Production of High Purity Hydrogen through Methanol Based Membrane Reformer

A thesis submitted in partial fulfillment of the requirements for the degree of

DOCTOR OF PHILOSOPHY

by

Richa Sharma

(126107017)

Department of Chemical Engineering

Indian Institute of Technology, Guwahati

May, 2018

CERTIFICATE

It is certified that the work contained in the thesis entitled **Production of High Purity Hydrogen Through Methanol Based Membrane Reformer** by **Richa Sharma**, a student in the Department of Chemical Engineering, Indian Institute of Technology Guwahati, Guwahati, India, for the award of the degree of Doctor of Philosophy has been carried out under our supervision and this work has not been submitted elsewhere for the degree.

Dr. Rajesh Kumar Upadhyay
Associate Professor
Department of Chemical Engineering
Indian Institute of Technology Guwahati
Guwahati 781039, Assam, India

Dr. Amit Kumar
Associate Professor
Department of Chemical Engineering
Indian Institute of Technology Guwahati
Guwahati 781039, Assam, India

ACKNOWLEDGEMENT

I am a part of the **CPEL team at IITG** and my journey as a Ph. D student has been worthwhile due to the motivation, suggestion and criticism that my team supported me with, for half a decade.

My friend once said, if I can learn and perform one thing well, I can surely handle the rest. Hence, I have surely come a long way with the timely motivation, guidance and critical discussions that nurtured me and allowed me to achieve my objectives. Expressing my gratitude by merely acknowledging the people who have supported me so far will be too small to what they have given me. Nonetheless, I would like to express my heartfelt thankfulness to all the people who have made this journey for me possible.

First and foremost, I am grateful to my supervisor Dr. Rajesh K. Upadhyay and co-supervisor Dr. Amit Kumar to teach me and groom me into the person that I am today. I thank them for opening up the whole new world of reactors to me which without a doubt I have loved working on. I also thank them for being kind and patient with me and giving me the time and space to grow and develop my understanding in this field. Their encouragements, advices and even sarcasms will always be the guiding light. I must also say that the exposure I received through them while working on this project is the confidence that shows in me.

I would also like to take this opportunity to thank my doctoral committee members Dr. Chandan Mukherjee, Dr. Chandan Das and Dr. Vaibhav Goud for their valuable suggestions and feedback on the work performed throughout my Ph.D. Moreover, I would especially like to express my heartfelt appreciation to Dr. **D**asmahapatra, Dr.

Mahuya De, Dr. Ghosh and Dr. Bandyopadhyay who despite minimal communication, have always inspired me to strive harder and achieve my goals.

My sincere gratitude also extends to Professor Moholkar and Professor Mandal current Head of Department (HoD) for allowing me to attend all the international conferences and providing me the timely grant that made the journeys comfortable. I also would like to acknowledge center for fire explosive and environment safety- defense research and development organization (CFEES, DRDO) to fund this project, Central instrumentation facility (CIF)-IIT Guwahati for providing the sophisticated tools to analyze my samples, administration (R&D, and academic office) for the timely help with the document processing and all the staff of department of chemical engineering especially Bhagya da, Deep da, Luko da, Debojeet da, Jayanta da, Ariful da and Jyotish da for all their co-operation and help whenever needed. I would also like to thank Dr. Pankaj Tiwari for all the help especially with gas cylinders he provided during the course of my work.

I am indebted to my friends Premkumar and Lipika who have always been there for me and have provided their support every time I asked for. I also wish to express my sincerest gratitude to my Lab mates (previous as well as current) especially Himadri, Tarang, Rawat, Trilok, Priyanka, Sonit, Shilpi Ma'am, Mamleshwar and Sreeram for their suggestions, unmatched help and above all for bearing with me. I also would like to thank Amrita Ma'am, Peeyu, Shiva, Rohit da and Rupak Sir for helping me innumerable times and believing in me. In addition, I would like to thank my friend Syam for giving me the space to discuss and unfold the intricacies of the systems I have dealt with during my Ph.D. I also thank him for being a true friend, a critique and a family during this journey.

Last but not the least, this journey would never have been steady and strong without the emotional support of my parents and my brother. I am forever indebted to the understanding they have showed and for standing by me through every thick and thin. This world is a better place because of you, Ma, Taji and Kunu. Thank You.

ABSTRACT

Commercial energy demand is largely met by fossil fuels globally. Burning of fossil fuel causes huge carbon emissions, which have created environmental menace due to ever increasing human population. Therefore, alternative energy production using renewable resources are considered a key player in minimizing the dependence on fossil fuels. Hydrogen is considered as a feasible alternative to fossil fuel. "Hydrogen" contains the highest energy to weight ratio with nearly three times the energy content of gasoline and diesel. Hydrogen can be used as a fuel in polymer electrolyte membrane (PEM) fuel cells that have potential to substitute internal combustion engines to provide on-board power for portable power generators and vehicles. However, storage and distribution of hydrogen is a major problem for fuel cell based stationary or mobile power generators. 'In-situ' generation and separation of hydrogen through 'membrane reformers' using steam reforming of alcohols can be a possible solution for this problem.

Membrane reformers couple reaction and separation in a single unit. However, achieving high hydrogen purity and high hydrogen flux through membrane reformer is a major challenge. The current work provides a comprehensive study on membrane reformer.

In the newly designed membrane reformer, hydrogen separation was carried out by using palladium based membranes to achieve high purity. Pd-based membranes supported on porous SS (PSS) and ceramic tubes were synthesized using electroless deposition until a dense (non-porous) surface morphology was

achieved. Membrane deposition was carried out for three combinations a) pure Pd, b) 90%Pd-10%Ag and c) 90%Pd-8%Ag-2%Au. Surface characterizations were performed with FESEM-EDX and AFM. Room temperature testing of the synthesized membrane was performed using bubble point methanol with argon as the purging gas inside the membrane dipped in water at different pressures. Further, the testing of prepared membranes were conducted with simulated compositions of reformate to determine membrane perm-selectivity as a separator for PSS as well as ceramic supported membranes to achieve high hydrogen purity.

Subsequently, membrane separator design was evaluated with the implementation of multi-pass inside it to achieve high hydrogen flux. Gas permeation studies were carried out using $50H_2$:$50N_2$ (v/v) feed composition for single and multiple membranes placed at different locations inside the multi-pass membrane separator. The best arrangement was then tested using a mixture composition such as $50H_2$:$30N_2$:$18CO_2$:2CO (v/v) that simulates a synthetic reformate mixture from methanol steam reforming.

Hydrogen generation was targeted with methanol steam reforming in a fixed bed reactor with different catalysts for variable temperature (150 to 400°C), feed rate and methanol to steam compositions. Reaction testing was performed with mono-metallic (Cu, Ni, Pd, Ru, Fe) and bimetallic (Cu-Fe, Ni-Fe, Ru-Fe, Cu-Ni and Cu-Ru) catalysts supported on alumina-zinc-zirconia composite. In bimetallic catalysts, Fe as a promoter was investigated to enhance hydrogen production rate as well as to determine its feasibility in inhibiting CO generation

even at high temperatures. Reaction performance was supported with material characterization tools such as XRD, TPR, TEM, FT-IR, TGA, DRIFT and Chemisorption. For the optimal catalyst, reaction mechanism was proposed and its long-term stability testing for 100 hours was carried out in order to confirm its viability for membrane reformer integration.

Finally, synthesized catalyst and prepared membrane are integrated in a single assemble, membrane reformer, and tested. The performance of in-house built membrane reformer was compared with commercially available membrane reformer unit "ME-100®" from REB Research and Consultancy, USA. The commercial unit comprise of an in-built reactor with 100 µm thick self-supported dense Pd-Ag membrane and a proprietary WGS catalyst. Experiments were performed to optimize the following parameters: a) feed composition (varied in the molar ratio of 1:1 to 1:18 methanol: water) b) temperature (between 623−723K) and c) pressure (between 3 and 5 bar). With the optimized operating conditions, the in-house developed membrane reformer was compared. Further, multiple membrane integration studies were also carried out to determine the maximum hydrogen flow rate in permeate of membrane reformer without compromising the purity of hydrogen.

Table of Contents

List of Figures

List of Tables

Chapter 1

Introduction

Abstract

This chapter discusses an overview of membrane reformers as 'on-board' hydrogen production units. In this study, membrane reformer/reactor (MR) integration using methanol steam reforming and palladium-based alloyed membranes is presented. A few major outcomes and challenges with MRs are also discussed. Lastly, the objectives of the thesis are highlighted followed with the structure of thesis.

1.1 Introduction

1.1.1 Hydrogen energy

Depleting fossil fuels directs the fuel economy to grow towards hydrogen. Hydrogen is the lightest element and possesses the highest energy-to-weight ratio, nearly three times the energy content of gasoline and diesel. It not only minimizes the dependence on fossil fuels but is also known as a clean-efficient energy carrier. This is because combustion of hydrogen to produce power releases only water as by-product. As an automotive fuel, burning of hydrogen in an internal combustion engine results in NOx formation and reduced power output particularly because of low volumetric density of hydrogen [1]. However, if converted to electrical energy using a fuel cell, the efficiency increases by 30% [2]. It facilitates power generation without putting much of CO_2 to the environment. The 'holy grail' of hydrogen fuel as energy carrier lies in its storage and transportation. Traditionally stored in compressed cylinders or as liquid in cryogenic containers,

hydrogen poses a safety threat due to its low volumetric density. In addition, it is highly challenging to compress hydrogen gas from 5,000 psi to 10,000 psi which is required for liquefying it [3]. Hydrogen can also be stored as metal hydrides and as a cryogenic liquid. Metal hydrides have low mass energy density which makes vehicles much heavier and less efficient than comparable gasoline vehicles. Further, cryogenic storage of liquid hydrogen for automotive incurs significant losses as 10–25% of fuel boils off during re-fuelling [4]. This brings huge capital costs, low energy content per unit volume, high tankage weights, and high storage vessel pressures. In order to abate these, 'on-board' generation of hydrogen seems to provide a feasible solution to storage. On-board hydrogen generators can further be integrated with polymer electrolyte membrane (PEM) fuel cells for power generation. A critical challenge in this integration is that PEM fuel cell requires hydrogen of 99.999% purity with CO content less than 1 ppm. This necessitates hydrogen separation from the amount generated to become an integral part of on-board hydrogen production unit. Moreover, generation and separation of hydrogen in a single unit should be compact for on-board applications.

1.1.2 Hydrogen generation

Hydrogen is a carrier; and its generation is usually accomplished using methane, gasoline, methanol, ethanol, coal and water as feed stock, by processes such as steam reforming, coal gasification, electrolysis and cracking. Depending on their stoichiometry, these processes when carried out in their respective operating conditions produce H_2 accompanied with by products such as CO, CO_2, O_2, C_2H_4, or CH_3CHO. Industrially, hydrogen generation is mostly carried out using methane steam reforming as shown in Fig. 1. However, temperature requirements for methane steam reforming are very high

(~850°C) to obtain a desirable conversion [5]. Further, low volumetric density of methane at ambient temperature and pressure provides substantial challenge in its storage and hence makes it unsuitable for on-board applications [6]. Furthermore, hydrogen can be generated through coal gasification. Coal is an abundant fossil fuel resource and is utilized for hydrogen production by reacting it with steam under high temperatures and pressures to form synthesis gas. However, hydrogen production using coal is an expensive process as most fossil fuels contain 0.5 to 5% total sulphur [7], removal of which is a significant challenge. Another promising technology for hydrogen generation is water electrolysis.

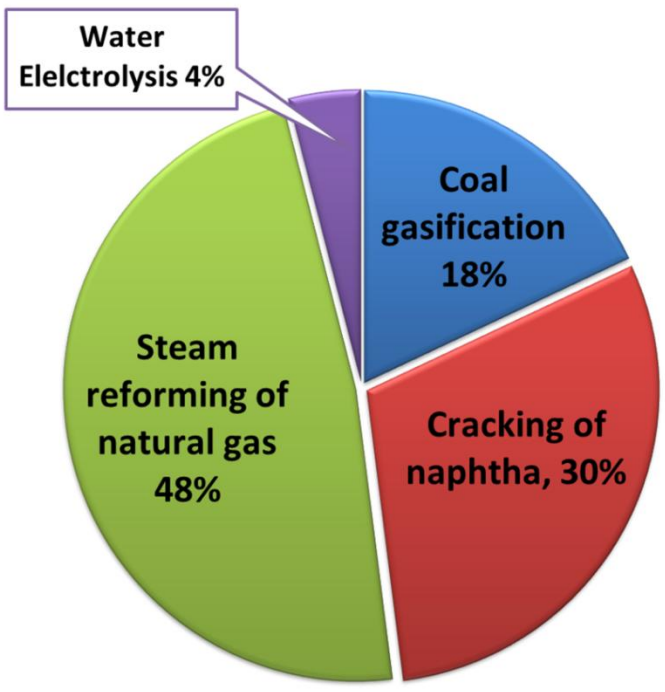

Fig. 1.1 Hydrogen generation processes (adapted from [8])

Since the 1920s, electrolysis has been used with water as feedstock to produce hydrogen industrially. It is a process which utilizes electricity to break the chemical bonds present in water molecule into hydrogen and oxygen. The energetic efficiency of electrolysis is

mostly between 50-70% [9]. High electricity consumption (4.5–5kW/m^3H_2) makes this process unsuitable for commercial hydrogen production [10]. Similar economically competitive hydrogen production process is direct methane cracking which has met huge interests due to increasing demand of CO free hydrogen. This reaction essentially produces hydrogen and filamentous carbon or carbon nanotubes. However, in order to achieve a reasonable yield, a temperature higher than 1200°C is required [11, 12]. In contrary to these processes, steam reforming of methanol is considered energy efficient with product gas containing 75% H_2 at relatively low reforming temperature (250-350°C). This is because there is no C-C bond cleavage in methanol steam reforming [13, 14]. In addition to methanol, ethanol and glycerol are also investigated widely for hydrogen production [15]. Though hydrogen yield through ethanol and glycerol is higher than methanol, the amount of CO generation and coke formation is also high. In order to minimize CO in the reformate stream, primary fuel can be combined with oxygen. Oxygen mixed with steam and hydrocarbon will result in heat from partial oxidation to provide heat for steam reforming reaction. This process is called as auto-thermal reforming [16]. In this method, careful control of oxygen content is essential to maintain the proper reaction temperatures thereby making it unsuitable [16].

A comparison between the energy efficiency of system with steam reforming of diesel, methanol and ethanol was recently reported [8] as shown in Fig. 2. In this study, methanol was reported to have maximum energy efficiency (~35%) followed with ethanol and diesel. It was reported that using ethanol, high conversion efficiency between 350-450°C can be achieved in comparison to methanol but the conversion products include acetaldehyde and methane besides hydrogen and CO/CO_2. Hence, higher

conversion does not necessarily imply high hydrogen production rate [8]. Based on this analysis, hydrogen production using methanol steam reforming appears to be the optimum choice for on-board hydrogen generation.

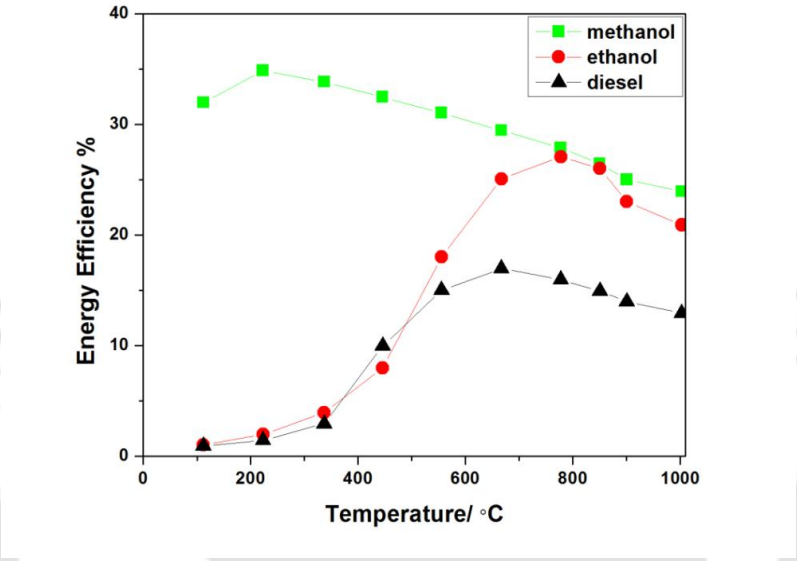

Fig. 1.2 Energy efficiency of systems employing steam reforming of methanol, ethanol and diesel to generate hydrogen (adapted from [8])

The reaction products using methanol steam reforming stoichiometrically include only CO_2 and H_2. However, CO formation has also been widely reported during the steam reforming of methanol due to methanol decomposition or reverse water gas shift reaction. In order to feed hydrogen to fuel cell for power generation, separation of hydrogen from CO and CO_2 is essential. The Pt-catalyst loaded on the anode of Proton Exchange Membrane (PEM) fuel cell requires feed that includes only dry H_2 typically of purity >99.999% [17]. Therefore, to obtain high purity hydrogen, effective separation of hydrogen from reformate mixture is vital.

1.1.3 Hydrogen separation

Gases can be purified through several techniques, such as pressure swing adsorption (PSA), temperature swing adsorption (TSA), cryogenic distillation and membrane separation. The separation methods mostly rely on either differences in physical properties (e.g., boiling point, size, solubility) or differences in chemical properties using sorbents with strong chemical interactions. Amongst physical separation techniques, PSA has been used for the past few decades in the chemical industry to carry out bulk gas separation and purification steps due to high selectivity, high throughput and high energy efficiency[18]. PSA operation involves the preferential adsorption of a species from a gas mixture at high pressure (10-40 bar) until equilibrium loading. Desorption is then carried out at nearly ambient pressure which regenerates the column. Adsorbents such as activated carbon, zeolites and carbon molecular sieves are extensively used for H_2 recovery from fuel gas, air separation and landfill gas separation respectively. Faster cycle times, lower size of equipment and thus lesser inventory of adsorbent makes PSA more attractive for bulk separation and purification in situations where adsorptive forces are relatively weak [19]. PSA process features very high product purity (99 % +) but moderate hydrogen recovery (65-90%). A continuous countercurrent process is mostly employed to maximize mass transfer and enhance recovery. In a similar manner, temperature swing adsorption is operated in cyclic batch mode, with at least two adsorbent beds: one for adsorption and the other for regeneration. Since adsorption is carried out at near ambient conditions, a portion of weakly adsorbing gas/hot inert purge or steam is used for regeneration. The main drawback of TSA is the long cycle time for bulk separation [20] compared to PSA. This is because increasing pressure does not take

time while changing temperature does. Further, long cycles in TSA mean large bed lengths, and therefore, large quantity of adsorbents; and if mass transfer zone is short, it leads to ineffective utilization of adsorbent. Further, PSA require very high pressure which is not desirable for on-board applications as it adds weight on the vehicle.

Another widely used method of separating fluid mixtures is cryogenic distillation process. The cryogenic process is a low temperature separation process which uses the difference in boiling temperatures of the feed components to effect the separation. Hydrogen has a high relative volatility compared to hydrocarbons. However, if the feed contains significant amounts of carbon monoxide (CO) and carbon dioxide (CO_2), a methane wash column is required to reduce the levels of these gases [21, 22]. Higher hydrogen recovery at moderate hydrogen purities (99%) is possible with a cryogenic system; however, very high hydrogen purity is not practical [23]. Further, it consumes a considerable amount of energy [21].

Apart from PSA, TSA and cryogenic distillation, membrane separation techniques have attracted wide interest. Membranes are barriers which, because of their physical nature, allow only selected materials to permeate across them. Some advantages of the membrane separation process over mature and commercially available technologies such as PSA and cryogenic distillation are as follows: ease of operation, low investment cost, low energy consumption, compact and cost effectiveness even at low gas volumes. They are classified based on their nature, geometry and separation regime such as organic, inorganic and inorganic/organic hybrids. Membranes can be homogeneous or heterogeneous, symmetric or asymmetric in structure; solid or liquid (organic thin layer) ; can possess positive or negative charge; and can be neutral or bipolar. But in all cases, the

major driving force that is applied to induce permeation through the membranes includes either a gradient of pressure or gradient of concentration or electric potential.

Separation of gases using membranes is a concentration driven process, i.e. directly related to the partial pressures of the gas species. Therefore, it is the pressure differential between the feed and permeate side that directly affects the effective performance of the membrane. Membranes comprise of organic such as polymeric membranes and inorganic membranes that can be of ceramic, glass or metal. Majority of industrial membrane processes are made up of either natural polymeric membranes such as wool, rubber (polyisoprene), cellulose or made up of synthetic polymers comprising polyamide, polystyrene and polytetrafluoroethylene (Teflon). Polymeric membranes are commercially emphasized to be very attractive with respect to its ease of processability, low operating temperatures and reasonable costs [24] However, the low solubility of hydrogen in polymeric membranes limits the rate of H_2 permeation fluxes. Also, high temperature instability problems especially in membrane reactors for hydrogen generation impede polymeric membranes feasibility [25]. In contrast to polymeric membrane's chemical and thermal instability, susceptibility to chemical attack, inorganic membranes are proposed to give much higher fluxes having operational stability and inertness to different conditions of temperature and chemical environment [26]. Transport through these membranes depends on whether the structure is porous or dense. The transport of gases through porous membranes may take place through any of the possible routes mentioned below:

a) Knudsen diffusion: When pore diameter d_p is smaller than the mean free path of the gas molecules λ, collisions between the gas molecules and the pore walls predominate

so that the transport of gas molecules is controlled by the thermal mean velocity of the gas molecules [27, 28].

b) Surface diffusion: It involves adsorption of permeating molecules on the surface (either physisorption or chemisorption) and migration along the surface.

c) Capillary condensation: It favour the transfer of relatively large molecules that condense within the pores due to capillary forces.

d) Molecular sieving: The pore diameter is very small so that it only allows the permeation of very small molecules and prevents larger molecules from passing through.

e) Poiseuille (viscous) flow: This occurs when the average pore diameter is bigger than the average free path of fluid molecules; such flow results in no separation [29].

f) Multi-layer diffusion: It results from strong molecule-surface interaction, and is considered an intermediate flow regime between surface diffusion and capillary condensation.

Contrary to porous membranes, dense membranes are non-porous, uniform and should be defect free for high hydrogen selectivity. Transport through dense membranes occurs by solution-diffusion mechanism wherein the gas dissolves in the membrane material and then diffuses through the membrane down a concentration gradient [30, 31]. This mechanism is driven by a difference in thermodynamic activity at the upstream and downstream faces of the membrane, as well as the interaction forces between the

molecules of the membrane matrix and the gases [32, 33]. The activity difference causes a concentration gradient that leads to diffusion in the direction of the reduced activity.

Among the several separation techniques discussed such as pressure swing adsorption (PSA), cryogenic distillation and membrane separation, membranes are widely preferred as it minimizes the energy consumption. Further, it also makes the system compact.

A comparative representation of various membrane types used for hydrogen separation is provided in Table 1.1. Thus, on the basis of compactness and high hydrogen selectivity as shown in Table 1.1, dense metallic membranes are considered a suitable choice for hydrogen separation. Metallic membranes of metals belonging to group 10 and some in groups 3–5 of the periodic table have the ability to dissociate and dissolve hydrogen.

Table 1.1 Overview of hydrogen separation techniques [10, 24, 34-36]

Separation Processes	**Adsorbent or Membrane Material**	**Separation Principle**	**Pore Size (nm)**	**Purity (%)**
Pressure Swing Adsorption	Carbon Molecular Sieves	Pressure driven	0.4-0.9	99.99
Temperature Swing Adsorption	Carbon Molecular Sieves	Temperature driven	0.4-0.9	-
Membrane Gas Separation	**Dense metallic membrane**	**Solution diffusion mechanism**	**Non-porous**	**99.999**
	Dense polymeric membranes	Solution diffusion mechanism	Non-porous	Low
Cryogenic Distillation	-not required-	Differing condensing/boiling points of the individual components	-NA-	Above 99% [21]

This property enables metallic membranes, especially palladium/palladium alloy membranes, to transport hydrogen with an outstanding ability due to higher hydrogen solubility over a wide range of temperature [30, 37-39]. Further, palladium has a higher phase transition temperature compared to other metals belonging in the same group [39, 40]. These properties and infinite hydrogen selectivity therefore make palladium membranes an ideal choice for hydrogen separation for 'on-board' applications.

1.2 Membrane reformers

Membrane reformers integrate hydrogen generation with simultaneous separation in a single unit. Using high energy density alcohols such as methanol, these membrane reformers are employed 'on-board' to produce high purity hydrogen for small scale vehicles, batteries and portable generators. Membrane reformers are especially advantageous for reactions limited by thermodynamic equilibrium such as steam reforming of methanol, as they can improve the reactant conversion by selective removal of hydrogen from the produced mixture. According to Le Chatelier's principle, continuous removal of H_2 shifts the equilibrium in the forward direction resulting in enhanced conversion. Moreover, increase in conversion increases the trans-membrane hydrogen partial pressure difference which results in better hydrogen permeation. Further, being an integrated assembly, membrane reformer does not require a dedicated separation unit which significantly reduces the size of the system and minimizes the downstream processing cost and product losses. This makes the membrane reformer more economical for commercial applications [3, 29, 41].

Integrated reaction-separation was first proposed by Professor Vladimir Gryaznov (Moscow University) in the year 1964. He proposed a method to carry out simultaneous evolution and consumption of H_2 in a dense tubular palladium membrane reactor where Pd is permeable to H_2 and also serves as a catalyst for the cyclohexane dehydrogenation to benzene. In the year 1990, a 4 Nm^3/h MR was developed by Tokyo Gas Co. Ltd with Mitsubishi Heavy Industries Ltd. In 2003, commercialized MR designs were reported by Reb Research and Consultancy (Prof. Buxbaum group)[42]. In addition to this, MR studies have been reported by ENEA (Prof. Sivano Tosti group), ITM-CNR (Dr. Angelo Basile group), Prof. Dittmeyer and Prof. Elnashaie group, fluidized membrane reactor by Prof. Kuipers and Prof. Sint Annaland group (University of Twente).

The system performance in case of a membrane reformer is both kinetically as well as diffusion controlled which thereby necessitates an optimal temperature, pressure and flow rate that will maintain stability of both the catalyst and the membrane.

1.2.1 Challenges of membrane reformer

Membrane reformer (MR) is an attractive tool to produce hydrogen for on-board applications. However, the following technological challenges associated with this system impede its fast commercialization.

- MR was developed with the critical objective of yield enhancement for equilibrium limited reactions. Therefore, the benefit of using a MR is the continuous permeation of product through the membrane that will simultaneously shift the equilibrium towards the product side (Le-Chatelier's principle). Thus, at a constant temperature, high

conversion in MR can be achieved compared to conventional techniques. However, membrane plays a critical role in the development of commercially viable MR.

- Inverse relationship that typically exists between permeability and selectivity (purity) necessitates a tradeoff for MR. Higher selectivity is obtained usually at the cost of low permeation values, which is economically not always justifiable. Selectivity and flux are two indispensable factors for the characterization of membrane reformers. It is well known that optimization of one factor sometimes has led to the deterioration of the other. For instance, Ligouri et al. [43] observed a higher hydrogen removal at higher pressure but also reported defects in membranes resulting in 0.21 and 0.25% CO in permeate. This necessitates a tradeoff between membrane thickness and hydrogen flux. Though a higher thickness may improve hydrogen selectivity but will increase metal required resulting in higher cost.
- Competitive adsorption of the species available in reactant and product reduces the separation efficiency and selectivity of the membranes which reduces the performance of MR. Further, concentration polarization in case of highly selective membrane is also an issue which affect the hydrogen permeation through it overtime thereby affecting MR stability [44, 45]
- Chiappetta et al. [46] assessed the effect of the membrane surface area, catalyst volume, reactant flow rate on the performance of methane fed membrane reformer. A surplus of hydrogen production with respect to available membrane surface area is also reported as an inadequate MR design due to low hydrogen recovery. At 550°C, highest recovery reported by Chiappetta et al. [46] was up to 45%. Moreover, inefficient seals (either glass enamel joints, glaze or graphite gaskets) used for

connecting membrane to the reactors are often reported to weaken during reaction conditions leading to huge losses in permeate hydrogen selectivity.

Thus, low hydrogen recovery and purity can be considered as a primary challenge with a membrane reformer. Surface to load ratio is also critical to determine membrane separation efficiency. Further, in order to minimize CO inhibition, steps are required which can negate its occurrence in the reaction. Therefore, better catalysts need to be designed.

1.3 Motivation

Membrane reformers are interesting process intensified units which have immense potential to emerge as a new technology for small scale portable hydrogen generators. The crux in the development of this technology is to obtain maximum hydrogen recovery, high hydrogen selectivity and high hydrogen flux.

Methanol is the simplest of alcohols that can be used to produce hydrogen. Steam reforming of methanol requires reaction temperatures in the range of 200–400°C which typically produces hydrogen (~60% by mole), the rest being CO, CO_2, unreacted H_2O and methanol. However, in order to decrease the startup time for a fuel cell, studies are targeted to achieve adequate conversion at even lower temperatures (120-170°C) [47, 48]. Various metal-metal and metal-support interactions are therefore studied to identify best performing catalysts for low temperature steam reforming of methanol. Further, in membrane reformers, reforming catalysts are intertwined with membranes which together control the performance of this system. Integration of endothermic steam reforming with membrane separation necessitates membranes which can sustain higher temperatures.

With evident superior thermal stability and acceptable tolerance to chemical attack, inorganic membranes are estimated to give much higher operational stability compared to polymeric membranes. Dense palladium membranes show large solubility of hydrogen over a wide temperature range compared to any other metal, which makes palladium the suitable material of choice for hydrogen separation. Palladium's catalytic ability allows molecular hydrogen to dissociate on its surface. The atomic hydrogen then diffuses across the palladium membrane to the permeate side, associates to molecular hydrogen and leaves the surface. Palladium membranes can provide infinite hydrogen selectivity when the surface is absolutely dense/non-porous. Pure palladium is mostly alloyed with elements such as Ag that lowers the critical phase transition temperature of palladium from 300°C to around room temperature. Further, addition of Ag to Pd also increases H_2 permeability because of the increase in average bond distance in the alloy in comparison to pure Pd. Numerous studies have reported the synthesis of Pd-alloy supported membranes over a range of thickness and compositions. However, there exists a tradeoff that is to be optimized between selectivity and flux to achieve optimal membrane performance. Although the overall concept of membrane reformer looks very simple, integrating a high temperature and low-pressure steam reforming reaction with low temperature and high-pressure membrane separation process is a major challenge. Broadly, the following three elements can be identified for the design of a membrane reformer:

i) Synthesis of suitable catalyst for steam reforming reaction, which can withstand high-pressure environment and can perform reaction at relatively low temperature.

ii) Preparation of dense palladium/palladium alloy membrane which can provide high selectivity and high flux at relatively low-pressure.

iii) Integration of above two in a single unit for production of ultra-pure hydrogen at high flux.

In the present work, all the three aspects of membrane reformer were addressed to design an optimal membrane reformer for production of ultra-pure hydrogen. Hydrogen generation by steam reforming of methanol was studied using synthesized Cu and Cu-based bimetallic supported catalysts. Catalyst testing was performed with varying operational parameters such as weight hour space velocity (WHSV, $kg_{cat}/mol_{methanol}.s$)), temperature and steam-to-methanol (S/M) ratio. Further, active metal% and bi-metal compositions were varied to study the product selectivity for the optimal reaction. To achieve high hydrogen purity, Pd-based dense supported membranes were employed after their synthesis and characterization. Dense Pd-based membranes were prepared using modified electroless deposition approach on porous SS (PSS) as well as porous alumina support. Yttria stabilized zirconia (YSZ) was applied as an intermediate layer that minimizes the intermetallic diffusion between Pd and SS. Further, Pd-Ag supported on alumina-based catalytic sol was coated on alumina supports to create a uniform surface morphology and reduce pore size. Optimization of standalone membranes as well as catalyst performance was performed prior to the integration. Finally, integration studies with prepared dense palladium alloy membranes and optimized catalysts were performed in a single unit. The performance of packed bed MR with varying parameters such as temperature and pressure, feed composition and bed configuration were tested to find the

optimal design and operating conditions for the newly developed methanol-based membrane reformer.

1.4 Objectives

The overall aim of current work was to design a methanol-based membrane reformer and find the suitable operating conditions for the same. The specific objectives of the work were as follows:

- Preparation, characterization and testing of dense palladium/palladium alloy membranes for separation of H_2
  - Optimization of membrane separator design
  - Performance comparison with commercial membrane
- Preparation, characterization and testing of supported catalysts for H_2 generation using methanol steam reforming
  - Effect of temperature and weight hourly space velocity (WHSV)
  - Effect of steam/methanol (S/M) ratio
- Integration, design and testing of a compact membrane reformer
  - Design of a compact membrane reformer
  - Optimization of operating condition

1.5 Structure of Thesis

The outline of the thesis is as follows:

In ***Chapter 2*** membrane preparation techniques are reviewed. Further, palladium-based alloy membranes such as Pd, Pd-Ag and Pd-Ag-Au supported on porous alumina and

porous stainless steel are prepared using electroless deposition. The extent of deposition was monitored using atomic absorbance spectroscopy (AAS). Characterization during each preparation step was performed using field emission scanning electron microscope-energy dispersive X-ray analysis (FESEM-EDX) and atomic force microscopy (AFM). Hydrogen permeation was tested using pure hydrogen at various temperatures and pressures.

In ***Chapter 3*** a multi-pass membrane separator design for high throughput applications is demonstrated. Using a commercial self-supported membrane, hydrogen permeation studies were carried out in the membrane separator with and without baffles. Self-supported membranes do not give any additional resistance to permeation and therefore were considered ideal to perform membrane separator optimization with baffles. Single membrane testing was performed at several membrane positions inside the reactor (with and without baffle). Further, multiple membrane arrangements using a four membrane assembly is devised. Temperature and velocity distributions inside the reactor (with and without baffles) are studied computationally to support and better explain the experimental observations. An optimal membrane arrangement comprising of 4 membranes is suggested which is lastly compared with the prepared four PSS supported Pd-Ag membranes. Hydrogen permeation is investigated using H_2/(Ar or N_2) and H_2/(Ar or N_2)/CO/CO_2 mixtures.

In ***Chapter 4*** development of catalysts for methanol steam reforming is discussed. Using incipient wetness impregnation, various monometallic and bimetallic catalysts supported on Al_2O_3-ZnO-ZrO_2 support are synthesized. Effect of Fe as promoter in the preparation of bimetallic catalyst is investigated owing to its high redox activity. Characterization of

the prepared catalysts is presented using Brunauer–Emmett–Teller (BET), X-ray diffraction (XRD), transmission electron microscope (TEM), temperature programmed reduction (TPR), FESEM-EDX and Fourier transform- infrared spectroscopy (FT-IR). Testing of catalysts is performed in a fixed bed reactor with varying temperature, steam/methanol (S/M) mole ratio and weight hourly space velocity (WHSV). This chapter further illustrates on the developed catalyst with zero CO selectivity at high temperatures. Lastly, the reaction mechanism for the developed Fe-promoted catalyst is also proposed using information from diffuse reflectance infrared fourier transform (DRIFT) analysis.

In ***Chapter 5*** membrane reformer integration studies are elaborated with two case studies: a) Commercial self-supported membrane integrated with proprietary high temperature MSR catalyst in ME-100® hydrogen generator (procured from REB Research and Consultancy, USA) and b) prepared Pd-Ag membrane supported on PSS with developed Cu-Fe catalyst supported on Al_2O_3-ZnO-ZrO_2. The effect of temperature and pressure is presented for both membrane reformer studies. Further, ME-100® is also compared with a membrane separator sequentially integrated with synthetic reformate mixture composition to evaluate the self-supported membrane performance. Effect of steam on hydrogen permeation is determined. Lastly, membrane reformer performance is demonstrated for supported Pd-Ag membranes with effect of reactor diameter, with and without baffle integration.

In **Chapter 6** broad inferences and conclusions are presented that elaborates on the significance of the study conducted. The effect of baffles to enhance hydrogen recovery

from a high throughput MR was presented. Further, the effect of developed low CO selective bi-metallic catalysts on MR performance is elaborated.

References

[1] S. Verhelst, Recent progress in the use of hydrogen as a fuel for internal combustion engines, International Journal of Hydrogen Energy, 39 (2014) 1071-1085.

[2] A. Schäfer, J.B. Heywood, M.A. Weiss, Future fuel cell and internal combustion engine automobile technologies: A 25-year life cycle and fleet impact assessment, Energy, 31 (2006) 2064-2087.

[3] L.M. Gandía, G. Arzamendi, P.M. Diéguez, Chapter 1 - Renewable Hydrogen Energy: An Overview, in: Renewable Hydrogen Technologies, Elsevier, Amsterdam, 2013, pp. 1-17.

[4] G.D. Berry, S.M. Aceves, Onboard Storage Alternatives for Hydrogen Vehicles, Energy & Fuels, 12 (1998) 49-55.

[5] V. Arcotumapathy, D.-V.N. Vo, D. Chesterfield, C.T. Tin, A. Siahvashi, F.P. Lucien, A.A. Adesina, Catalyst design for methane steam reforming, Applied Catalysis A: General, 479 (2014) 87-102.

[6] J.A. Mason, J. Oktawiec, M.K. Taylor, M.R. Hudson, J. Rodriguez, J.E. Bachman, M.I. Gonzalez, A. Cervellino, A. Guagliardi, C.M. Brown, P.L. Llewellyn, N. Masciocchi, J.R. Long, Methane storage in flexible metal–organic frameworks with intrinsic thermal management, Nature, 527 (2015) 357-361.

[7] C.-L. Chou, Sulfur in coals: A review of geochemistry and origins, International Journal of Coal Geology, 100 (2012) 1-13.

[8] S.M. Mousavi Ehteshami, S.H. Chan, Techno-Economic Study of Hydrogen Production via Steam Reforming of Methanol, Ethanol, and Diesel, Energy Technology & Policy, 1 (2014) 15-22.

[9] C. M. Kalamaras, A. Efstathiou, Hydrogen Production Technologies: Current State and Future Developments, 2013.

[10] D.L. Stojić, M.P. Marčeta, S.P. Sovilj, Š.S. Miljanić, Hydrogen generation from water electrolysis—possibilities of energy saving, Journal of Power Sources, 118 (2003) 315-319.

[11] A.M. Amin, E. Croiset, W. Epling, Review of methane catalytic cracking for hydrogen production, International Journal of Hydrogen Energy, 36 (2011) 2904-2935.

[12] H.F. Abbas, W.M.A.W. Daud, Hydrogen production by thermocatalytic decomposition of methane using a fixed bed activated carbon in a pilot scale unit: Apparent kinetic, deactivation and diffusional limitation studies, International Journal of Hydrogen Energy, 35 (2010) 12268-12276.

[13] O. Sanz, I. Velasco, I. Pérez-Miqueo, R. Poyato, J.A. Odriozola, M. Montes, Intensification of hydrogen production by methanol steam reforming, International Journal of Hydrogen Energy, 41 (2016) 5250-5259.

[14] S. Sá, H. Silva, L. Brandão, J.M. Sousa, A. Mendes, Catalysts for methanol steam reforming—A review, Applied Catalysis B: Environmental, 99 (2010) 43-57.

[15] B. Zhang, X. Tang, Y. Li, Y. Xu, W. Shen, Hydrogen production from steam reforming of ethanol and glycerol over ceria-supported metal catalysts, International Journal of Hydrogen Energy, 32 (2007) 2367-2373.

[16] L. F. Brown, A comparative study of fuels for on-board hydrogen production for fuel-cell-powered automobiles, International Journal of Hydrogen Energy, 26 (2001) 381-397.

[17] F. de Bruijn, The current status of fuel cell technology for mobile and stationary applications, Green Chemistry, 7 (2005) 132-150.

[18] S. Jain, A.S. Moharir, P. Li, G. Wozny, Heuristic design of pressure swing adsorption: a preliminary study, Separation and Purification Technology, 33 (2003) 25-43.

[19] W.J. Thomas, B. Crittenden, 4 - Rates of adsorption of gases and vapours by porous media, in: Adsorption Technology & Design, Butterworth-Heinemann, Oxford, 1998, pp. 66-95.

[20] T. Eriksson, Y. Kiros, Temperature swing adsorption device for oxygen-enriched air, Journal of Cleaner Production, 76 (2014) 174-179.

[21] A.B. Hinchliffe, K.E. Porter, A Comparison of Membrane Separation and Distillation, Chemical Engineering Research and Design, 78 (2000) 255-268.

[22] S. Adhikari, S. Fernando, Hydrogen Membrane Separation Techniques, Industrial & Engineering Chemistry Research, 45 (2006) 875-881.

[23] S. Peramanu, B.G. Cox, B.B. Pruden, Economics of hydrogen recovery processes for the purification of hydroprocessor purge and off-gases, International Journal of Hydrogen Energy, 24 (1999) 405-424.

[24] D.F. Sanders, Z.P. Smith, R. Guo, L.M. Robeson, J.E. McGrath, D.R. Paul, B.D. Freeman, Energy-efficient polymeric gas separation membranes for a sustainable future: A review, Polymer, 54 (2013) 4729-4761.

[25] T. M. Nenoff, R. Spontak, C. M. Aberg, Membranes for Hydrogen Purification: An Important Step toward a Hydrogen-Based Economy, 2006.

[26] N.W. Ockwig, T.M. Nenoff, Membranes for Hydrogen Separation, Chemical Reviews, 107 (2007) 4078-4110.

[27] W. He, W. Lv, J.H. Dickerson, Gas Diffusion Mechanisms and Models, in: Gas Transport in Solid Oxide Fuel Cells, Springer International Publishing, Cham, 2014, pp. 9-17.

[28] H.A. Jakobsen, Elementary Kinetic Theory of Gases, in: Chemical Reactor Modeling: Multiphase Reactive Flows, Springer International Publishing, Cham, 2014, pp. 183-365.

[29] A. Basile, A. Iulianelli, J. Tong, 6 - Membrane reactors for the conversion of methanol and ethanol to hydrogen, in: Membrane Reactors for Energy Applications and Basic Chemical Production, Woodhead Publishing, 2015, pp. 187-208.

[30] T.L. Ward, T. Dao, Model of hydrogen permeation behavior in palladium membranes, Journal of Membrane Science, 153 (1999) 211-231.

[31] J.G. Wijmans, R.W. Baker, The solution-diffusion model: a review, Journal of Membrane Science, 107 (1995) 1-21.

[32] P. Pandey, R.S. Chauhan, Membranes for gas separation, Progress in Polymer Science, 26 (2001) 853-893.

[33] H.L. Frisch, "Diffusion in polymers" edited by J. Crank and G. S. Park, Academic Press, London and New York, 1968; 452 pg, Journal of Applied Polymer Science, 14 (1970) 1657-1657.

[34] W. Liemberger, M. Groß, M. Miltner, M. Harasek, Experimental analysis of membrane and pressure swing adsorption (PSA) for the hydrogen separation from natural gas, Journal of Cleaner Production, 167 (2017) 896-907.

[35] A. Ntiamoah, J. Ling, P. Xiao, P.A. Webley, Y. Zhai, CO2 Capture by Temperature Swing Adsorption: Use of Hot CO2-Rich Gas for Regeneration, Industrial & Engineering Chemistry Research, 55 (2016) 703-713.

[36] T. Sata, Ion exchange membranes and separation processes with chemical reactions, Journal of Applied Electrochemistry, 21 (1991) 283-294.

[37] N.A. Al-Mufachi, N.V. Rees, R. Steinberger-Wilkens, Hydrogen selective membranes: A review of palladium-based dense metal membranes, Renewable and Sustainable Energy Reviews, 47 (2015) 540-551.

[38] K. Atsonios, K.D. Panopoulos, A. Doukelis, A.K. Koumanakos, E. Kakaras, T.A. Peters, Y.C. van Delft, 1 - Introduction to palladium membrane technology, in: Palladium Membrane Technology for Hydrogen Production, Carbon Capture and Other Applications, Woodhead Publishing, 2015, pp. 1-21.

[39] S. Yun, S. Ted Oyama, Correlations in palladium membranes for hydrogen separation: A review, Journal of Membrane Science, 375 (2011) 28-45.

[40] F.A. Lewis, The palladium-hydrogen system: Structures near phase transition and critical points, International Journal of Hydrogen Energy, 20 (1995) 587-592.

[41] F. Gallucci, E. Fernandez, P. Corengia, M. van Sint Annaland, Recent advances on membranes and membrane reactors for hydrogen production, Chemical Engineering Science, 92 (2013) 40-66.

[42] R. Buxbaum, H. Lei, Power output and load following in a fuel cell fueled by membrane reactor hydrogen, Journal of Power Sources, 123 (2003) 43-47.

[43] S. Liguori, A. Iulianelli, F. Dalena, V. Piemonte, Y. Huang, A. Basile, Methanol steam reforming in an Al2O3 supported thin Pd-layer membrane reactor over Cu/ZnO/Al2O3 catalyst, International Journal of Hydrogen Energy, 39 (2014) 18702-18710.

[44] A. Caravella, G. Barbieri, E. Drioli, Concentration polarization analysis in self-supported Pd-based membranes, Separation and Purification Technology, 66 (2009) 613-624.

[45] T.A. Peters, M. Stange, H. Klette, R. Bredesen, High pressure performance of thin Pd–23%Ag/stainless steel composite membranes in water gas shift gas mixtures; influence of dilution, mass transfer and surface effects on the hydrogen flux, Journal of Membrane Science, 316 (2008) 119-127.

[46] G. Chiappetta, G. Barbieri, E. Drioli, Pd/Ag-based membrane reactors on small scale: Assessment of the feed pressure and design parameters effect on the

performance, Chemical Engineering and Processing: Process Intensification, 49 (2010) 722-731.

[47] K.M.K. Yu, W. Tong, A. West, K. Cheung, T. Li, G. Smith, Y. Guo, S.C.E. Tsang, Non-syngas direct steam reforming of methanol to hydrogen and carbon dioxide at low temperature, Nature Communications, 3 (2012) 1230.

[48] X.-R. Zhang, L.-C. Wang, C.-Z. Yao, Y. Cao, W.-L. Dai, H.-Y. He, K.-N. Fan, A highly efficient Cu/ZnO/Al2O3 catalyst via gel-coprecipitation of oxalate precursors for low-temperature steam reforming of methanol, Catalysis Letters, 102 (2005) 183-190.

Chapter 2

Hydrogen Separation: Membrane Preparation, Characterization and Testing

Abstract

In this chapter, palladium (Pd) membranes supported on porous alumina and porous stainless steel (SS) were prepared by electroless deposition using a modified contacting approach. Through this approach in addition to Pd, Pd-alloyed with silver (Ag) and Pd-Ag-gold (Au) were synthesized characterized and tested. Based on the support, intermediate sol layers of catalytic sol and yttria stabilized zirconia (YSZ) were deposited on alumina and SS, respectively. The surface structure and morphology of the prepared membranes were analyzed by field emission scanning electron microscope (FESEM) and atomic force microscopy (AFM). Extent of deposition was monitored by bubble point testing to determine the pressure that the membrane can sustain in contrast to bare support. Further, with the same methodology pin-holes on the membrane were also identified and cured with multiple deposition cycles. Lastly, hydrogen selectivity of the prepared membranes was obtained with gas permeation studies performed in an 'in-house designed' membrane separator unit using pure hydrogen and H_2/Ar mixtures.

2.1 Membranes for hydrogen separation

Separation of hydrogen using membranes mostly comprise of inorganic, organic polymers and dense ion transport membranes based on proton conducting materials. On

the basis of membrane material property, hydrogen permeation through it will vary. In addition, the criterion to choose a feasible membrane for hydrogen separation through it depends on its hydrogen selectivity, flux, stability at the operating temperature, pressures and in the presence of other mixture components. Based on these requirements, a brief comparison between the membranes used for hydrogen separation is made as shown in Table 2.1.

Polymeric membranes have low cost and provide ease of processing and high packing density. However, they cannot withstand high temperature, aggressive chemical environment and can be swollen or plasticized when exposed to hydrocarbons or CO_2 at high partial pressures [1]. This results in instant damage in material property and separation capabilities.

High thermal and chemical stability of inorganic membranes on the other hand make them a feasible choice for hydrogen separation studies [2]. Inorganic membranes include metallic, carbon and ceramic membranes broadly. Ceramic membranes are a combination of a metal with a non-metal in the form of an oxide, nitride or carbide. Ceramic include dense ceramics (perovskites) and porous (zeolites) membranes. Porous ceramics generally comprise of aluminium, titanium, zirconia or silica oxides. They are chemically inert and characterized by high permeability, thermal stability but low selectivity [3]. Chemical stability of these membranes makes them suitable for food, biotechnology and pharmaceutical applications for microfiltration and ultrafiltration within the 0.01µm to 10µm produced by slip coating procedure. Silica membranes degrade in water containing atmospheres therefore doping with TiO_2, Al_2O_3, NiO and ZrO_2 are performed to enhance

material stability. While zeolites act as natural molecular sieves but separation of hydrogen through them is still limited [4].

On the other hand, ion transport membranes are mostly dense ceramic membranes with mixed ion and electron transport capabilities. Hydrogen permeation through these membranes also follows solution diffusion mechanism. These membranes include dense ceramics-perovskite $SrCeO_{3-\delta}$, $BaCeO_{3-\delta}$ and are mostly called as proton conducting membranes (or proton exchange membranes). They operate at 600-900^{0}C and transport hydrogen as ions (protons) which make them highly hydrogen selective. However, these materials are too basic and suffer from material degradation [5].

Carbon membranes exhibit good thermal and chemical stability. They contain a pore system with wide pore openings and narrow constrictions which approaches molecular dimensions. This property of carbon membranes in contrast to silica based membranes aids in separation of gas molecules with similar size effectively. However, their brittle nature and low hydrogen permeability restricts its application for hydrogen separation studies [6].

Amongst all the above, metal membranes are of particular interest for separation of hydrogen from gas stream. Metals such as palladium, niobium, tantalum, vanadium, copper, gold, iron, cobalt and platinum are extremely hydrogen selective and thermally stable. A comparative review on the advantages and disadvantages of different membranes used for hydrogen separation are illustrated in Table 2.1. Out of these metals, palladium membranes have high hydrogen permeability over a wide temperature range which makes them an ideal candidate for H_2 separation.

Table 2.1 Membranes for hydrogen separation [1-3, 6]

S. No.	Membranes	Advantages	Dis-advantages
1	Metallic	Stable at high temperatures Long lifetime Resistant to chemicals at wide pH Strong structural integrity High flux Highly selective	Brittle at low temperatures e.g. **Pd** Not cost effective
2	Polymeric	Cost effective Efficient for mass production	Cannot sustain high temperature Short life Low selectivity
3	Ceramic	Operating temp: 200-600^{0}C Stability in H_2O vapor	Susceptible to H_2S.
4	Carbon	Operates at 500-900^{0}C Separation of non-(or weakly) absorbable gases such as H_2S, NH_3 and CFC_s.	Susceptible to organic traces or other strongly adsorbing vapors. Requires non-oxidizing environment Brittle in nature Costly
5	Ion transport membranes	$BaCe_{0.9}Y_{0.1}$ $O_{3-\alpha}$ (BCY) Operating temperature 500-900^{0}C	High hydrogen permeability and selectivity is only obtained above 600^{0}C

2.2 Palladium membranes

Palladium has a very high affinity for dissociating molecular hydrogen into its atomic state. The face centered cubic (f.c.c.) structure of palladium lattice has four octahedral

and eight tetrahedral sites. It is at these two sites in the palladium lattice that the potential energy of a hydrogen atom is at a minimum. Thus, atomic diffusion of hydrogen through bulk palladium occurs by the H-atom jumping between the nearest neighbor octahedral sites while passing through tetrahedral sites. Palladium (Pd) membranes are chemically compatible with many hydrocarbon containing gas streams and have theoretical infinite hydrogen selectivity which makes Pd a widely studied material for hydrogen separation.

Extreme solubility of hydrogen in palladium below 300°C leads to the formation of a separate palladium-hydride phase that causes embrittlement. This transition occurs from a stable α-phase (interstitial hydrogen in solid solution) to β-phase i.e. palladium hydride (Pd-H) resulting in a 10% volume expansion that cause internal stress, crystalline structure distortion and mechanical failure of the membrane [7, 8]. Therefore, phase transition restricts the operating temperature to be above 300°C for pure Pd. To overcome hydrogen embrittlement, Pd can be alloyed with Ag, Cu, Ni, Au and Y that reduces the phase transition temperature and also enhances hydrogen permeability. Palladium alloys lower the critical temperature and pressure for the phase transition by narrowing the α/β-Pd hydride miscibility gap and the difference between the sizes of the α- and β-Pd lattice constant [9, 10]. Increase in hydrogen permeability with Pd-Ag alloys is widely reported because of the increase in average bond distance of the alloys in comparison to pure Pd. Transport of hydrogen through a dense Pd or Pd-Ag membrane is characterized by solution-diffusion mechanism which follows a six step mechanism presented in Fig. 2.1:

(a) Adsorption of hydrogen molecules on the high pressure side of the membrane surface;

(b) Dissociation of the chemisorbed molecule into $H^{\bullet}$ species, consisting of a proton and an electron;

(c) Dissolution of the hydrogen atoms $H^{\bullet}$ (proton and electron) into the lattice of the metal;

(d) Diffusion of hydrogen atoms $H^{\bullet}$ (proton and electron) through the lattice from the high pressure side to the low pressure side of the membrane surface;

(e) Re-association of hydrogen atoms $H^{\bullet}$ (proton and electron) to form hydrogen molecules at the low pressure side of the membrane surface;

(f) Desorption of hydrogen from the low pressure side membrane side to the bulk.

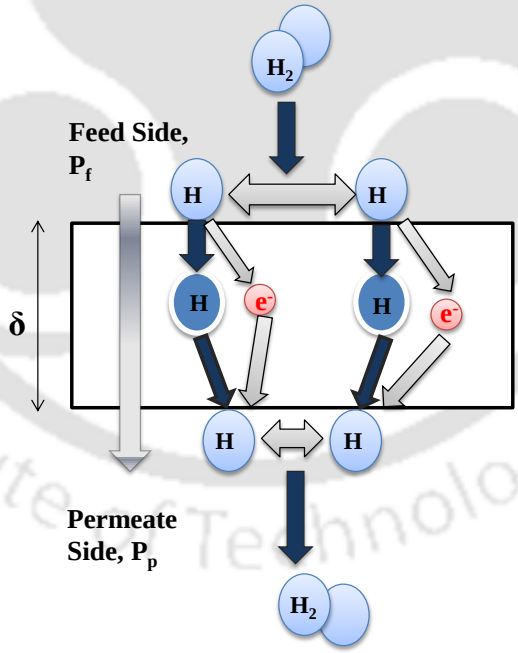

Fig. 2.1 Solution-diffusion mechanism H_2 permeation through dense Pd membranes

The individual steps in hydrogen permeation through palladium have very different kinetics which has been studied in detail by Ward and Dao [11]. The exponent (n) in

equation 2.1 varies from n=0.5 to 1 depending on the rate limiting step. If the diffusion of atomic hydrogen through the metal bulk of the membrane is rate determining step and hydrogen concentration in the Pd based lattice (H/Pd) is lower than 1, the Sieverts law should be valid for which the exponent is 0.5. For n in the range 0.5 to 1, mass transport to or from the surface and dissociative or associative adsorption becomes rate limiting.

$$\textbf{Permeability (Pe)} = \frac{j_{H_2} \times \delta}{\left(p^n_{H_{2retentate}} - p^n_{H_{2,permeate}}\right)} \quad \text{where } n = 0.5 \qquad (2.1)$$

It is mostly reported that n is in the range of 0.6 to 1 is indicative of palladium layer thinner than 5 µm. In addition, in case of thicker membranes (>5 µm) a value of n = 1 is indicative of defects or pinholes in the membrane.

2.3 Supported membranes

Palladium membranes reported in literature are either self-supported or supported. Self-supported Pd foils or membranes are extremely expensive and normally >30µm in thickness in order to remain durable. However, Pd membranes can be deposited onto asymmetric porous supports. This porous support can be utilized to prepare comparatively thinner membrane (for higher flux) and thus reduce the preparation cost. Depending on the support type and substrate to be coated, morphology or the micro-structure formed plays a key role in deciding membrane performance based on its perm selectivity, permeability and thermal stability.

2.3.1 Preparation techniques for palladium membranes

In this section, the preparation of supported palladium membranes is discussed. Supported palladium membranes are prepared by deposition of palladium or Pd-alloys on a multi-layer porous ceramic or porous stainless steel (PSS) support. Some well-known thin film deposition techniques are discussed below:

Sputtering

Sputtering is a process which results in ejection of atoms by the bombardment of a solid or liquid target by energetic particles, mostly ions [12]. The ions necessary for bombardment are extracted from argon plasma that burns between the cathode (target) and anode (substrate). Both target and substrate are planar plates arranged close to the argon plasma as shown in Fig. 2.2:

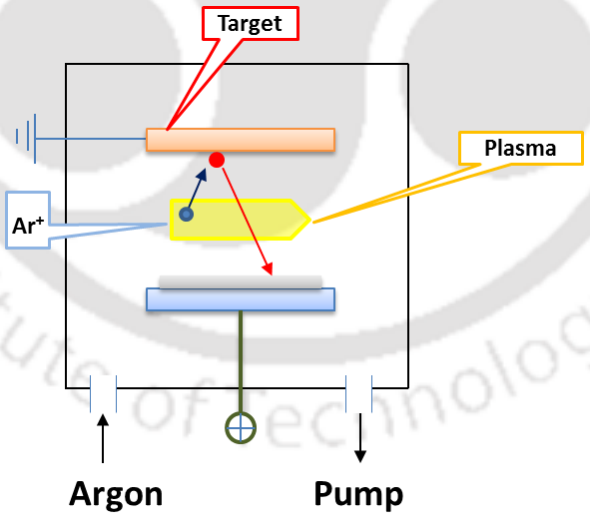

Fig. 2.2 Schematic of sputtering [13]

The high energy and positively charged argon (Ar^+) bombards the negatively charged target to liberate atoms from the target. The liberated atoms move in all directions, where

some atoms hit the substrate with large enough energy that they stick to the substrate. Therefore, the composition of the deposited atoms will be same as that of target. The advantage of sputtering is that it gives a uniform coverage of deposited material over the substrate and accuracy in controlling thickness. However, high cost of deposition set up, operating cost and poor crystallinity of sputtered layers [13] makes it un-economical on a wider scale.

Chemical vapor deposition (CVD)

CVD involves film deposition using a precursor gas or gases that flow into a chamber containing one or more heated objects to be coated. This technique requires volatile, reactive and thermally stable molecular precursors to transport and deposit growth materials in a kinetically controlled manner. Chemical reactions occur on or near the hot surface, resulting in the deposition of a thin film on the surface. Deposition using this chemical reaction results in formation of by-products that are exhausted out of the chamber along with unreacted pre-cursor gases. CVD results in uniform, conformal and high purity films [14]. However, deposition of films only occurs at elevated temperatures which imposes restrictions on the kind of substrates that can be coated [15]. Further, high temperature leads to stresses in films deposited with materials having different thermal expansion co-efficient, which can cause mechanical instabilities in the deposited films [15].

Electroplating

In electroplating, electric current reduces the desired metal cations on the substrate surface thereby causing metal deposition. This technique is used for metal coating on to a

metallic or a conducting surface by an electrochemical process. Non-conducting substrates such as ceramics as well as plastics require pre-treatment prior to be electroplated. In the electrolysis cell, the substrate being deposited acts as a cathode (negative electrode) which is immersed in an aqueous solution containing the metal to be deposited and anode is a conducting Pt electrode. When a direct electric current is passed, according to Faraday's law, deposition takes place in the following manner.

$$\textit{At Cathode} \qquad M^{2+}(aq) + ze^{-} \rightarrow M(s) \qquad (2.2)$$

$$\textit{At Anode} \qquad M(s) \rightarrow M^{2+}(aq) + ze^{-} \qquad (2.3)$$

The cation concentration, bath temperature and current density determine the deposition rate. The control over deposition rate is achieved by controlling the amount of current passed through the electroplating cell depending on the standard electrode potential of the metal. Thickness of the electroplated layer on the substrate is determined by the time duration of plating. Longer is the plating time, higher is the thickness. However, co-deposition of two metals with more than one volt difference in standard electrode potential is difficult. Further, one of the major reasons why electroplating has not been much successful so far for palladium film deposition is the evolution of hydrogen on the substrate surface.

Electroless plating (ELP)

ELP is an autocatalytic process. A chemical reaction between a reducing agent and the precursor of metal ion in the solution causes either formation of metallic phase in bulk or a thin film due to precipitation on a localized solid surface. The reduction product (metal)

then acts as a catalyst to continue metal deposition or coating of unlimited thickness in principle. In addition, no external electrical current is provided; so deposition is performed using immersion and contact plating methods. For these reasons, surface materials such as non-conductors, semi-conductors and metals are used for deposition. Rhoda; Athavale and Totlani [16, 17] reported the chemical reactions involved in ELP.

An electroless plating bath for palladium comprise $Pd(NH_3)_4Cl_2$, $PdCl_2$ as the metal ion source while silver plating comprises $AgNO_3$. Complexing agent such as ethylene di-amine tetra acetic acid (EDTA), and ammonium hydroxide are used. Hydrazine, sodium hypophosphite and trimethyl amine borane are used as reducing agents along with stabilizers and accelerators. Reducing agent affects the plating rate [18].

However, electroless plating bath is unstable in nature. Some of the characteristics related to this aspect are presented next.

- Higher hydrazine concentration increases the catalytic activity of Pd. At higher concentrations (> 3.6 mM) in case of Pd-Ag bath, Pd is favored more than Ag [18, 19]. However, at a further higher hydrazine concentration (5.4 mM), altering of Ag plating followed by decrease in pH is observed. This decrease in pH has been reported to signify a complete stop in plating thereby leading to bulk precipitation. It was reported by Rothenberger et al.[19] that during electroless plating deposition rate of palladium decreased with the depletion of palladium ions and hydrazine, leading to a decrease in pH. This led to replacing of plating solution every 90 mins.

- High Pd ion concentration (metal ion concentration) leads to decrease in plating reaction conversion. As the reaction stoichiometry between hydrazine: Pd ion

concentration should be 1:2 a very high initial Pd metal ion concentration makes hydrazine act as a limiting reagent thereby resulting in a decrease in conversion [20].

- Ammonium hydroxide is mostly used as a complexing agent, and EDTA is applied as a stabilizing agent. This is because in the absence of EDTA, the instability of the electroless bath leads to spontaneous precipitation above 70°C. Another peculiar characteristic observed in the electroless bath is the reduction of plating rate attributed to the catalytic decomposition of hydrazine by palladium. Usually electroless plating is carried out at alkaline pH (10–11). Electrons released from the reaction between hydrazine and hydroxide ions at the anode initiate the reduction of Pd^{2+} complex to Pd. The main product of this reaction is nitrogen. Ayturk et al.,[18] reported that above 60°C, excess amount of NH_4OH undergoes significant evaporation, thereby resulting in unstable electroless bath leading to easy decomposition. The change in pH causes bulk precipitation of the Pd and Ag metals in the plating solution.

2.3.2 Procedures followed in electroless plating

Cleaning

Mardilovich et al.[21] reported that thorough surface cleaning is required to provide a clean and an optimum rough surface structure for high adhesion in metal to metal bonds. It mostly comprises of mechanical cleaning with abrasion (sand paper, stainless steel brush, file etc) and chemical cleaning using ammonia solution, isopropanol, sodium hydroxide, sodium bicarbonate, di-sodium phosphate, hydrochloric acid, organic detergent, ethanol at 60°C. Mardilovich et al.[21] showed that initial polishing of the PSS sample of 0.5 μm grade showed large number of pores in the size range 20–30 μm on the

surface. These large pores remained only at the entrance which continued to become narrower below the surface (< 8 μm). Mechanical treatment (sandpaper, file) reduced the porosity of support making the treated surface almost impermeable. Cleaning with alkaline solution not only removes any dirt or grease on the surface of the support but also increases the permeability. HCl treatment should be short term such that it does not affect the pore size.

Activation

This is performed either with a combination of $SnCl_2/PdCl_2$ or palladium acetate in chloroform repeated cycles until dark-brown. Chemical activation with $SnCl_2$ leads to formation of tin hydroxyl chlorides on the PSS surface whose composition, structure and thickness is highly dependent on $HCl/SnCl_2$, support surface structure, roughness etc [21]. An excess of Sn^{2+} leads to loose crumbly easy to peel layer, while deficiency can cause non-uniform seeding of Pd nuclei. Mardilovich et al. [21] reported an activation solution containing Sn 1 g/L with 37% HCl 1 ml/L and Pd 0.1 g/L with 37% HCl 1 ml/L at 20°C for 5 min each cycle.

Deposition

Once activation of support is complete with Pd nucleation on the surface turning it shiny brown, deposition is then carried out by immersing the support in electroless bath with intermittent addition of hydrazine at a controlled rate. In addition, a controlled rotation of the support to ensure uniform deposition of Pd on the PSS tube is also reported [18, 21, 22]. Rate of Pd deposition was measured based on $2Pd/N_2$ (based on reaction 2.4). The quantity deposited can be measured by the gas flow measurement and integration of this

data, simultaneous weighing of support before and after the deposition and finally SEM analysis can be performed as well.

$$2Pd^{2+} + H_2NNH_2 + 4OH^- \rightarrow 2Pd^0 + N_2 + 4H_2O \quad (2.4)$$

2.4 Literature review on preparation of Pd-based composite membranes

Fabrication of metal composite dense alloys has been widely studied to separate hydrogen from the reformate gas mixtures [23-27]. The high selectivity and high temperature resistance of Pd and Pd/Ag alloys always makes them a preferred material choice. Likewise, easy deposition on any conducting or non-conducting material with uniform or non-uniform surface gives electroless plating (ELP) an edge over the other less cost-effective methods. In conventional ELP, reducing agent and Pd-containing electroless bath are mixed together and used for deposition on supports. However, this instant mixing results in bulk Pd precipitation in bath. Further, deposits using ELP are mostly columnlike and with defects. The occurrence of these defects immensely lowers hydrogen selectivity of these membranes. These defects are more evident when thickness of membranes is low. Therefore, significant research is focused on making Pd films using ELP denser and thinner while still maintaining high hydrogen selectivity. Numerous works have illustrated Pd deposition on wide variety of supports which include tantalum and niobium (Buxbaum and Marker, [28], Buxbaum and Kinney, [28]), porous glass (Uemiya et al. [29, 30]), alumina (Kikuchi and Uemiya [22], Lim and Oyama, [31], Kim et al. [32] and Zeng et al.[33]) and porous stainless steel (Shu et al. [34], Mardilovich et al. [21], Dittmeyer et al. [26], Huang and Dittmeyer [35, 36], Ayturk and Ma [18], Guazzone and Ma [28], Guazzone et al. [37, 38] etc.). Many authors have also reported

effect of modified activation, effect of inter-diffusion barriers in case of PSS, effect of different annealing temperatures and effect of modified ELP plating techniques such as simultaneous electroless plating, sequential electroless plating and pore plating [20, 39-41]. In the present work, two kinds of support material have been investigated: a) porous alumina and b) porous SS. Table 2.2 provides the literature review on palladium based membrane preparation studies reported.

Mardilovich et al. [21] reported dense palladium membranes of 20 μm thickness supported on PSS using electroless deposition. For uniform deposition of Pd on PSS tube, a controlled rotation for the support was maintained, while the flow of gases evolved from the reaction (equation III) was measured by a soap bubble meter. A total of 9 plating cycles were reported in order to reach surface densification.

Kitiwan et al. [42] studied the influence of porosity of α-alumina support on Pd deposition. Deposition morphology was investigated at four different sintering temperatures: 1200, 1300, 1400 and 1500°C. Pore size of support varied from 0.25–0.35μm. It was reported that higher temperature gave a larger and smoother grain while a lower temperature exhibits bimodal grain size structure. Selectivity was found to be poorer for more porous support but could be improved with higher plating time.

Okajaki et al. [43] reported membrane preparation with vacuum ELP and simultaneous deposition on α-alumina support. Alloying of Pd with Ag was performed at temperatures higher than 230°C. The alloy progressed effectively at temperature 550 to 600°C with sharp XRD peaks. Temperature higher than 600°C caused formation of a lesser hydrogen

permeable alloy of Pd-Al. Maximum permeability was observed at 550°C with 0.8 mol/m^2s.

Tanaka et al. [44] too suggested 500°C (thermal treatment) for alloy formation in order to minimize defects. It was suggested that in simultaneous deposition, Ag is preferentially deposited on Pd seed nuclei and therefore shields active Pd particle and prohibits plating reaction. Therefore control of deposition rate with proper Pd/Ag ratio is important. Annealing was optimized at 500°C under hydrogen stream for 4 h, and precipitation in the plating solution was stabilized using ammonia and EDTA, which control the deposition rates of individual metals by modifying the redox potentials.

Tanaka et al. [45] reported yttria stabilized zirconia (YSZ) mixed sol in 8–20 nm size range as an intermediate layer deposition on to ϒ-alumina support under vacuum suction. Coating this layer was followed by seeding, and additional sol layer and finally Pd coating. Though no significant defect was observed, it was reported that the effective area occupied by Pd became narrower by the co-presence of YSZ-gamma alumina that hindered H_2 permeation.

In addition to this, application of ceramic (20%YSZ-80%alumina) based interdiffusion barriers were also investigated recently by Fernandez et al. [46] prior to Pd-Ag deposition on porous hastelloy. The deposition of 2–5 layers of YSZ-alumina was carried out using atmospheric plasma spraying (APS) and dip coating. The resulting thickness of the layer after sintering and reduction was reported 40 μm. Pd-Ag deposition of 3–5μm thickness was further carried out with simultaneous deposition.

Further, Straczewski et al. [47] reported comparison of YSZ coating using APS and TiO_2 coating using wet powder spraying (WPS) prior to Pd deposition on to PSS. Nearly 80–100 μm thick YSZ layer was coated while poor adhesion in case TiO_2 was reported. It was clearly reported that completely defect free membranes were not observed for all tubes prepared. Rust formation, especially visible after palladium coating, has been reported to induce large defects. In addition, variation in the alloy composition at the weld seams that includes porous tube, dense adapter and additional weld material could induce the formation of a contact material that causes preferential corrosion in SS 310. The final thickness of Pd membrane was reported 14.4–25μm with H_2/N_2 selectivity in the range of 60–120.

From the above studies, it is becomes clear that deposition of palladium on to both ceramic and SS still remains a challenge. Moreover, the pore size distribution of both supports is distinctly diverse. This variation in pore sizes eventually plays a crucial role in surface densification of palladium deposited. Difference in membrane deposition between porous SS and porous ceramic to achieve faster densification is therefore crucial to determine maximum hydrogen flux. This comparative information is not available in literature, especially with regards to how palladium consumption for dense membrane synthesis can be decreased by change of support porosity. Decrease in palladium consumption will drastically reduce the membrane preparation cost and lower thickness on the other hand will improve hydrogen flux as well. These parameters are therefore critical for palladium membrane synthesis.

Table 2.2 Literature review on preparation of Pd-based composite membranes

S. No.	Author	Support	Intermetallic alloy	Preparation Method and Details	T and pH	δ (μm)	H_2 Flux mol/m^2 s	N_2 Flux
1	Mardilovich et al.[21]	**PSS** 316L cups and tubes (Mott) 0.5 μm O.d.15.9 mm, 12.7 mm Thickness 1.6 mm , L=19–25 mm	-nil-	ELP Ultrasonic clean in alkaline solution Activation: acidified $SnCl_2$ and $PdCl_2$ Deposition: $Pd(NH_3)_4Cl_2.H_2O$: 4 g/L NH_4OH:198 ml/L, Na_2EDTA 40.1 g/L N_2H_4 5.6–7.6 ml/L	60°C at 10.4 pH	19–28	2 to 4 $m^3/m^2.h$ @ 350 and 500°C	0.008 $m^3/m^2.h$
2	Hollen et al. [48]	**α-alumina** pore size 100 nm, PSS <500 nm O.d. 10 mm and I.d 6 mm	Ceramic layer with slip coating and metal wet powder spaying	ELP $PdCl_2$ 5 g/L $Na_2EDTA.2H_2O$ 70 g/L NH_4OH 500 ml/L N_2H_4 10 ml/L	60°C at 10.4 pH	15	0. 3	0.01 cm^3/cm^2 min
3	Huang and Dittmeyer et al.[49]	**PSS** O.d. 10 mm, I.d.6 mm L=11 cm	Ceramic (ZrO_2YSZ) and TiO_2 by atmospheric plasma spray, magnetron sputter and wet powder spray	ELP Clean in NH_3H_2O, water and isopropanol Activation:$SnCl_2$.$PdCl_2$ $PdCl_2$5 g/L, $Na_2EDTA.2H_2O$ 70 g/L; NH_4OH 250 ml/L N_2H_4 1 ml/L (in breaks) 200 rpm	60°C at 10.4 pH	7–12	11 $m^3/m^2.h$@ 500°C	0.06 $m^3/m^2.h$
4	Ayturk and Ma, [18]	**PSS** 0.5μm, O.d. 1.27cm, L=2.54 cm and porous Inconel (MOTT) 0.1 μm,	Oxidized @ 600–800°C for 12h	ELP Activation $SnCl_2/PdCl_2$ Deposition $Pd(NH_3)_4Cl_2$ 2–4 g/L	20–60°C @10 –11	17–20	-NA-	Instead of N_2 helium was used. An increase

		O.d.1.27 cm, L=6.35 cm		$AgNO_3$ 0.5–2.1 g/L $Na_2EDTA.2H_2O$ 40 g/L NH_4OH 198 ml/L N_2H_4 2.5–7.5 ml/L @ 400 rpm	pH			in Helium rate was reported with increasing with temp.
5	Lim and Oyama, [50]	**α-alumina** (Pall corp.) 5 nm pore size, O.d. 10 mm, I.d. 7 mm, L=24 cm	Boehmite sols of diff. particle sizes	ELP Activation: dip coating in Pd acetate (0.05M) Deposition $Pd(NH_3)_4Cl_2.H_2O$: 4 g/L NH_4OH:198 ml/L, Na_2EDTA 40.1 g/L N_2H_4 5.6- 6 ml/L	60°C @10 –11 pH	10	0.6	-NA-
6	Guazzone et al. [38]	The composite Pd membranes were prepared on porous stainless steel (**PSS**) supports 1"OD, 10" long 200 cm^2 permeable surface area	Gamma alumina with Pd cemented	Pd/Au/Pt Pd ELP coating Au electrocoated at 60°C and Δ V 0.55V and current density 0.! 3mA/cm^2 All membranes were protected with a special oxide coating to avoid scratches on the membrane surface during the mounting (oxide coating did not affect H_2 permeance)	450° C H_2 perm eatio n testin g 12.6 bar	8–13	26.6 to 16.3 $m^3/m^2.h$	0.5–<0.1 ml/min bar at 25°C minimum leak. after testing 99.89% during 200 h
7	Kim et al. [32]	500µm Cu(II)O/**Al_2O_3** catalyst film washcoated on top of 27 µm ELP coated Pd	PSS substrate 0.5 µm grade OD 0.5 in., porous length 2 in.	Oxidation at 673 K for 4 h using a heating and cooling rate of 3 K min^{-1}. The oxidation step is intended to grow a native surface oxide on the cleaned PSS tube	623–773K	27 µm Pd and 500 µm catalyst	0.025	0.015

8	Zeng et al. [33]	Pd/Ag plating on **porous alumina** supports was investigated The inner and outer diameters and the length of the tubes are 7, 10 and 35 mm	activated by dipping into a aqueous Pd solution containing 10 mmol/L PdSO4 and 1 mmol/L Na2EDTA, reduced with hydrazine	The final bath contained 75 mL solution of 3.1 mmol/L PdCl2, 1.0 mmol/L AgNO3, 5 mol/L NH4OH, 0.12 mol/L Na2EDTA, and 6 mmol/L N2H4 E_a = 5.5 kJ/mol		1.5 to 2.6µm	0.8	0.41×10^{-3}
9	Pujari et al. [51]	Effect of Ni inter diffusion barrier on palladium densification on **PSS** supports of 0.1 µm pore size	PSS circular discs (dia of 36 mm and thickness of 1 mm) 0.1 µm and 0.5 µm	ELP PdCl2 0.886 g/l CTAB 2CMC	60°C at pH 11	2.52-8.88 µm for Pd/PSS 3.14 to 11.16 µm to Pd/Ni/PSS	-NA-	Ni negatively affects the palladium densification; Ni was plated electrolessly Novel identified surfactant CTAB
10	Mardilovich et al. [52]	Porous stainless steel (**PSS**) tubular supports with an outer diameter of 0.025 m and a length of 0.254 m. The total porous surface area of the	Activated Al_2O_3 particles were used to grade the previously oxidized supports and were cemented	Pd plating with standard ELP Gold and Platinum were deposited by electro-deposition followed by alloying in situ H_2/helium selectivity >2500	450° C	8–15µm	0.093	9.6µm thick Pd membrane decrease up to 87% Pd/Au 99% Pd/Pt/Pd remained

		membrane was 200 cm^2.	with Pd				98% Pd/Au/Pt 10099.91% for 700h
11	Chi et al. [53]	Effect of rotating 0-200 rpm PSS support on Pd deposition -alumina particle with lithium aluminide ingot was used to produce a hydroxide intermetallic layer	PSS 0.3 µm, 1 mm o.d., 150 mm length and 0.89 mm thickness	$PdCl_2$ 4g/L Nh_4OH 200ml/L N_2H_4 0.5–4ml/L Naa_2EDTA 40g/L pH 10–11 Temperature 60°C Increased rotation increased the deposition thickness of the membrane	350–450° C and 1–4 bar	5µm	137.5 $m^3/m^2.h$	<0.01m^3/m^2.h Pin holes and other defects were reported even after deposition of 240 min; with 200 rpm it gets minimized
12	Kim et al. [54]	Nano scale layers of Pd were deposited with advanced sputtering under high vacuum	Porous nickel support	Successive in-situ DC magnetron sputtering, Au metal was used for alloying and surface densification as well as to increase the resistance against poisoning by hydrogen sulfide and sulfurous constituents E_a = 12–14.9 kJ/mol	723K	5 to 5.5	2	Voids exists with sputtering -N_2 flux not mentioned Selectivity up to 5000 was reported

δ here represents thickness of metallic layer and T is temperature

2.5 Experimental Methods

2.5.1 Techniques used for support characterization

BET (Brunauer Emmett Teller) Technique

Gas adsorbs on the external and internal surfaces of a porous material in equilibrium at temperature (T) and relative vapor pressure p/p_0. The relation between relative vapor pressure and amount of adsorbed gas (N_2) at a constant temperature (77 K) is called an adsorption isotherm. N_2 Adsorption isotherms of porous materials can be used for the determination of specific surface area by BET theory. The basic equation for calculation of specific surface area from adsorption data is given in equation 2.5

$$S = \frac{X_m}{M}.N.A_m \qquad (2.5)$$

Here X_m is the mass of adsorbate forming a monolayer on unit mass of adsorbent, M is the molecular weight of adsorbate, A_m is the area occupied by one adsorbate molecule in the monolayer and N is the Avogadro's number [55]. In order to determine X_m, Brunauer, Emmett and Teller based their theory on the following assumption to derive equation 2.6 mostly referred to as the BET equation. The assumptions are: a) gas molecules physically adsorb in infinite layers on the solid, b) there is no interaction between molecules in different sites, c) heat of adsorption and condensation in all layers above the first are equal to those of bulk and d) condensation constant = evaporation constant (at dynamic equilibrium). On this basis, BET equation as mentioned in 2.6 was derived [56]. The linear relationship of this equation is maintained only in the range of $0.05 < P/P_0 < 0.35$.

$$\frac{1}{v\left[\left(\frac{P_0}{P}\right)-1\right]} = \frac{c-1}{v_m c}\left(\frac{P}{P_0}\right) + \frac{1}{v_m c} \qquad (2.6)$$

BJH (Barrett-Joyner-Halenda) Method [57]

In addition, since the gas is used below its critical point, pore size distribution is analyzed by capillary condensation as a function of the relative pressure of the adsorptive. Capillary/pore condensation represents a phenomenon whereby gas condenses to a liquid like phase in pores at a pressure less than saturation pressure of bulk fluid. Since decrease of saturated vapor pressure takes place over the concave meniscus, it is described by Kelvin equation (equation 2.7).

$$\ln\frac{P}{P_0} = \frac{-2\gamma V_{liq}\cos\theta}{rRT} \qquad (2.7)$$

Here, P = actual vapour pressure (bar),

P_0 = saturated vapour pressure (bar),

γ = surface tension (J/m^2),

r = radius of curvature of the adsorptive condensed in the pore (m),

V_{liq} = molar gas volume of an ideal gas (m^3/mol),

θ = contact angle,

R = ideal gas constant (J/molK),

T = temperature (K),

Surface area and pore size distribution of both porous alumina as well as porous SS was evaluated using Quanta chrome Autosorb iQ automated gas sorption analyzer at the temperature of liquid nitrogen (77 K) and degassing temperature of 200°C. Samples for BET analysis were pieces of porous ceramic and porous SS cut into smaller dimensions such that it can fit the BET tubes for testing.

Field Emission Scanning Electron Microscopy (FESEM)

FESEM scans the surface of a sample by raster scanning over it with a high energy beam of electrons. The electrons generated from an electron gun enter the sample surface to release many low energy secondary electrons. The intensity of these secondary electrons is governed by the surface topography of the sample. Therefore, an image is constructed by measuring secondary electron intensity as a function of position of the scanning primary electron beam. Further, in addition to FESEM, energy dispersive X-ray spectroscopy (EDX) is also a simple and powerful tool to determine elemental composition of a material. The technique is non-destructive wherein the electron beam excites the atoms in the sample that subsequently produce X-rays to discharge the excess energy. The energy of X-ray is characteristic of the atoms that produced it thereby forming peaks in the spectrum.

Unmodified supports as well as Pd-deposited supports were analyzed using FESEM-EDX (ZEISS-FESEM Sigma). Samples were sputter coated with gold and then analyzed under high vacuum at varying magnifications. Further, for this analysis planar surface of porous SS (disks) and ceramic (squares) were purchased. Planar surface enhances the image

focus of the samples used for analysis. Further, the composition and surface morphology of these planar supports are identical to the tubes used for membrane preparation.

Atomic Force Microscopy (AFM)

AFM is a kind of scanning probe technique which essentially uses touch to image a surface unlike light or electron microscope. It relies on the force between the tip and sample where force is not measured directly but calculated by measuring the deflection of the lever, knowing the stiffness of the cantilever by Hooke's law as stated in equation 2.8:

$$F = -kz \tag{2.8}$$

Where, F is the force, k is the stiffness of the lever, and z is the distance lever is bent.

Planar samples with thin deposited intermediate layers and Pd were analyzed using AFM (Agilent, Model 5500 series). Measurements were performed in air, operating in non-tapping mode with silicon cantilevers (nominal radius of 10 nm). From the AFM images, the surface roughness was obtained by using the software WSxM 5.0.

Water Bubble Point Testing

Bubble point is a test designed to determine a pressure at which continuous stream of bubbles are visible from a wetted porous material under gas pressure. The pressure at which steady stream of bubbles are noticed is called bubble point. This study was used to determine average pore size of the membrane support, pore size distribution and most importantly to identify the defects in palladium-deposited tubes. The methodology was adapted from Jakobs and Koros, 1997 [58]. Water held inside pores by capillary forces

can be expelled by increasing the pressure difference. For a pore with radius r (μm), this pressure difference is given by the Laplace equation:

$$\Delta P = 2 \text{ x } \sigma \text{ x } H \tag{2.9}$$

where σ is the interfacial tension (N/m) of the fluid-fluid system and H is the mean curvature of the meniscus. The radius of the meniscus relates to the pore radius (r) via the contact angle φ of the fluid-fluid-membrane system by the following equation

$$\Delta P = \frac{(2 \times \sigma \times \cos \varphi)}{r} \tag{2.10}$$

Atomic Absorbance Spectroscopy (AAS)

AAS was used for measurement of concentration of Pd metal in plating solutions. AAS was carried out by using Varian Atomic Absorption Spectroscopy equipped with air-acetylene burner. Standard calibration curve was generated, using 5, 10, 15, 20, 25, 35 and 40 ppm solutions of palladium chloride, to determine the concentration of palladium in plating solution before and after plating. The corresponding calibration curve is shown in Appendix A. The total loading of palladium was calculated based on the difference between initial and final concentration.

2.5.2 Technique used for membrane deposition

Support for Membrane Deposition

Porous alumina and porous SS (PSS) tubes were used as support in this study to deposit palladium membranes on them. Porous alumina tubes were purchased from Kumar Ceramics, Orissa-India while porous SS tubes were purchased from Applied Porous,

USA. The porous alumina tubes had 10% porosity with 80 mm length and 10 mm outer diameter. On the other hand, porous SS tubes (Material SS-316) of 0.2 microns, 150 mm length and 6.35 mm outer diameter were used.

Cleaning

Prior to sol treatment, activation and deposition, all tubes were cleaned in alkaline solution in ultra-sonication for 1 h washed in de-ionized water or isopropyl alcohol and dried. Chemicals used for the porous alumina and PSS are detailed in Table 2.3

Table 2.3 Chemical composition for cleaning of supports [18, 59]

	Chemicals	**Porous alumina**	**Porous SS (PSS)**
Alkaline bath	Sodium phosphate	45 g/L	45 g/L
	Sodium carbonate	65 g/L	65 g/L
	Sodium hydroxide	45 g/L	45 g/L
	Detergent	5 mL	5 mL
Acidic bath	HCl	0.1M	-NA-
Neutral bath	Isopropyl alcohol (91%)	-NA-	yes

Intermediate Sol Layer

In order to minimize the surface roughness of the support and membrane thickness, a thin intermediate layer between the support and membrane can be applied. On the basis of the reported literature [20, 36, 45] as also stated in section 2.3.2, intermediate layers for porous alumina and SS tubes were synthesized respectively. Studies have illustrated the

effect gamma alumina based intermediate layers on the dense membrane synthesis and its stability [18, 60]. Recent studies have also highlighted the importance of thin and uniform activation layer deposition with the use of sophisticated tools such as sputtering and atmospheric plasma spraying [61, 62]. The large columnar micro structure reported with sputtering based techniques and cauliflower like morphology mostly reported for electrolessly plated palladium membranes tend to form micro-pores upon heat treatment. In comparison to these methods, dip coating provides easy applicability for metal deposition on any support and is feasible for economical scale up point of view. Therefore, in this regard, catalytic materials such as supported Pd/Ag on alumina for sol preparation were synthesized that can be effectively utilized to achieve thinner and uniformly deposited palladium membranes. Alumina, being the same material as ceramic substrate will bind to it easily. In addition, finely dispersed palladium-silver catalyst on alumina allows the surface characteristic to not only provide a uniform base but be catalytically active as well. In addition to catalytic sol for alumina supports, yttia stabilized zirconia (YSZ) for porous SS supports were synthesized as per reported literature [63]. YSZ minimizes the intermetallic diffusion between Pd and SS because of thermal expansion co-efficient between Pd and SS [9, 64]. Therefore, YSZ minimizes the inter-metallic diffusion between Pd and SS when operated in higher temperatures.

For catalytic sol synthesis, Pd-Ag on powdered alumina catalysts was synthesized by electroless plating process. The alumina used for catalyst synthesis was prepared by co-precipitation method. 20 wt% of catalyst was peptized in HNO_3 for 6–7 h prior to sol preparation, filtered and dried. 5 g poly vinyl alcohol (PVA) solution in water was further added in synthesized reduced palladium catalysts to prepare catalytic sol. The sol was

further deposited onto porous alumina using dip coating. Clean alumina tube was introduced into the sol for 30 s and then withdrawn at a controlled rate of 2–3 cm/min. According to dip coating theory, the withdrawal velocity affects the thickness of coating and thereby plays a key role in this process. The sol-coated tube was then dried overnight at 90°C and further calcined at 300°C. The deposited sol morphology as well as cross-section was observed with FESEM. For porous SS, YSZ sol was synthesized to deposit as an intermediate layer. In this case, yttria-stabilized zirconia (YSZ) was first synthesized by citric acid reduction method using yttrium nitrate and zirconyl nitrate as precursors. Addition of citric acid to the salt solution of mixed yttrium and zirconyl nitrate leads to generation of a colloidal solution that was stirred for 3–4 h. The sol was then evaporated until a white yellowish powder appears. The prepared YSZ powder was then crushed for several hours in a mortar pestle until a fine powder of YSZ is achieved. In order to prepare the sol, 0.5% dispersant (tri-sodium citrate) and 5% PVA was added to prepare a sol. With vacuum assisted dip coating, a fine layer of YSZ was deposited on porous SS tubes followed by room temperature drying overnight and then sintering at 800°C.

Activation

The standard $SnCl_2$-$PdCl_2$ activation method was applied on porous alumina tubes [18, 21, 22, 52]. Both $SnCl_2$ and $PdCl_2$ are prepared with 3-4 drops of HCl in water. This is because $PdCl_2$ only dissolves in acidic water. Further, $SnCl_2$ is not stable in water as it gets hydrolyzed to form a colloidal basic salt. Hence, in order to obtain a clean Tin (II) chloride ($SnCl_2$) solution, acidic water is essential. In this method, a cycle is followed by dipping porous alumina in acidic $SnCl_2$ (5 mins), distilled water (1 min), acidic $PdCl_2$ (5

mins) and 0.01 M HCl (1 min) [60]. This cycle was continued until was surface displayed uniform brown Pd seeds on the entire surface of alumina.

In case of porous SS, Pd (II) acetate activation was performed. This is because $PdCl_2$ was observed to corrode SS immensely. Further, corrosion pits on PSS formed also hindered membrane deposition as it reoccurs even after tedious cleaning. Oxalic acid (1M) was observed the best in cleaning corrosion completely from the surface. Oxalic acid solution dissolves the rust in it which shows changes the transparent solution to green. Oxalic acid is an iron complexing agent that once in contact with a surface having rust form a ferrioxalate ion which is soluble in hot water. In Pd (II) acetate activation method, Pd (II)-acetate (0.1 g/L) dissolved in chloroform (Pd-acetate solution) was used [42, 65, 66]. In this case, PSS substrate was dipped in Pd (II) acetate solution for 10 mins followed by dipping in 1 mol/L hydrazine in aqueous ammonia. This was followed by dipping the substrate in 0.2 mol/L NaOH for 10 minutes rinsed in water and dried at 110°C. Further, Pd (II) acetate activation and hydrazine reduction with vacuum was also performed to make sure that uniform and in-depth activation was obtained.

Modified Electroless Deposition

In the present work, dense Pd membranes on porous alumina as well as porous stainless steel (PSS) were prepared using modified electroless plating process. The standard $SnCl_2$-$PdCl_2$ activation method [18, 42, 45, 54, 60, 62] was applied on alumina to pre-nucleate the tubes with palladium. On the other hand, porous SS tubes were activated using Pd-acetate in order to avoid corrosion of SS tubes due to $PdCl_2$. The method as described above was followed as reported in literature [42, 65, 66].

Deposition of palladium on pre-activated porous alumina and PSS tube was performed using hydrazine by a modified contacting pattern devised in-house. Instead of hydrazine bulk addition to the plating bath in conventional plating, both substrates were soaked in dilute hydrazine of 10 mM concentration outside the bath and then subjected to plating under continuous vacuum until no further bubbles were observed. The composition, temperature and pH of the plating bath maintained during the process are listed in Table 2.4. Thus, the complete methodology for the deposition of palladium on supports (porous alumina as well as porous SS) followed was as mentioned in the schematic below Fig. 2.3.

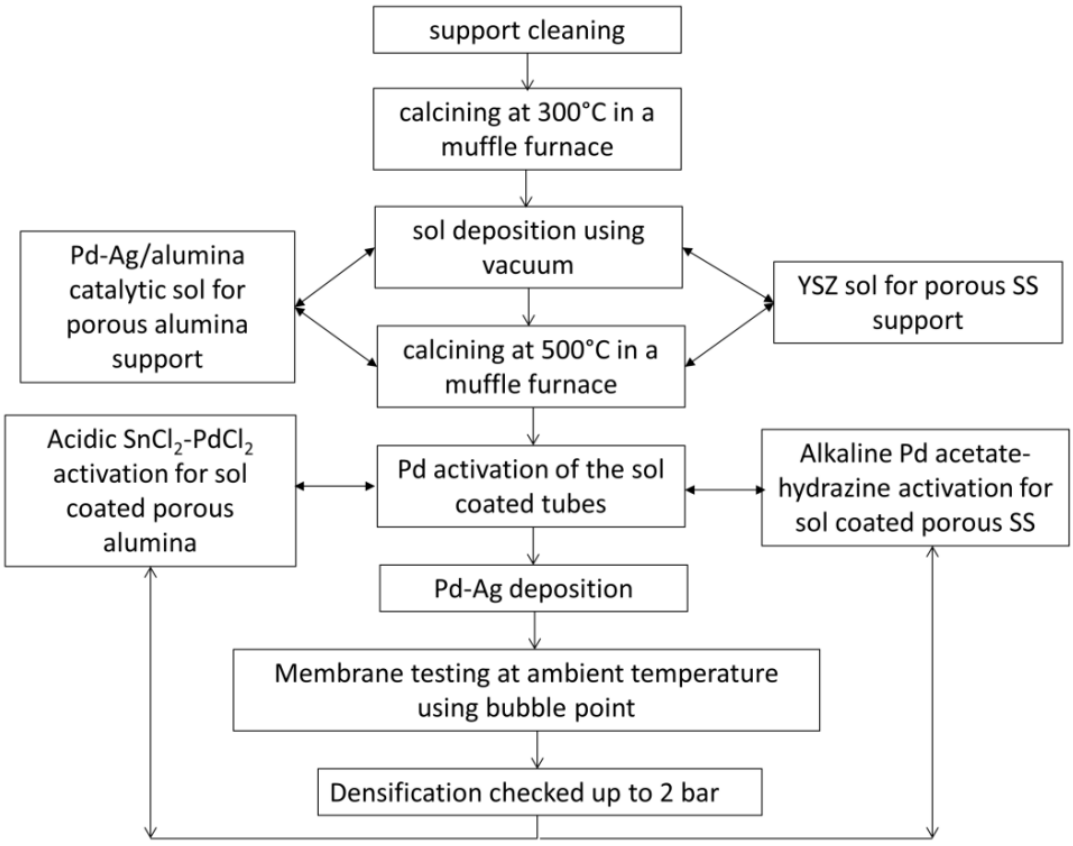

Fig. 2.3 Schematic of Pd-Ag membrane deposition steps for porous alumina and porous SS

The coating thickness was calculated gravimetrically using the known density of palladium (~12 g/cm^3). Characterization of tubular structures using FESEM and AFM causes problems in image focusing. Hence, square plates of alumina tube and porous SS disks with same composition as that of tubes were used for effective characterization simultaneously at each preparatory step.

Table 2.4 Plating bath composition

Plating bath components/conditions	Amount/Value
$PdCl_2$ (g/L)	4
NH_4OH (28 wt. %) (ml/L)	200
Na_2 EDTA (g/L)	70
N_2H_4 (0.37 M) (ml/L)	5.6
Temperature (°C)	60
pH	10

2.6 Results and discussion

2.6.1 Support characterization and testing

The pictorial description and complete surface morphology of porous alumina and SS is presented in Fig. 2.4a and 2.4b respectively. In case of porous alumina tube, the porous section was connected to dense (non-porous) ceramic using glass enamel at both ends and heat treated at 1000°C. Slow heating and cooling was followed in this step to achieve crack free enamel coating on to the ceramic. Further, multiple coatings were applied until a leak free joint was observed using water bubble point testing. For SS, the porous

section is welded to the non-porous end by diffusion bonding by the makers. The non-porous end consists of a metal nut with ferrule bonded to it.

FESEM images in Fig. 2.4a show that the alumina substrate surface was extremely rough with large voids distributed unevenly. Similar non-uniformities on surface morphology of the SS were also found in Fig. 2.4b. FESEM image analysis was performed using ImageJ software to determine the pore size distribution of both supports. Fig. 2.4c shows that alumina has much narrower pore size distribution than SS. This indicates that the amount of Pd required to have a dense membrane supported on SS would be much higher than that needed for alumina.

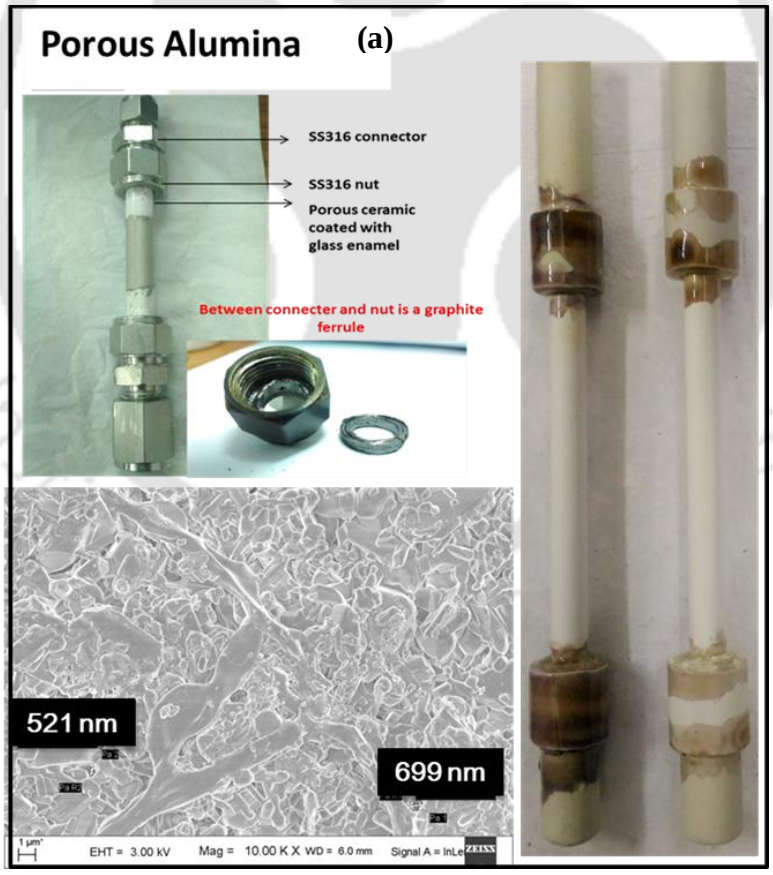

Fig. 2.4a Support assembly FESEM images of porous alumina

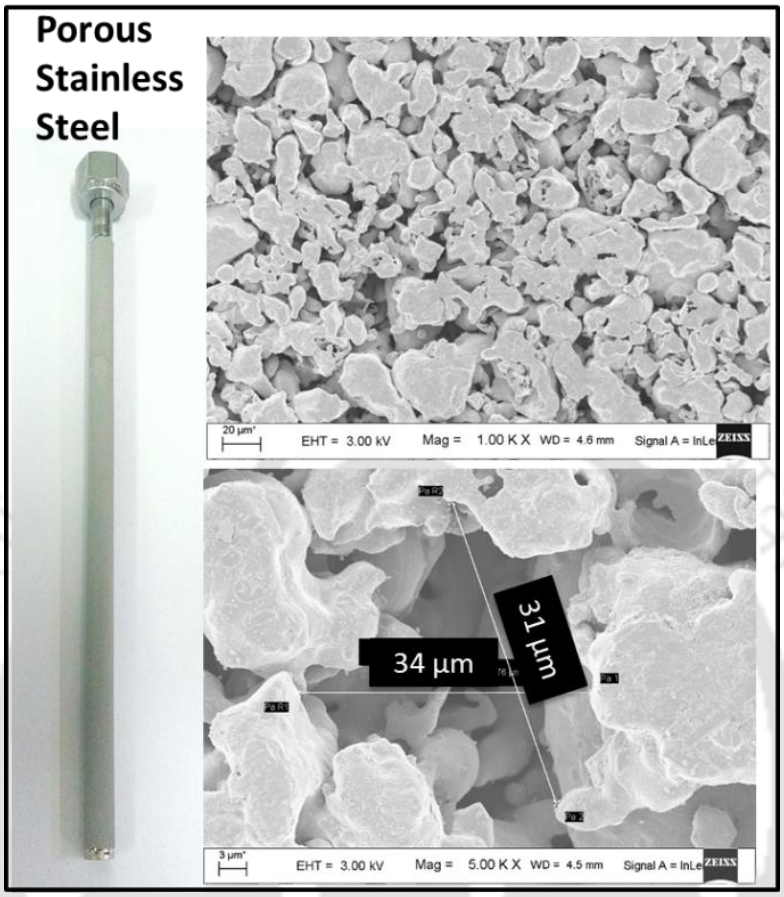

Fig. 2.4b Support assembly FESEM images of porous SS

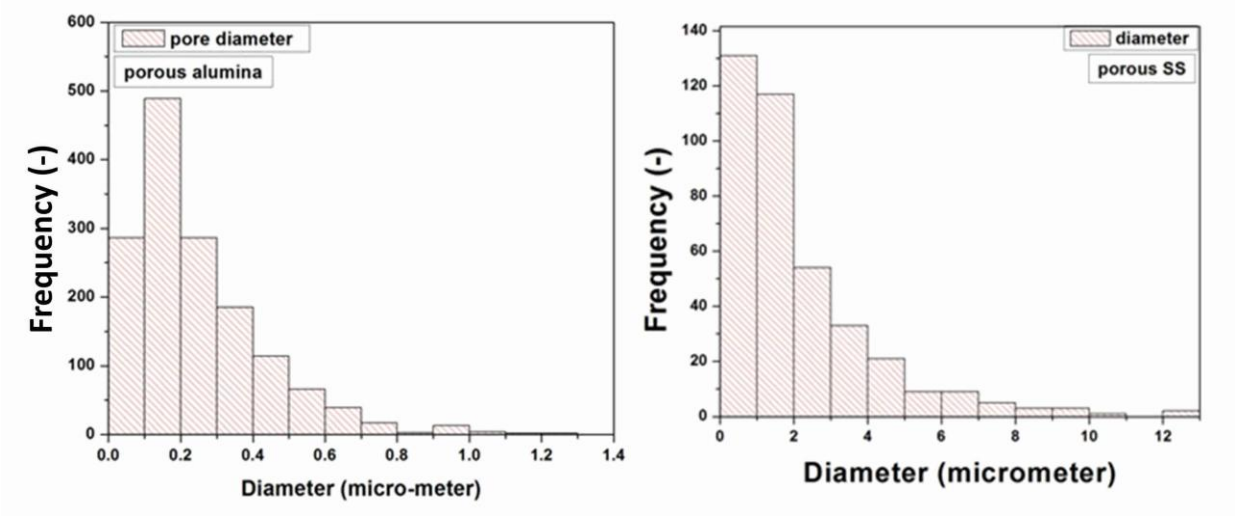

Fig. 2.4c Pore size distribution of porous alumina and porous SS

Further, elemental distribution of porous alumina and SS from EDX analysis in Fig. 2.5a and Fig. 2.5b is presented. The compositions observed matches the standard elemental distribution mostly reported for alumina and SS 316 [67-69].

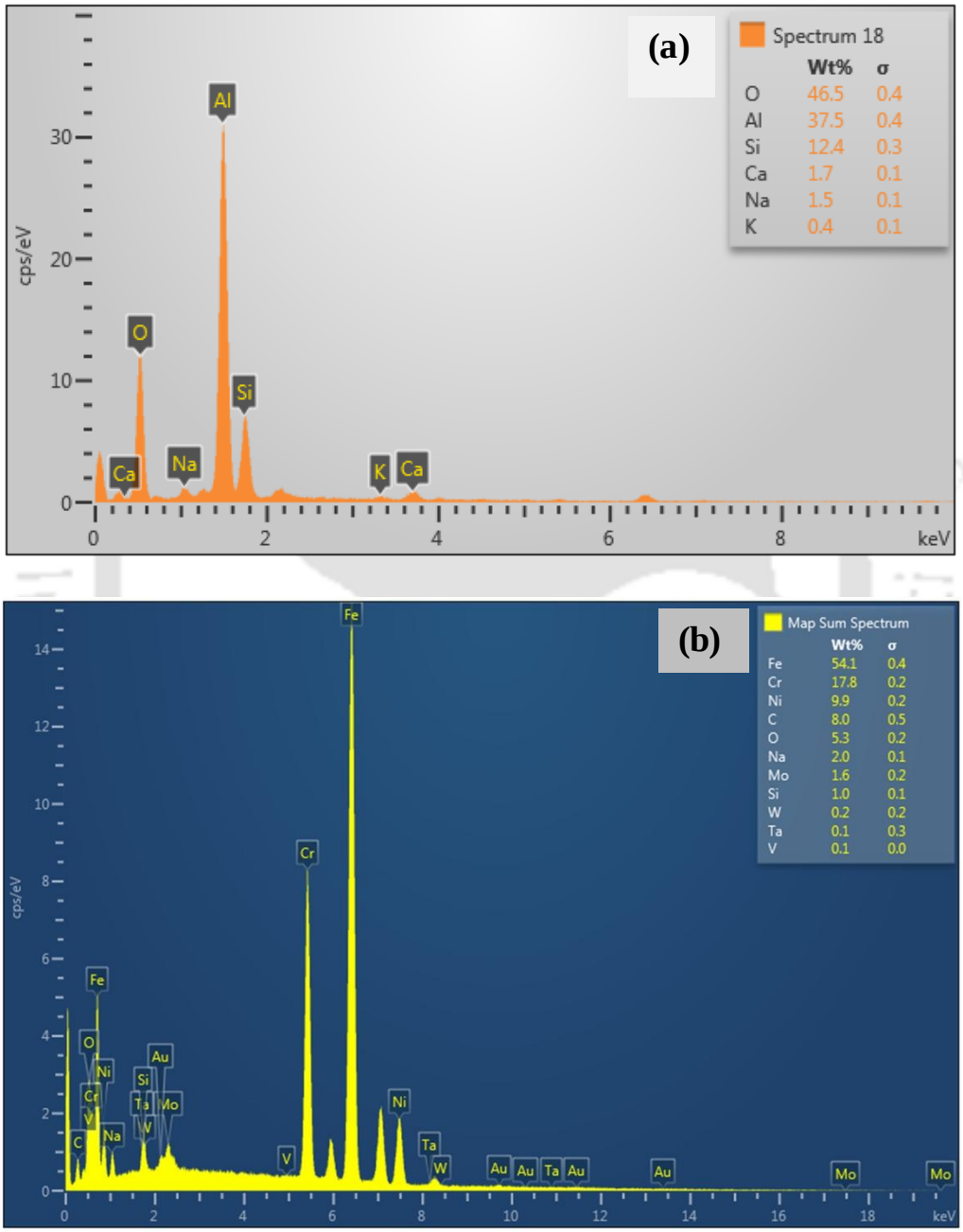

Fig. 2.5 Elemental distribution of porous alumina and SS from EDX analysis a) porous alumina and b) porous SS

Bubble Point Testing

Fig. 2.6 shows that PSS consists of much larger pore size which thereby requires minimum pressure of 0.5 bar for the gas flow. In contrary, porous alumina requires minimum 1 bar pressure for bubbles to emerge and hence confirms the presence of relatively smaller pores in comparison to porous SS. A pictorial representation of the same has also been shown in Fig. 2.7. It can be observed that PSS required a minimum pressure of 0.4-0.5 bar for bubbles to arise while porous alumina required a pressure >1 bar. Higher the pressure required for the bubbles to emerge smaller is the pore diameter. This analysis also coincides with the pore size distribution observed using FESEM. Thus, higher pore diameters suggest that it would provide minimum resistance to gas flow. However, in terms of membrane synthesis that necessitates a morphology which is non-porous or dense for hydrogen separation, the amount of palladium required to fabricate it will be huge. Further, the coarse surface morphology will also hinder uniform metal deposition. Hence, in order to create a uniform surface on top of the pores and between Pd membranes, intermediate layers have been prepared.

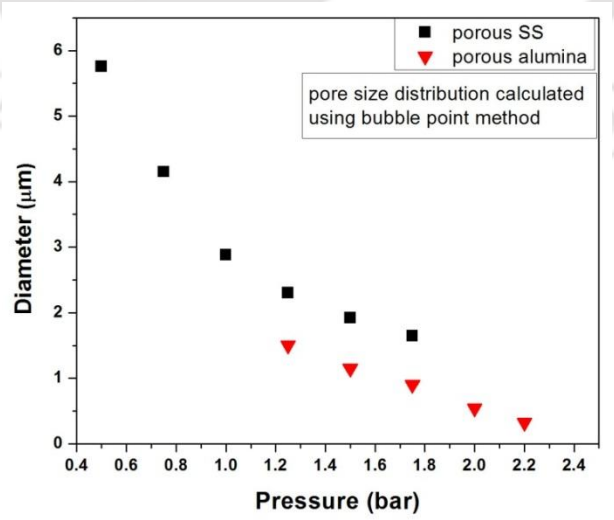

Fig. 2.6 Bubble point testing of porous alumina and SS

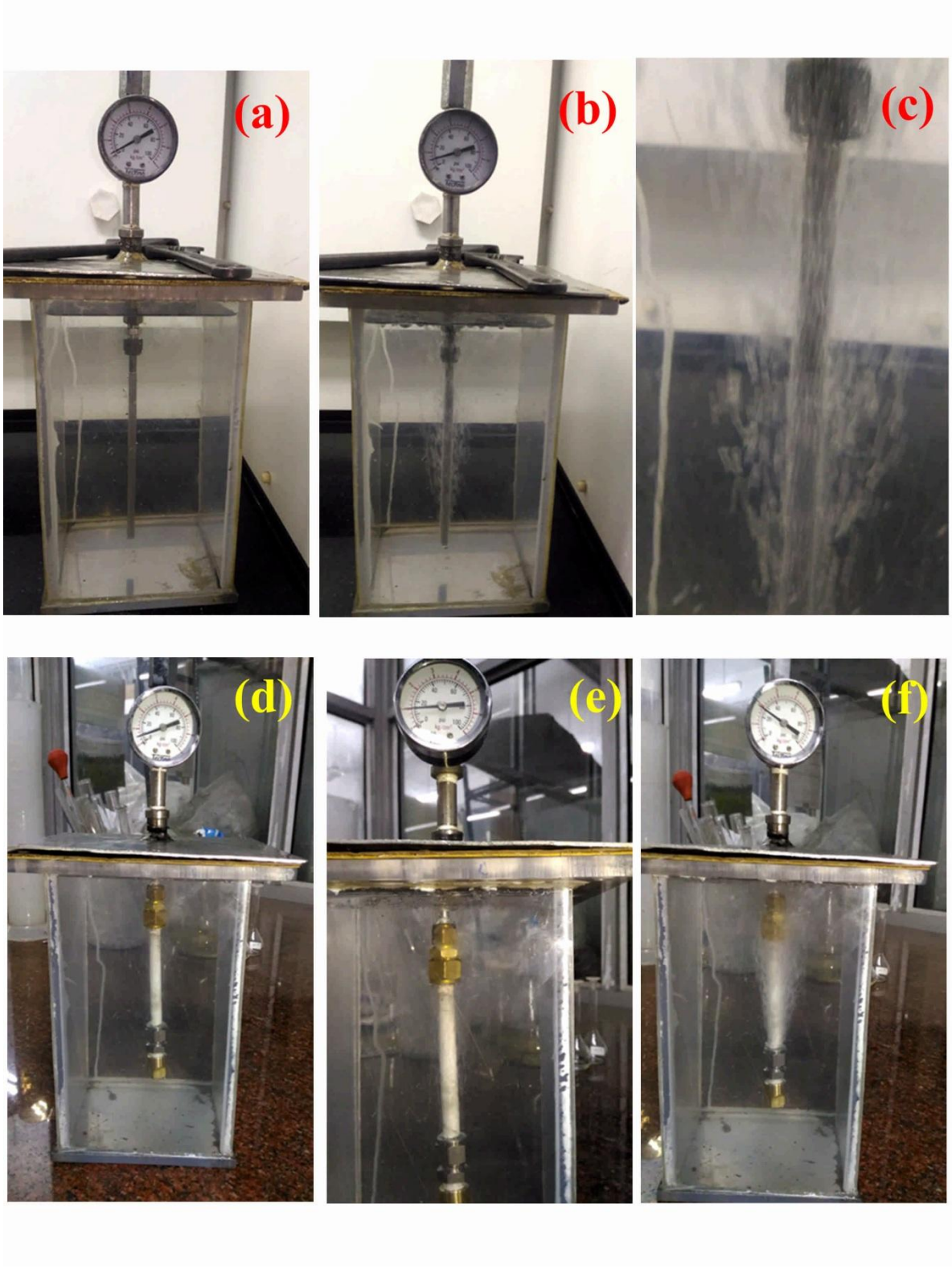

Fig. 2.7 Pictorial representation of porous SS (a-c) and alumina (d-f) with bubble point testing

2.6.2 Intermediate sol layer for porous alumina

Fig. 2.8 shows the Pd-Ag/alumina catalytic sol prepared using electroless deposition. The figure shows fine dispersion of active metals on the support with total 4% metal by weight Pd (2.4%) and Ag (1.6%). Fig. 2.8a shows uniform dispersion of metal on alumina catalysts. Therefore, the same catalysts when deposited on the tube as a sol provide an easy methodology to create a catalytic dense surface on alumina by improving its surface properties for metal deposition. The sol having the same base material as the alumina support showed good adherence with the support. Further, the pore size distribution with catalytic sol was reduced to 4-6 nm as shown in the Fig. 2.8b. Hence, with kinetic diameter of hydrogen about 0.289 nm, no resistance to its flow was assumed.

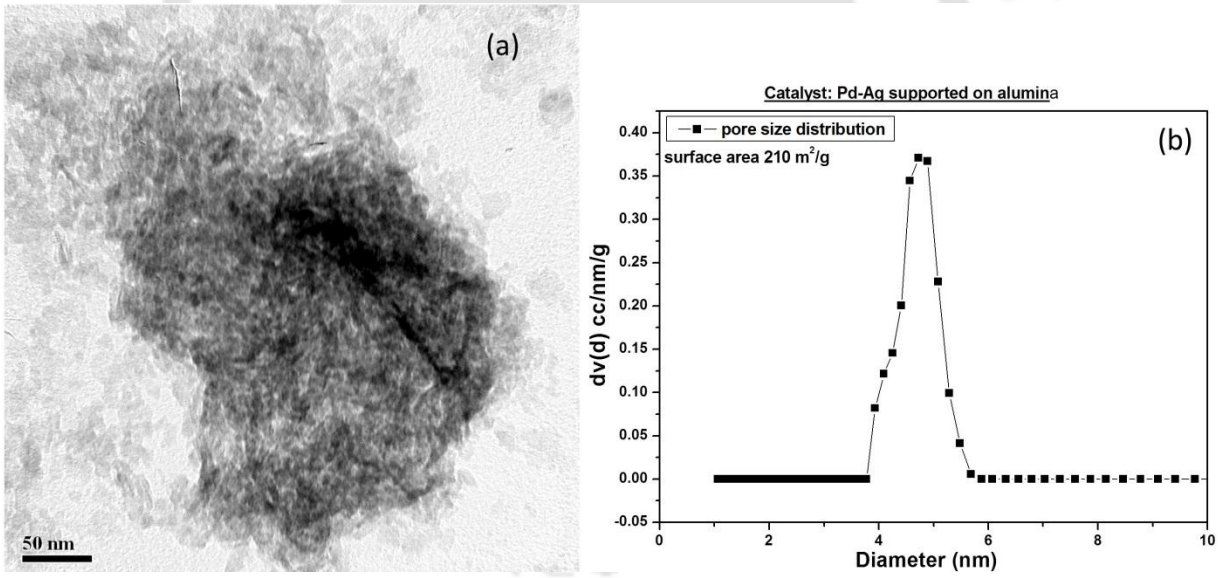

Fig. 2.8 (a-b) Pd-Ag/alumina catalysts for catalytic sol synthesis TEM image of the catalyst and pore size distribution of prepared Pd-Ag catalyst

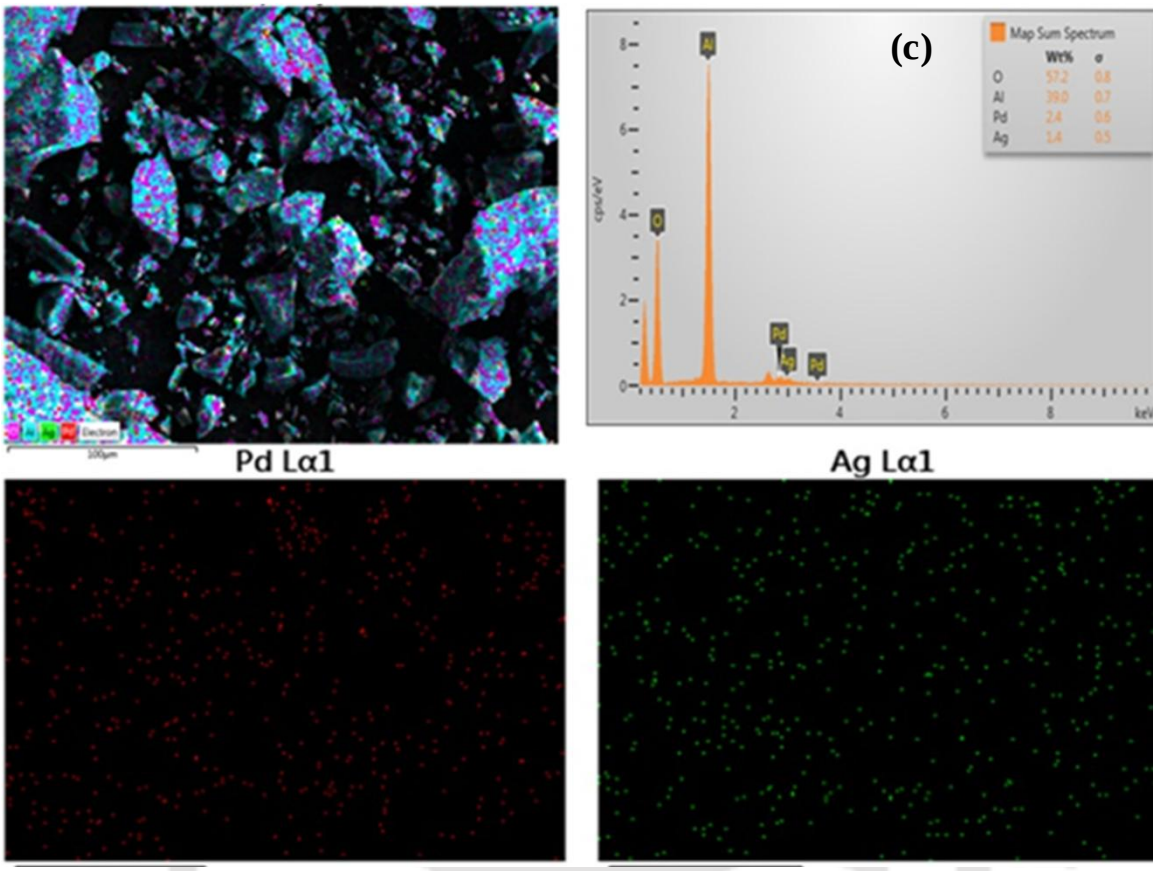

Fig. 2.8c Pd-Ag/alumina catalysts for catalytic sol synthesis: EDX analysis of the catalyst

The catalytic sol comprises 3 wt.% Pd-Ag on γ-alumina as shown in Fig. 2.8c was deposited on to the ceramic support by washcoating followed with drying at 90°C overnight and calcining at 300°C thereafter. Since self-diffusion in alumina occurs at temperatures > 1200 °C, the catalytic sol deposited on supports cannot be called as an inter-diffusion layer. The sol was applied to minimize surface roughness of the alumina support. Fig. 2.9 shows the FESEM image of the sol-deposited alumina tube. A smooth morphology was observed with a thickness of approximately 83 µm. In order to distinguish the effect of catalytic sol to smoothen the support surface, AFM analysis was performed. From Fig. 2.10, it can be observed that sol deposition immensely improves Pd morphology on support. Deposition of catalytic sol on alumina support reduced its

surface roughness and provided a uniform surface with smooth finish. The root mean square or roughness (RMS) roughness of ceramic tube was 0.2398 without sol coating while the RMS roughness for ceramic with sol was 0.0237.

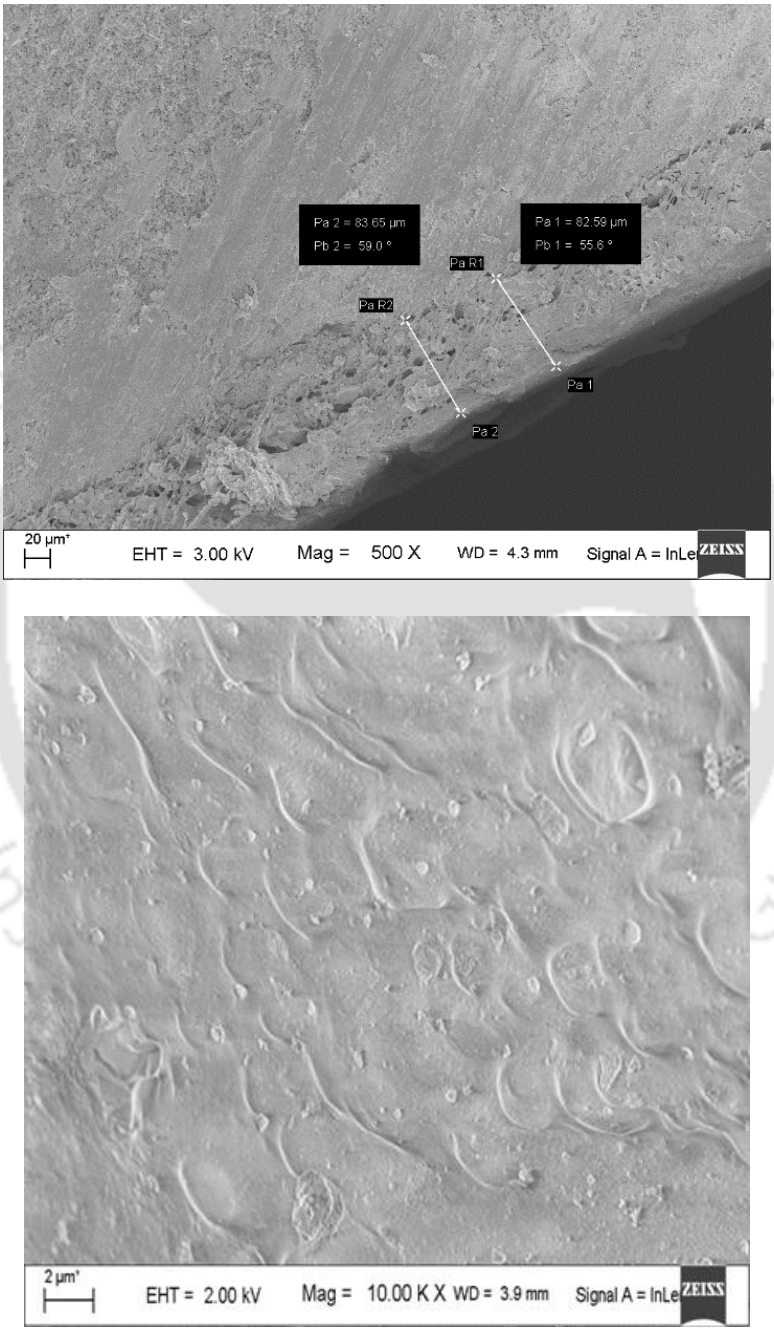

Fig. 2.9 FESEM analysis of Pd membrane deposited on alumina a) cross-section and b) morphology

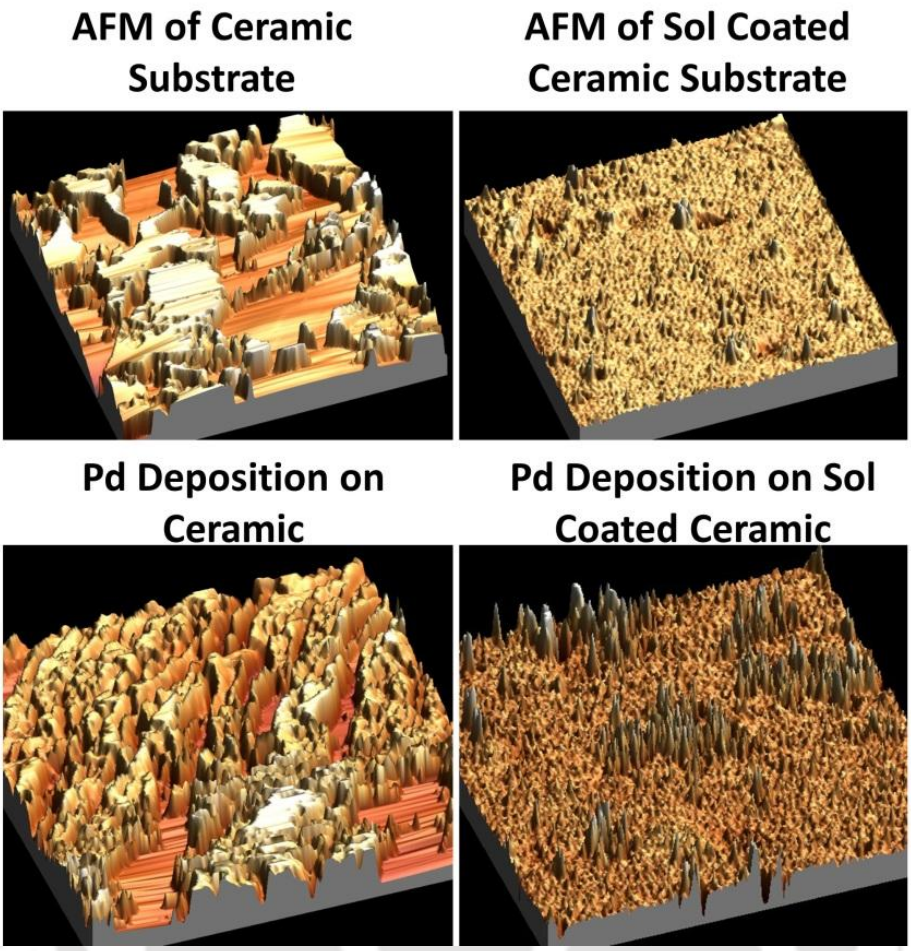

Fig. 2.10 AFM analysis of catalytic sol deposited on alumina

2.6.3 Pd membrane deposition on porous alumina

Palladium membrane deposition on porous alumina with and without sol was compared. In the direct palladium deposition method (without sol), prior to Pd plating, the alumina tubes were activated with alternate dipping in acidic $SnCl_2$ and $PdCl_2$, to create a nucleated layer of Pd on the non-conducting alumina surface until the whole surface of alumina turns brown. Fig. 2.11 shows the pictorial representation of the alumina tube at different stages in direct palladium deposition method.

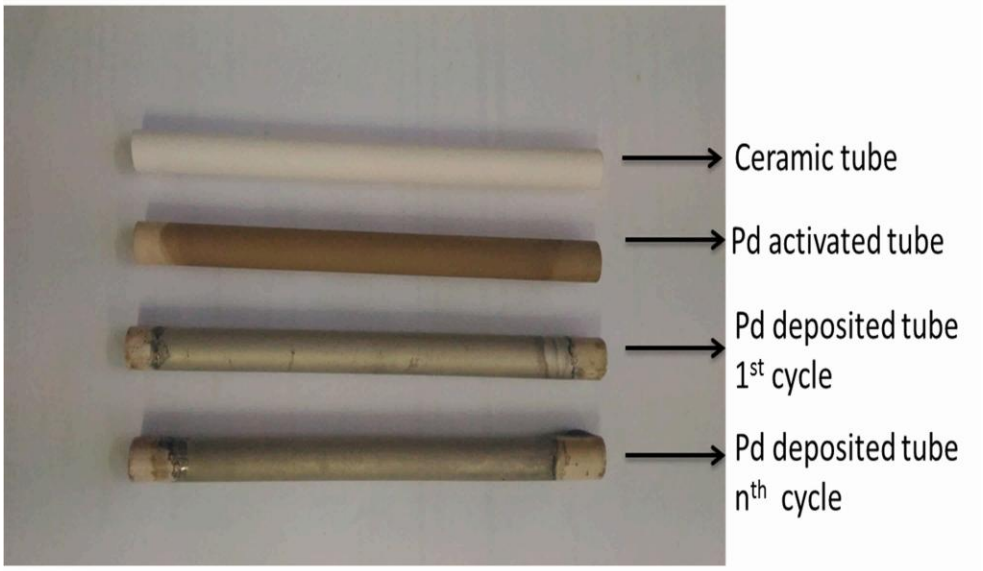

Fig. 2.11 Stages to membrane preparation by direct Pd deposition using modified electroless plating

The use of a relatively weak reducing agent such as $SnCl_2$ leads to a finely dispersed Pd layer over the length of the tube. This pre-nucleated layer then acts as a catalyst during subsequent hydrazine-led reduction cycles for the growth of multiple Pd layers until complete densification of surface occurs. In conventional electroless plating, reducing agent is directly mixed with plating solution for metal deposition on the substrate. In contrast to the conventional method, reduction in the present method was targeted only on the substrate with controlled addition of reducing agent on the substrate. The substrate surface covered with reducing solution was then dipped in the plating bath and left until the bubbles stop emerging. According to the reaction mentioned in reaction 2.4 nitrogen bubbles will evolve which suggests that reaction is occurring. A smooth gray metallic finish on surface was observed after one full cycle of coating as shown in Figure 2.11. Further, using such contacting pattern, bulk reduction of Pd in the plating solution was minimized. With the same methodology, square samples were also plated simultaneously

with Pd to analyze the surface characteristics. Fig. 2.12 shows the morphology of deposited palladium on alumina surface after first deposition cycle and after sixth cycle.

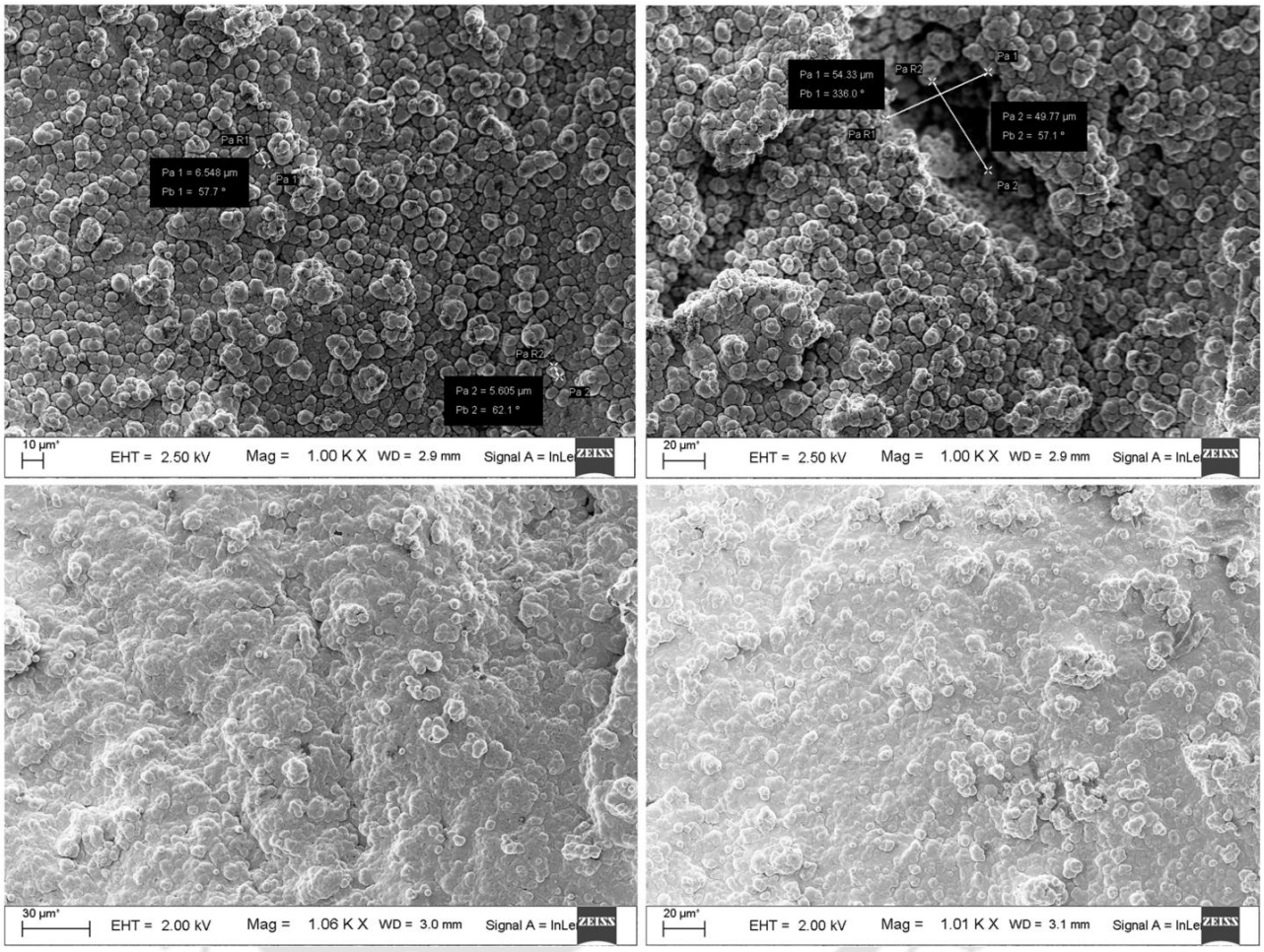

Fig. 2.12 FESEM images of Pd deposition on alumina with direction deposition method

It was observed that Pd particles grow perpendicularly and laterally around the nucleated Pd, forming cauliflower-like agglomerated structure. During this stage, some pits on the surface could also be observed. This may be due to insufficient surface coverage of palladium. With six continuous deposition cycles a much better surface coverage was observed. However, despite a wide surface coverage with increased plating cycles, complete densification of the surface was not achieved. This may be due to minor pits

created due to bubble adherence on the surface and some spalling that occurred during heat treatment. Non-uniform deposition as presented above and peculiar pin hole positions on the tube were observed with the help of in-house built gas tightness testing setup. It is believed that these peculiar pin holes may be generated by the non-uniformities of the alumina substrate. Therefore, in order to cover the non-uniformities of the substrate, a novel catalytic sol was synthesized. On top of a sol-coated alumina tube, palladium deposition was performed in a similar manner as before until the entire surface turned metallic grey. Surface characterization of sol-coated Pd membranes showed no apparent crevices or pits as can be observed in Fig. 2.13. Further, the thickness of Pd deposited on sol-coated alumina tube was also calculated. Nearly similar thickness of Pd membrane in case of direct Pd deposition and Pd deposition on top of catalytic sol was observed as presented in Table 2.5.

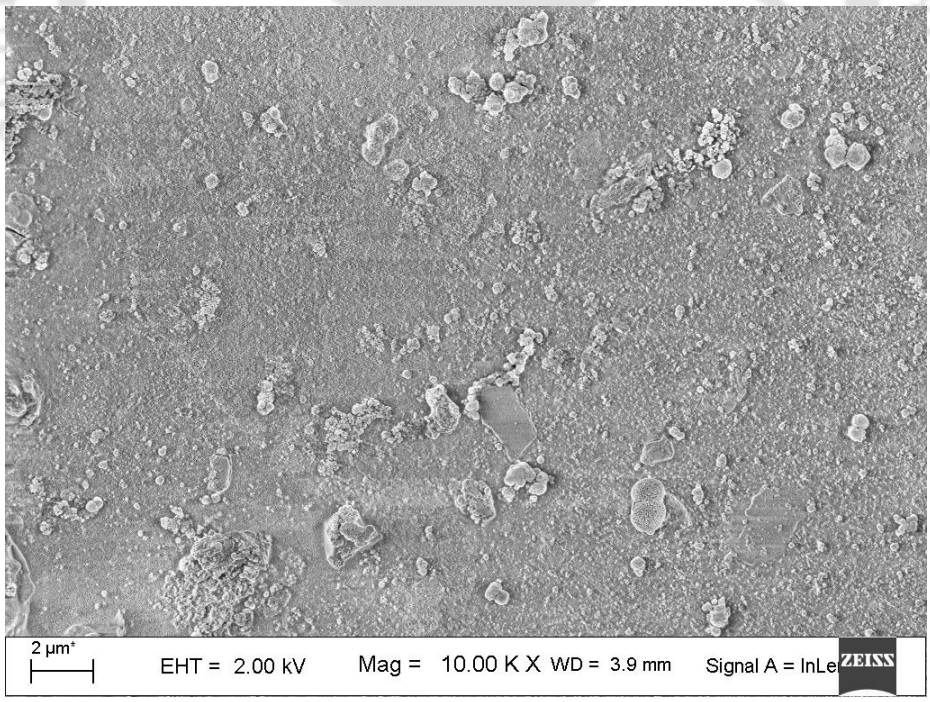

Fig. 2.13 Pd membrane deposited on sol-coated alumina tubes

Table 2.5 Comparison of membrane thickness with and without sol coating

S. No.	Membrane	Weight of alumina (g)	Weight of tube after sol deposition (g)	Weight of tube after two cycles of palladium deposition (g)	Palladium thickness (µm)
1	Direct palladium deposition on γ-alumina tube with modified ELP	10.2903	-NA-	10.4878	5.2
2	Palladium deposition on catalytic sol coated γ-alumina tube	10.2199	10.4869	10.6785	5.08

On this basis, we may suggest that catalytic washcoating is a viable technique to deposit uniform and dense palladium surface for hydrogen separation studies. Further, catalytic sol minimizes the use of rigorous electroless plating cycles to achieve dense Pd membranes. Therefore, with the use of electroless plating a thin layer of reduced palladium can be deposited on top of a dense catalytic sol surface wherein the catalyst particles are also embedded in a reduced state.

2.6.4 Atomic Absorbance Spectroscopy (AAS)

Pd deposition was carried out using electroless plating by external contacting of hydrazine with the membrane. Plating was carried out in multiple cycles and the amount of Pd deposited was monitored using timely sample analysis using AAS. It can be

observed from Fig. 2.14 that with the bare support, the deposited Pd in the first plating is higher than the rest. Pd deposition also followed a sigmoidal curve which indicates that after a given length of time, deposition gets stagnant. This may be because of the decreasing amount of ammonia complexed $PdCl_2$ in solution with increasing plating time.

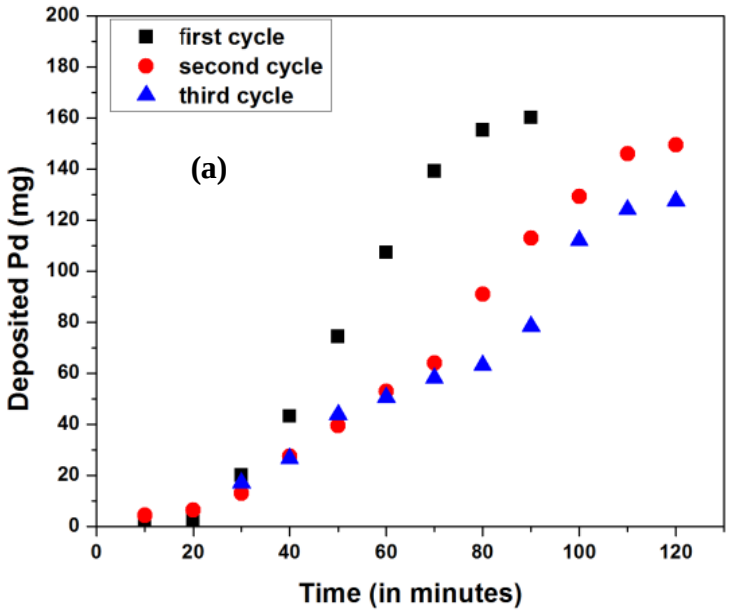

Fig. 2.14 Atomic absorbance analysis of palladium deposition a) deposition with increasing cycle

2.6.5 Pd-Ag and Pd-Ag-Au membrane deposition on alumina

Pd/Ag has large lattice constant and therefore could suppress the induced lattice expansion upon adsorption of hydrogen that causes embrittlement in pure Pd. Pd/Ag is co-plated in a Pd-rich bath because silver deposition is faster than Pd, and higher Pd content covers most of the active sites which otherwise in case of silver-rich bath get passivated. Therefore, silver addition was performed intermittently during the Pd plating

cycles. Alloying of palladium with silver increases hydrogen solubility. Silver has Tammann temperature of 344°C [18, 20, 23, 33, 60] and therefore can be alloyed by heating at 400°C. Elemental distribution of Ag deposited on Pd membranes is showed in Fig. 2.15a. Further, cross-sectional elemental distribution was also observed as shown in Fig. 2.15b. The thin membrane outline on the cross section of alumina can be distinctly observed through this image.

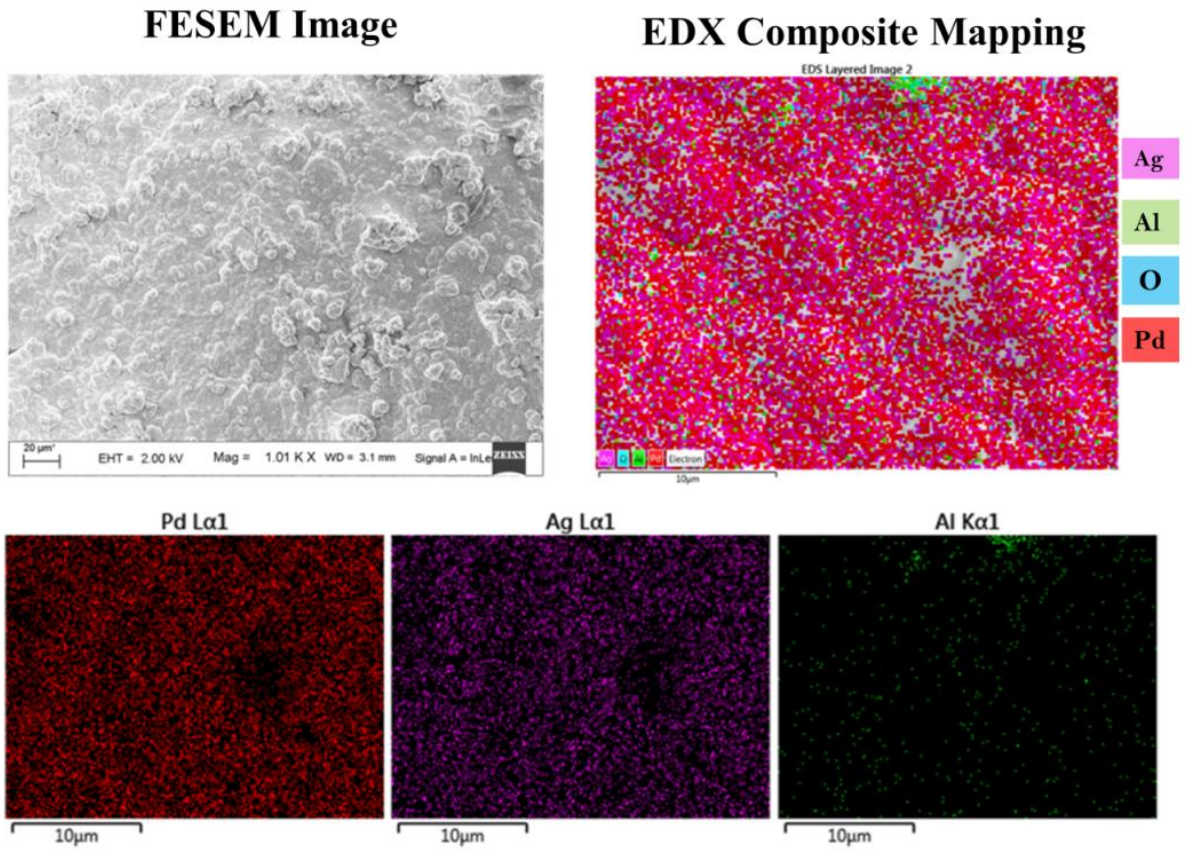

Fig. 2.15a EDX analysis Pd-Ag membrane elemental distributions

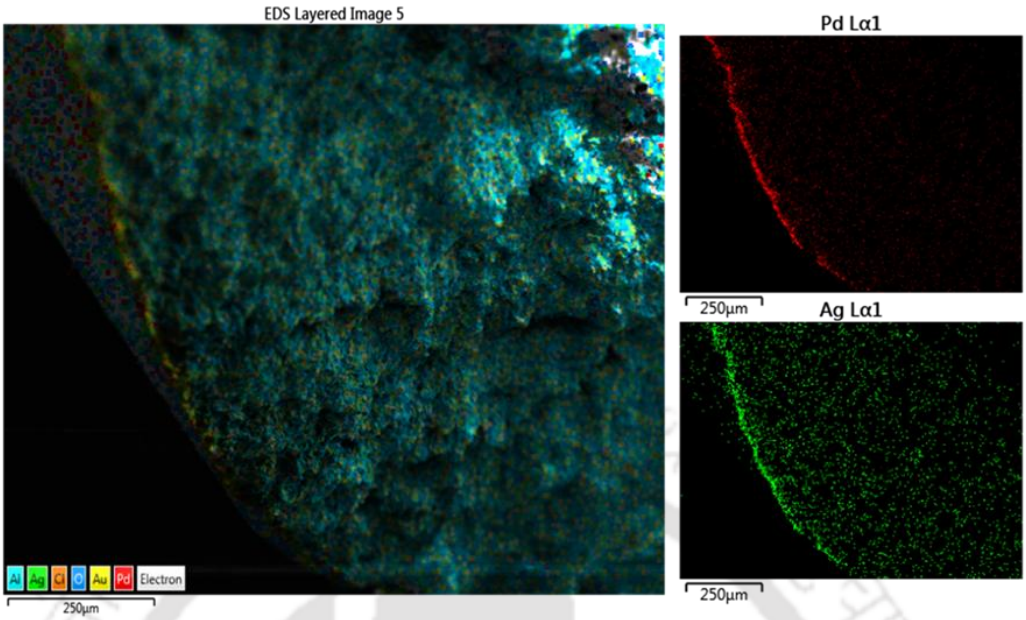

Fig. 2.15b EDX analysis Cross-section of Pd-Ag membrane deposited on alumina

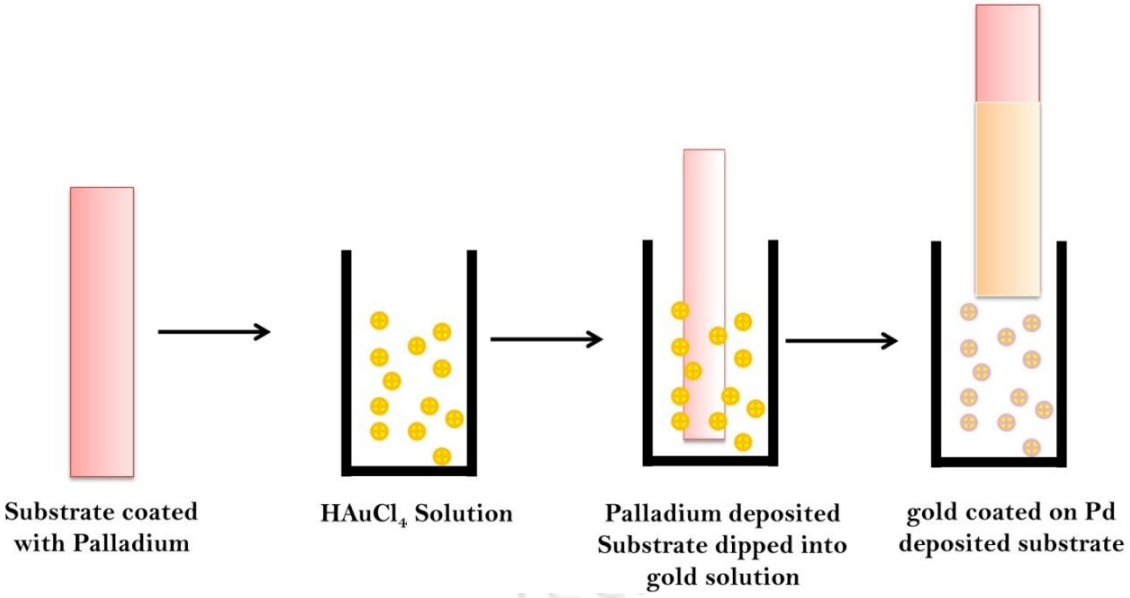

Fig. 2.16 Galvanic displacement for Pd-Ag-Au membrane supported on alumina

Further, for Pd-Ag-Au membrane preparation, galvanic displacement was employed (see Fig. 2.16). According to this methodology, a more noble metal is deposited on a less noble metal and the dissolution of the less noble metal maintains the electroneutrality of

the reaction. This means that there is oxidation of substrate and consequent reduction of the ions of more positive element based on the standard reduction potential of metals [70, 71]. This result in a uniform Au layer deposition on the membrane once dipped in an aqueous Au solution.

Metal composition of all membranes prepared was studied using energy dispersive X-ray spectroscopy (EDX). The metal composition of Pd-Ag membrane was 90 wt. % Pd and 10 wt. % Ag. Further, Pd-Ag-Au membrane composition was 80 wt. % Pd- 14 wt. % Ag- 6 wt. % Au. Table 2.6 shows the metal composition of all prepared membranes.

Table 2.6 EDX metal composition of all prepared membranes

Metal Composition	EDX
Pd-Ag	90 wt. % Pd and 10 wt. % Ag
Pd-Ag-Au	80 wt. % Pd- 14 wt. % Ag- 6 wt. % Au

2.6.6 Argon permeation in Pd, Pd-Ag and Pd-Ag-Au membranes supported on alumina

A comparison of argon permeation through alumina tube with and without sol is also presented as shown in Fig. 2.17a. At 673 K and increasing inlet pressure of pure argon as feed, this testing was carried out to observe the argon permeation through the tubes. Studies are conducted at relatively high temperature and at variable pressure to represent hydrogen permeation conditions which is mostly performed beyond 623 K to avoid membrane embrittlement in the presence of hydrogen. Further, the diffusivity of gases at higher temperature also affects permeation behavior. Therefore, argon testing for all the

tubes was carried out at 673 K. The scope of the study however, was limited to only argon testing which will be used to validate the proposed hypothesis on better densification using catalytic sol.

To carry out this study, all the tubes were connected to Swagelok SS316 fittings with graphite ferrules in order to be connected to the membrane reactor (in this study, no reaction was involved; only pure argon permeation). Further, argon permeation through palladium membranes was carried out after 12 h of heat treatment in hydrogen atmosphere to completely reduce the membranes and avoid presence of any oxide layers. At constant inlet feed rate of 0.5 LPM, it can be observed that argon permeation achieves a constant flow rate above 0.5 bar feed pressure for alumina tube as inlet rate becomes equal to the outlet. Further, with effect of varying metal composition of membrane, no significant change in argon permeation was observed. Pure Pd, Pd-Ag and Pd-Ag-Au supported on alumina nearly similar argon permeation rates as shown in Fig. 2.17a. Hence, 25-50% of Ar was able permeate through the membrane. This signifies that the support non-uniformity is critical to fabricate dense membranes. Hence, inter-mediate layers using a catalyst sol (Pd-Ag supported of alumina and dispersed in PVA) was used to smoothens the rough support surface and enable reduction of argon permeation. Fig. 2.17b compares argon permeation through no sol coated and sol coated alumina tubes as well as pure Pd membrane. It can be observed that using catalytic sol coating, an additional restriction to argon permeation causes the permeate rate to decrease compared to pure alumina and thus achieves steady flow rate of nearly 0.4 LPM above 1 bar pressure. Further, it has been noticed that reduction in permeate flow rate for catalytic sol-coated membrane is much higher compared to without sol-coated membrane for the

same thickness of palladium layer (~5 µm). Moreover, metal deposition was then continued to achieve maximum densification. The maximum membrane thickness at which hydrogen selectivity of at least 100 was observed was ~16 µm, as presented in Fig. 2.17c. All permeation studies were therefore carried out with sol coated tubes followed with metal deposition until a minimal H_2/Ar selectivity of up to 100 was obtained.

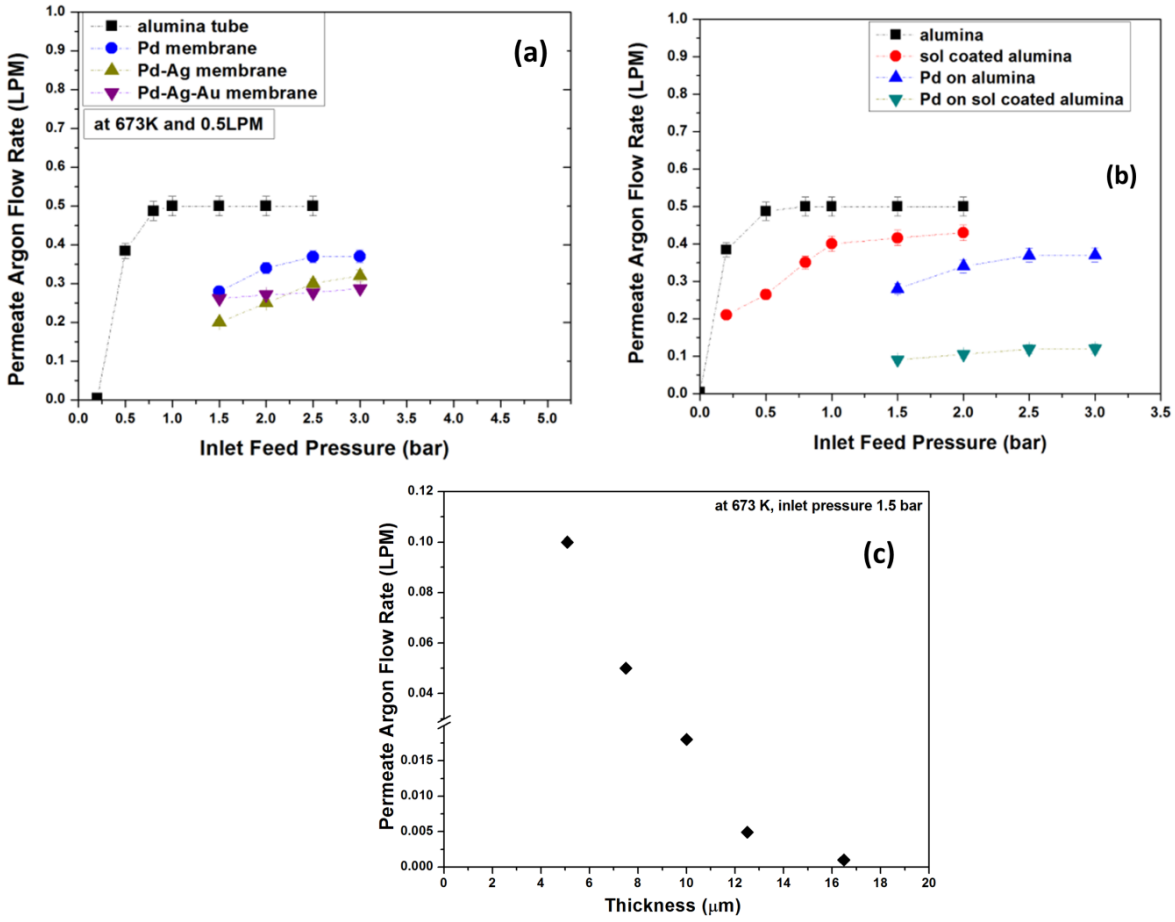

Fig. 2.17 Argon permeation through (a) through no sol coated pure Pd-, Pd-Ag, Pd-Ag-Au membrane, (b) sol coated tubes, and (c) permeated argon vs. membrane thickness

2.6.7 Hydrogen permeation testing through prepared membranes

Permeation of hydrogen through palladium occurs by solution-diffusion mechanism which involves several steps. The exponent (n) of equation 2.1 varies from n = 0.5 to 1

depending on the rate limiting step. If the diffusion of atomic hydrogen through the metal bulk of the membrane is rate determining step and hydrogen concentration in the Pd based lattice (H/Pd) is lower than 1, the Sieverts law should be valid for which the exponent is 0.5.

In this study, gold deposition on Pd-based membranes was carried out to minimize gas leaks from the welds as well as small pin-holes on the surface. Pd-Au alloys are widely reported in literature primarily to overcome H_2S poisoning. However it is important to note that improvement in hydrogen permeability occurs only with 10 wt. % of Au. Beyond this point, hydrogen flux starts to decrease down to zero [72]. Fig. 2.18a shows the picture of membranes used for hydrogen testing. Hydrogen permeance from the prepared Pd, Pd-Ag and Pd-Ag-Au membranes supported on alumina is further shown in Fig. 2.18b. The highest hydrogen permeance was observed with Pd-Ag membrane. This is because addition of Ag to Pd membrane makes hydrogen permeation not only through the octahedral Pd sites but also tetrahedral Ag sites. However, gold addition showed a drastic decrease in hydrogen permeability. This may be because hydrogen permeability through gold is inherently small and therefore may require much higher trans-membrane pressure for hydrogen permeation to occur. In contrast to the reported literature, it was observed that even with 6 wt. % of Au, hydrogen permeability was negligible. This may be because Au addition improves hydrogen permeation when added to only pure Pd and not Pd-Ag. In this context, a recent article has also reported the activation energies for $Pd_{94.9}Ag_{5.1}$ and $Pd_{90.5}$-$Ag_{4.6}$-$Au_{4.9}$ membranes to be 9.5 kJ/mol and 16 kJ/mol respectively [72]; thus, the activation energy increases upon addition of Au to the Pd-Ag alloy. This suggests that addition of Au affects the adsorption and dissociation steps in the solution-

diffusion model of H_2 transport through Pd-based membranes. Hence, Pd-Ag composition was observed the best for hydrogen permeation. Further, the same composition was then deposited on to porous SS support. Table 2.7 shows the comparison between all prepared membranes.

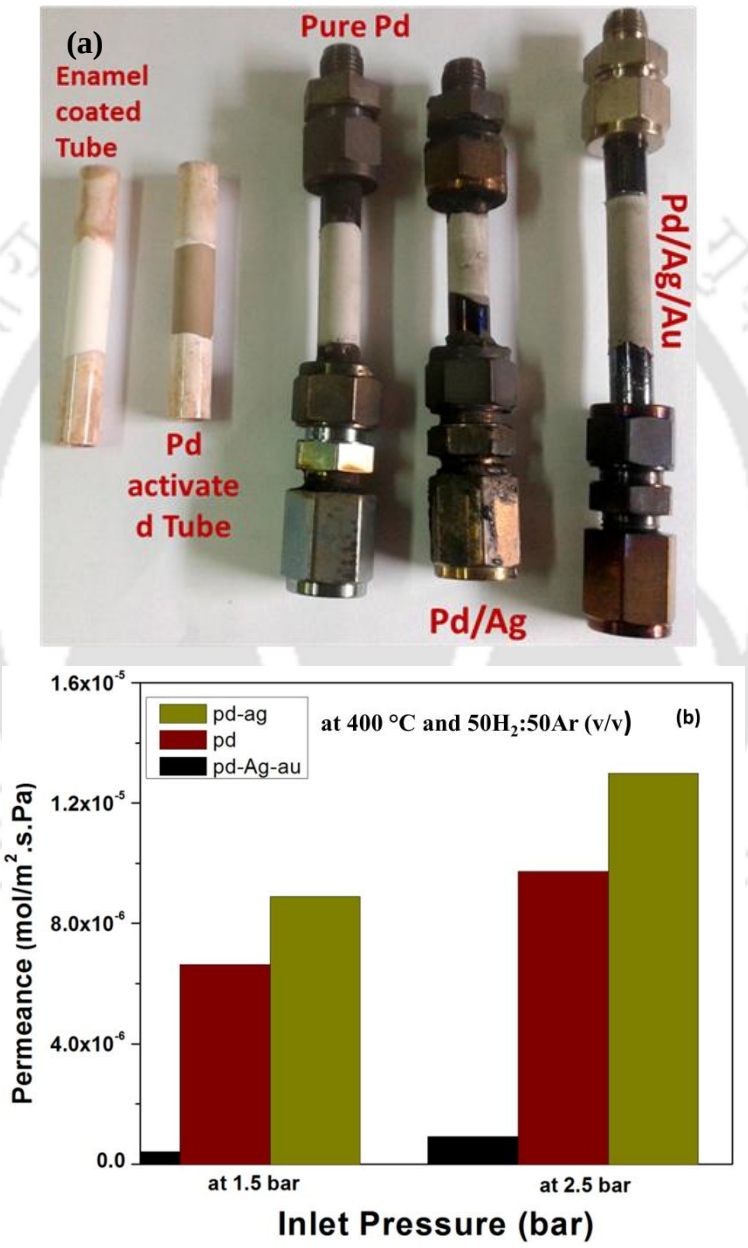

Fig. 2.18 Prepared pure Pd, Pd-Ag and Pd-Ag-Au membranes a) picture and b) Hydrogen permeability tested

Table 2.7 Comparative performance of alumina supported Pd-membranes at 400 °C, pressure 1.5 bar and 50H_2:50Ar (v/v) feed

Alumina-Supported Membranes	Permeance (mol s^{-1} m^{-2} Pa^{-1})	H_2/Ar Selectivity (-)
Pure Pd	6.6×10^{-6}	123
Pd-Ag	8.9×10^{-6}	107
Pd-Ag-Au	4×10^{-7}	114

2.7 Pd-Ag membrane deposition on porous SS

Using similar electroless deposition methodology as detailed in the previous section, Pd-Ag membrane on sol coated PSS was synthesized. YSZ sol was coated on the PSS support using vacuum to obtain a uniform smooth texture on the support as shown in Fig. 2.19. Pd-acetate activation with vacuum was performed further until the surface achieves a shiny black texture. This tube was then dried at 110°C followed with Pd-Ag deposition sequentially. Nearly 10 deposition cycles, consisting of 0.5 g $PdCl_2$ in each cycle, was required in order to obtain dense membrane morphology. Fig. 2.19 also shows the stages to Pd-Ag membrane synthesis with FESEM images starting from granular coarse surface to a smoother membrane surface. The final Pd-Ag membrane was observed dense up to 1 bar. Fig. 2.20 shows the YSZ elemental distribution used prior to Pd deposition.

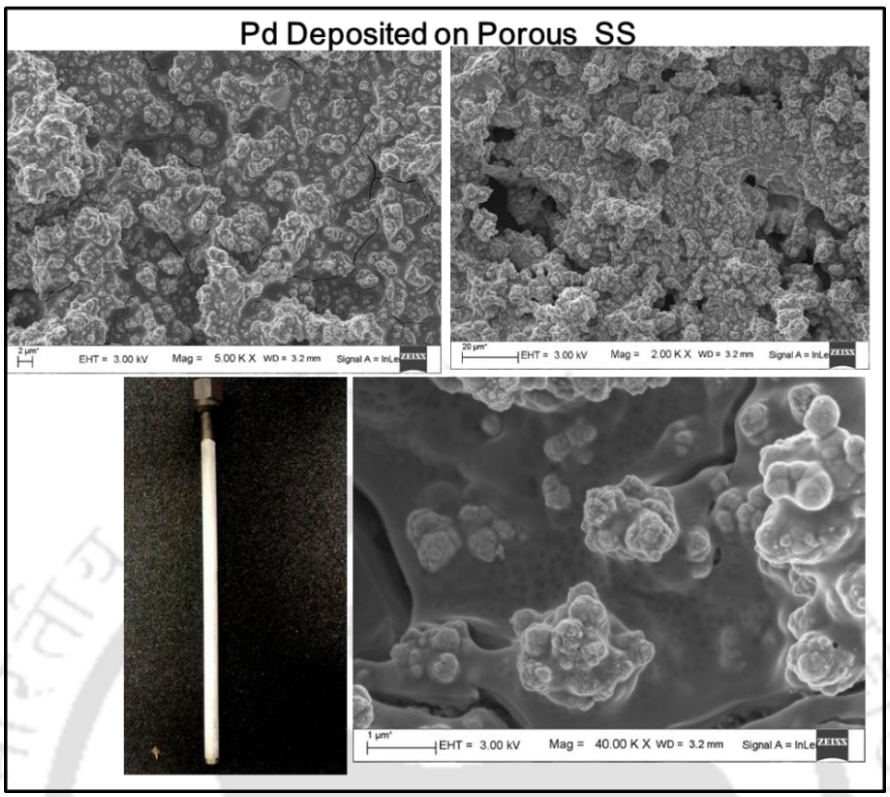

Fig. 2.19 Pd-Ag membrane on YSZ coated PSS support

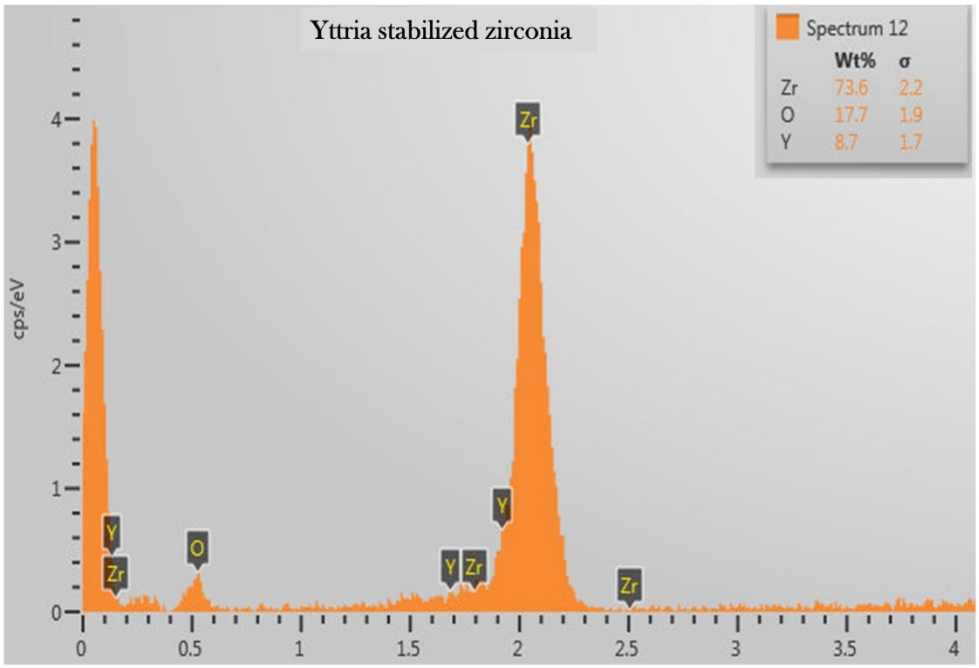

Fig. 2.20 Elemental distribution of YSZ synthesized

2.8 Hydrogen permeation through Pd membrane supported on porous SS

Fig. 2. 21 shows that permeate hydrogen flux through PSS supported membrane increases with increase in trans-membrane pressure difference as well as temperature. The observed activation energy for the prepared membrane matches the values reported in literature [7, 33, 45, 52, 59, 60, 66]. Hydrogen permeation was tested at temperatures ranging from 200 to 400°C. A maximum hydrogen flux of 1 mol/m^2.s was achieved using pure H_2 as feed with increasing pressure difference with Pd-Ag membrane supported on YSZ coated porous SS.

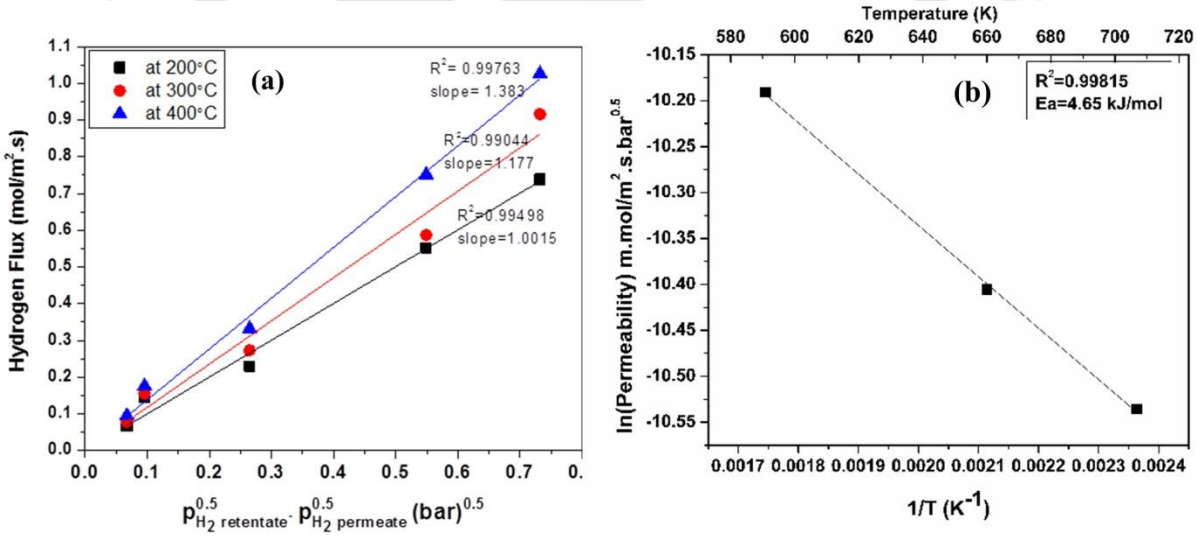

Fig. 2.21 Hydrogen permeation through Pd-Ag membrane supported on PSS a) Hydrogen flux and b) activation energy

2.9 Supported Pd-membranes performance comparison

Fig. 2.22 shows that the hydrogen permeation rate through porous SS was much higher than alumina-supported membrane. At all temperatures, hydrogen permeation rate

through PSS tube was observed higher. This may be due to larger pore size in case of porous SS in comparison to porous alumina. A large pore size therefore will reduce the resistance to gas flow through the membrane and hence improve the permeation rate. Moreover, due to higher pore size, the minimum pressure required for gas flow to occur in case of PSS is also low. Therefore, it may be suggested that there always lie a tradeoff between the pore size that provides minimal resistance and amount of Pd required for its densification.

In comparison to porous alumina tube, the requirement of Pd was higher in SS. However, with higher hydrogen flow rate, the performance of Pd-Ag membrane supported on YSZ coated PSS tube may be suggested as more efficient. Moreover, a comparative chart of prepared membrane performance with the reported literature is presented in Table 2.8.

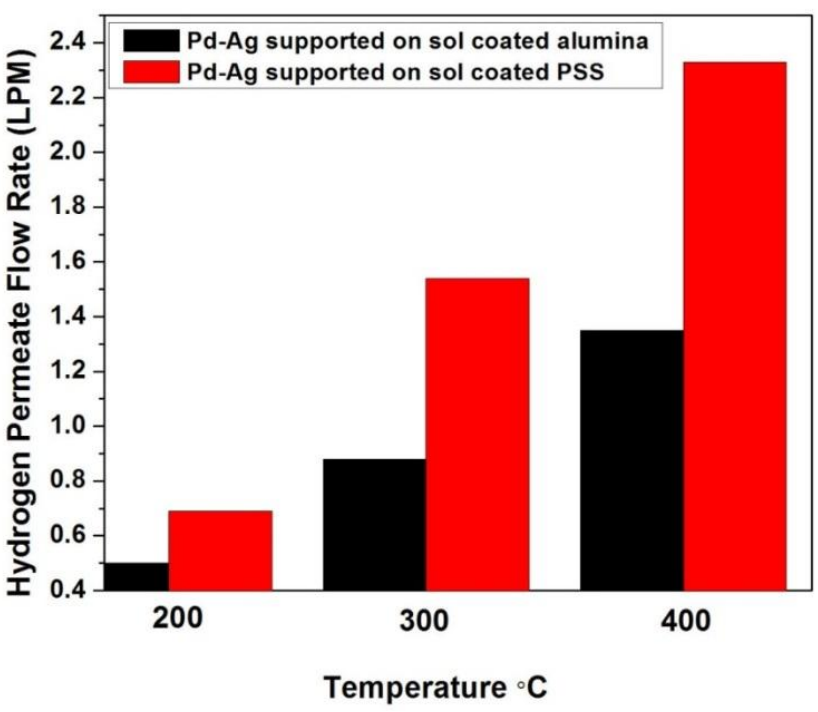

Fig. 2.22 Comparison of SS and ceramic supported Pd membranes

Table 2.8 Comparative literature review

S. No	Membrane	Intermediate Layer (particle size)	Membrane Preparation Method	Reactor ID (cm)	Operating Temperature (°C)	Pressure Difference (bar)	H_2 Permeance (mol s^{-1} m^{-2} Pa^{-1})	H_2/Ar Selectivity (-)	Ref.
			Membrane Supported on Porous Alumina						
1	$Pd_{90.5}Ag_{4.6}Au_{4.9}$	ZrO_2 (110 nm)	ELP	10.2	600	1	5×10^{-6}	2557	[72]
2	Pd	YSZ and YSZ-γ-Al_2O_3 mixed sol (7-15 nm)	ELP	-NA-	550	1	1.76×10^{-7}	50	[63]
3	Pd	nil	ELP	-NA-	300	1	1.9×10^{-3}	384	[73]
4	Pd	YSZ-γ-Al_2O_3 mixed sol (5-20 nm)			500	1	2×10^{-6}	>350	[45]
5	Pd_{95}-Ag_5	Pd-Ag followed by YSZ-γ-Al_2O_3 mixed sol	ELP	4.27	500	1	4.6×10^{-6}	2000	[74]
6	Pd-Ag	PVA	ELP	-NA-	500	1	-nil-	958	[75]
7	Pd_{90}-Ag_{10}	Pd-Ag on γ-Al_2O_3 catalytic sol	ELP	14.5	400	1	8.9×10^{-6}	107	**This work**
			Membrane Supported on Porous Stainless Steel (PSS)						
8	Pd	Metal oxide	ELP	1.35	450	25	2.51×10^{-5}	100	[19]
9	Pd Pd-27Pt Pd-0.3Ru	-nil-	ELP	-NA-	550	6	2.3×10^{-3} 1×10^{-3} 2.4×10^{-3}	1750 626 1860	[76]
10	Pd-Ag	Oxidized support + γ-Al_2O_3+ Pd- γ-Al_2O_3	ELP	0.8	400	1.5	-NA-	400 (oxidized support)	[77]
11	Pd-Ag	γ-Al_2O_3 mixed sol or in-situ hydrothermal synthesis of NaA zeolite	ELP	-NA-	450	1	9.1×10^{-4}	300	[66]
12	Pd_{90}-Ag_{10}	YSZ	ELP	14.5	400	1	1.473×10^{-5}	122	**This work**

3.0 Summary

Chapter 2 focuses on methodology and challenges related to membrane deposition on alumina as well as SS supports. Therefore, the primary aim of this chapter was to present systematic synthesis procedure and characterization of membranes prior to ideal hydrogen flux testing. Hence, with the maximum hydrogen selectivity of 100 observed in the current work, chapter 2 only shows the ideal hydrogen flux at varying trans-membrane pressure differences.

In this chapter, preparation of dense palladium membranes was investigated using electroless deposition on two different supports, porous SS and porous alumina. A modification in conventional electroless deposition methodology was applied by contacting hydrazine to the support external instead of the plating solution. Progress in reaction was observed using atomic absorbance spectroscopy with a dilution factor of 100. Continuous deposition was simultaneously assisted with bubble point testing in order to identify points from where leak occurs at the desired operating pressure. Following can be outlined as the major observations from the current chapter:

- Hydrogen permeation rate through Pd-Ag deposited on YSZ coated PSS was observed to be higher than Pd-Ag on alumina. A higher area used for Pd-Ag membrane supported on PSS results in this enhancement. Further, the large pore size in PSS provides minimum resistance for gas flow. This behavior was observed using bubble point testing wherein a minimal pressure required for gas to flow through uncoated PSS was 0.5 bar in contrary to porous alumina which was more than 1 bar.

- Pd-Ag membrane deposited on porous SS and porous alumina supports provide certain advantages as well as disadvantages: Brittle nature of ceramic tubes causes immense loss during its connection with SS fittings. Narrow pore size distribution of the alumina support required pressure more than 1 bar for gas to pass through the pores which in case of PSS was 0.5 bar. However, a narrow pore size led to a reduced amount of $PdCl_2$ required for membrane densification in case of porous alumina.

- In case of PSS, excessive corrosion of SS tubes affects the deposition process resulting in pinhole creation. This was minimized using Pd-acetate activation methodology and by avoiding direct contact of PSS with either HCl and $PdCl_2$. Further, effective removal of rust was observed using oxalic acid. Further, SS strength minimizes breakage and loss of membrane deposited tubes in comparison to huge losses incurred with membrane deposited on porous alumina. Higher pore size in porous SS necessitates increased number of deposition cycles for membrane densification.

- Lastly, from these observations PSS-supported Pd membranes showed better performance than Pd-Ag on alumina and were therefore considered for integration studies.

References

[1] D.F. Sanders, Z.P. Smith, R. Guo, L.M. Robeson, J.E. McGrath, D.R. Paul, B.D. Freeman, Energy-efficient polymeric gas separation membranes for a sustainable future: A review, Polymer, 54 (2013) 4729-4761.

[2] G.Q. Lu, J.C. Diniz da Costa, M. Duke, S. Giessler, R. Socolow, R.H. Williams, T. Kreutz, Inorganic membranes for hydrogen production and purification: A critical

review and perspective, Journal of Colloid and Interface Science, 314 (2007) 589-603.

[3] T. M. Nenoff, R. Spontak, C. M. Aberg, Membranes for Hydrogen Purification: An Important Step toward a Hydrogen-Based Economy, 2006.

[4] M. Hong, J.L. Falconer, R.D. Noble, Modification of Zeolite Membranes for H2 Separation by Catalytic Cracking of Methyldiethoxysilane, Industrial & Engineering Chemistry Research, 44 (2005) 4035-4041.

[5] T. Norby, R. Haugsrud, Dense Ceramic Membranes for Hydrogen Separation, in: Nonporous Inorganic Membranes, Wiley-VCH Verlag GmbH & Co. KGaA, 2006, pp. 1-48.

[6] J.W. Phair, S.P.S. Badwal, Materials for separation membranes in hydrogen and oxygen production and future power generation, Science and Technology of Advanced Materials, 7 (2006) 792-805.

[7] J.J. Conde, M. Maroño, J.M. Sánchez-Hervás, Pd-Based Membranes for Hydrogen Separation: Review of Alloying Elements and Their Influence on Membrane Properties, Separation & Purification Reviews, 46 (2017) 152-177.

[8] F.A. Lewis, The palladium-hydrogen system: Structures near phase transition and critical points, International Journal of Hydrogen Energy, 20 (1995) 587-592.

[9] S.N. Paglieri, J.D. Way, INNOVATIONS IN PALLADIUM MEMBRANE RESEARCH, Separation and Purification Methods, 31 (2002) 1-169.

[10] A. Knapton, Palladium alloys for hydrogen diffusion membranes, Platinum Metals Review, 21 (1977) 44-50.

[11] T.L. Ward, T. Dao, Model of hydrogen permeation behavior in palladium membranes, Journal of Membrane Science, 153 (1999) 211-231.

[12] D. Depla, S. Mahieu, J.E. Greene, Chapter 5 - Sputter Deposition Processes A2 - Martin, Peter M, in: Handbook of Deposition Technologies for Films and Coatings (Third Edition), William Andrew Publishing, Boston, 2010, pp. 253-296.

[13] C. Bechtold, A. Lotnyk, B. Erkartal, L. Kienle, E. Quandt, Structural Characterization of Sputtered Fe70Pd30 Thin Films During Ex Situ and In Situ TEM Heating, Advanced Engineering Materials, 14 (2012) 716-723.

[14] S.E. Koponen, P.G. Gordon, S.T. Barry, Principles of precursor design for vapour deposition methods, Polyhedron, 108 (2016) 59-66.

[15] J. Creighton, P. Ho, Introduction to chemical vapor deposition (CVD), Chemical vapor deposition, 2 (2001) 1-22.

[16] R.N. Rhoda, Electroless Palladium Plating, Transactions of the IMF, 36 (1959) 82-85.

[17] Chapter 3 Materials and preparation of inorganic membranes, in: H.P. Hsieh (Ed.) Membrane Science and Technology, Elsevier, 1996, pp. 23-92.

[18] M.E. Ayturk, Y.H. Ma, Electroless Pd and Ag deposition kinetics of the composite Pd and Pd/Ag membranes synthesized from agitated plating baths, Journal of Membrane Science, 330 (2009) 233-245.

[19] K.S. Rothenberger, A.V. Cugini, B.H. Howard, R.P. Killmeyer, M.V. Ciocco, B.D. Morreale, R.M. Enick, F. Bustamante, I.P. Mardilovich, Y.H. Ma, High pressure hydrogen permeance of porous stainless steel coated with a thin palladium film via electroless plating, Journal of Membrane Science, 244 (2004) 55-68.

[20] Y.H. Ma, B.C. Akis, M.E. Ayturk, F. Guazzone, E.E. Engwall, I.P. Mardilovich, Characterization of Intermetallic Diffusion Barrier and Alloy Formation for Pd/Cu and Pd/Ag Porous Stainless Steel Composite Membranes, Industrial & Engineering Chemistry Research, 43 (2004) 2936-2945.

[21] P.P. Mardilovich, Y. She, Y.H. Ma, M.-H. Rei, Defect-free palladium membranes on porous stainless-steel support, AIChE Journal, 44 (1998) 310-322.

[22] E. Kikuchi, S. Uemiya, Preparation of supported thin palladium-silver alloy membranes and their characteristics for hydrogen separation, Gas separation & purification, 5 (1991) 261-266.

[23] H. Amandusson, L.G. Ekedahl, H. Dannetun, Hydrogen permeation through surface modified Pd and PdAg membranes, Journal of Membrane Science, 193 (2001) 35-47.

[24] M.M. Barreiro, M. Maroño, J.M. Sánchez, Hydrogen permeation through a Pd-based membrane and RWGS conversion in H2/CO2, H2/N2/CO2 and H2/H2O/CO2 mixtures, International Journal of Hydrogen Energy, 39 (2014) 4710-4716.

[25] F. Pinto, R.N. André, C. Franco, C. Carolino, I. Gulyurtlu, Effect of syngas composition on hydrogen permeation through a Pd–Ag membrane, Fuel, 103 (2013) 444-453.

[26] J. Boon, J.A.Z. Pieterse, F.P.F. van Berkel, Y.C. van Delft, M. van Sint Annaland, Hydrogen permeation through palladium membranes and inhibition by carbon monoxide, carbon dioxide, and steam, Journal of Membrane Science, 496 (2015) 344-358.

[27] J. Catalano, M. Giacinti Baschetti, G.C. Sarti, Influence of the gas phase resistance on hydrogen flux through thin palladium–silver membranes, Journal of Membrane Science, 339 (2009) 57-67.

[28] R.E. Buxbaum, A.B. Kinney, Hydrogen Transport through Tubular Membranes of Palladium-Coated Tantalum and Niobium, Industrial & Engineering Chemistry Research, 35 (1996) 530-537.

[29] S. Uemiya, N. Sato, H. Ando, Y. Kude, T. Matsuda, E. Kikuchi, Separation of hydrogen through palladium thin film supported on a porous glass tube, Journal of Membrane Science, 56 (1991) 303-313.

[30] S. Uemiya, Y. Kude, K. Sugino, N. Sato, T. Matsuda, E. Kikuchi, A palladium/porous-glass composite membrane for hydrogen separation, Chemistry Letters, 17 (1988) 1687-1690.

[31] S. Yun, S. Ted Oyama, Correlations in palladium membranes for hydrogen separation: A review, Journal of Membrane Science, 375 (2011) 28-45.

[32] S.S. Kim, N. Xu, A. Li, J.R. Grace, C.J. Lim, S.-K. Ryi, Development of a new porous metal support based on nickel and its application for Pd based composite membranes, International Journal of Hydrogen Energy, 40 (2015) 3520-3527.

[33] G. Zeng, L. Shi, Y. Liu, Y. Zhang, Y. Sun, A simple approach to uniform PdAg alloy membranes: Comparative study of conventional and silver concentration-controlled co-plating, International Journal of Hydrogen Energy, 39 (2014) 4427-4436.

[34] J. Shu, B.P.A. Grandjean, S. Kaliaguine, Methane steam reforming in asymmetric Pd- and Pd-Ag/porous SS membrane reactors, Applied Catalysis A: General, 119 (1994) 305-325.

[35] R. Dittmeyer, V. Höllein, K. Daub, Membrane reactors for hydrogenation and dehydrogenation processes based on supported palladium, Journal of Molecular Catalysis A: Chemical, 173 (2001) 135-184.

[36] Y. Huang, R. Dittmeyer, Preparation and characterization of composite palladium membranes on sinter-metal supports with a ceramic barrier against intermetallic diffusion, Journal of Membrane Science, 282 (2006) 296-310.

[37] F. Guazzone, Y.H. Ma, Leak growth mechanism in composite Pd membranes prepared by the electroless deposition method, AIChE Journal, 54 (2008) 487-494.

[38] F. Guazzone, E.A. Payzant, S.A. Speakman, Y.H. Ma, Microstrains and Stresses Analysis in Electroless Deposited Thin Pd Films, Industrial & Engineering Chemistry Research, 45 (2006) 8145-8153.

[39] P. Pinacci, F. Drago, Influence of the support on permeation of palladium composite membranes in presence of sweep gas, Catalysis Today, 193 (2012) 186-193.

[40] M. Vadrucci, F. Borgognoni, A. Moriani, A. Santucci, S. Tosti, Hydrogen permeation through Pd–Ag membranes: Surface effects and Sieverts' law, International Journal of Hydrogen Energy, 38 (2013) 4144-4152.

[41] H.W. Abu El Hawa, S.-T.B. Lundin, S.N. Paglieri, A. Harale, J. Douglas Way, The influence of heat treatment on the thermal stability of Pd composite membranes, Journal of Membrane Science, 494 (2015) 113-120.

[42] M. Kitiwan, D. Atong, Effects of Porous Alumina Support and Plating Time on Electroless Plating of Palladium Membrane, Journal of Materials Science & Technology, 26 (2010) 1148-1152.

[43] J. Okazaki, T. Ikeda, D.A.P. Tanaka, K. Sato, T.M. Suzuki, F. Mizukami, An investigation of thermal stability of thin palladium–silver alloy membranes for high temperature hydrogen separation, Journal of Membrane Science, 366 (2011) 212-219.

[44] D.A. Pacheco Tanaka, M.A. Llosa Tanco, T. Nagase, J. Okazaki, Y. Wakui, F. Mizukami, T.M. Suzuki, Fabrication of Hydrogen-Permeable Composite Membranes Packed with Palladium Nanoparticles, Advanced Materials, 18 (2006) 630-632.

[45] D.A. Pacheco Tanaka, M.A. Llosa Tanco, J. Okazaki, Y. Wakui, F. Mizukami, T.M. Suzuki, Preparation of "pore-fill" type Pd–YSZ–γ-Al2O3 composite membrane supported on α-Al2O3 tube for hydrogen separation, Journal of Membrane Science, 320 (2008) 436-441.

[46] E. Fernandez, A. Helmi, J.A. Medrano, K. Coenen, A. Arratibel, J. Melendez, N.C.A. de Nooijer, V. Spallina, J.L. Viviente, J. Zuñiga, M. van Sint Annaland, D.A. Pacheco Tanaka, F. Gallucci, Palladium based membranes and membrane reactors for hydrogen production and purification: An overview of research activities at Tecnalia and TU/e, International Journal of Hydrogen Energy, 42 (2017) 13763-13776.

[47] G. Straczewski, J. Völler-Blumenroth, H. Beyer, P. Pfeifer, M. Steffen, I. Felden, A. Heinzel, M. Wessling, R. Dittmeyer, Development of thin palladium membranes supported on large porous 310L tubes for a steam reformer operated with gas-to-liquid fuel, Chemical Engineering and Processing: Process Intensification, 81 (2014) 13-23.

[48] V. Höllein, M. Thornton, P. Quicker, R. Dittmeyer, Preparation and characterization of palladium composite membranes for hydrogen removal in hydrocarbon dehydrogenation membrane reactors, Catalysis Today, 67 (2001) 33-42.

[49] Y. Huang, R. Dittmeyer, Preparation of thin palladium membranes on a porous support with rough surface, Journal of Membrane Science, 302 (2007) 160-170.

[50] H. Lim, S.T. Oyama, Hydrogen selective thin palladium–copper composite membranes on alumina supports, Journal of Membrane Science, 378 (2011) 179-185.

[51] M. Pujari, A. Agarwal, R. Uppaluri, A. Verma, Role of electroless nickel diffusion barrier on the combinatorial plating characteristics of dense Pd/Ni/PSS composite membranes, Applied Surface Science, 305 (2014) 658-664.

[52] I.P. Mardilovich, B. Castro-Dominguez, N.K. Kazantzis, T. Wu, Y.H. Ma, A comprehensive performance assessment study of pilot-scale Pd and Pd/alloy membranes under extended coal-derived syngas atmosphere testing, International Journal of Hydrogen Energy, 40 (2015) 6107-6117.

[53] Y.-H. Chi, J.-J. Lin, Y.-L. Lin, C.-C. Yang, J.-H. Huang, Influence of the rotation rate of porous stainless steel tubes on electroless palladium deposition, Journal of Membrane Science, 475 (2015) 259-265.

[54] C.-H. Kim, J.-Y. Han, N.-C. Kim, S.-K. Ryi, D.-W. Kim, Characteristics of dense palladium alloy membranes formed by nano-scale nucleation and lateral growth, Journal of Membrane Science, 502 (2016) 57-64.

[55] G. Fagerlund, Determination of specific surface by the BET method, Matériaux et Construction, 6 (1973) 239-245.

[56] S. Brunauer, P.H. Emmett, E. Teller, Adsorption of Gases in Multimolecular Layers, Journal of the American Chemical Society, 60 (1938) 309-319.

[57] E.P. Barrett, L.G. Joyner, P.P. Halenda, The Determination of Pore Volume and Area Distributions in Porous Substances. I. Computations from Nitrogen Isotherms, Journal of the American Chemical Society, 73 (1951) 373-380.

[58] E. Jakobs, W.J. Koros, Ceramic membrane characterization via the bubble point technique, Journal of Membrane Science, 124 (1997) 149-159.

[59] F. Guazzone, E.E. Engwall, Y.H. Ma, Effects of surface activity, defects and mass transfer on hydrogen permeance and n-value in composite palladium-porous stainless steel membranes, Catalysis Today, 118 (2006) 24-31.

[60] R. Bhandari, Y.H. Ma, Pd–Ag membrane synthesis: The electroless and electro-plating conditions and their effect on the deposits morphology, Journal of Membrane Science, 334 (2009) 50-63.

[61] V. Jayaraman, Y.S. Lin, M. Pakala, R.Y. Lin, Fabrication of ultrathin metallic membranes on ceramic supports by sputter deposition, Journal of Membrane Science, 99 (1995) 89-100.

[62] S. Yan, H. Maeda, K. Kusakabe, S. Morooka, Thin Palladium Membrane Formed in Support Pores by Metal-Organic Chemical Vapor Deposition Method and Application to Hydrogen Separation, Industrial & Engineering Chemistry Research, 33 (1994) 616-622.

[63] A. Arratibel, U. Astobieta Urigüen, D. Tanaka, M. Annaland, F. Gallucci, N2, He and CO2 diffusion mechanism through nanoporous YSZ/γ-Al2O3 layers and their use in a pore-filled membrane for hydrogen membrane reactors, 2015.

[64] J. Kim, Y.S. Lin, Synthesis and oxygen-permeation properties of thin YSZ/Pd composite membranes, AIChE Journal, 46 (2000) 1521-1529.

[65] S.N. Paglieri, K.Y. Foo, J.D. Way, J.P. Collins, D.L. Harper-Nixon, A New Preparation Technique for Pd/Alumina Membranes with Enhanced High-Temperature Stability, Industrial & Engineering Chemistry Research, 38 (1999) 1925-1936.

[66] M.L. Bosko, E.A. Lombardo, L.M. Cornaglia, The effect of electroless plating time on the morphology, alloy formation and H2 transport properties of Pd–Ag composite membranes, International Journal of Hydrogen Energy, 36 (2011) 4068-4078.

[67] U. Savitha, G. Jagan Reddy, A. Venkataramana, A. Sambasiva Rao, A.A. Gokhale, M. Sundararaman, Chemical analysis, structure and mechanical properties of discrete and compositionally graded SS316–IN625 dual materials, Materials Science and Engineering: A, 647 (2015) 344-352.

[68] D. Kuscer, I. Bantan, M. Hrovat, B. Malič, The microstructure, coefficient of thermal expansion and flexural strength of cordierite ceramics prepared from alumina with different particle sizes, Journal of the European Ceramic Society, 37 (2017) 739-746.

[69] C. Sadik, I.-E.E. Amrani, A. Albizane, Processing and characterization of alumina–mullite ceramics, Journal of Asian Ceramic Societies, 2 (2014) 310-316.

[70] C.K. Srikanth, P. Jeevanandam, Comparison of galvanic displacement and electroless methods for deposition of gold nanoparticles on synthetic calcite, Bulletin of Materials Science, 35 (2012) 939-946.

[71] H.O. Ali, I.R.A. Christie, A review of electroless gold deposition processes, Gold Bulletin, 17 (1984) 118-127.

[72] J. Melendez, N. de Nooijer, K. Coenen, E. Fernandez, J.L. Viviente, M. van Sint Annaland, P.L. Arias, D.A.P. Tanaka, F. Gallucci, Effect of Au addition on hydrogen permeation and the resistance to H2S on Pd-Ag alloy membranes, Journal of Membrane Science, 542 (2017) 329-341.

[73] D.A. Pacheco Tanaka, M.A. Llosa Tanco, S.-i. Niwa, Y. Wakui, F. Mizukami, T. Namba, T.M. Suzuki, Preparation of palladium and silver alloy membrane on a

porous α-alumina tube via simultaneous electroless plating, Journal of Membrane Science, 247 (2005) 21-27.

[74] A. Arratibel, A. Pacheco Tanaka, I. Laso, M. van Sint Annaland, F. Gallucci, Development of Pd-based double-skinned membranes for hydrogen production in fluidized bed membrane reactors, Journal of Membrane Science, 550 (2018) 536-544.

[75] Y. Guo, H. Wu, X. Fan, L. Zhou, Q. Chen, Palladium composite membrane fabricated on rough porous alumina tube without intermediate layer for hydrogen separation, International Journal of Hydrogen Energy, 42 (2017) 9958-9965.

[76] H.W. Abu El Hawa, S.N. Paglieri, C.C. Morris, A. Harale, J. Douglas Way, Identification of thermally stable Pd-alloy composite membranes for high temperature applications, Journal of Membrane Science, 466 (2014) 151-160.

[77] D. Yepes, L.M. Cornaglia, S. Irusta, E.A. Lombardo, Different oxides used as diffusion barriers in composite hydrogen permeable membranes, Journal of Membrane Science, 274 (2006) 92-101.

Chapter 3

Hydrogen Separation: Optimization of Membrane Separator Design

Abstract

This chapter discusses the design and optimization of membrane separator with baffles to determine the hydrogen separation efficiency of self-supported Pd-Ag membranes. Separation of hydrogen with high purity as well high recovery is a challenging task. Pd-Ag membranes can achieve both provided the membrane surface is non-porous, surface inhibition is negligible and a high H_2 partial pressure difference across membrane is maintained. However, it was observed that hydrogen partial pressure not only changes across the length of membrane but also changes radially along the length of separator. Therefore, membrane separator with three longitudinal baffles arranged in zigzag fashion inside the separator was devised. Gas permeation studies were carried out using $50H_2$:$50N_2$ (v/v) feed composition. The final arrangement was tested using a mixture composition of $50H_2$:$30N_2$:$18CO_2$:2CO (v/v) that simulates a synthetic reformate mixture from methanol steam reforming.

Hydrogen permeation was quantified through single membrane at different positions inside the separator. With this study multiple membrane arrangements were identified to optimize hydrogen flux from a multi-pass high throughput membrane separator unit. Consequently, flow dynamics inside the reactor was simulated using ANSYS 14.5 under

similar conditions as that of gas permeation studies performed. An optimal arrangement identified 33% enhancement in hydrogen recovery with multi-pass in comparison to single pass. Further, with the optimal membrane arrangement in a multi-pass membrane separator, the performance of supported Pd-Ag membranes was also compared.

3.1 Introduction

Membrane separator is principally a purifier that is used to separate hydrogen from various components of reaction products such as CO_2, CH_4, CO, unreacted CH_3OH and H_2O. A critical parameter that is required to be optimized from a membrane separator is hydrogen recovery. Hydrogen recovery through membrane mainly depends on trans-membrane hydrogen partial pressure, temperature, competitive adsorption of different species present in the mixture and concentration polarization. For high hydrogen selective membranes, the continuous permeation of hydrogen will essentially develop a layer of non-permeable gases present in the mixture, which acts as a barrier. This barrier is often termed as concentration polarization. Hence, in order to obtain maximum hydrogen recovery, separator design can be developed which minimizes the occurrence of concentration polarization and competitive adsorption of different species on membrane surface. One of the typical ways to minimize both is sequential integration of reaction assembly in series with the membrane separation assembly. Sequential integration provides the benefit of removing the excess steam and unreacted methanol before the gases produced by the reaction contact with the membrane. Such segregation allows independent control of temperature for both reaction and membrane end but makes the system bulky.

Using Pd-Ag membranes for hydrogen separation, this chapter discusses the role of separator design and membrane arrangements to improve hydrogen recovery from the synthetic mixtures gases (without methanol and water). Hence, the results can also be seen as an output of sequentially integrated membrane with reaction assembly as methanol and water vapour is separated. In literature, studies on hydrogen permeation through dense Pd-Ag membranes are widely reported [1-7]. The flux of hydrogen permeating through the membrane (j_{H2}) is proportional to hydrogen partial pressure difference and inversely proportional to the thickness (δ) of membrane layer as shown in equation 3.1. The proportionality constant is the membrane permeability (Pe).

$$j_{H_2} = \frac{Pe}{\delta}\left(p^n_{H_2,\,retentate} - p^n_{H_2,\,permeate} \right) \tag{3.1}$$

According to Sieverts law, if the diffusion of atomic hydrogen through the metal bulk of the membrane is the rate-determining step and hydrogen concentration in the Pd lattice (H/Pd) is lower than 1, the value of exponent, n, is 0.5 [8, 9]. In literature, slight deviation in the n value from 0.5 to 1 is reported for mixture gases [7, 10, 11]. This is mostly attributed to decrease in hydrogen flux due to the following reasons: i) competitive inhibition in the presence of other gases such as CO and CO_2 blocking hydrogen adsorption sites [2, 10] and ii) decrease in hydrogen permeability due to concentration polarization [10, 12, 13]. Inhibition of hydrogen permeation by the CO and CO_2 can be minimized at higher temperatures (≥ 673 K), as was also observed in our earlier study [14]. However, in concentration polarization, a concentration boundary layer develops along the membrane surface due to accumulation of less permeable species. This leads to decrease in hydrogen permeation due to extra resistance [12, 13, 15, 16]. Though

increasing the feed flow rate can help in minimizing the concentration polarization, a decrease in contact time with an increase in flow rate will drastically reduce the permeate H_2 recovery [2, 17, 18]. Introduction of sweep gas on the permeate side therefore is also reported in the literature to reduce the concentration polarization [19-22]. It is found that sweep gas flow rate (co-current or counter-current) lowers the hydrogen partial pressure on the permeate side which increases the trans-membrane pressure difference and hence increases the hydrogen flux. However, beyond a critical sweep gas velocity, both H_2 flux and H_2 recovery become constant, and sweep gas plays only a marginal role in improving hydrogen permeation [23, 24]. Recently, baffles were used to minimize the concentration polarization [18, 23, 25-29]. Mori et al. [29] investigated reactors with different diameters rand reactors with baffle plates to reduce the concentration polarization. It was reported that an increase in linear velocity of gas flow could reduce the concentration polarization due to decrease in contact time. This can be achieved by either reducing the diameter of the reactor or with baffle. The use of baffle was found to be more effective [29]. Chen et al. [18, 23, 25] have numerically investigated the effect of baffle location, baffle pattern and baffle diameter to shell diameter ratio on hydrogen separation through Pd membrane in the presence of sweep gas. Noticeable improvement in hydrogen recovery using one axial baffle around a single membrane was observed. However, hydrogen recovery was found not to increase proportionally with increase in the number of baffles around the membrane. Apart from these studies, baffle inserted inside membranes [26, 28] and slit-type baffles incorporates on the surface of the membrane [27] have also been reported to improve flux as a result of intense fluctuations of local wall velocity and wall shear stress. It becomes clear from these studies that with a suitable reactor configuration using

baffles, concentration polarization can be minimized that can result in higher hydrogen flux.

In all the above-reported studies, baffles are placed along the length of the membrane which effectively reduces the diameter of the separator and generates instabilities which start at the baffle tip. This baffle-generated instability/turbulence reduces the thickness of concentration boundary layer by increasing mixing and minimizes the effect of concentration polarization. However, most of these studies are based on numerical approach and reported for single membrane in a relatively small diameter system while extensive experimental data are missing. Further, no study is reported for longitudinal baffle arrangements in a large diameter system, which is inevitable for high throughput system due to the requirement of a large number of membrane tubes. The use of longitudinal baffle not only changes the diameter of the separator and hence enhances mixing, but also provides flexibility for multi-pass membrane separator system. This multi-pass membrane arrangement system can provide better control on hydrogen partial pressure in each pass by varying the number of membranes and hence can significantly increase the hydrogen recovery. With the aforementioned hypothesis, in the present chapter experimental and simulation studies are reported for a membrane separator system with and without longitudinal baffle assembly. Initially, experiments are performed without baffle with a single membrane to determine the maximum hydrogen flux and recovery for a binary gas mixture at varying temperature and pressure conditions. Thereafter, experiments are performed with three longitudinally baffles (which provide four passes) arranging the single membrane at different locations to find the effect of location on permeate flux in a large diameter system. Further, experiments

are performed with and without baffle with multiple membranes, arranging the membranes at different locations inside the separator, to find the most effective membrane assembly which provides high hydrogen recovery and flux. Computational fluid dynamics (CFD) simulations are performed to understand the effect of baffles on gas velocity and flow path. Finally, performance of single and multiple membrane separators with and without baffles are compared to quantify the effect of baffles on hydrogen flux and recovery.

3.2 Literature review of gas separation studies using Pd-based membranes

Hydrogen separation from mixtures gases has been widely studied in order to determine the hydrogen permeation rate through the membrane in the presence of other gas components. The permeation performance depends on hydrogen selectivity of the membrane and hydrogen permeation in the presence of other gas components. Hence, hydrogen permeation at varying temperatures, pressures, feed composition and sweep gases are widely reported.

Cheng et al. [30] reported the performance of palladium membrane using commercial alumina as support for permeation of single gas and town gas mixture which consist of 49% H_2, 28.5%CH_4, 19.5% CO_2 and 3% CO. Hydrogen flux in the mixture was reported to be less than $1/5^{th}$ of that observed for pure gas permeation of hydrogen. Decrease in gas permeation was due to CO blocking the hydrogen adsorption and dissociation sites, as also reported by Amandusson et al. [31]. It was also reported that under certain conditions, carbon dioxide reacts with hydrogen on the palladium membrane to form

more carbon monoxide and water. However, the membrane did not suffer any irreversible damage with repeated separation and pure hydrogen permeation conducted alternately. Lowered hydrogen flux also caused decrease in hydrogen purity, with CO concentration in permeate ranging from 0.03–0.8%.

Sanchez et al. [32] performed separation of syngas synthesized from gasification of coal, biomass or wastes using a Pd membrane (OD = 2.54 cm, L = 15 cm) over 593–873 K and 0.15–1.2 MPa. Three gas compositions were studied: (i) 63.9% N_2, 17.2% H_2 and 18.9% CO, (ii) 69.8% N_2, 25% H_2 and 5.2% CO, and (iii) a synthetic unconverted shift gas mixture with 17% H_2, 19%CO, 7%CO_2 and 57% H_2O. It was reported that at feed pressures above 150 kPa all hydrogen was able to permeate through the membrane. An increase in permeability from 0.153 $mol.m^{-2}s^{-1}$ at 593 K to 0.215 $mol.m^{-2}s^{-1}$ at 723 K was reported because the reduction in exothermic hydrogen adsorption on palladium at high temperatures was dominated by increase in the rate of diffusion. Presence of N_2 was reported to decrease H_2 permeation flux in H_2/N_2 mixtures due to concentration polarization and hydrogen depletion along the membrane. Presence of steam also caused lesser stability in hydrogen permeation due to axial and longitudinal concentration gradients. Carbon monoxide caused severe deactivation of palladium-based membranes due to competitive adsorption. However, at higher temperatures inhibition was milder as permeation flux was observed to be 0.022 mol m^{-2} s^{-1} at 593 K and 0.040 mol m^{-2} s^{-1} at 723 K. H_2 recovery was reported to be much smaller, 47% at 11.5 kPa (feed pressure 1 MPa), with simultaneous presence of N_2, CO_2, steam and CO compared to pure H_2 permeation, 100% at 723 K and driving force 6.8 $kPa^{0.5}$ (feed pressure 10 kPa).

Augustine et al. [17] studied palladium supported on Inconel using three gas mixtures: 61.7% H_2 and 38.3% He (mixture A); 61.7% H_2 and 38.3% CO_2 (mixture B); 61.7% H_2, 37.1% CO_2 and 1.2% CO (mixture C) using reaction pressure 14.4 bar and temperature 500°C. At GHSV exceeding 30,000 h^{-1} and 14.4 bar feed pressure, hydrogen flux was reported 98% of the pure hydrogen flux for mixture A, 76% for mixture B and 74% for mixture C. With mixture B, decrease in hydrogen permeation with the presence of CO_2 was reported to occur due to boundary layer resistance in addition to CO_2 inhibitory effect. Further, increase in temperature did not result in any change in hydrogen permeation in the presence of CO_2. Contrary to this, presence of CO using mixture C was reported to immensely affect hydrogen permeation behavior. They reported that hydrogen flux at 350°C was 65% of the pure hydrogen flux and increased to 74% at 500°C. Hence, strong inhibitory effect of CO was reported at lower temperatures.

Gallucci et al. [2] investigated the surface effects of N_2, Ar, CO and CO_2 on hydrogen permeation through Pd membrane at temperature 250–450°C and 2–3.5 bar. It was suggested that a long term permeation test (>200 h) is necessary to find stationary value of the hydrogen permeation flux as a non-constant hydrogen flux through Pd is always reported in literature (Dittmeyer et al.[33] , Mardilovich et al.[34] and Lessing et al. [35]). Dilution of H_2 in feed causes decrease in H_2 permeation rate and so % H_2 decreases. At low temperatures (<350°C), strong interactions between CO and palladium atoms (surface effect) were reported which caused some induced modifications on the surface leading to nonlinear slope of hydrogen flux in contrast to H_2/N_2. High temperatures result in less pronounced surface effects of CO.

Hou and Hughes [36] evaluated the effect of external mass transfer, competitive adsorption and coking on Pd/Ag supported on alumina at 275–450°C and pressure of 4 bar. Ratios of the experimental hydrogen flow (F_{exp}) to the predicted H_2 flow ($F_{predicted}$) were plotted to give a measure of the effects of competitive adsorption of other species with hydrogen on hydrogen permeation through the membrane. Nitrogen was observed to have negligible adsorption effect, while 1% steam was observed to decrease permeation by 60%, 1% CO_2 reduces H_2 permeation by 10% and 1% CO decreases permeation by 40%. However these negative effects decrease with increase in temperature from 350–450°C.

3.3 Experimental and simulation details

All the experiments were performed using 100 µm thick, 15.2 cm^2 area self-supported dense commercial Pd-Ag membranes, as they give no additional resistance to permeation. They also avoid the formation of micro-cracks on the metallic surfaces. These membranes were supplied by REB Research & Consultancy®, USA having tube outer diameter of 1/8 inch with one end closed and the other bonded to a metal stub that could be connected with Swagelok® fittings to the reactor as shown in Fig. 3.1.

Fig. 3.1 Self-supported Pd-Ag membrane connected to the reactor

Initial membrane surface characterization studies were performed with field emission scanning electron microscope (FESEM) to measure the thickness and observe the surface morphology. Elemental composition of the membrane film was determined by the energy dispersive X-ray spectroscopy (EDX). Fig. 3.2 shows the schematic of multi-pass membrane separator used in the current study. The inner diameter of the membrane separator was 14.5 cm and height was 40 cm. The separator was made of SS310 so that it can safely be operated at high temperature. A large volume reactor was designed to accommodate three baffles of 30 cm length each. Two baffles were assembled closer to the edges of the reactor vessel while one baffle was affixed at the center of the tube sheet at the top of the reactor. Baffles were designed of same material SS 310 as the reactor.

Although the reactor can accommodate 10 membrane tubes, in the current study a maximum of four self-supported Pd-Ag membrane tubes from REB Research and Consultancy® USA were used. These membranes were 6 in. long, 1/8 in. diameter with Pd-Ag layer thickness of 0.1 mm and composition 78.65% Pd and 21.35% Ag. To strengthen the membrane tube, the manufacturer has inserted a spring that prevents collapse under high pressure. These membranes are dead-end type membranes with one end welded and the other end brazed to a SS stub by the manufacturer. The SS stub can be fitted to the reactor using gas tight Swagelok® fittings.

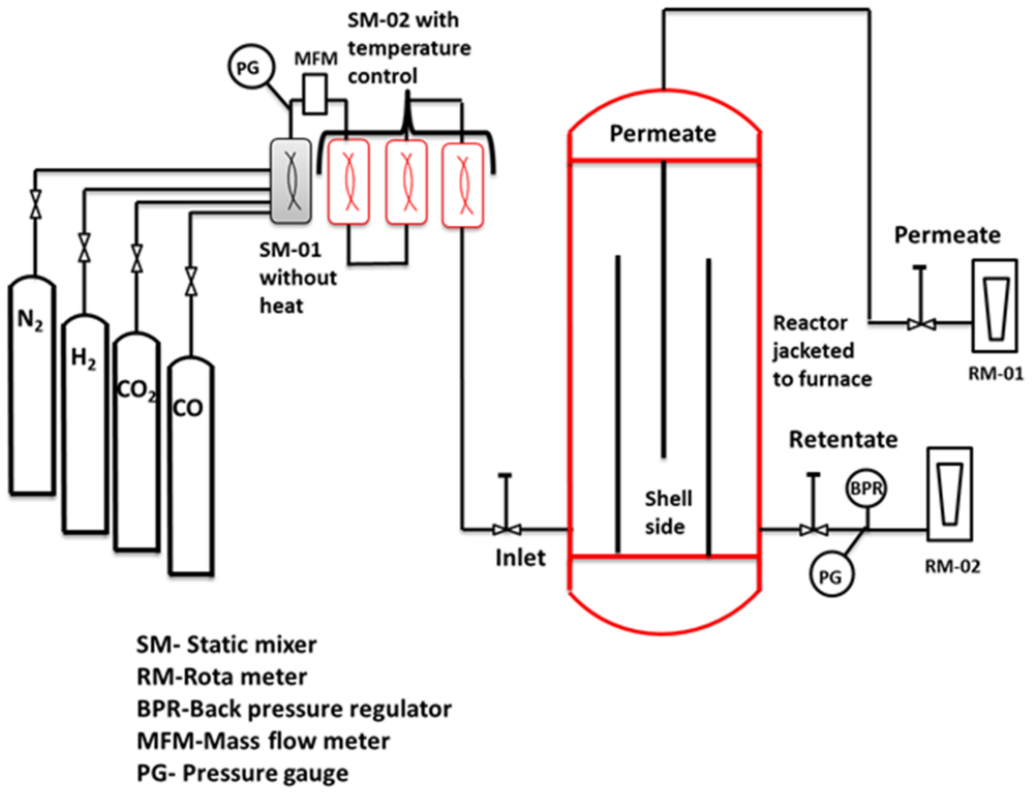

Fig. 3.2 Schematic of multi-pass membrane separator

Preliminary permeation studies were performed at temperatures ranging from 623–723 K, inlet feed rate of 0.3–1 LPM and gauge pressure ranging from 2.5–3.5 bar with no sweep gas. The optimized condition from the single membrane performance was then studied to observe the hydrogen separation behavior for multiple membranes (4 membranes in number) with composition $50H_2$:$50N_2$ v/v. Using baffles, different membrane arrangements were tested to find the best arrangement for enhanced H_2 recovery and flux. To observe any effect of CO/CO_2 inhibitions, optimal membrane arrangement, performance was further studied with synthetic reformate mixture composition $50H_2$:$30N_2$:$18CO_2$:2CO by volume. The volume fractions of 18 CO_2 v/v and 2 CO v/v were taken to simulate a reformate fraction on dry basis. For each experiment, continuous

analysis of feed, retentate and permeate side gases were performed by using gas chromatography (GC) with a series arrangement of column porapak Q and molecular sieve. Thermal conductivity detector was used for this purpose with argon as carrier gas. For all the cases, the performance of membrane was quantified based on hydrogen flux on the permeate side (equation 3.1), % H_2 recovery (equation 3.2) and gas hourly space velocity (equation 3.3).

$$\textbf{Hydrogen Recovery} = \frac{F_{H2,\,permeate}}{\left(F_{H2,\,permeate} + F_{H2,retentate}\right)} \tag{3.2}$$

$$\textbf{GHSV}(h^{-1}) = \frac{\textbf{volumetric flow rate}}{\textbf{reactor volume}} \tag{3.3}$$

Equation 3.2 defines hydrogen recovered at the permeate side which is the ratio of mass flow rate of hydrogen on permeate side $F_{H_2,permeate}$ to the total hydrogen in feed.

3.3.1 Numerical Simulation

The flow dynamics in membrane separator were simulated by using commercial software ANSYS 14.5®. The simulation geometry was kept exactly same as of the experimental setup. Mesh was created using Gambit® 2.4.6 without baffle and with baffle arrangements. Unsteady state simulations are performed with pure hydrogen gas as the feed. Continuity, momentum and energy equations (shown in Table 3.1) are solved to find the temperature and velocity profile inside the separator.

Table 3.1 Governing equations for numerical simulation of the membrane separator

Governing equation	
Continuity equation	$\frac{\partial}{\partial t}(\rho)+\nabla.(\rho\vec{v})=0$
Momentum equation	$\frac{\partial}{\partial t}(\rho\vec{v})+\nabla.(\rho\vec{v}\vec{v})=-\nabla p+\nabla.\vec{\vec{\tau}}+\rho g$
Energy equation	$\frac{\partial}{\partial t}(\rho h)+\nabla.(\rho h\vec{v})=\nabla.(k\nabla T)$

To find the flow path line, discrete phase model (DPM) simulations are performed where neutrally buoyant particles of very small size are injected through the inlet. To achieve a smooth curve, 1000 particles are injected at a given time and their path lines are recorded for both with-baffle and without-baffle case. The detailed simulation parameters are given in Table 3.2. Simulations were performed for 100 s with 75 s time averaging period.

3.4. Membrane preliminary characterization

Initial membrane characterization studies were performed to observe dense surface morphology, thickness and composition of the membrane. Using scanning electron microscopy (SEM) analysis presented in Fig. 3.3a, the thickness of the membrane cross-section was determined to be 0.1mm.

Table 3.2 Outline of simulation parameters and boundary conditions

Simulation Parameters	
Mesh grid size	3x3 mm
Time	Transient
Model	Single phase mixture model Energy On Viscous Laminar
Boundary conditions	Velocity inlet: 0.15 m/s; temperature 300 K Left wall: stationary; No slip; temperature 673 K Right wall: stationary; No slip; temperature 673 K Top wall: stationary; No slip; temperature 500 K Bottom wall: stationary; No slip; temperature 500 K Outlet: Pressure outlet
Fluid	Pure H_2
Pressure–velocity coupling	SIMPLE
Spatial discretization	Gradient: Green–Gauss cell based Pressure: Standard Momentum: Second order upwind Energy: Second order upwind
Time step size (s)	0.00001

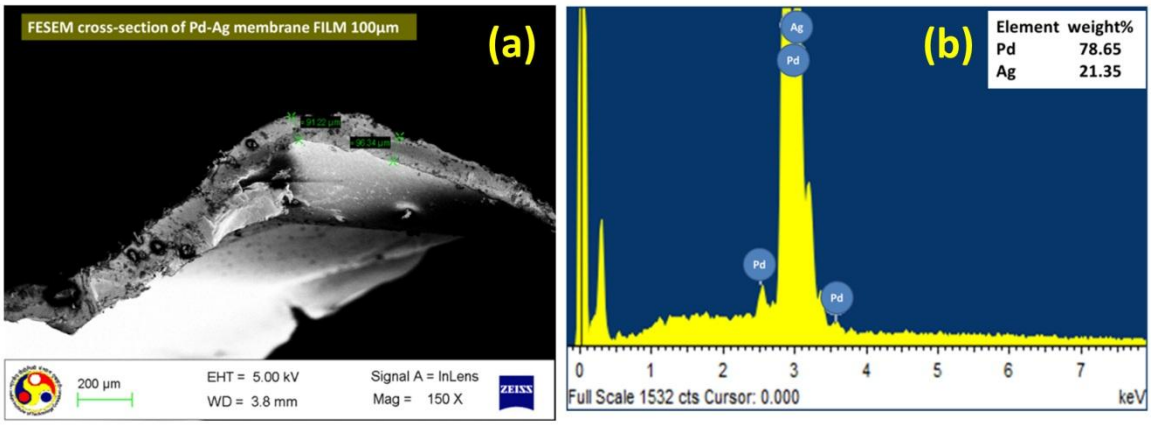

Fig. 3.3 Self-supported Pd-Ag film: a) cross-section with FESEM and b) elemental detection using EDX

The composition of the membrane determined using EDX analysis was 78.65% Pd and 21.35% Ag, as presented in Fig. 3.3b. The dense surface morphology of the Pd-Ag membrane was also observed with FESEM analysis at 3KX followed with maximum resolution up to 18KX as presented in Fig. 3.4a and 3.4b. It was observed that apart from distinct grain boundaries no pinholes were present on the membrane surface.

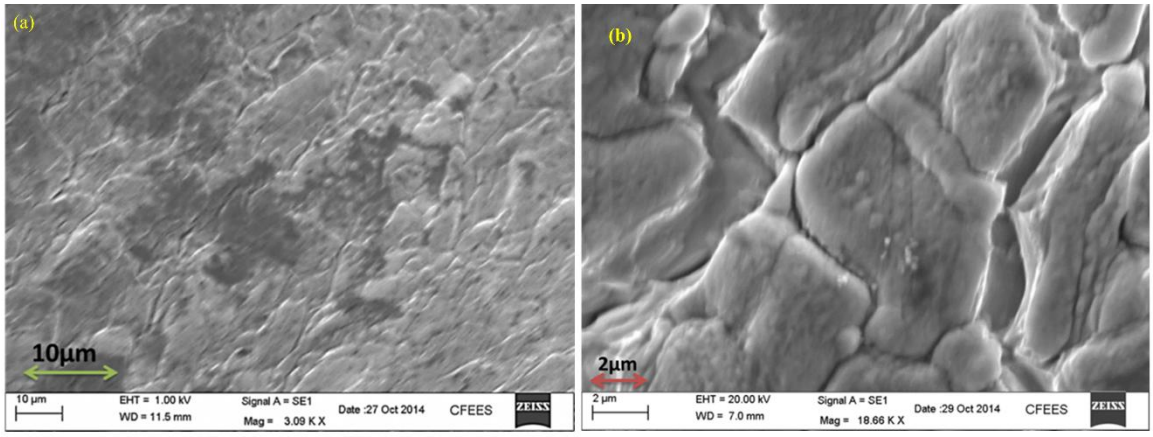

Fig. 3.4 Self-supported Pd-Ag film surface analysis with FESEM: a) at 3KX and b) at 18KX

3.5. Membrane separator

A "multi-pass" membrane separator was designed 'in-house' to study the hydrogen permeation behavior of self-supported Pd-Ag membranes. Initially, for a single membrane, hydrogen permeation studies were performed at different temperatures and pressures using 50 H_2:50 N_2 v/v as feed. Using the same binary gas mixture, experiments were performed to estimate the change in hydrogen recovery with increasing gas-hourly space velocity (GHSV). Further, as the experiments are performed in a relatively larger diameter vessel, effect of membrane position on the hydrogen recovery was studied for single as well as multiple membranes. Flow inside the membrane separator was simulated using commercial software ANSYS 14.5 for two case studies: with and without baffle. The effect of baffles on hydrogen recovery was studied to find the optimal membrane arrangements for larger diameter system. In the last stage, the experiment was performed with mixture gases (H_2, CO_2, CO and N_2) using the best possible membrane arrangement and at the optimized process conditions to find the inhibition effect of CO and CO_2 on hydrogen separation.

3.5.1 Optimization of process conditions

The first stage of hydrogen separation using the multi-pass membrane separator requires process optimization for single membrane. Thermal activation of Pd-Ag membranes was performed in pure H_2 environment for 3–4 hours at 400°C in order to make sure that the surface is clean from any contaminants that may have been introduced during the manufacturing process. Flow stabilization was performed for the system to achieve steady state. Initial experiments were performed with a binary gas mixture in which

hydrogen was diluted with an equal amount of nitrogen, i.e. using a composition $50H_2$:$50N_2$ v/v. The feed composition of $50H_2$:$50N_2$ (v/v) was used in order to simulate 50% by volume of hydrogen mostly present in a typical methanol reformate product stream [2, 12, 37, 38]. Nitrogen was used as a diluent as it causes no inhibition to hydrogen permeation [14, 39]. The same was determined in our previous study where similar permeate flux was observed for pure H_2 and $50H_2$:$50N_2$ for the membranes used in the current work [14, 40]. Therefore, single membrane permeation performance was investigated with $50H_2$:$50N_2$ as feed by increasing the feed pressure from 2 to 3 bar, temperature 623–723 K at a constant inlet feed rate of 0.3 LPM. The permeate side volumetric flow rates of gases were measured by using a soap bubble flow meter. The hydrogen permeate flux was calculated by dividing the permeate flow rate at steady state conditions by the membrane surface area (15.2 cm^2 for single membrane). With hydrogen flux vs. difference in the square root of the partial pressures between retentate and permeate plot, linearity of slope was identified (Fig. 3.5).

The slope of flux versus the difference of square root of the hydrogen partial pressures provides H_2 permeance of the membrane wherein a linear fit of slope with pressure exponent n= 0.5 indicates that bulk diffusion of hydrogen through palladium layer is the rate controlling step. Further, hydrogen permeation not only increases with pressure but also with temperature, as shown in Fig. 3.5. An increase in pressure increases the adsorption of hydrogen on palladium surface and an increase in temperature increases the hydrogen diffusivity through the membrane, and hence both increase the hydrogen flux. Hydrogen flux at all temperatures and 3 bar pressure ranged between 0.095 and 0.13 $mol/m^2.s$.

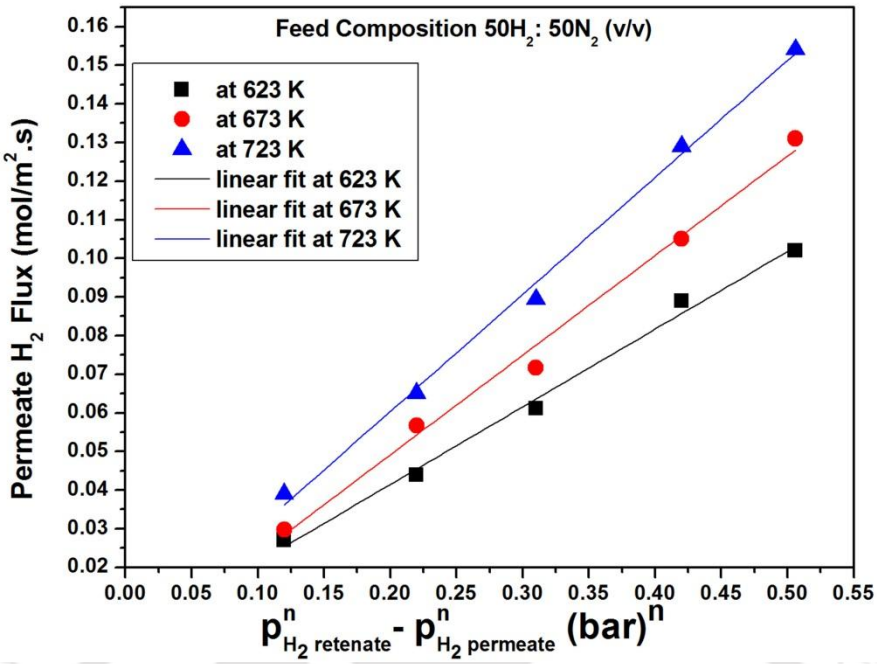

Fig. 3.5 Effect of increasing pressure and temperature on permeate hydrogen flux

Further, at constant temperature (673 K) and pressure (3 bar), the effect of increasing GHSV was investigated as shown in Fig. 3.6.

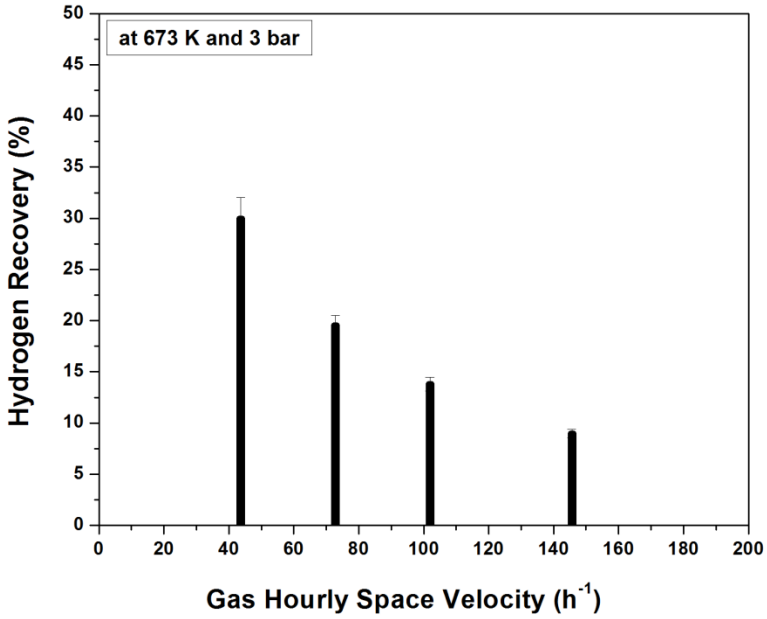

Fig. 3.6 Effect of increasing gas hourly space velocity (GHSV) on hydrogen recovery

Increasing GHSV as shown in equation 3.3, increases the inlet feed rate, which reduces the contact time of gases with the membrane and hence decreases the permeate hydrogen recovery. These results clearly indicate that contacting between feed gas and membrane plays a critical role in hydrogen permeation and it can be modified by controlling the contact time and pattern. The contacting becomes more critical when membrane is used in a large diameter system and/or when several membranes are used for the separation. Therefore, further studies were performed by placing the membrane at different locations inside the membrane separator at a fixed operating condition.

3.5.2 Effect of membrane positioning on single membrane performance: with and without baffle

The overall objective of the study reported in this section was to find the effect of membrane positioning on the hydrogen flux. In contrast to the single-membrane studies of the previous section, where single membrane was located at the outlet position for its process optimization study, the current section investigates the performance of the same single membrane with respect to its location in a large diameter membrane separator. For each test, a single membrane was kept at inlet, center and outlet side individually, one at each time for each cycle. Each cycle refers to heating the system under nitrogen at desired operating conditions, balancing the composition, measuring the H_2 flux obtained at steady state and finally cooling the system to ambient temperature and pressure under continuous nitrogen flow. After the flow was stabilized, the hydrogen permeate flow rate was measured to determine the hydrogen recovery for each membrane position. A schematic representation of each experimental run performed to investigate single

membrane performance at three locations within the shell: inlet, center and outlet, is shown in Fig. 3.7a.

Corresponding to Fig. 3.7a, the hydrogen recovery measured for each membrane position is presented in Fig 3.7b. It can be observed that H_2 recovery without baffle shows a marginal increasing trend from inlet to center while it abruptly declines at the outlet side. This was surprising as the membrane contact area, inlet feed rate, temperature and pressure were same in all the conditions, and hence the only possible reason for such behavior can be the contacting pattern.

To infer on gas flow pattern inside the membrane separator, simulations were performed in ANSYS 14.5 at the same operating conditions as of experiments in an empty separator without membrane. The CFD simulation was performed in 2D. The CFD simulation was performed to study the flow dynamics and to understand effect of baffles on flow profiles. This work presents simulated velocity profiles inside reactor (with and without baffle) performed using ANSYS Fluent under similar operating conditions as that of experiments. Further, no membrane was considered during this simulation. The local velocity around the baffles affect the residence time of gases in that region. Hence the analogy was presented to support the experimental observations with simulated velocity profiles.

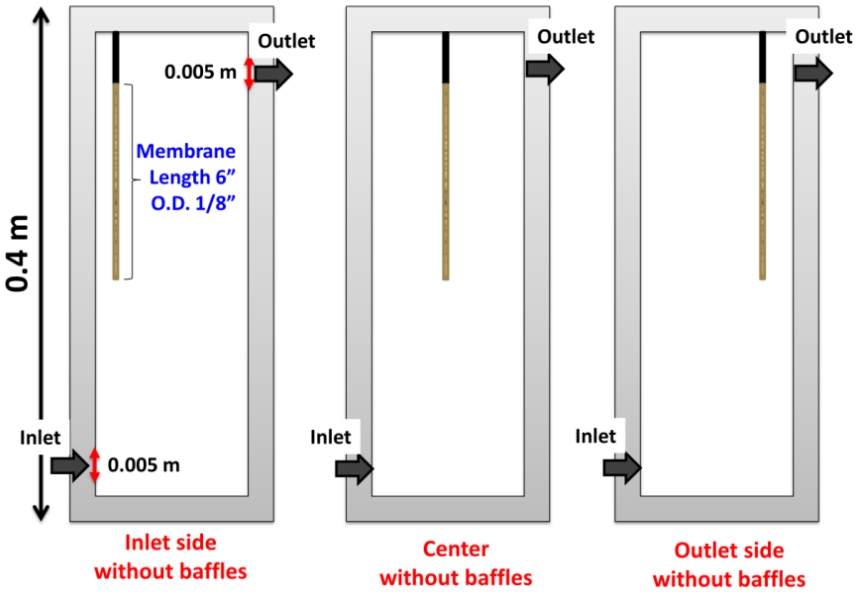

Fig. 3.7a Schematic of single membrane at three locations within the shell: Inlet, center and outlet

Fig. 3.8a and 3.8b show the contour of grid independent axial gas velocity and tracer particle path lines (colored according to time spent by the particle inside the separator) which are injected to find the contacting pattern.

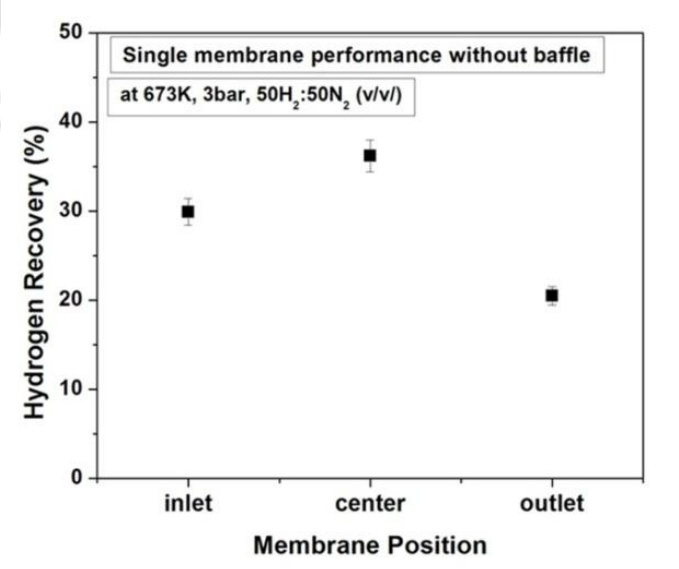

Fig. 3.7b Effect of membrane position on hydrogen recovery

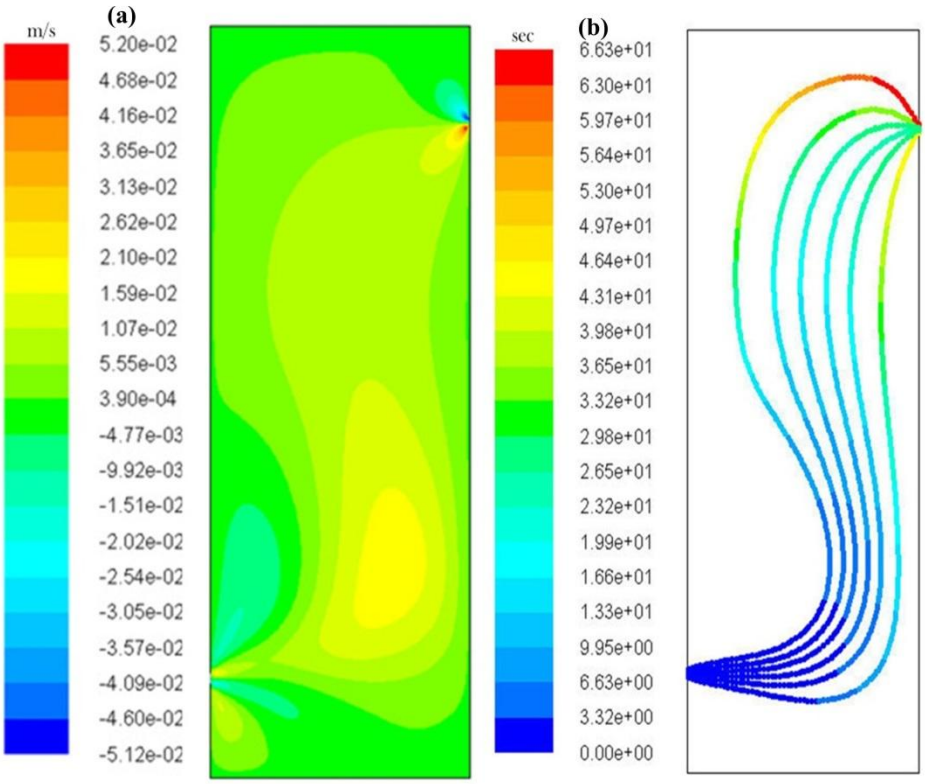

Fig. 3.8 a) Contour of grid independent axial gas velocity and b) tracer particle path lines, obtained from CFD simulations.

Fig. 3.8a and 3.8b clearly indicate that both velocity and gas contact change significantly with change in position. Near the inlet or outlet position, gas contacting with the membrane was observed minimal. . However, at the center better contacting is evident due to the path of gas that showed maximum flow at the center. This resulted in higher hydrogen recovery at the center of the column. To improve the contacting pattern of inlet gas with membrane, baffles are introduced in the longitudinal direction as shown in the schematic Fig. 3.9a. Similar to previous studies, a single membrane is placed at three different locations (inlet, center and outlet) inside the separator in the presence of the baffles.

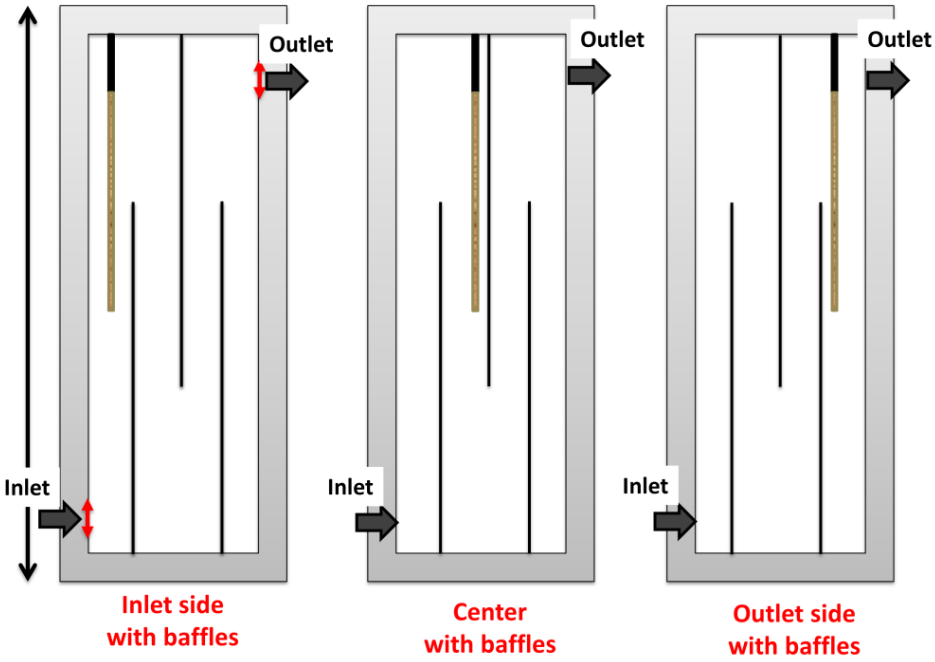

Fig. 3.9a Schematic of single membrane at three locations within the shell: inlet, center and outlet (with baffle)

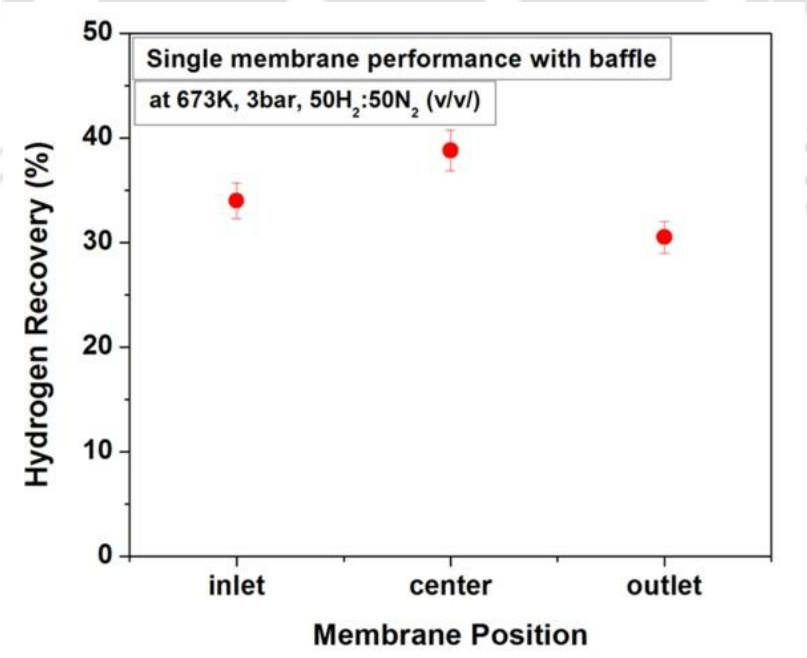

Fig. 3.9b Effect of membrane position on hydrogen recovery with baffle

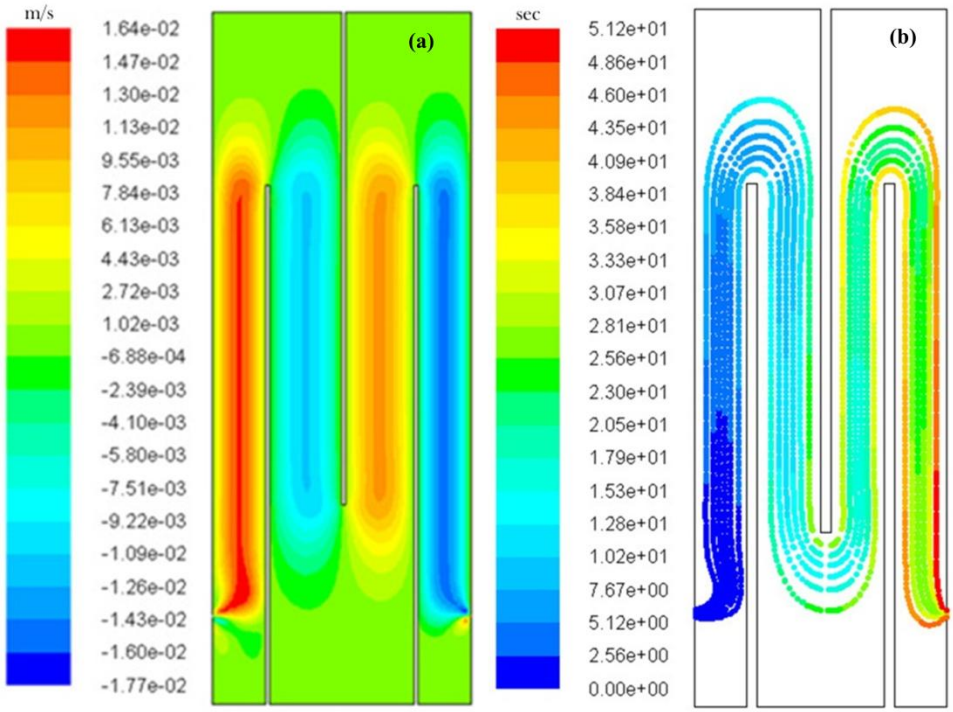

Fig. 3.9 c) Contour of grid independent axial gas velocity with baffle and d) tracer particle path lines with baffle

Fig. 3.9b shows that in the presence of baffles, for each position higher hydrogen recovery was achieved compared to without baffles (see Fig. 3.7b) for the same operating condition. However, even in the presence of baffles, maximum recovery was observed when the membrane was placed at the center location. Further, the recovery at the outlet position was marginally lower than the inlet position. This was mainly because of better contacting between the gas and membrane in the presence of baffles, which is shown in Fig. 3.9c and Fig. 3.9d. It can be observed that at the inlet and outlet, the velocity of the gas is marginally higher due to higher pressure gradient, and hence the residence times of tracer at these zones are lower compared to that at the center of the column. Therefore, higher recovery was observed at the center compared to the inlet and outlet zones. However, in each case the recovery in the presence of baffles was significantly higher

than without baffles. The maximum flux achieved experimentally using a single membrane at center position was approximately 0.035 mol/m^2.s (corresponding to 36% H_2 recovery) without baffle and 0.04 mol/m^2.s (corresponding to 39% H_2 recovery) with baffle at 673 K, 3 bar, inlet feed rate 0.3 LPM and $50H_2$:$50N_2$ v/v feed composition. A comparative chart of this work with reported literature is presented in Table 3.3.

3.5.3 Multi-pass Arrangements Using Multiple Membranes

A major advantage of using "multi-pass" was not only to increase the path length of gases, but also the extent of gas back-mixing caused by the insertion of baffles that improved hydrogen recovery through the membrane. However, this also indicates that due to the same gas back-mixing, contacting between the membrane and gas improved. Therefore, through the same length of membrane tested with and without baffle, the residence time of gases around the membranes improved, resulting in better contacting and thereby higher hydrogen recovery. This resulted in designing different membrane arrangements.

To find the optimal membrane arrangement which can provide maximum hydrogen recovery and flux, six different arrangements were studied as shown in Fig 3.10a. Three baffles were used at different zones inside the shell of the reactor to provide systematic flow direction to inlet gases. In *case I*, all the four membranes are placed at the center of the shell and were separated by a central baffle. In *case II*, two membranes were placed near the inlet and one membrane each was placed at the center and near the outlet. In *case III*, two membranes were placed at the center of the shell and one membrane each at the inlet and at the outlet side. In *case IV*, all the four membranes were uniformly distributed

across the shell while in *case V*, one membrane each was placed at the center and the inlet, whereas two membranes were placed near the outlet. To compare the effect of baffles and membrane arrangements on overall separation, experiments were also performed with four membranes at the center of the shell without having any baffle as shown in *case VI*. It is worthy to note that in the case of a single membrane without baffles, maximum recovery was achieved when the membrane was placed at the center. Hence, *case VI* represents the best possible arrangement in the absence of the baffles.

The performance studies of different arrangements as discussed are presented in Fig. 3.10b. The maximum hydrogen recovery and flux from permeate side was observed for *case I* and minimum was observed for *case VI*. Significant differences in permeate flux and hydrogen recovery were observed between *case II* and *case V* in relation to hydrogen recovery for single membrane which was obtained nearly similar when placed at the inlet and the outlet as shown in Fig. 3.9b.

This is mainly because of partial pressure across the membranes, which changes significantly with change in membrane location in case of multi-pass arrangement. For *case II*, two membranes are placed at the inlet where they come in contact with fresh feed, and hence the separation is more as the partial pressure of hydrogen across these two membranes is higher. However, for *case V*, two membranes are placed at the outlet where the partial pressure of hydrogen across the membranes is lower due to the separation of hydrogen by the membranes placed at the inlet and center of the column. Therefore, these results also suggest that partial pressure across the membrane plays a critical role and can be tuned with suitable membrane and baffle arrangements.

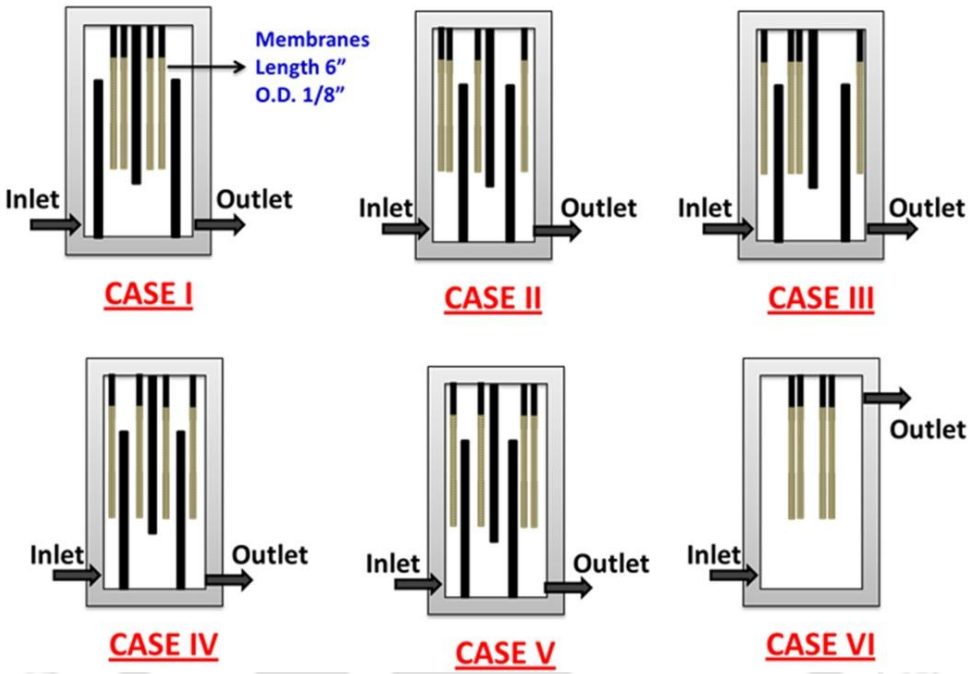

Fig. 3.10a Multi-pass membrane separator: schematic of multiple membrane arrangements with baffle

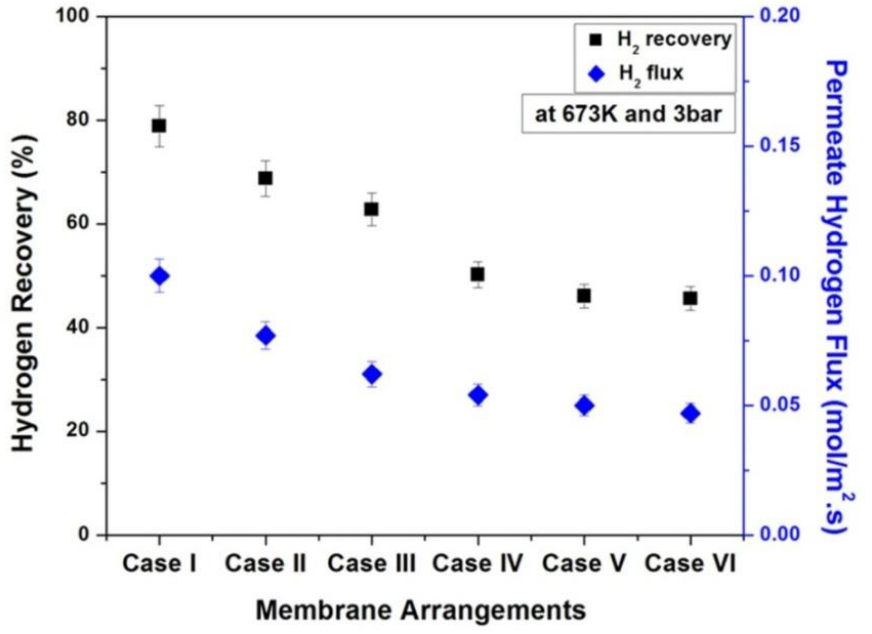

Fig. 3.10b Multi-pass membrane separator: performance of different membrane arrangements on hydrogen recovery

Similar reason is valid for relatively low hydrogen flux and recovery in *case III* compared to *case II*. *Case I* had the maximum hydrogen flux and recovery mainly due to relatively high contact time (low velocity) at the center position of the separator as shown in Fig. 3.9c and d. With the baffle in place, 33% more recovery was found compared to the case when baffles were not present. A direct comparison of single and multiple membrane performance with and without baffles is presented in Fig. 3.11.

For a single membrane, not much difference in H_2 recovery could be witnessed with or without baffles. This is evident because the partial pressure over a single membrane cannot change much with or without baffles and the change in recovery is mainly due to the contacting pattern and time. In case of multiple membranes, when separation study was performed without baffles (*case VI*) hydrogen recovery was 47% in comparison to 79%, observed in *case I* with baffles. Comparing the above inferences, it can be reported that using baffles, a major increase in H_2 recovery from 47% (single pass *case VI*) to 79% (multi-pass *case I*) was witnessed as a result of the huge role played by hydrogen partial pressure inside the shell and the enhanced gas residence time.

Further, in terms of scalability, an increase in the number of membranes did not necessarily increase the hydrogen recovery proportionally. Without baffles, a single membrane at the center of the shell resulted in 36% hydrogen recovery whereas four membranes at the center led to 47% hydrogen recovery (*case VI*). Similarly, using baffles single membrane gave 38% hydrogen recovery while 79% recovery was observed with four membranes. Therefore, the loss in overall hydrogen recovery with baffles was much lesser compared to the loss in recovery without baffles.

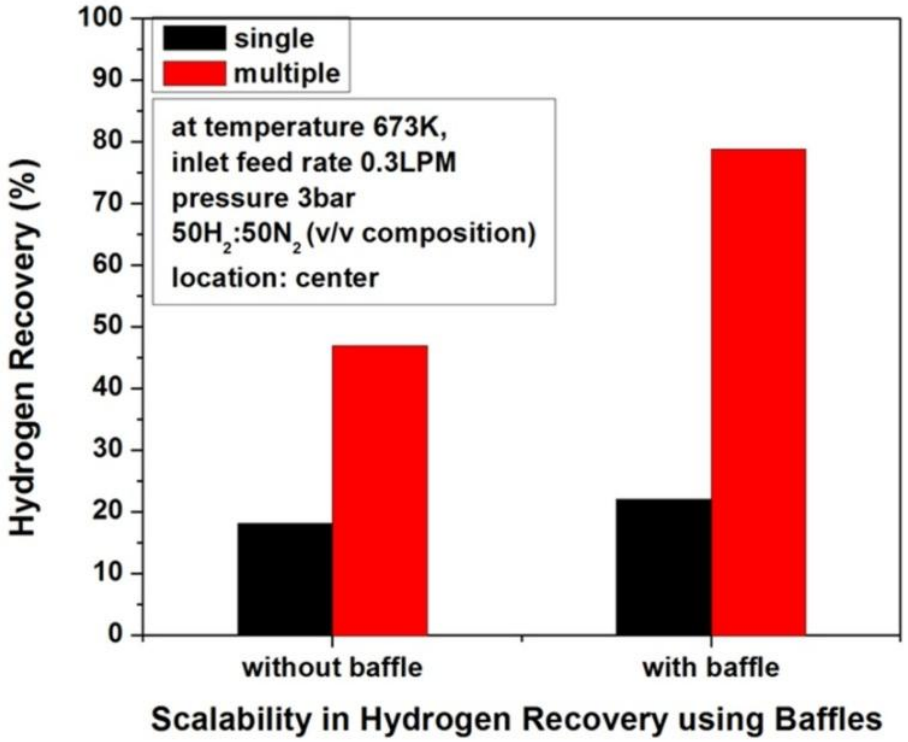

Fig. 3.11 Comparison of single and multiple membrane performance with and without baffle

Hence, it can be stated that a major portion of loss can be recovered using baffles inside a membrane reactor for enhanced hydrogen recovery. Table 3.3 shows the comparison of the results of the current study with the results available in the literature, for synthetic gas mixture as a feed against dense Pd-Ag membranes. However, no literature report was found where the effect of multi-pass was investigated on enhancing hydrogen recovery experimentally. Few simulation-based studies are available wherein the effect of baffles has been reported. Amongst these, Chen et al. [18] reported H_2 recovery up to 37% using radial baffles in their numerical study using Pd/Ag membrane of 20 µm thickness at 10 bar inlet feed pressure. In comparison, a similar trend has also been observed in the current study using longitudinal baffles with maximum hydrogen recovery of 79% using

four self-supported Pd-Ag membrane of 0.1 mm thickness at 3 bar inlet feed pressure, 0.3 LPM inlet feed rate and 673 K temperature.

3.5.4 Mixture composition

From various membrane arrangements studied, the best arrangement (*case I*) was then utilized to investigate the effect of CO and CO_2 on the hydrogen recovery and flux at the same operating condition (673 K, 3 bar) using a mixture gas composition of $50H_2$:$30N_2$:$18CO_2$:2CO by volume. Fig. 3.12 shows a slight reduction in hydrogen permeance with mixture composition; however, no drastic decline was observed.

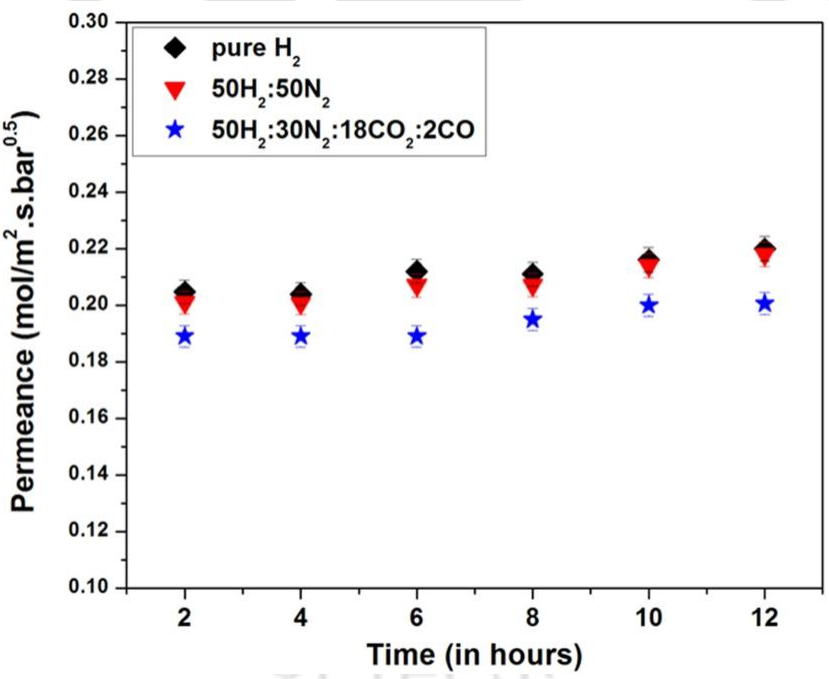

Fig. 3.12 Hydrogen permeance with optimal membrane arrangement using pure H_2, $50H_2$:$50N_2$ and $50H_2$:$30N_2$:$18CO_2$:2CO

Table 3.3 shows a comparative chart of the hydrogen permeance and recovery through the multi-pass membrane separator in comparison to the reported literature. The observed

permeance is akin to the reported literature. Further, what needs to be noted is the hydrogen recovery. It may be suggested that baffles may indeed be used to minimize recovery losses in these systems.

3.6 Comparison of performance of self-supported membrane with prepared supported membranes

A comparative hydrogen flux testing between self and supported Pd membrane without baffles was performed. Preparation and testing of supported membranes was detailed in chapter 2. Fig. 3.13 shows that hydrogen permeation rate of supported Pd membrane was much higher than self-supported Pd. For self-supported membrane thickness of Pd was 0.1 mm because higher thickness gives the necessary mechanical strength to the self-supported membrane. In contrast, the thickness of supported Pd membranes is approximately 30 μm each. Reduced thickness thereby improves flux. At similar trans-membrane hydrogen partial pressure difference, Pd supported on PSS showed the maximum flux. As discussed in the chapter 2, the pore size distribution of PSS was much wider than alumina. Ideally, lower pore size supports are considered viable for faster dense membrane preparation. However, PSS despite having higher pore size gave a significant improvement in hydrogen flux.

3.6.1 Membrane separator with baffle for prepared membranes

In order to observe the effect of baffle, self-supported membrane performance was also observed with the prepared Pd-Ag membranes supported on PSS. Fig. 3.14 shows the increase in hydrogen flux compared to Fig. 3.13 for both self-supported and supported membranes.

Table 3.3 Comparative literature review of membrane as separator

No. of Pd tubes	Feed	Membrane Thickness (µm)	Permeance (mol/m^2.s.Pa)	% H_2 Recovery	H_2 Purity (%)	Ref.
3	$50H_2$/ $50N_2$	84	2.4×10^{-7}	-NA-	-NA-	[32]
-NA-	$17H_2$/ 19CO/ $7CO_2$/ $64N_2$/ 57steam	-na-	1.3×10^{-6}	Below 50%	-NA-	[38]
9	$80H_2$ / $20N_2$	20	4×10^{-8}	10-90%	99.6	[41]
1	$28H_2$/ 4.7CO/ $10CO_2$/ N_2 (balance) / 34.7steam	50	1×10^{-7}	80%	-NA-	[17]
-NA-	$70H_2$/ 18CO/ $12CO_2$	13.8	1.33×10^{-7}	-NA-	-NA-	[29]
-NA-	$50H_2$/ $50N_2$	7.2	4×10^{-7}	18	99.7	[39]
4	$80H_2$ / $20CO_2$	4	1.1×10^{-6}	90	>99.5	[10]
1	$61H_2$/ $37CO_2$/ 1.2CO	10.5	2×10^{-6}	85	97.5	[42]
1	$60H_2$/ $10CH_4$/ $30CO_2$	100	3.5×10^{-7}	7.5	>99	[17]
1	$50H_2$/ $50N_2$	45	1.01×10^{-8}	-NA-	-NA-	[2]
1	$50H_2$/ $50N_2$	60	2.13×10^{-8}	-NA-	-NA-	[43]
1	$80H_2$/ 10CO/ $10N_2$	2.2	7.4×10^{-7}	-NA-	>99	[44]
1	$50H_2$/ 50Ar	1	1.9×10^{-6}	-NA-	-NA-	[45]
1 without baffles	**$50H_2$/ $50N_2$**	**100**	1.13×10^{-6}	**36**	**99.997**	**This work**
1 with baffles	**$50H_2$/ $50N_2$**	**100**	1.29×10^{-6}	**38**	**99.997**	**This work**
4 without baffles	**$50H_2$/ $50N_2$**	**100**	1.61×10^{-6}	**46**	**99.997**	**This work**
4 With baffles (Case 4)	**$50H_2$/ $50N_2$**	**100**	2×10^{-6}	**79**	**99.997**	**This work**
Case 4 With baffles	**$50H_2$: $30N_2$: $18CO_2$: 2CO**	**100**	1.78×10^{-6}	**74.4**	**98 due to CO & CO_2 leak**	**This work**

Moreover, it can further be stated that Pd-Ag supported on PSS was observed to give the best performance as membrane separator both with and without baffles.

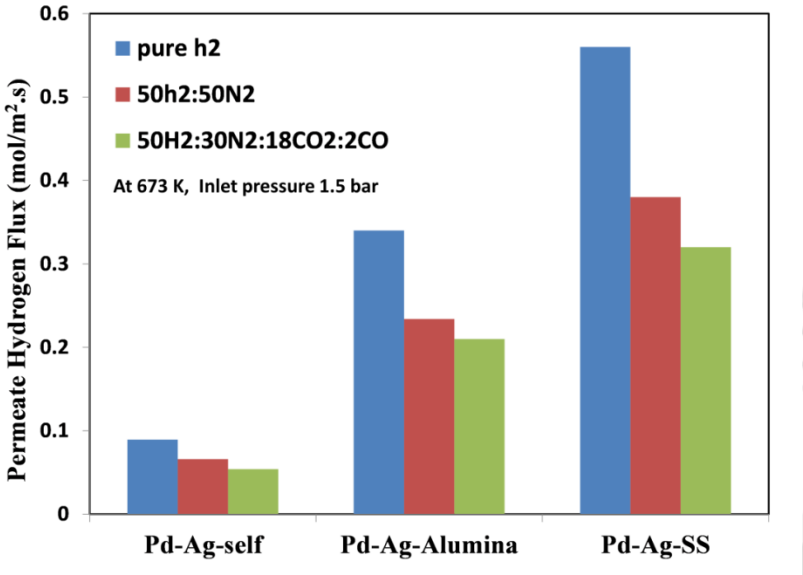

Fig. 3.13 Hydrogen flux comparison between self-supported and supported Pd membranes

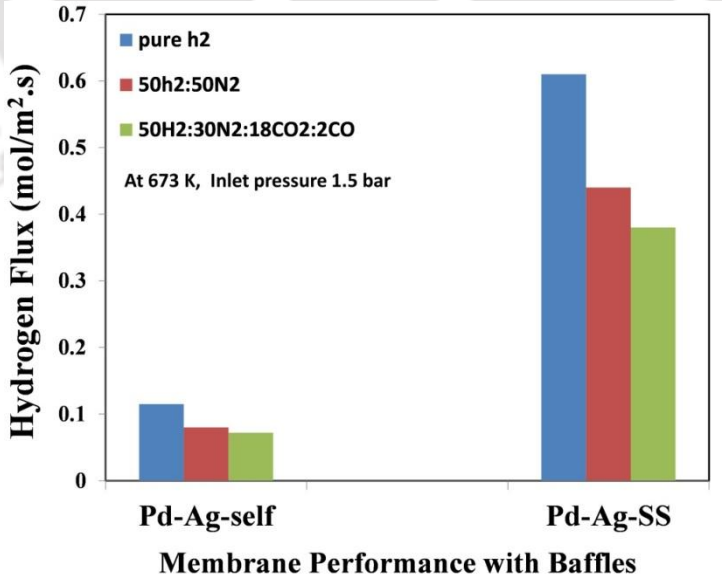

Fig. 3.14 Hydrogen flux comparison between self-supported and PSS supported Pd membranes with baffles

3.5 Summary

In the current study, a 'multi-pass' modular shell and tube based membrane separator was used to optimize the separation performance of 0.1 mm thick self-supported Pd-Ag membranes. The performance of both single as well as multiple membranes (total four in number) was evaluated. The effect of single membrane positioning and multiple membrane arrangements was studied to enhance hydrogen recovery at low pressures. These membrane arrangements were made with the aid of "multi-pass" by placing baffles on the shell-side that would eventually increase the path length of gases, thereby providing higher residence time for effective gas separation. Initially, single membrane gas separation performance optimization was carried out using binary gas, $50H_2$:$50N_2$ (v/v), mixtures.

- Under the optimum operating condition observed, i.e. 673 K temperature and 3 bar pressure, multiple membrane performance was studied by using different arrangements separated with baffles. It was observed that hydrogen recovery changed with different membrane arrangements. This indicates that these arrangements cause the H_2 partial pressure inside the shell to either fall progressively (observed in case II to case IV) or abruptly (observed in case I and VI) thus strongly affecting the hydrogen recovery. The maximum hydrogen recovery (79%) was observed for case I at temperature 673 K, pressure 3 bar, inlet feed rate 0.3 LPM and composition $50H_2$:$50N_2$ v/v. In order to observe the effect of baffles on these membrane performances, both single membrane and multiple membranes (optimal arrangement) were studied without baffles.

- It was observed that for a single membrane only a marginal improvement in hydrogen recovery (2.5–3%) was found in the presence of baffles. In contrast, the performance of multiple membranes showed 46% hydrogen recovery without baffles and 79% with baffles. Therefore, nearly 33% enhancement in hydrogen recovery was observed in the presence of baffles.
- In addition, an important aspect to be noted here is that the loss in hydrogen recovery with multiple membranes was immensely reduced due to the baffles. Lastly, the optimal arrangement was tested using a simulated reformate mixture composition of $50H_2$:$35N_2$:$14CO_2$:3CO by volume at same operating conditions. In this case, a marginal decrease in hydrogen permeance was observed, but no significant inhibition by CO and CO_2 was found.
- Based on the comparison with literature presented in Table 3.3, this study stands at par with other reported works despite a high membrane thickness of 0.1 mm and the lower total surface area available (because of the use of only four membranes). In the presence of baffles, maximum 79% hydrogen was recovered (case I) at 3 bar pressure. Further, due to the increased contact time using baffles under adequate pressures, hydrogen recovery through a membrane reactor can be vastly benefitted. These parameters may aid in achieving targeted scale up for future studies.
- Lastly, membrane performance was also compared between self-supported and the in-house prepared membranes. Hydrogen flux for the prepared membranes both on porous alumina as well as PSS was observed higher than self-supported membranes. Increase in flux with the prepared membranes may be because of the reduced thickness of membrane using the porous supports in comparison with 0.1mm thick self-

supported membranes. Further, higher flux using the prepared Pd-Ag membrane on PSS was also observed as multi-pass separator.

- Higher performance of the prepared membranes than the self-supported also indicates the feasibility of the synthesized membranes for further integration studies.

3.6 Nomenclature

Pe	Permeability, $m.mol/m^2.s.bar^{0.5}$
j_{H_2}	Hydrogen permeate flux, $mol/m^2.h$
$p^n_{H_2,permeate}$	Partial pressure of hydrogen in permeate, n=0.5
$p^n_{H_2,retentate}$	Partial pressure of hydrogen in retentate, n=0.5
δ	Thickness of membrane, m
$\mathbf{F}_{H_2,permeate}$,	Mass flow rate of H_2 in permeate, kg /s
$\mathbf{F}_{H_2,retentate}$	Mass flow rate of H_2 in retentate, kg /s
v	Velocity, m/s
ρ	Density, kg/m^3
p	Pressure, Pa
h	Enthalpy, kcal/kg

T	Temperature, K
g	Acceleration due to gravity, m/s^2
k	Thermal conductivity, W/m. K
τ	Shear stress, Pa

References

[1] H.W. Abu El Hawa, S.N. Paglieri, C.C. Morris, A. Harale, J. Douglas Way, Identification of thermally stable Pd-alloy composite membranes for high temperature applications, Journal of Membrane Science, 466 (2014) 151-160.

[2] F. Gallucci, F. Chiaravalloti, S. Tosti, E. Drioli, A. Basile, The effect of mixture gas on hydrogen permeation through a palladium membrane: Experimental study and theoretical approach, International Journal of Hydrogen Energy, 32 (2007) 1837-1845.

[3] D.N. Jewett, A.C. Makrides, Diffusion of hydrogen through palladium and palladium-silver alloys, Transactions of the Faraday Society, 61 (1965) 932-939.

[4] D. Mendes, V. Chibante, J.-M. Zheng, S. Tosti, F. Borgognoni, A. Mendes, L.M. Madeira, Enhancing the production of hydrogen via water–gas shift reaction using Pd-based membrane reactors, International Journal of Hydrogen Energy, 35 (2010) 12596-12608.

[5] Y. Sakamoto, S. Hirata, H. Nishikawa, Diffusivity and solubility of hydrogen in Pd-Ag and Pd-Au alloys, Journal of the Less Common Metals, 88 (1982) 387-395.

[6] J.W. Simons, T.B. Flanagan, Absorption Isotherms of Hydrogen in the α-Phase of the Hydrogen-Palladium System, The Journal of Physical Chemistry, 69 (1965) 3773-3781.

[7] N. Vicinanza, I.-H. Svenum, L.N. Næss, T.A. Peters, R. Bredesen, A. Borg, H.J. Venvik, Thickness dependent effects of solubility and surface phenomena on the

hydrogen transport properties of sputtered Pd77%Ag23% thin film membranes, Journal of Membrane Science, 476 (2015) 602-608.

[8] A. Caravella, F. Scura, G. Barbieri, E. Drioli, Sieverts Law Empirical Exponent for Pd-Based Membranes: Critical Analysis in Pure H2 Permeation, The Journal of Physical Chemistry B, 114 (2010) 6033-6047.

[9] T.L. Ward, T. Dao, Model of hydrogen permeation behavior in palladium membranes, Journal of Membrane Science, 153 (1999) 211-231.

[10] F. Pinto, R.N. André, C. Franco, C. Carolino, I. Gulyurtlu, Effect of syngas composition on hydrogen permeation through a Pd–Ag membrane, Fuel, 103 (2013) 444-453.

[11] M. Vadrucci, F. Borgognoni, A. Moriani, A. Santucci, S. Tosti, Hydrogen permeation through Pd–Ag membranes: Surface effects and Sieverts' law, International Journal of Hydrogen Energy, 38 (2013) 4144-4152.

[12] J. Catalano, M. Giacinti Baschetti, G.C. Sarti, Influence of the gas phase resistance on hydrogen flux through thin palladium–silver membranes, Journal of Membrane Science, 339 (2009) 57-67.

[13] O. Lüdtke, R.D. Behling, K. Ohlrogge, Concentration polarization in gas permeation, Journal of Membrane Science, 146 (1998) 145-157.

[14] R. Sharma, A. Kumar, R.K. Upadhyay, Performance comparison of methanol steam reforming integrated to Pd-Ag membrane: Membrane reformer vs. membrane separator, Separation and Purification Technology, 183 (2017) 194-203.

[15] N. Itoh, W.C. Xu, K. Haraya, Radial mixing diffusion of hydrogen in a packed-bed type of palladium membrane reactor, Industrial & Engineering Chemistry Research, 33 (1994) 197-202.

[16] J. Zhang, D. Liu, M. He, H. Xu, W. Li, Experimental and simulation studies on concentration polarization in H2 enrichment by highly permeable and selective Pd membranes, Journal of Membrane Science, 274 (2006) 83-91.

[17] A.S. Augustine, Y.H. Ma, N.K. Kazantzis, High pressure palladium membrane reactor for the high temperature water–gas shift reaction, International Journal of Hydrogen Energy, 36 (2011) 5350-5360.

[18] W.-H. Chen, W.-Z. Syu, C.-I. Hung, Y.-L. Lin, C.-C. Yang, Influences of geometry and flow pattern on hydrogen separation in a Pd-based membrane tube, International Journal of Hydrogen Energy, 38 (2013) 1145-1156.

[19] M.E. Adrover, D. Borio, M. Pedernera, Comparison between WGS membrane reactors operating with and without sweep gas: Limiting conditions for co-current flow, International Journal of Hydrogen Energy, 42 (2017) 5139-5149.

[20] J. Boon, J.A.Z. Pieterse, F.P.F. van Berkel, Y.C. van Delft, M. van Sint Annaland, Hydrogen permeation through palladium membranes and inhibition by carbon monoxide, carbon dioxide, and steam, Journal of Membrane Science, 496 (2015) 344-358.

[21] X. Li, A. Li, C.J. Lim, J.R. Grace, Hydrogen permeation through Pd-based composite membranes: Effects of porous substrate, diffusion barrier and sweep gas, Journal of Membrane Science, 499 (2016) 143-155.

[22] P. Pinacci, F. Drago, Influence of the support on permeation of palladium composite membranes in presence of sweep gas, Catalysis Today, 193 (2012) 186-193.

[23] W.-H. Chen, W.-Z. Syu, C.-I. Hung, Y.-L. Lin, C.-C. Yang, A numerical approach of conjugate hydrogen permeation and polarization in a Pd membrane tube, International Journal of Hydrogen Energy, 37 (2012) 12666-12679.

[24] M. Coroneo, G. Montante, A. Paglianti, Numerical and Experimental Fluid-Dynamic Analysis To Improve the Mass Transfer Performances of Pd−Ag Membrane Modules for Hydrogen Purification, Industrial & Engineering Chemistry Research, 49 (2010) 9300-9309.

[25] W.-H. Chen, C.-H. Lin, Y.-L. Lin, Flow-field design for improving hydrogen recovery in a palladium membrane tube, Journal of Membrane Science, 472 (2014) 45-54.

[26] M. Jafarkhani, M.K. Moraveji, R. Davarnejad, F. Moztarzadeh, M. Mozafari, Three-dimensional simulation of turbulent flow in a membrane tube filled with semi-circular baffles, Desalination, 294 (2012) 8-16.

[27] S.X. Liu, M. Peng, L.M. Vane, CFD simulation of effect of baffle on mass transfer in a slit-type pervaporation module, Journal of Membrane Science, 265 (2005) 124-136.

[28] Y. Liu, G. He, X. Liu, G. Xiao, B. Li, CFD simulations of turbulent flow in baffle-filled membrane tubes, Separation and Purification Technology, 67 (2009) 14-20.

[29] N. Mori, T. Nakamura, K.-i. Noda, O. Sakai, A. Takahashi, N. Ogawa, H. Sakai, Y. Iwamoto, T. Hattori, Reactor Configuration and Concentration Polarization in Methane Steam Reforming by a Membrane Reactor with a Highly Hydrogen-Permeable Membrane, Industrial & Engineering Chemistry Research, 46 (2007) 1952-1958.

[30] Y.S. Cheng, M.A. Peña, J.L. Fierro, D.C.W. Hui, K.L. Yeung, Performance of alumina, zeolite, palladium, Pd–Ag alloy membranes for hydrogen separation from Towngas mixture, Journal of Membrane Science, 204 (2002) 329-340.

[31] H. Amandusson, L.G. Ekedahl, H. Dannetun, Hydrogen permeation through surface modified Pd and PdAg membranes, Journal of Membrane Science, 193 (2001) 35-47.

[32] J.M. Sánchez, M.M. Barreiro, M. Maroño, Bench-scale study of separation of hydrogen from gasification gases using a palladium-based membrane reactor, Fuel, 116 (2014) 894-903.

[33] Y. Huang, R. Dittmeyer, Preparation and characterization of composite palladium membranes on sinter-metal supports with a ceramic barrier against intermetallic diffusion, Journal of Membrane Science, 282 (2006) 296-310.

[34] P.P. Mardilovich, Y. She, Y.H. Ma, M.-H. Rei, Defect-free palladium membranes on porous stainless-steel support, AIChE Journal, 44 (1998) 310-322.

[35] P.A. Lessing, H.C. Wood, L.D. Zuck, Low temperature hydrogen transport using a palladium/copper membrane, Journal of Materials Science, 38 (2003) 2401-2408.

[36] K. Hou, R. Hughes, The effect of external mass transfer, competitive adsorption and coking on hydrogen permeation through thin Pd/Ag membranes, Journal of Membrane Science, 206 (2002) 119-130.

[37] J. Catalano, F. Guazzone, I.P. Mardilovich, N.K. Kazantzis, Y.H. Ma, Hydrogen Production in a Large Scale Water–Gas Shift Pd-Based Catalytic Membrane Reactor, Industrial & Engineering Chemistry Research, 52 (2013) 1042-1055.

[38] A. Iulianelli, T. Longo, A. Basile, Methanol steam reforming in a dense Pd–Ag membrane reactor: The pressure and WHSV effects on CO-free H2 production, Journal of Membrane Science, 323 (2008) 235-240.

[39] A. Basile, F. Gallucci, A. Iulianelli, G.F. Tereschenko, M.M. Ermilova, N.V. Orekhova, Ti–Ni–Pd dense membranes—The effect of the gas mixtures on the hydrogen permeation, Journal of Membrane Science, 310 (2008) 44-50.

[40] R. Sharma, A. Kumar, K. Upadhyay Rajesh, Catalytic Sol Assisted Dense Pd/γ-Al2O3 Membrane using Modified Electroless Plating: Effect of Process on Surface Morphology, in: Chemical Product and Process Modeling, 2016.

[41] J.A. Calles, R. Sanz, D. Alique, L. Furones, Thermal stability and effect of typical water gas shift reactant composition on H2 permeability through a Pd-YSZ-PSS composite membrane, International Journal of Hydrogen Energy, 39 (2014) 1398-1409.

[42] Z.W. Dunbar, I.C. Lee, Effects of elevated temperatures and contaminated hydrogen gas mixtures on novel ultrathin palladium composite membranes, International Journal of Hydrogen Energy, 42 (2017) 29310-29319.

[43] Y.-M. Lin, M.-H. Rei, Separation of hydrogen from the gas mixture out of catalytic reformer by using supported palladium membrane, Separation and Purification Technology, 25 (2001) 87-95.

[44] T.A. Peters, M. Stange, H. Klette, R. Bredesen, High pressure performance of thin Pd–23%Ag/stainless steel composite membranes in water gas shift gas mixtures; influence of dilution, mass transfer and surface effects on the hydrogen flux, Journal of Membrane Science, 316 (2008) 119-127.

[45] A. Santucci, F. Borgognoni, M. Vadrucci, S. Tosti, Testing of dense Pd–Ag tubes: Effect of pressure and membrane thickness on the hydrogen permeability, Journal of Membrane Science, 444 (2013) 378-383.

Chapter 4

Catalysts for Methanol Steam Reforming: Preparation, Characterization and Testing

Abstract

The current work investigates multiple monometallic as well as bimetallic catalysts supported on Al_2O_3-Zn-ZrO_2 to determine a catalyst with minimal CO selectivity at higher temperatures for methanol steam reforming. Using incipient wetness impregnation, monometallic catalysts with Cu, Ni, Fe, Pd and Ru as active metal were synthesized and compared with bimetallic catalysts having Fe as the second metal. Bimetallic catalysts such as Cu-Fe, Ni-Fe and Ru-Fe were synthesized, characterized and tested along with Ni-Cu and Cu-Ru supported on Al_2O_3-Zn-ZrO_2. For all catalysts, metal-support interactions were characterized in detail using temperature programmed reduction (TPR). Activity testing was performed in a fixed bed reactor at 350°C, gas hourly space velocity (GHSV) of 9000h^{-1} and steam-to-methanol (S/M) ratio of 3 (molar ratio). Nearly zero CO selectivity was determined for Cu-Fe supported on Al_2O_3-Zn-ZrO_2 up to a temperature of 450˚C. Further, nearly 4 to 5 times enhancement in hydrogen production rate was observed with Cu-Fe supported on Al_2O_3-Zn-ZrO_2 in comparison to its monometallic counterparts.

The optimized Cu-Fe supported on Al_2O_3-Zn-ZrO_2 was further tested at varying metal molar compositions, temperatures, steam-to-methanol (S/M) molar ratios and weight

hour space velocity W/F ratio. Here, W refers to the mass of catalyst and F referes to the molar flow rate of methanol in feed. Lastly, reaction mechanism was proposed using information from in situ DRIFT IR analysis.

4.1 Introduction

Production of hydrogen using organic resources such as water, methane, methanol and ethanol via electrolysis, steam reforming, cracking, dry reforming, partial oxidation or auto-thermal reforming is widely studied [1-7]. Amongst these, hydrogen production using methanol via steam reforming is a widely applied process due to its high efficiency both at laboratory and pilot plant scale. The benefit of steam reforming is high hydrogen yield at relatively low temperature. Under favorable conditions, steam reforming can generate a product stream containing 75% H_2 and 25% CO_2 on a dry basis. However, since steam reforming is an endothermic reaction, higher H_2 yield has only been reported at higher temperatures, but it comes at the cost of increasing CO [8-13]. Presence of CO can be dis-advantageous for following reasons: a) excess CO generation deteriorates the reforming catalyst's activity over time and also causes poisoning, b) excess CO also has poisoning effect on palladium membrane used for hydrogen separation, and c) CO above 10ppm contaminates the Pt-catalyst loaded in the fuel cell anode. Therefore, it is important for a membrane reformer to design a catalyst that has minimal CO selectivity.

In literature, catalysts used for methanol steam reforming mostly include transition metals (belonging to the group 8–10) because of their high catalytic activity. Such high activity results from their ability to adopt multiple oxidation states and thereby provide path with lower activation energy. Noble metal catalysts have been reported with sufficient

reforming activity over a wide temperature range; however, their high cost limits large scale implementation. Amongst noble metal, Pd and Ru are considered active catalysts for methanol reforming but both show high CO selectivity as well [16, 17]. High CO selectivity in these catalysts is primarily suggested to occur by methanol decomposition [17]. In contrast, non-precious metal catalysts for methanol steam reforming mostly include Cu, Ni and Fe. Copper is a low cost, highly abundant metal well known to transport oxygen, catalyze oxidation-reduction reactions and possess high hydrogen selectivity. High metal surface area and low metal particle size are mostly targeted to attain highly active copper catalysts. To attain that, addition of ZnO and ZrO_2 to copper-based alumina-supported catalysts has been reported [13, 18]. Addition of zinc oxide improves copper dispersion while ZrO_2 reduces the CO yield [18, 19]. In addition to that, supports such as CeO_2 [20], $ZnO\text{-}Al_2O_3$ [11, 13, 17, 21], ZrO_2 [12] and MgO [22] have also been extensively studied to prepare the catalysts with minimal CO selectivity. The combined interaction between the active metal and the support brings about the complete catalytic functionality. This is because the physico-chemical properties of a carrier significantly affects the existing surface reactions either by modifying the electrical properties of the metal or by promoting the activation of intermediate species [7].

Ni-based catalysts are mostly applied due to their inherent activity towards C-C and C-H bond cleavage [14]. However, Ni-based catalysts are susceptible to carbon formation that results in faster deactivation of these catalysts when exposed to hydrocarbon fuels for long term applications [15]. In comparison to Ni and Cu, Fe is also an abundant transition metal with a number of different oxidation states and ability to oxidize and reduce easily. Faster oxidation of Fe results in decomposition of Fe-metal to metal oxides during

catalysis which is considered less catalytically active. Therefore, in order to improve the catalyst performance Fe is mostly incorporated with other metals [16]. With different supports, CO formation in Cu and Ni monometallic catalysts has mostly been reported in the range of 3-18% while it is 30-40% CO in case of Pd, Ru and Fe supported on Al_2O_3 or ZrO_2 or CeO_2, supports and up to 0.8-6% for Pd, Ru and Fe supported on In_2O_3, ZnO and Ga_2O_3.[17].

A drastic change in CO selectivity with In_2O_3, ZnO and Ga_2O_3 was reported to occur due to alloy formation. In order to further investigate on effect of alloy formation on CO selectivity, bimetallic catalysts have recently gained wide attention. Bimetallic catalysts show distinct electronic and chemical properties in comparison to parent metal. Cooperative interactions between two metals in a bimetallic catalyst show different structures according to metal properties, metal-support interactions, atmosphere (oxidative and reductive) and temperature. Depending on these interactions, bimetallic structures in the form of heteroatom and nano-alloys have mostly been reported in literature [18]. For instance, rapid decrease in catalytic activity of Ni due to metal sintering and coke deposition can be partially inhibited using additional metals such as Cu [19]. In a similar manner, addition of Fe to Ni supported on cerium has also been reported to suppress carbon formation rate. High redox property of Fe causes the transfer of oxygen atoms from Fe to Ni which thereby promotes reaction between carbonaceous species and oxygen species [20, 21]. Therefore, with the literature reported, it is evident that in order to eliminate CO formation bimetallic catalysts are indeed promising. However, to negate CO formation even at higher temperatures, choice of optimal bimetallic catalysts still remains an open question.

In the current work, range of monometallic (Cu, Ni, Fe, Pd and Ru) as well as bimetallic (Cu-Fe, Ru-Fe, Ni-Fe, Ni-Cu and Cu-Ru) catalysts with 3% metal loading supported on $70Al_2O_3$-15Zn-12ZrO_2 were synthesized using incipient wetness impregnation method. As copper is the primary metal targeted for optimization studies, support composition chosen was adapted from literature that reported the synergistic effects that exist between copper and Al_2O_3-ZnO-ZrO_2 [11, 12, 22-24]. Further, alumina as base also provides high surface area as well as required thermal stability to the catalyst. Catalyst activity of monometallic vs. bimetallic was compared at a constant temperature of 350°C, gas hourly space velocity (GHSV) of 9000h^{-1} and steam-to-methanol molar ratio (S/M) of 3. Morphological as well as microstructure characterization was performed using field emission scanning electron microscopy (FESEM) and transmission electron microscopy (TEM). The best performing bimetallic catalyst was targeted to achieve maximum hydrogen yield with effect to increasing metal loading in the range of 3 to 33% and zero CO selectivity.

4.2 Methanol steam reforming (MSR)

4.2.1 Literature survey on catalysts for methanol steam reforming

Catalysts for methanol steam reforming include active noble metal catalysts like Ir, Au, Ru, Pd, Pt and Rh, non-noble metal catalysts like Cu, Ni and Co, and oxide catalysts such as MgO, Al_2O_3, V_2O_5, ZnO, TiO_2, ZrO_2, CeO_2, Sm_2O_3, La_2O_3-Al_2O_3, CeO_2-Al_2O_3, MgO-Al_2O_3 etc. As the small metal particles tend to sinter at low temperatures, they are applied onto a pre-existing support material which is thermally more stable and maintains high surface area even at high temperatures, affecting dispersion and stability of the metal. For

instance, ZnO increases copper dispersion and reducibility of Cu/ZnO. Al_2O_3 improves surface area of copper thereby preventing it from sintering during calcination. ZrO_2 enhances catalytic activity of the catalyst. ZrO_2 can also easily adsorb methanol and improve the mobility of lattice oxygen. It thereby inhibits thermal sintering of the particles, prevents poisoning of the active metal surface and ensures additional chemical and thermal performance stability which is very important for industrial catalysts.

Table 4.1 shows a brief literature review on the catalysts tested for MSR.

From Table 4.1 it can be summarized that in methanol steam reforming many literatures has reported the presence of CO in reformate with increasing temperatures. This occurrence is mostly suggested due to reverse water gas shift that causes CO_2 utilization resulting in CO production. Since reforming is an endothermic reaction, higher H_2 yield has only been reported higher with higher temperatures but it comes with at the cost of increasing CO. Therefore it is essential to synthesize catalysts that can give 100% conversion at low temperatures, in order to minimize CO production or completely inhibit CO generation without affecting the hydrogen yield.

Table 4.1 Literature review on catalysts for MSR

Catalytic composition	Catalyst amount (g)	S/M ratio (-)	Operating Conditions	Support surface area (m^2/g)	Reactor i.d.* (mm)	H_2 outlet flow rate (mmol/ kgcat.s)	CO mole %	Conversion (%)	Ref.
15atomic%Cu-$Ce_{0.6}$ $Zr_{0.4}$ mixed oxides	0.1	1/1	**Temperature** 200–330°C **Inlet Flow Rate** 0.4mL/hr **GHSV** 40,000 h^{-1}	100–125	6	-NA-	0-18	73 @ 250°C 90 @ 275°C 100 @300°C	[25]
Cu/ Zn/Zr/Al (SP) 70/18/10/2	0.1	1.3/1	**Inlet Flow Rate** 38.6 mL/min; **methanol** (16.6 mL//min) **Temperature** 140–345°C **W/F** 0.00259 g/(cm^3/min)	119	-NA-	186	-nil-	100 at temperature ≥345°C	[9]
Cu–Zn– Al–O catalysts (CP)	2	1.3/1	**Temperature** 250°C	56	12	-NA-	-NA-	100	[10]
Cu60/Zn/Zr /15wt% Al_2O_3	-NA-	1.3/1	**Temperature** 200–300°C **Space velocity** 10,000h^{-1}	111	25with 22mm monolith	-NA-	0.43	-not mentioned-	[26]
Cu3–12%/Zn/Zr /15wt% Al_2O_3	15	1.3/1	**Temperature** 200–300°C **GHSV** 25000 h^{-1}	184	25	180	0.4-1.2	100	[11]

6.4 wt.% Pd/ZnO	0.3	-NA-	**Methanol WHSV** 47 h^{-1}	--NA-	-NA-	-NA-	15	60	[27]
Cu/Zn/Zr/Al 8/4/2/86	3	1.4/1	**Temperature** 260°C **Inlet flow rate** 0.26mL/min **WHSV** 11 kg cat/(mol.s) **S/M** 1.4	162	19	217	1.2	81	[12]
M-MCM-41 (10wt.%M:Cu, Co, Ni, Pd, Zn and Sn)		3/1	**GHSV** 2838 h^{-1} **Temperature** 350°C	1039	6.2	-NA-	17.7	82 (highest with Cu)	[8]
CuZnGaOx	0.4	2/1	**Temperature** 150–200 **W/F** 180 kg_{cat}.s/mol **Inlet Feed Rate** 0.1mL/min Cu Dispersion 30.52	79	4	-NA-	0	22.5 @150°C	[28]

*Here, i.d. refers to internal diameter,

In order to investigate the mechanism of CO formation in methanol steam reforming as a secondary byproduct, Breen and Ross [9] conducted a kinetic study by testing $Cu/ZnO/ZrO_2/Al_2O_3$ at varying W/F ratio (0.001 to 0.0013 g/min.cm^3) and temperatures (200 and 300°C). In-situ DRIFTS analysis was further performed to analyze the reaction intermediates. CO formation was reported to occur at higher contact times and not below 0.003 g/min.cm^3. 100% methanol conversion was reported at 300°C. DRIFTS analysis was reported with generation of formate species once water is added to methanol. Conversion of formaldehyde and methoxy species produced formate species. No evidence of gas phase CO or adsorbed CO was reported. Further, with the kinetic study it was reported that CO did not form when methanol was present, and that CO_2 and H_2 were the primary products. However, when methanol was fully converted, CO was evident in the gas stream.

Idem and Bakhshi, [29] tested copper alumina catalysts with Cu concentrations ranging up to 27.8 wt.% at 170–250°C and WHSV of 16.7 h^{-1}. The catalysts were prepared by co-precipitation and tested with respect to varying calcination temperature. It was reported that copper dispersion did not play a significant role in methanol conversion. Higher calcination temperature results in the formation of large amounts of $CuAl_2O_4$ and metallic Cu with subsequent reduction. Thus, higher calcination temperature resulted in formation of highly dispersed Cu crystallites and large metallic copper area. However, increasing metal dispersion was reported to decrease turn over number (TON) for methanol conversion. This indicates that metallic Cu obtained from $CuAl_2O_4$ is less efficient for methanol conversion than metallic Cu obtained from the reduction of CuO, Cu_2O and

$Cu_2(OH)_2CO_3$. CO formation for methanol steam reforming was reported in the range of 0 to 1.5 (mol%) at 170–250°C.

Lindstorm et al. [11] tested three sets of copper (3 to 12 wt. %) based catalysts: $Cu/Zn/ZrO_2$, $Cu/Cr/Al_2O_3$ and $Cu/Zr/Al_2O_3$ to investigate the influence of catalyst on methanol reforming and formation of CO. Testing of the catalysts was performed in a fixed bed reactor with 15g catalyst pellets, at 25000 GHSV h^{--1} over a temperature range of 150 to 300°C. Reactants were fed with 30% excess steam. Lowest CO formation was reported with Cu/Zr, while highest activity was reported with Cu/Zn.

Similar study to investigate CO formation using Cu (Zn) (Zr)-alumina was reported by Pant et al. [12] using different catalyst preparation methods such as co-precipitation and wetness impregnation. Addition of ZnO and ZrO_2 as promoters was reported to enhance the surface area of the catalysts in case of co-precipitated catalysts. Further, ZrO_2 addition was reported to enhance catalyst surface area with wetness impregnation in contrast to only zinc. At W/F 11 kg_{cat} mol^{-1} s, S/M 1.4/1 and temperature range 200–260°C, CO mol % with precipitated CuZnZrAl catalyst was reported between 0 to 0.8 mol % while for wetness impregnation it was between 0.7 to 2.5 mol %. Stable activity of precipitated CuZnZrAl was observed for a period of 20 h.

In addition to noble metal based catalysts, bimetallic catalysts have received considerable attention owing to cooperative interactions between two metals that result in stable and optimal catalytic performances. This interaction between two metals can be a structural as well as a surface (geometric and electronic) phenomenon. It mostly results in the formation of a hetero-structure to core shell, nano-alloys or intermetallic. Further, electronic density increase or decrease also results in a change in activity and selectivity

of the catalysts. Generally, formation of a surface alloy is considered as a determinant for the chemical behavior of bimetallic system. Bimetallic catalysts reported for methanol steam reforming include Ni-Cu/Al_2O_3 [19, 30], Au-Cu [31], Au-Ni [31] supported on multiwall carbon nanotubes (MWCNTs) and Pd-Zn supported on alumina [32, 33], ceria [34] and zinc oxide[35].

Copper-based catalysts are widely reported in literature for their high hydrogen selectivity. However, the inherent disadvantages of copper-based catalysts such as sintering above 260–280°C, self-healing properties which may negatively impact operation and handling procedures lead to substantial loss of activity. Hence, noble metals such as Pd for methanol steam reforming activity are also tested. Ilinich et al. [34] reported power law kinetic equations for methanol steam reforming activity using a ceria-supported Pd-Zn catalyst which was promoted with yttrium (developed by BASF). Alloy formation between Pd-Zn was reported. However, contrary to reported literature, CO formation was reported as a consequence of direct methanol decomposition. Rate of methanol decomposition (MD) was reported to be significantly higher than reverse water gas shift (rWGS) which establishes that methanol decomposition is a dominant pathway for CO generation using Pd-based catalysts supported on alumina as well as ceria. Role of yttria was not significantly highlighted in this study.

Hence, it can be observed that metal support interaction and metal-metal interaction plays a significant role in determining the catalyst activity. A schematic to describe the effect of such metal support interaction that results in a change in reaction mechanism is presented in Fig. 4.1. It illustrates that for non-noble metal such as Cu showed in Fig. 4.1a, catalyst activity with ZnO and ZrO_2 promoted alumina results in the formation of

formate species as intermediate product that gives CO_2 and H_2 as final product. The acidity and basicity of the support governs the synergistic effect of the metal clusters interaction with the supports that causes an increase in metal surface area, metal dispersion and easier reduction of metal oxide. Similarly, with noble metal, a distinct change in reaction mechanism can be observed with ZnO and ZrO_2 in comparison to alumina as presented in Fig. 4.1b. However, a high methanol decomposition (MD) activity with noble metals such as Pd results in final product composition of CO and CO_2.

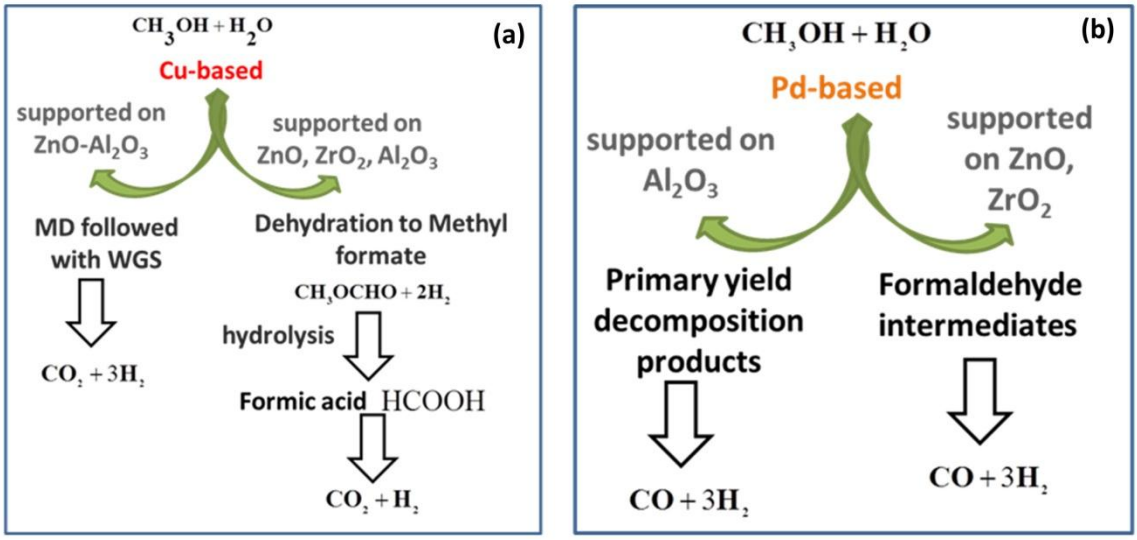

Fig. 4.1 Schematic of reaction mechanism for methanol steam reforming (MSR): a) Cu-based catalysts and b) Pd-based catalyst

4.2.2 Catalysts preparation methods

The two widely applied techniques for catalyst preparation includes co-precipitation and impregnation. Co-precipitation provides high metal dispersion with high attainable metal loading up to 60-80%, because of which catalysts prepared by this method are also termed as bulk catalysts [36]. However, this process creates lot of problem with its super saturation conditions above which the product is to be separated from the large quantities

of waste salt generation. Impregnation on the other hand is a widely applied process not only on lab scale but also industrially [37]. It primarily refers to the contacting of a solid and a liquid phase and adsorption of the latter by the former. Dry incipient wetness refers to the impregnation of the previously dried support with a solution containing precursor of the active phase i.e. $V=V_{pore}$. The solution gets sucked in the pores by capillary action and in case of proper wetting no excess solution is left outside, henceforth called dry or incipient wetness impregnation.

4.3 Experimental

4.3.1 Catalyst preparation

All monometallic and bimetallic catalyst preparation was carried out using incipient wetness impregnation. Metal salts such as copper II nitrate trihydrate (Merck, reagent grade), ferric nitrate nonahydrate (Loba chemie), nickel II nitrate hexahydrate (Merck, reagent grade), palladium chloride (Spectrochem), ruthenium (III) chloride hydrate (Alfa Aesar), zinc nitrate hexahydrate (Merck), zirconyl nitrate (Loba) and aluminium nitrate nonahydrate (Merck) were used as raw materials. Metal loading for all catalysts was 3% with support of fixed composition Al_2O_3-Zn-Zr (70:15:12). To prepare the support, alumina was synthesized using ammonium hydroxide and cetyltrimethylammonium bromide (CTAB) as surfactant with precipitation method at pH 10.5 [38]. The precipitated alumina was further calcined at 500°C followed by crushing and sieving the alumina power to the size of 200 µm. Zinc nitrate and zirconyl nitrate were then added to the alumina by incipient wetness impregnation.

4.3.2 Catalyst characterization

All catalysts and supports were calcined after preparation at 500°C for 5 h. Surface area determination of porous supports was performed using Brunauer-Emmett-Teller (BET) [39] analysis from N_2 adsorption-desorption isotherms at 77 K, degassing at 200°C for 2 h (Quanta chrome Autosorb iQ). Pore volume was calculated using Barrett-Joyner-Halenda (BJH) models [40].

Temperature programmed reduction (TPR) experiments were performed for all catalysts. The equipment used for the TPR experiment was CHEMISORB 2720. For a typical experiment, 40 mg of catalyst was placed in the center of a quartz reactor using quartz wool. The temperature of the catalyst was recorded by a thermocouple inside the catalyst bed which was connected to a temperature controller. The reactor tube was heated by an electric furnace. The calcined catalyst was degassed in situ at 200°C under flow of Ar (30 ml/min). After cooling the sample to approximately 25°C, the temperature programmed reduction was performed using 9.35% H_2/Ar gas mixture as reducing gas. The sample was heated up to 850°C at a rate of 10°C/min.

Particle size distribution was studied using TEM (JEOL) images for the best performing catalyst. The morphology of the reduced and reacted catalysts was analyzed by FESEM (ZEISS-FESEM, Sigma) technique to determine the nature of the agglomerates on the catalyst. Further, Raman spectroscopy was performed to determine any carbon present on the spent catalysts.

4.3.3 Catalyst activity

Steam reforming of methanol (SRM, equation 4.1) was performed in a fixed bed reactor made of SS 310 with 20 mm inner diameter, 600 mm length. The reactor is assembled with electrically heated furnace and PID controllers. 1.8 gm of pre-calcined catalyst mixed with quartz of same size in a ratio of 1:2 respectively was used in all the experiments. Catalyst bed height of 2 cm, GHSV 9000 h^{-1}, temperature 350°C and S/M ratio 3:1 (mol: mol) were kept constant throughout. The value of S/M ratio was selected based on our previous work [41]. Two thermocouples were connected to the reactor, wherein one thermowell was kept just on top of the catalyst bed while the second was maintained at the lower end of the reactor to observe the temperature gradients. The catalysts were reduced 'in situ' with the stream of H_2/N_2 mixture for 1–2 hours before starting the reaction. A mixture of steam and methanol was passed through a pre-evaporator along with nitrogen prior to entering the reactor. The product effluent was passed through the condenser in order to separate the produced reformate gas mixture from unreacted methanol and water. Reformate gas produced was analyzed by Nucon® 5765 Gas Chromatograph equipped with thermal conductivity detector (TCD) having carbosphere packed bed column. All catalysts were synthesized with total 3% metal loading and support composition of 15Zn-12 ZrO_2-70Al_2O_3 (wt.% basis). A total metal percentage of 3 was used to determine the best performing metal and metal composition catalyst prior to optimizing the metal loading.

Hydrogen production using methanol mostly occurs in stages of three processes: steam reforming of methanol (SRM, equation 4.1), methanol decomposition (MD, equation 4.2)

and water gas shift (WGS, equation 4.3) depending on the reaction condition and type of catalyst used.

SRM: $CH_3OH + H_2O \leftrightarrow 3H_2 + CO_2 \quad \Delta H_r = 49.7 \text{ kJ mol}^{-1}$ (I)

MD: $CH_3OH \leftrightarrow CO + 2H_2 \quad \Delta H_r = 90.2 \text{ kJ mol}^{-1}$ (II)

WGS: $CO + H_2O \leftrightarrow CO_2 + H_2 \quad \Delta H_r = -41.2 \text{ kJ mol}^{-1}$ (III)

The catalyst activity for the SRM reaction was evaluated in terms of methanol conversion (equation 4.4), CO selectivity (equation 4.5), hydrogen production rate (equation 4.6) and hydrogen yield (equation 4.7) as given below:

$$\text{Methanol conversion } (\%) = \frac{F_{CO}+F_{CO_2}}{F_{meoh}} \times 100\% \quad (4.4)$$

$$\text{CO selectivity } (\%) = \frac{F_{CO}}{F_{CO_2}+F_{CO}+F_{H_2}} \quad (4.5)$$

$$H_2 \text{ production rate (mmol/ kg}_{cat}\text{.s)} = \frac{F_{H_2}}{W_{catalyst}} \quad (4.6)$$

$$H_2 \text{ yield } = \frac{F_{H_2}}{F_{methanol}} \quad (4.7)$$

4.4. Results and Discussion

4.4.1 Support Characterization

In this study, optimization of metal composition for methanol steam reforming is performed to achieve zero CO selectivity at higher temperatures. Fig. 4.2a and 4.2b show the BET surface area and pore size distribution of the synthesized support.

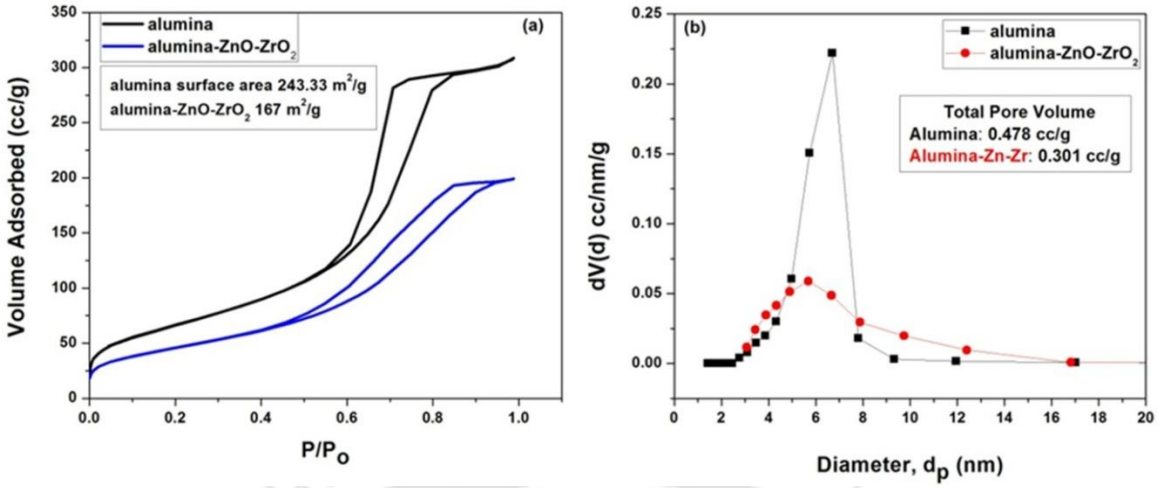

Fig. 4.2 Surface area characterization of prepared supports: a) Nitrogen adsorption isotherms at 77 K and b) Pore size distribution

N_2 adsorption-desorption isotherms of aluminium oxide as well as alumina-ZnO-ZrO_2 (AZZ) at 77 K were observed to follow Type IV isotherm with H1 hysteresis loop [42]. Alumina synthesized thus falls in the mesoporous range with a narrow pore size distribution as mostly reported for H1 hysteresis loop and evident from Fig 4.2b. In addition, impregnation of Zn and Zr plugs some pores of alumina which causes reduction in the surface area of AZZ obtained.

All catalyst testing studies were indeed performed in kinetically controlled regime. The catalyst particle size was ~ 0.25 mm that was chosen as per the range reported in literature [43] for reactor with similar dimensions. It was reported that for catalyst testing set up with internal diameter 19 mm, methanol conversion remained constant for particle size below 0.7 mm. Further in our work plug flow conditions were maintained using $D/D_p > 30$ and $L/D_p > 50$.

4.4.2 Monometallic catalyst activity

Monometallic catalysts tested for methanol steam reforming includes Cu, Ni, Pd, Fe and Ru supported on synthesized AZZ support with 3% total metal loading. Fig. 4.3a and 4.3b show methanol steam reforming activity and CO selectivity respectively at 350°C and 9000 h^{-1} GHSV. Since methanol conversion is a direct function of CO and CO_2 produced by the catalyst per molar flow rate of methanol fed, higher methanol conversion was observed with Fe, Pd and Ru as a consequence of high CO selectivity in comparison to Cu and Ni monometallic catalysts. This is because higher number of oxidation states in Pd, Ru and Fe gives them enhanced activity compared to Cu and Ni. As the pathway chosen by the individual metal oxidation state may differ, higher number of oxidation states leads to an increase in the number of intermediates/side reactions resulting in higher methanol conversion.

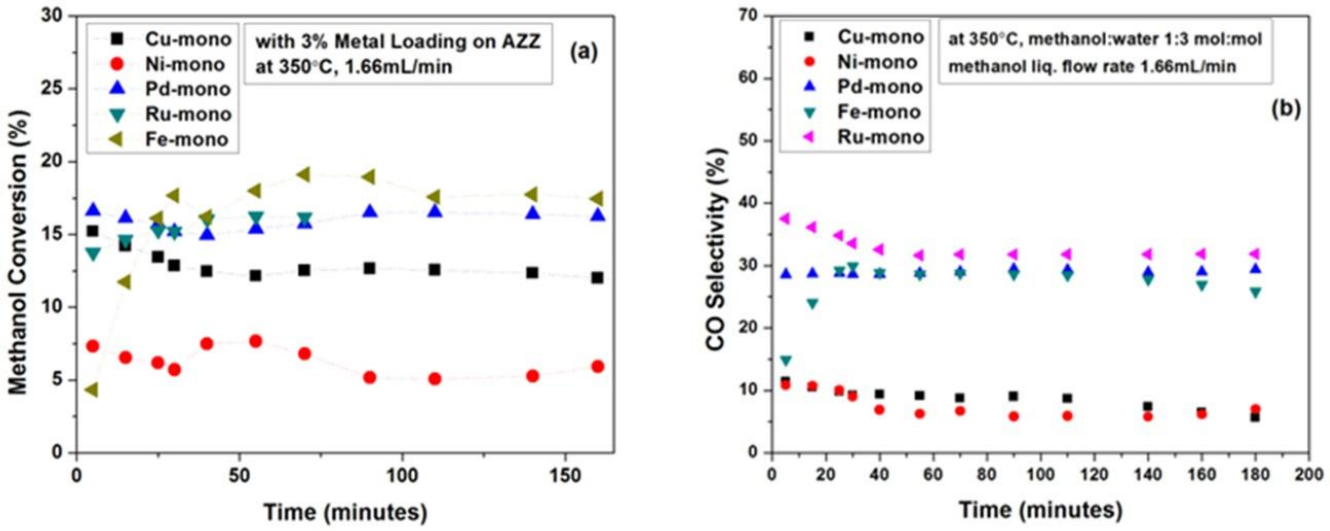

Fig. 4.3 Monometallic catalyst activity: a) Methanol conversion for prepared monometallic catalysts, b) CO selectivity of the prepared monometallic catalysts (dotted lines are guides to the eye)

A prominent product distribution difference was observed between Pd, Fe, Ru and Cu, Ni. It can be observed from Fig. 4.4a, 4.4b and 4.4c that CO selectivity for Fe, Pd and Ru catalysts was much higher than CO_2 in contrast to Cu and Ni as shown in Fig. 4.4d and 4.4e. This behavior has also been reported in previous studies [21, 27, 30]. For elemental Pd supported on non-reactive inert supports such as alumina, CO selectivity is higher because of its tendency to catalyze methanol decomposition as per equation 4.2 [44]. Similarly for Ru, CO formation is always high considering its high selectivity towards methanol decomposition [45, 46] while for Fe, despite being a high temperature water gas shift catalyst, a high CO selectivity is mostly reported as a result of possible side reaction such as reverse water gas shift reaction [47].

Moreover, it is important to point out that a higher CO selectivity reduces the hydrogen production rate. Fig. 4.5 shows the hydrogen production rate for all the monometallic catalysts tested. Depending on the operational condition and type of catalyst used, reaction 4.1 to 4.3 occurs simultaneously.

As reported in literature, excess CO generation in methanol steam reforming mostly occurs by reverse water gas shift that causes consumption of hydrogen produced. Hence, despite higher methanol conversion observed with Pd, Fe and Ru, hydrogen production rate was observed highest with Cu. Further, high hydrogen selectivity of Cu is well addressed in literature [8, 9, 11, 12]. The low hydrogen production rate with Ni may be attributed to the minimal conversion as observed from Fig. 4.3a. Low activity with Ni-based catalysts may be because of high C-C breaking activity rather than C-H causing a sharp increase in CO_2 formation as observed in Fig. 4.4d.

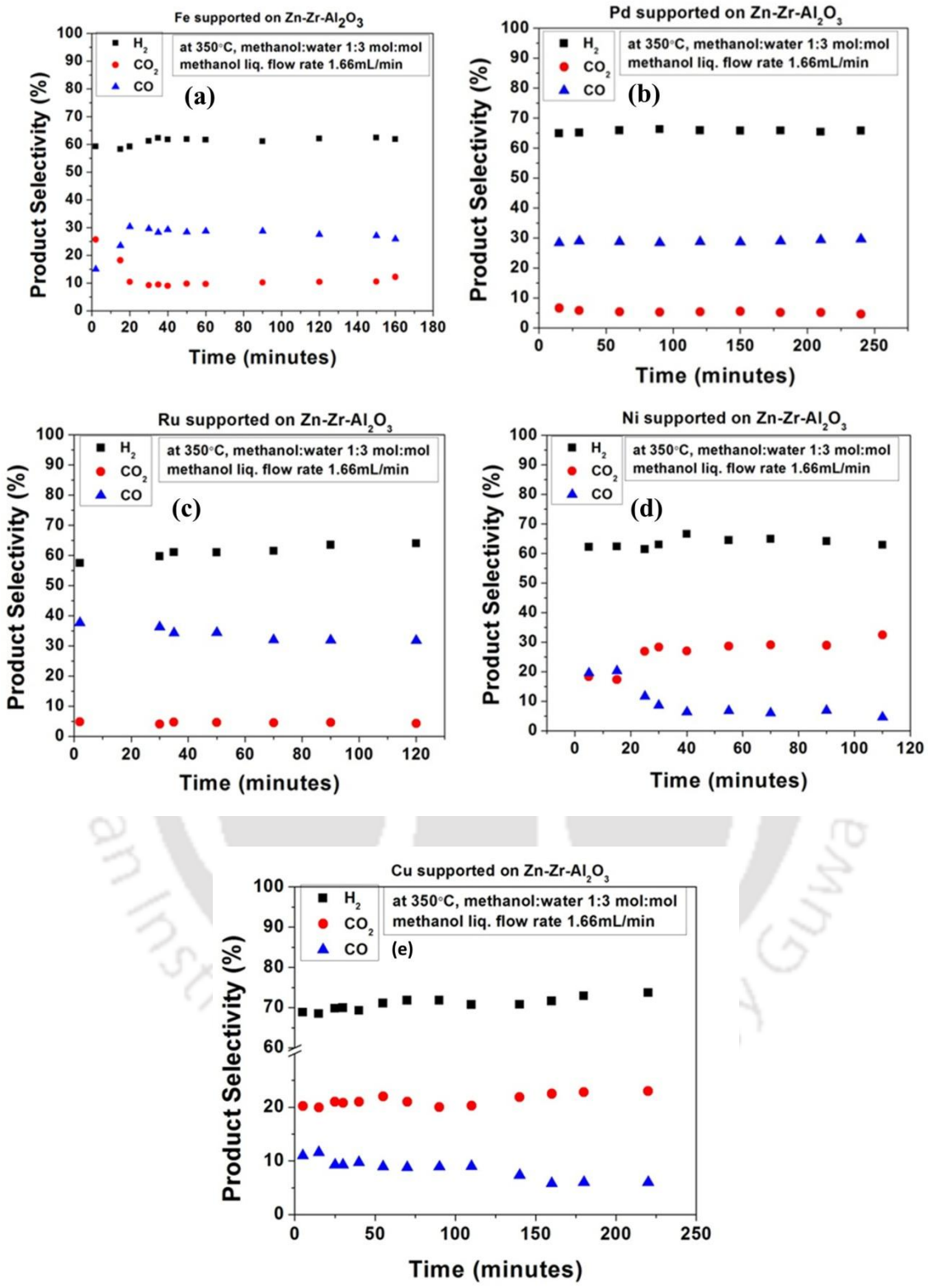

Fig. 4.4 Monometallic catalysts product selectivity: a) Fe-supported, b) Pd-supported, c) Ru-supported, d) Ni-supported and e) Cu-supported

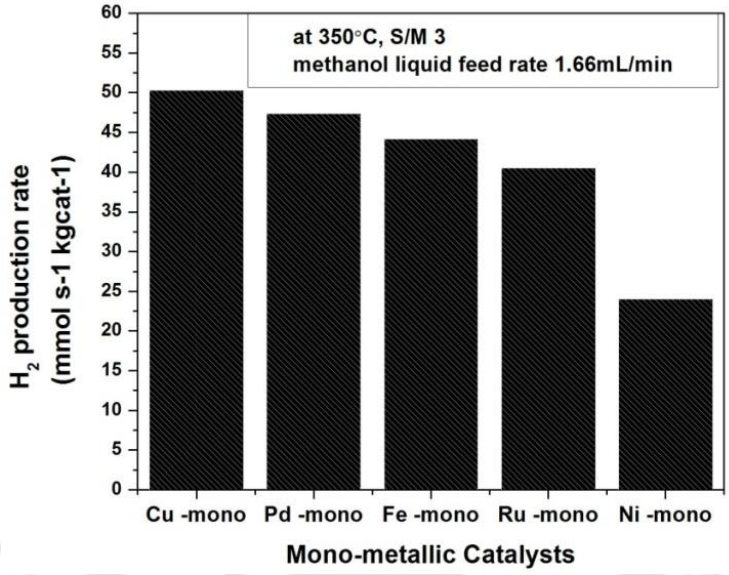

Fig. 4.5 Hydrogen production rate with the monometallic catalysts synthesized

4.4.3 Bimetallic catalysts

In the previous section, it was observed that hydrogen selectivity for all monometallic catalysts was in the range of 60–70%. However, what drastically varied was CO selectivity between precious and non-precious metals. This observation was consistent with the reported literature [19, 28, 30, 31, 34]. In order to lower the CO selectivity of catalysts prepared for MSR, a range of bimetallic catalysts were also synthesized. In bimetallic catalysts, co-operative interactions between two metals occur when one metal is miscible in the lattice of the other [48]. This results in the formation of alloy structures. Alloyed structures exhibit chemical properties very different from those of the pure metals. Moreover, formation of alloys results in reducing the bimetal particle size and change in its activity as well as selectivity.

Recently, it has been found that Fe as a co-catalyst for hydrocarbon reforming reactions provides enhanced catalytic activity, improved metal dispersion and low carbon

deposition by increasing the coverage of oxygen species during the reforming reaction [49-52]. However, effect of Fe as co-catalysts for methanol steam reforming has not been reported so far. In the current work, Fe was selected as a co-metal for Cu, Ni and Ru. Further, Cu-Ni [19] and Cu-Ru [6] were synthesized as reference catalysts to compare the performance of Fe-based bimetallic catalysts.

4.4.4 Characterization of bi-metallic catalysts with TPR

Temperature-programmed reduction profiles of Al_2O_3-Zn-ZrO_2 supported monometallic as well as bimetallic catalysts are presented in Fig. 4.6 (a–e). All catalysts with 3% total metal loading were used.

In the case of monometallic catalysts in Fig. 4.6 (a–e), Cu showed a broad single peak in the range of 200–500°C indicating reduction of CuO to Cu. Further, ruthenium oxide can be easily reduced at lower temperatures which therefore results in a broad peak between 180 and 350°C. Such broad single peak has also been reported in literature [53], due to the interactions between Ru and alumina-ZnO doped with ZrO_2 as support. In comparison to Cu and Ru, both Fe and Ni showed dual peaks. A wide temperature range for Ni as well as Fe may imply a great variety of oxidation states in these catalysts. Depending on the metal oxide interaction, for Ni supported on AZZ the first peak was observed between 400 and 500°C, and second peak in the range of 600 to 700°C. According to literature [5, 54], the first peak corresponds to NiO_x in strong interaction with the support while peak at high temperature shows reduction of bulk $NiAl_2O_4$ formed by Ni^{2+} migration into the Al_2O_3 lattice. Further, Fe supported on AZZ showed typical reduction peaks of Fe_2O_3 [55] wherein the first peak in the range of 280 to 500°C is

normally ascribed to Fe_2O_3 to Fe_3O_4 which after further reduction from 500 to 750°C reduces to Fe°. Once Fe as second metal is added, bimetallic catalysts such as Ni-Fe, Ru-Fe and Cu-Fe showed distinct characteristics. In all cases, Fe as second metal promotes the bimetal formation resulting in a temperature shift. This shift is approximately 22% (between Ni and Fe) for Ni-Fe, 28.5% (between Ru and Fe) for Ru-Fe and 43.7% (before Cu and Fe) for Cu-Fe supported on AZZ. Higher the shift more is the tendency for the bimetal to form an alloy. However, the variation in this shift is caused by the difference in the reduction potential of two metals. Based on these differences, they require different treatments to form a bimetallic alloy. For example, Ni-Fe cannot be mixed thermodynamically [56]; therefore $NaNH_4$ reduction or hydrogen reduction treatment at more than 700°C is required to form a bimetallic alloy. In addition, in case of Ru-Fe, the introduction of non-noble metal with high valence has a negative effect on the ease of reducibility of noble metal [57, 58]. Therefore, addition of Fe to Ru shifts the bimetal peak to a higher temperature compared to Ru monometallic catalyst. However, in comparison to monometallic Fe, presence of Ru shifts the peak to a lower temperature because of the easy activation of H_2 molecules on noble metals [58, 59].

In comparison to Ni-Fe and Ru-Fe, Cu-Fe showed a distinct lower temperature shift than its monometallic counterparts. Addition of Fe improves the reducibility of Cu thereby resulting in a sharp peak at lower temperature which was attributed to the reduction of CuO to Cu. Further, the subsequent broad peak may account for the existence of Cu-Fe as an alloy while the high temperature peak can be attributed to reduction of Fe_3O_4 to Fe° [60]. In addition to that, H_2-TPR profiles of the Fe-promoted bimetallic catalysts were

also compared with Ni-Cu and Cu-Ru as the reference catalyst. The high miscibility of Ni with Cu to form a solid solution results in an easy bimetal formation that showed a lower temperature peak between 200 and 400°C associated with reduction of Cu along with a subsequent peak associated with the reduction of Ni species promoted by the presence of metallic Cu. Lastly, addition of Ru to Cu did not show any improvement in reducibility of Cu; however, a broad single peak corresponding to both Cu and Ru was observed. Therefore, it can be stated that in case of Cu-Fe high metal-metal interaction resulted in an alloy formation once heated in the presence of hydrogen thereby giving a lower temperature shift. In contrast to this, the other bimetallic compositions showed prominent metal-support interaction once heated in the presence of hydrogen and hence, resulted in a higher temperature shift.

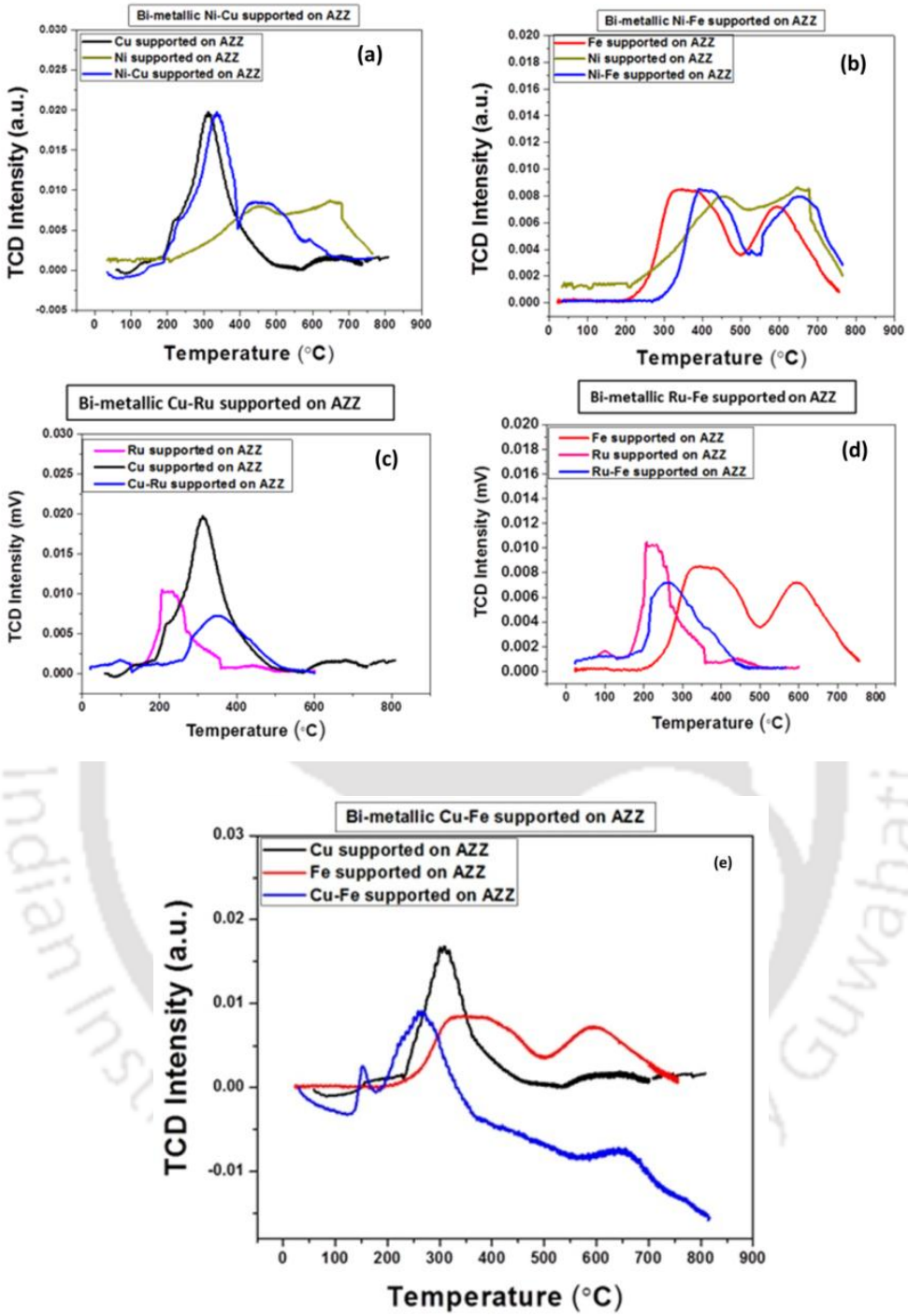

Fig. 4.6 H_2-temperature programmed reduction profiles for monometallic and bimetallic catalysts

4.4.5 Bimetallic catalyst testing

With the above H_2-TPR studies, catalyst activity testing was further carried out after reduction at 400°C using S/M of 3:1, GHSV of 9000 h^{-1} and operating temperature of 350°C. Fig. 4.7a and 4.7b show the methanol conversion and CO selectivity of Cu-Fe, Ni-Fe, Ru-Fe, Ni-Cu and Cu-Ru supported on AZZ.

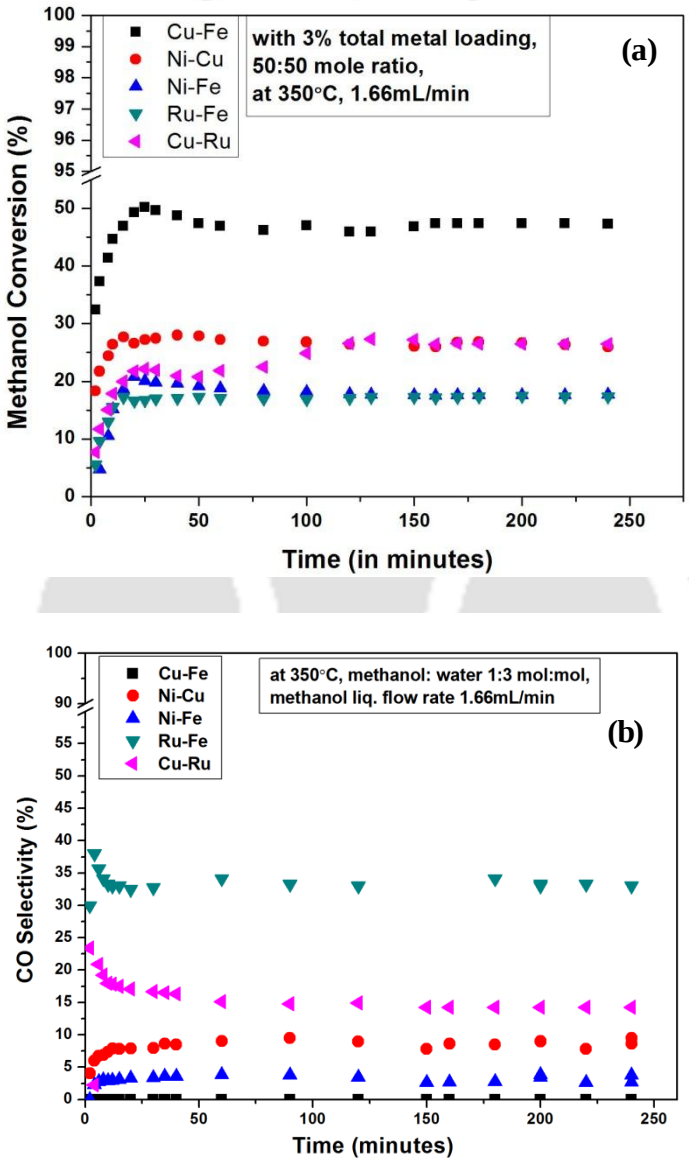

Fig. 4.7 Bimetallic catalyst activity: a) Methanol conversion of prepared bimetallic catalysts and b) CO selectivity of the prepared bimetallic catalysts

It can be observed from Fig. 4.7a and 4.7b that in comparison to all bimetallic catalysts, Cu-Fe (50:50 molar ratio) supported on AZZ gave maximum methanol conversion (~48%) along with zero CO selectivity. The next best methanol conversion was observed using Ni-Cu and Cu-Ru supported on AZZ. Addition of noble metal to a non-noble metal enhances the catalytic activity in case of Cu-Ru because of its co-existence as a bimetal observed in Fig. 4.6c. Further, high miscibility of Ni-Cu also improves its catalytic performance. However, for Ni-Cu and Cu-Ru, the CO selectivity was also observed to be 10 and 15% respectively (see Fig. 4.7b). In addition to these, performance of Ru-Fe and Ni-Fe supported on AZZ in terms of methanol conversion was minimal. It is to be noted that alloy formation is hindered if any of the following factors is not optimal: metal-metal interaction, metal-metal composition, calcination and reduction temperature. Since the scope of the current research was to determine the best performing bimetallic catalyst with low CO selectivity, optimization of the individual bimetallic activity was not performed. As can be observed from the previous section, Cu-Fe supported on AZZ showed a distinct alloy formation which thereby explains the enhancement in catalyst activity. Low CO selectivity (0–1.05 %) with 26 wt.% Cu-Fe_2O_4 spinel compounds was also reported by Huang et al [60] in the range of 240–320°C. In comparison to this study, the current work reports Cu-Fe (50:50) supported on 15Zn-12 Zr-70Al_2O_3 (wt. % basis) with no CO selectivity up 450°C. Fig. 4.8 shows the CO selectivity in a temperature range of 150 to 500°C with Cu-Fe (50:50) supported on AZZ.

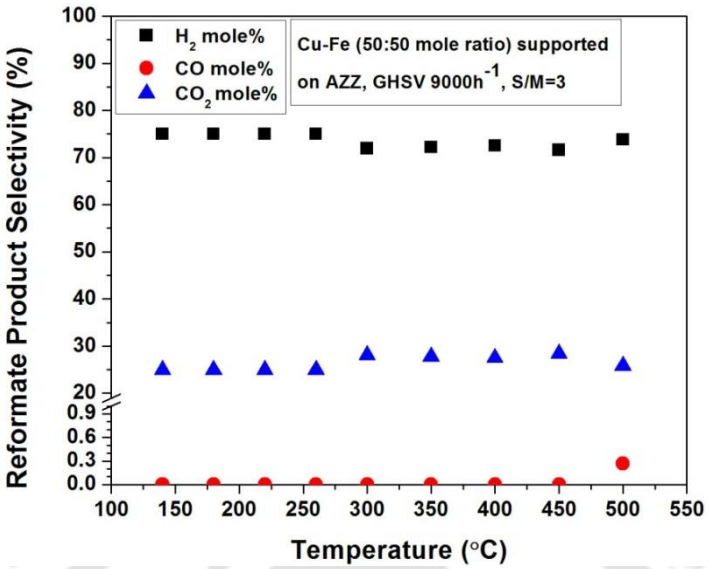

Fig. 4.8 CO selectivity using Cu-Fe (50:50) supported on AZZ at different temperatures

Therefore, it can be suggested that interaction of Cu-Fe with AZZ support strongly promotes the reducibility of the active metals which thereby leads to its enhanced activity. It is widely reported that incorporation of second metal mostly increases the reducibility of the first metal [60] as well as decreases the size of the catalyst [18]. Comparison of mono-metallic Cu and Fe with bimetallic CuFe supported on AZZ using TEM was performed. Fig. 9a shows that Cu supported on AZZ comprises of an amorphous morphology with metal present as clusters on the support. On the other hand, Fe supported on AZZ shows a more crytalline and uniform morphology. A higher crystallanity with Fe supported on AZZ occurs due to strong metal support interaction that exists between Group VIII metals and various metal oxides [61]. Once Cu and Fe are mixed together, similar atomic sizes and lesser electronegativity difference between the two metals results in the formation of an alloy [62]. Alloy formation was also confirmed with the decrease in metal particle size as obtained from the TEM data shown in Fig. 4.9b. Decrease in particle size occurs due to incorporation of Cu (atomic size 128 pm)

into the lattice of Fe (atomic size 126pm) that results in a solid solution or alloy [63]. Hence, lower the particle size, higher is the catalytic surface area thereby resulting in enhanced catalytic activity. This also justifies the enhanced hydrogen production rate with Cu-Fe supported on AZZ shown in Fig. 4.10 in comparison to total monometallic Cu, monometallic Fe (shown in Fig. 4.5) and rest of the bimetallic catalysts synthesized, as shown in Fig 4.10.

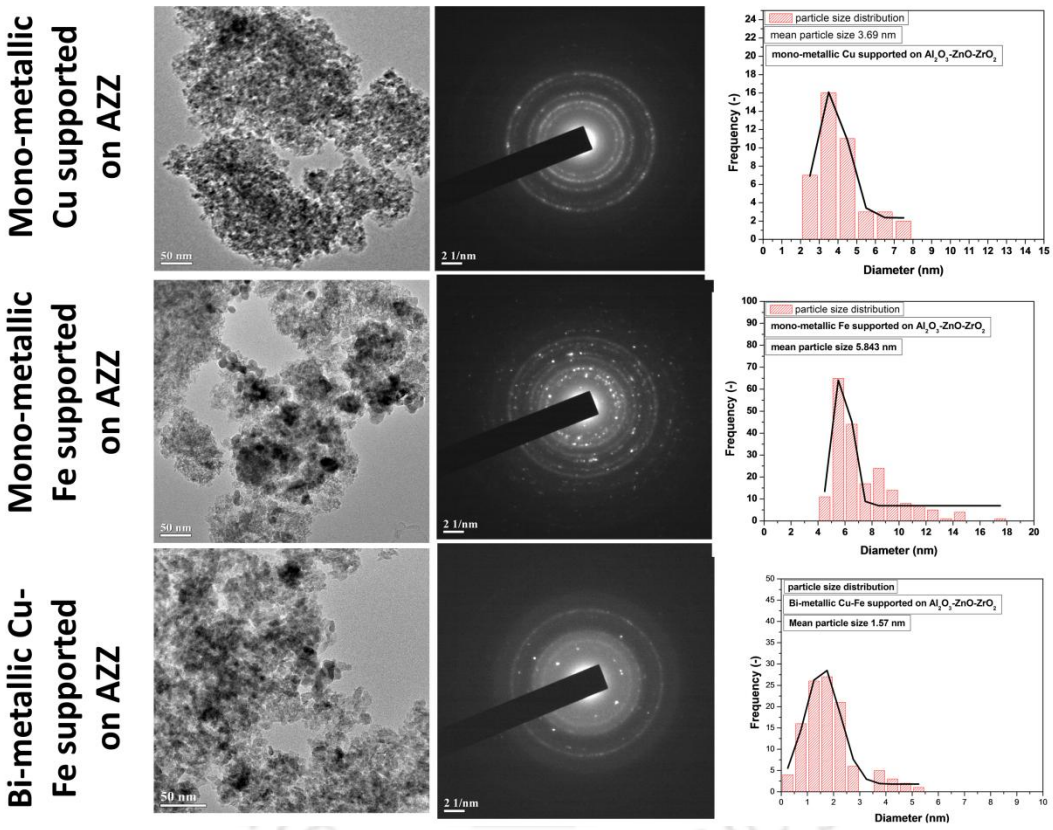

Fig. 4.9a TEM Characterization of monometallic Cu, Fe and bimetallic Cu-Fe supported on AZZ catalysts

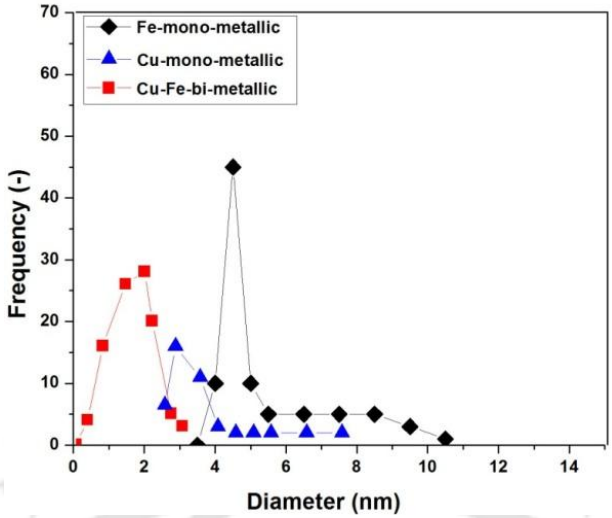

Fig. 4.9b Characterization of monometallic Cu, Fe and bimetallic Cu-Fe supported on AZZ catalysts particle size distribution calculated using TEM data

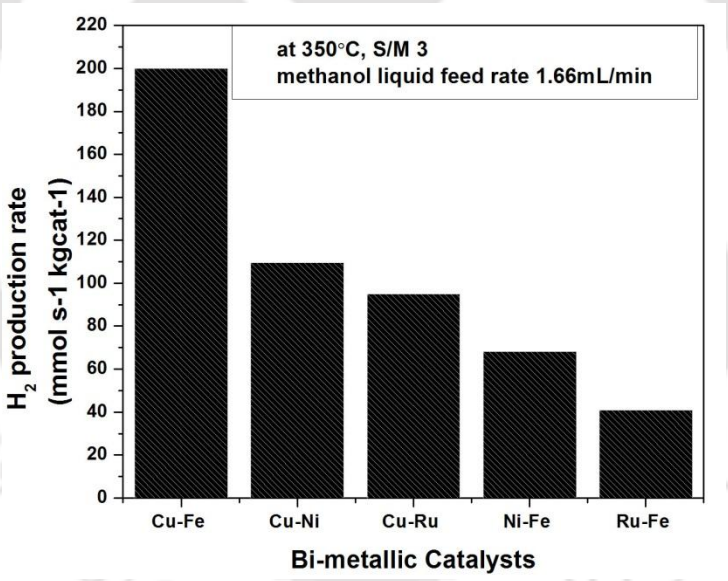

Fig. 4.10 Hydrogen production rate for bimetallic catalysts

Formation of Cu-Fe alloy was also analyzed using X-ray diffraction (XRD) as shown in Fig. 4.11. All catalysts were characterized after two hours of reduction treatment in H_2/N_2 mixture at 450°C. Fig. 4.11 compares the XRD peaks of mono-metallic Cu and Fe catalysts with bimetallic Cu-Fe prepared in different molar ratios such as 25/75, 50/50 and 75/25. Mono-metallic Fe showed the peaks characteristic of rhombohedral hematite

Fe_2O_3 structure at 32.94° (104 plane) and 35.54° (110 plane) [63]. In case of mono-metallic Cu supported on AZZ, the peaks are a characteristic of crystalline CuO (32°, 35.6°, 38.5°, 37.5°) phase with tenorite structure (JCPS 481548). No peaks of ZnO, ZrO_2 and Al_2O_3 further indicates that they are well dispersed and in an amorphous state [64-66]. Bi-metallic Cu-Fe supported on AZZ catalysts on the other hand show a distinct peak at 2θ=20.5° that appeared especially with Cu-Fe 50/50 and 75/25 molar ratios. This peak corresponds to the tetragonal structure of copper ferrite $CuFe_2O_4$ according to the JCPDS file No. 34-0425 [67, 68].

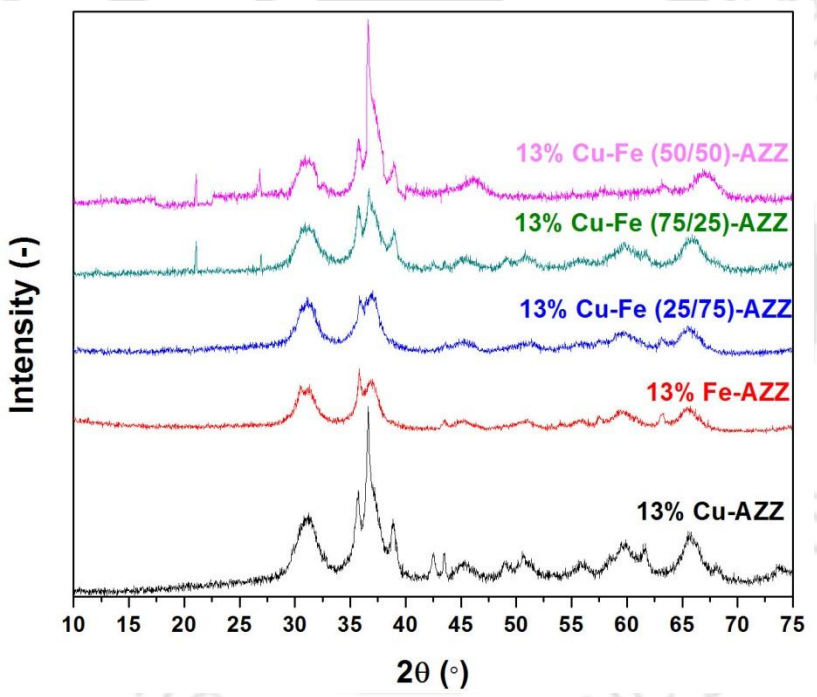

Fig. 4.11 XRD analysis for the mono-metallic and bimetallic Cu, Fe series

The catalysts activity with similar Cu-Fe molar ratios was performed as shown in Fig. 4.12. It was observed that catalysts activity with 50/50 molar ratio was the highest. Interestingly, CO selectivity was below detection limit for Cu-Fe combinations either equimolar, or higher Cu percentage. Further, higher Fe percentage in Cu-Fe bimetallic catalyst was observed to deteriorate the catalyst performance. Further, TEM analysis for

Cu-Fe bimetallic catalysts was also performed. Fig. 4.13 shows that the d-spacing with Cu-Fe (50/50) molar ratio was smallest followed closely with Cu-Fe (75/25). Reduced d-spacing thereby establishes formation of solid solution that is an alloy.

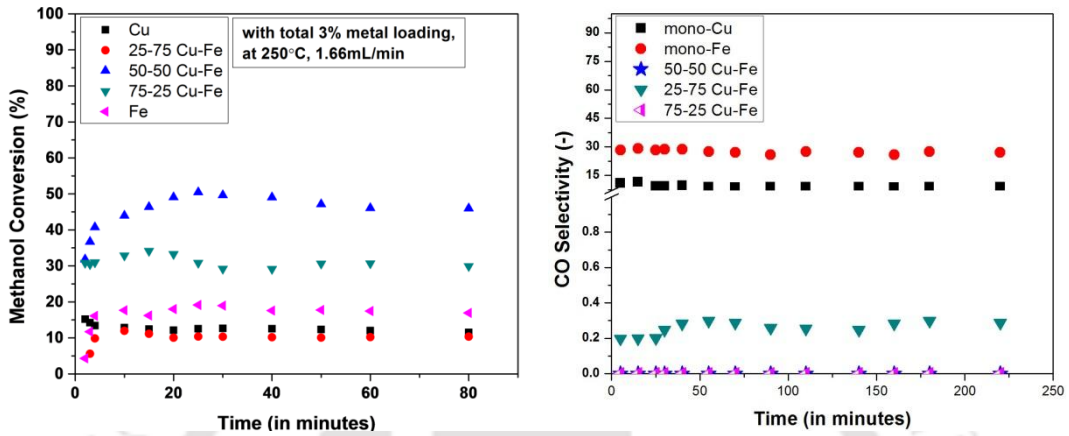

Fig. 4.12 Catalysts activity of Cu-Fe bimetallic series: a) Methanol conversion and b) CO selectivity

Hence, in order to have higher catalytic activity, Fe beyond 6 wt. % corresponding to Cu-Fe (50/50) molar ratio should not be used.

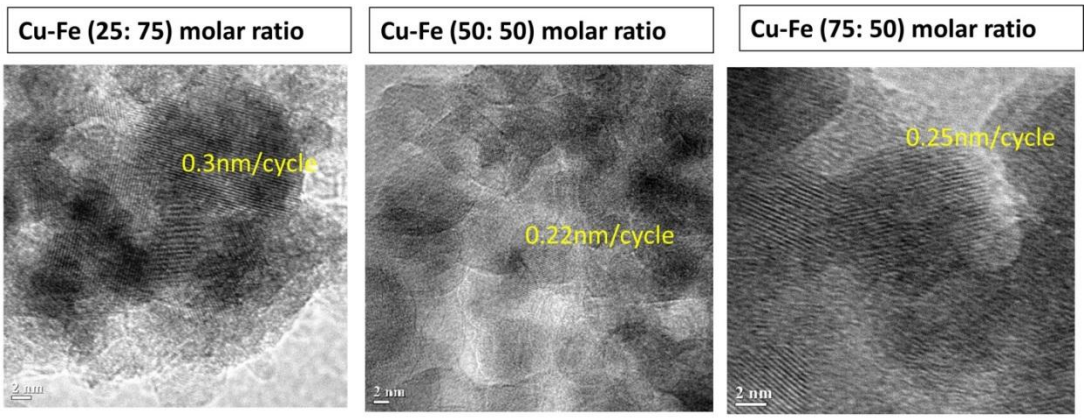

Fig. 4.13 **TEM characterization of Cu-Fe with varying molar ratio**

4.4.6 Activity testing

With the best performing catalyst that is Cu-Fe (50/50) supported on AZZ was tested against two variables: a) steam to methanol (S/M) ratio, b) weight of catalyst/molar flow rate of methanol (W/F)

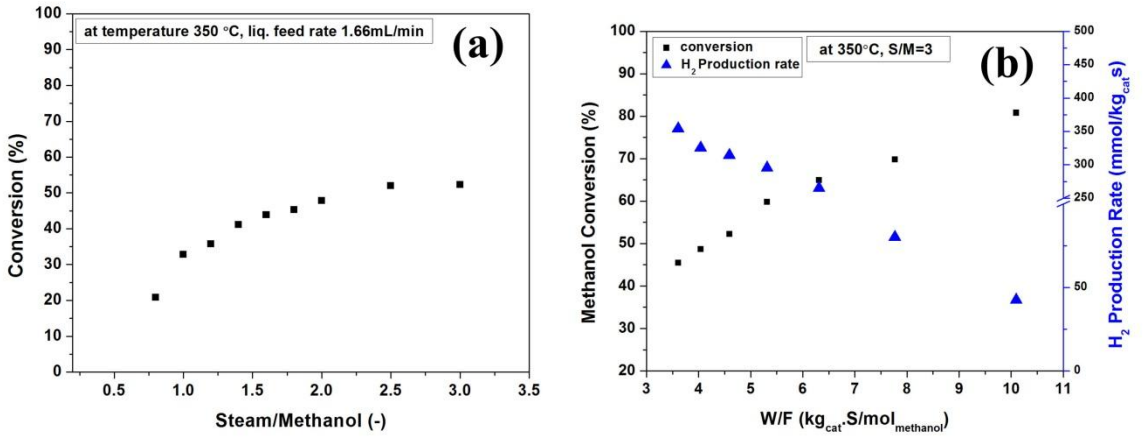

Fig. 4.14 Catalyst activity: a) Effect of S/M ratio and b) Effect of W/F

Fig. 4.14a shows that increasing steam in feed increases methanol conversion up to S/M equal to 2/1. Beyond this feed composition, methanol conversion remains constant. Increase in methanol conversion with steam occurs due to shift in reaction equilibrium towards water gas shift as mentioned in reaction 4.2. As a result of this, additional moles of hydrogen are produced. However, beyond 2/1 feed composition methanol dilution causes no further increase in hydrogen production thereby CO_2 generation also becomes constant. Further, Fig. 4.14b shows the effect of contact time on catalysts performance. Catalysts mass was maintained while flow rate was increased. This explains the decrease in hydrogen production rate with increasing W/F. Higher methanol flow rate with W/F 3 results in maximum hydrogen produced. This is because moles of hydrogen produced are a function of methanol molar flow fed. With increasing W/F on the other hand, flow rate

is continuously decreasing that enhances the contact time with the catalysts and hence improves conversion.

4.4.7 Effect of temperature on catalysts activity

Methanol steam reforming as shown in reaction 4.1 is an endothermic reaction. Hence, increase in temperature improves the methanol conversion with all the catalysts. Fig. 15a shows the performance of all bimetallic catalysts and Cu-Fe with different molar ratios in comparison with monometallic Cu and Fe. The total metal loading for the catalysts tested was 13%. As shown in Fig. 15b, methanol steam reforming activity was observed to be maximum with 13% metal. Beyond 13% metal loading, deterioration in catalysts activity was also observed. This may occur due to clogging of pore mouth with excess metal. Hence, 13% metal loading was used to observe the effect of temperature on all catalysts performance.

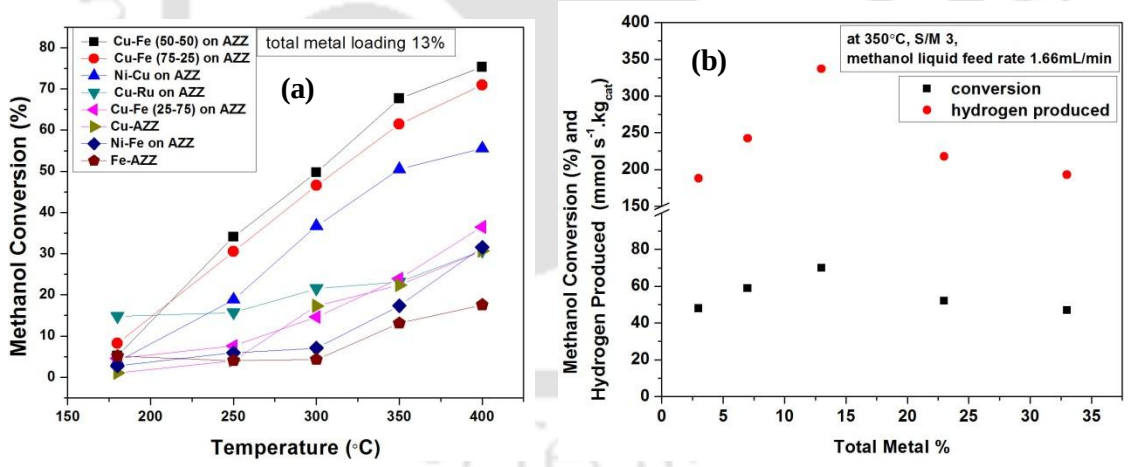

Fig. 4.15a Catalysts activity: a) Effect of temperature and b) Effect on increasing metal loading

From Fig. 15a it can be clearly stated that Cu-Fe (50-50 and 75-25) are the best performing catalysts in all temperature range.

4.4.8 Optimal Catalyst Testing with DRIFT

Fig. 4.16 shows the DRIFT study performed to analyze the intermediate formed with methanol steam reforming at varying temperatures for Cu-Fe (50-50) supported on AZZ. With this study, change in methanol-water vibration spectra at increasing temperatures was observed. Further, catalyst testing with DRIFT was also performed after hydrogen reduction as carried out during reaction. From Fig. 4.16 it can be observed that no C-O stretching showed at all temperatures tested. This confirms the negligence of CO selectivity with the developed catalyst. Further, methoxy stretch observed at 2950 and 2836 cm^{-1} also indicates the readily adsorption of methanol even at 50°C. Decrease in the intensity of these methoxy characteristic peaks suggests conversion to occur rapidly beyond 150°C. In addition to this, with increasing temperature intensity of peak at 1600 cm^{-1} is increasing. This indicates the occurrence of bi-carbonate species. It is reported that methoxy species are converted to formate and bicarbonate species. This observation is consistent with the reaction mechanism reported in literature.

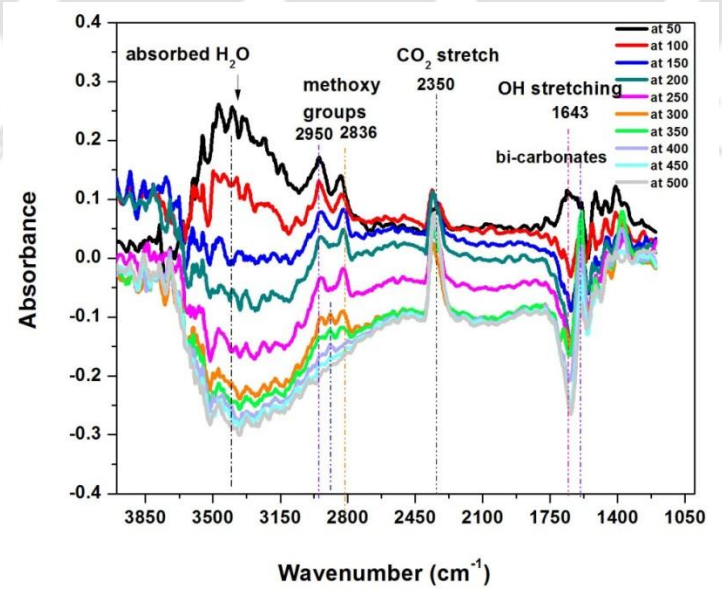

Fig. 4.16 DRIFT analysis for Cu-Fe supported on AZZ

Hence, with this confirmation that the developed catalyst follows the formate pathway and with the presence of Fe_2O_3 determined using XRD, the reaction mechanism for the developed catalyst was proposed. Fig. 4.17 shows that with Cu-Fe supported on AZZ, presence of Fe_2O_3 as surface species converts the CO produced to CO_2 resulting in no detectable CO in the final product stream. A high redox activity of Fe thereby not only enhances the hydrogen production rate but helps enable to produce CO free product with methanol steam reforming even at high temperatures.

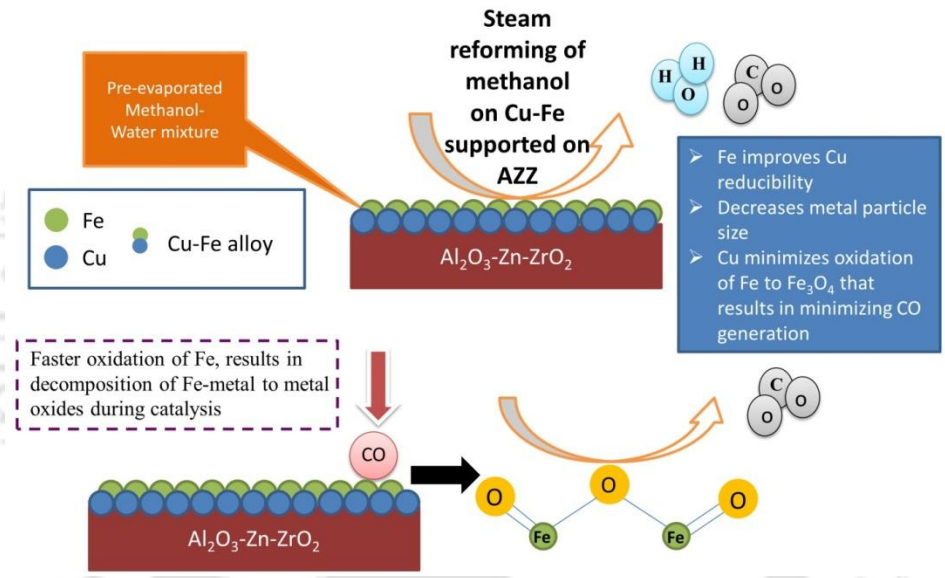

Fig. 4.17 Proposed mechanism for Cu-Fe supported on AZZ

4.4.9 Catalyst Stability

The optimized catalyst was hereby tested for a period of 100 hours to evaluate its stability over time. Fig. 4.18 shows no decrease in activity throughout the 100 hour run. The initial increase in methanol conversion results from the complete utilization of the catalysts surface. Beyond this point a slight decrease in mass transfer was observed that resulted in slight decrease in conversion. However, beyond this point, the catalysts

performance was observed stable. This suggests that the developed catalyst can be utilized for pilot scale performance with the integrated membrane reformer designed.

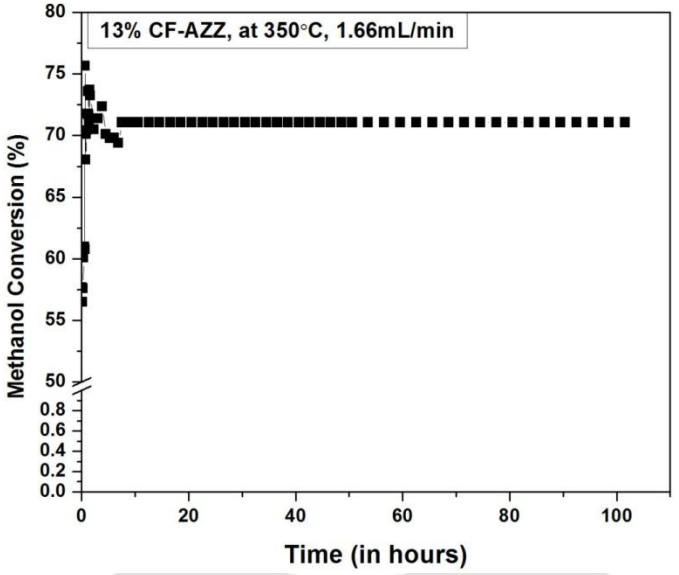

Fig. 4.18 **Stability of Cu-Fe supported on AZZ**

4.5 Summary

In the current study, series of mono-metallic and bi-metallic catalysts were synthesized using incipient wetness impregnation with 3% metal supported on Al_2O_3-Zn-Zr. Catalyst characterization was carried out using TPR, FESEM and particle size distribution analysis of TEM images. Further, all catalyst testing for methanol steam reforming at temperature 350˚C, GHSV 9000h^{-1} and S/M ratio 3 was carried out. The objective of the study was to determine a catalyst which can provide minimal CO selectivity for methanol steam reforming at higher temperature.

Mono-metallic catalysts such as Cu, Ni, Pd, Ru and Fe supported on Al_2O_3-Zn-ZrO_2 were tested. A distinct difference in CO selectivity between noble and non-noble metals was

observed. Further, Fe as promoter was studied owing to its fast reduction characteristics in the synthesis of bi-metallic catalysts. An interesting synergy between Cu and Fe supported on AZZ was observed which resulted in lower metal particle size, enhanced catalytic activity as well as zero CO selectivity. Addition of Fe to Cu reduced the metal particle size that indicates the formation of alloy at 50:50 (mol: mol) composition. The drastic reduction in CO selectivity in comparison to mono-metallic can therefore be justified with the alloy formed that also resulted in enhanced activity observed in terms of hydrogen production rate (~200 mmol/ kg_{cat}.s with 3% total metal). At 350˚C, W/F 5 kg_{cat}.s/$mol_{methanol}$ and S/M ratio 3, Cu-Fe was provides ~48% methanol conversion with 3% total metal loading and up to 70% methanol conversion with 13% total metal loading. Further, the optimal catalyst with 13% metal loading was also tested with effect of S/M ratio, W/F, temperature and lastly its stability for up to 100 hours was performed. In addition to this, no occurrence of CO with the developed Cu-Fe supported on AZZ catalyst was also demonstrated with DRIFT. On the basis of the analysis, the reaction mechanism was also proposed.Thus, with the current observations, we report Cu-Fe supported on Al_2O_3-Zn-Zr as a promising catalyst with zero CO selectivity up to 400°C at GHSV 9000h^{-1} and S/M 3 molar ratio.

References

[1] A. Farsi, S.S. Mansouri, Influence of nanocatalyst on oxidative coupling, steam and dry reforming of methane: A short review, Arabian Journal of Chemistry, 9 (2016) S28-S34.

[2] S. Freni, S. Cavallaro, N. Mondello, L. Spadaro, F. Frusteri, Production of hydrogen for MC fuel cell by steam reforming of ethanol over MgO supported Ni and Co catalysts, Catalysis Communications, 4 (2003) 259-268.

[3] G. Guan, M. Kaewpanha, X. Hao, A. Abudula, Catalytic steam reforming of biomass tar: Prospects and challenges, Renewable and Sustainable Energy Reviews, 58 (2016) 450-461.

[4] A. Haryanto, S. Fernando, N. Murali, S. Adhikari, Current Status of Hydrogen Production Techniques by Steam Reforming of Ethanol: A Review, Energy & Fuels, 19 (2005) 2098-2106.

[5] Y. Qian, S. Liang, T. Wang, Z. Wang, W. Xie, X. Xu, Enhancement of pyrolysis gasoline hydrogenation over Zn- and Mo-promoted Ni/γ-Al2O3 catalysts, Catalysis Communications, 12 (2011) 851-853.

[6] J.M. Sieben, V. Comignani, A.E. Alvarez, M.M.E. Duarte, Synthesis and characterization of Cu core Pt–Ru shell nanoparticles for the electro-oxidation of alcohols, International Journal of Hydrogen Energy, 39 (2014) 8667-8674.

[7] P.D. Vaidya, A.E. Rodrigues, Insight into steam reforming of ethanol to produce hydrogen for fuel cells, Chemical Engineering Journal, 117 (2006) 39-49.

[8] R.Y. Abrokwah, V.G. Deshmane, D. Kuila, Comparative performance of M-MCM-41 (M: Cu, Co, Ni, Pd, Zn and Sn) catalysts for steam reforming of methanol, Journal of Molecular Catalysis A: Chemical, 425 (2016) 10-20.

[9] J.P. Breen, J.R.H. Ross, Methanol reforming for fuel-cell applications: development of zirconia-containing Cu–Zn–Al catalysts, Catalysis Today, 51 (1999) 521-533.

[10] V. Durga Kumari, M. Subrahmanyam, A. Ratnamala, D. Venugopal, B. Srinivas, M.V. Phanikrishna Sharma, S.S. Madhavendra, B. Bikshapathi, K. Venkateswarlu, T. Krishnudu, K.B.S. Prasad, K.V. Raghavan, Correlation of activity and stability of CuO/ZnO/Al2O3 methanol steam reforming catalysts with Cu/Zn composition obtained by SEM–EDAX analysis, Catalysis Communications, 3 (2002) 417-424.

[11] B. Lindström, L.J. Pettersson, P. Govind Menon, Activity and characterization of Cu/Zn, Cu/Cr and Cu/Zr on γ-alumina for methanol reforming for fuel cell vehicles, Applied Catalysis A: General, 234 (2002) 111-125.

[12] S. Patel, K.K. Pant, Influence of preparation method on performance of Cu(Zn)(Zr)-alumina catalysts for the hydrogen production via steam reforming of methanol, Journal of Porous Materials, 13 (2006) 373-378.

[13] M. Yang, S. Li, G. Chen, High-temperature steam reforming of methanol over ZnO–Al2O3 catalysts, Applied Catalysis B: Environmental, 101 (2011) 409-416.

[14] J. Sehested, Four challenges for nickel steam-reforming catalysts, Catalysis Today, 111 (2006) 103-110.

[15] W. Tao, H. Cheng, W. Yao, X. Lu, Q. Zhu, G. Li, Z. Zhou, Syngas production by CO2 reforming of coke oven gas over Ni/La2O3–ZrO2 catalysts, International Journal of Hydrogen Energy, 39 (2014) 18650-18658.

[16] T. Umile, Catalysts and Sustainability, in: Catalysis for Sustainability, CRC Press, 2015, pp. 1-22.

[17] N. Iwasa, N. Takezawa, New Supported Pd and Pt Alloy Catalysts for Steam Reforming and Dehydrogenation of Methanol, Topics in Catalysis, 22 (2003) 215-224.

[18] V. Dal Santo, A. Gallo, A. Naldoni, M. Guidotti, R. Psaro, Bimetallic heterogeneous catalysts for hydrogen production, Catalysis Today, 197 (2012) 190-205.

[19] L. De Rogatis, T. Montini, B. Lorenzut, P. Fornasiero, NixCuy/Al2O3 based catalysts for hydrogen production, Energy & Environmental Science, 1 (2008) 501-509.

[20] S. Hu, L. He, Y. Wang, S. Su, L. Jiang, Q. Chen, Q. Liu, H. Chi, J. Xiang, L. Sun, Effects of oxygen species from Fe addition on promoting steam reforming of toluene over Fe–Ni/Al2O3 catalysts, International Journal of Hydrogen Energy, 41 (2016) 17967-17975.

[21] L. Wang, D. Li, M. Koike, S. Koso, Y. Nakagawa, Y. Xu, K. Tomishige, Catalytic performance and characterization of Ni-Fe catalysts for the steam reforming of tar from biomass pyrolysis to synthesis gas, Applied Catalysis A: General, 392 (2011) 248-255.

[22] J. Agrell, H. Birgersson, M. Boutonnet, I. Melián-Cabrera, R.M. Navarro, J.L.G. Fierro, Production of hydrogen from methanol over Cu/ZnO catalysts promoted by ZrO2 and Al2O3, Journal of Catalysis, 219 (2003) 389-403.

[23] H. Jeong, K.I. Kim, T.H. Kim, C.H. Ko, H.C. Park, I.K. Song, Hydrogen production by steam reforming of methanol in a micro-channel reactor coated with Cu/ZnO/ZrO2/Al2O3 catalyst, Journal of Power Sources, 159 (2006) 1296-1299.

[24] S. Velu, K. Suzuki, M. Okazaki, M.P. Kapoor, T. Osaki, F. Ohashi, Oxidative Steam Reforming of Methanol over CuZnAl(Zr)-Oxide Catalysts for the Selective Production of Hydrogen for Fuel Cells: Catalyst Characterization and Performance Evaluation, Journal of Catalysis, 194 (2000) 373-384.

[25] D. Das, J. Llorca, M. Dominguez, S. Colussi, A. Trovarelli, A. Gayen, Methanol steam reforming behavior of copper impregnated over CeO2–ZrO2 derived from a surfactant assisted coprecipitation route, International Journal of Hydrogen Energy, 40 (2015) 10463-10479.

[26] B. Lindström, L.J. Pettersson, Steam reforming of methanol over copper-based monoliths: the effects of zirconia doping, Journal of Power Sources, 106 (2002) 264-273.

[27] S. Liu, K. Takahashi, H. Eguchi, K. Uematsu, Hydrogen production by oxidative methanol reforming on Pd/ZnO: Catalyst preparation and supporting materials, Catalysis Today, 129 (2007) 287-292.

[28] K.M.K. Yu, W. Tong, A. West, K. Cheung, T. Li, G. Smith, Y. Guo, S.C.E. Tsang, Non-syngas direct steam reforming of methanol to hydrogen and carbon dioxide at low temperature, Nature Communications, 3 (2012) 1230.

[29] R.O. Idem, N.N. Bakhshi, Production of Hydrogen From Methanol. 2. Experimental Studies, Industrial & Engineering Chemistry Research, 33 (1994) 2056-2065.

[30] A.A. Lytkina, N.A. Zhilyaeva, M.M. Ermilova, N.V. Orekhova, A.B. Yaroslavtsev, Influence of the support structure and composition of Ni–Cu-based catalysts on hydrogen production by methanol steam reforming, International Journal of Hydrogen Energy, 40 (2015) 9677-9684.

[31] P. Mierczynski, K. Vasilev, A. Mierczynska, W. Maniukiewicz, M.I. Szynkowska, T.P. Maniecki, Bimetallic Au–Cu, Au–Ni catalysts supported on MWCNTs for oxy-steam reforming of methanol, Applied Catalysis B: Environmental, 185 (2016) 281-294.

[32] Y. Matsumura, Enhancement in activity of Pd–Zn catalyst for methanol steam reforming by coprecipitation on zirconia support, Applied Catalysis A: General, 468 (2013) 350-358.

[33] T. Conant, A.M. Karim, V. Lebarbier, Y. Wang, F. Girgsdies, R. Schlögl, A. Datye, Stability of bimetallic Pd–Zn catalysts for the steam reforming of methanol, Journal of Catalysis, 257 (2008) 64-70.

[34] O.M. Ilinich, Y. Liu, E.M. Waterman, R.J. Farrauto, Kinetics of Methanol Steam Reforming with a Pd–Zn–Y/CeO2 Catalyst under Realistic Operating Conditions of a Portable Reformer in Fuel Cell Applications, Industrial & Engineering Chemistry Research, 52 (2013) 638-644.

[35] K.M. Eblagon, P.H. Concepción, H. Silva, A. Mendes, Ultraselective low temperature steam reforming of methanol over PdZn/ZnO catalysts—Influence of induced support defects on catalytic performance, Applied Catalysis B: Environmental, 154 (2014) 316-328.

[36] G.J.K. Acres, A.J. Bird, J.W. Jenkins, F. King, The design and preparation of supported catalysts, in: C. Kemball, D.A. Dowden (Eds.) Catalysis: Volume 4, The Royal Society of Chemistry, 1981, pp. 1-30.

[37] E. Marceau, X. Carrier, M. Che, Impregnation and Drying, in: Synthesis of Solid Catalysts, Wiley-VCH Verlag GmbH & Co. KGaA, 2009, pp. 59-82.

[38] C. Kumar Patel, P. Jyoti Sarma, M. De, Comparative parametric study on development of porous structure of aluminium oxide in presence of anionic and cationic surfactants, Ceramics International, 41 (2015) 3578-3588.

[39] S. Brunauer, P.H. Emmett, E. Teller, Adsorption of Gases in Multimolecular Layers, Journal of the American Chemical Society, 60 (1938) 309-319.

[40] E.P. Barrett, L.G. Joyner, P.P. Halenda, The Determination of Pore Volume and Area Distributions in Porous Substances. I. Computations from Nitrogen Isotherms, Journal of the American Chemical Society, 73 (1951) 373-380.

[41] R. Sharma, A. Kumar, R.K. Upadhyay, Performance comparison of methanol steam reforming integrated to Pd-Ag membrane: Membrane reformer vs. membrane separator, Separation and Purification Technology, 183 (2017) 194-203.

[42] K.S.W. Sing, D.H. Everett, R.A.W. Haul, L. Moscou, R.A. Pierotti, J. Rouquerol, T. Siemieniewska, Reporting Physisorption Data for Gas/Solid Systems, in: Handbook of Heterogeneous Catalysis, Wiley-VCH Verlag GmbH & Co. KGaA, 2008.

[43] S. Patel, K.K. Pant, Experimental study and mechanistic kinetic modeling for selective production of hydrogen via catalytic steam reforming of methanol, Chemical Engineering Science, 62 (2007) 5425-5435.

[44] K. Föttinger, J.A. van Bokhoven, M. Nachtegaal, G. Rupprechter, Dynamic Structure of a Working Methanol Steam Reforming Catalyst: In Situ Quick-EXAFS on Pd/ZnO Nanoparticles, The Journal of Physical Chemistry Letters, 2 (2011) 428-433.

[45] F.-W. Chang, L.S. Roselin, T.-C. Ou, Hydrogen production by partial oxidation of methanol over bimetallic Au–Ru/Fe2O3 catalysts, Applied Catalysis A: General, 334 (2008) 147-155.

[46] S. Aouad, C. Gennequin, M. Mrad, H.L. Tidahy, J. Estephane, A. Aboukaïs, E. Abi-Aad, Steam reforming of methanol over ruthenium impregnated ceria, alumina and ceria–alumina catalysts, International Journal of Energy Research, 40 (2016) 1287-1292.

[47] M. Konsolakis, Z. Ioakimidis, T. Kraia, G. Marnellos, Hydrogen Production by Ethanol Steam Reforming (ESR) over CeO2 Supported Transition Metal (Fe, Co, Ni, Cu) Catalysts: Insight into the Structure-Activity Relationship, Catalysts, 6 (2016) 39.

[48] J. Zhang, H. Li, PEM Fuel Cell Electrocatalysts and Catalyst Layers: Fundamentals and Applications, 2008.

[49] J. Ashok, S. Kawi, Nickel–Iron Alloy Supported over Iron–Alumina Catalysts for Steam Reforming of Biomass Tar Model Compound, ACS Catalysis, 4 (2014) 289-301.

[50] M. Koike, D. Li, Y. Nakagawa, K. Tomishige, A Highly Active and Coke-Resistant Steam Reforming Catalyst Comprising Uniform Nickel–Iron Alloy Nanoparticles, ChemSusChem, 5 (2012) 2312-2314.

[51] A. Djaidja, A. Kiennemann, A. Barama, Effect of Fe or Cu addition on Ni/Mg-Al and Ni/MgO catalysts in the steam-reforming of methane, Studies in Surface Science and Catalysis, 162 (2006) 945-952.

[52] Y. Kathiraser, J. Ashok, S. Kawi, Synthesis and evaluation of highly dispersed SBA-15 supported Ni-Fe bimetallic catalysts for steam reforming of biomass derived tar reaction, Catalysis Science & Technology, 6 (2016) 4327-4336.

[53] A.V.H. Soares, J.B. Salazar, D.D. Falcone, F.A. Vasconcellos, R.J. Davis, F.B. Passos, A study of glycerol hydrogenolysis over Ru–Cu/Al2O3 and Ru–Cu/ZrO2 catalysts, Journal of Molecular Catalysis A: Chemical, 415 (2016) 27-36.

[54] R. Molina, G. Poncelet, α-Alumina-Supported Nickel Catalysts Prepared from Nickel Acetylacetonate: A TPR Study, Journal of Catalysis, 173 (1998) 257-267.

[55] J. Zieliński, I. Zglinicka, L. Znak, Z. Kaszkur, Reduction of Fe2O3 with hydrogen, Applied Catalysis A: General, 381 (2010) 191-196.

[56] S.K. Singh, A.K. Singh, K. Aranishi, Q. Xu, Noble-Metal-Free Bimetallic Nanoparticle-Catalyzed Selective Hydrogen Generation from Hydrous Hydrazine for Chemical Hydrogen Storage, Journal of the American Chemical Society, 133 (2011) 19638-19641.

[57] R. Burch, M.J. Hayes, The Preparation and Characterisation of Fe-Promoted Al2O3-Supported Rh Catalysts for the Selective Production of Ethanol from Syngas, Journal of Catalysis, 165 (1997) 249-261.

[58] W. Li, L. Ye, P. Long, J. Chen, H. Ariga, K. Asakura, Y. Yuan, Efficient Ru-Fe catalyzed selective hydrogenolysis of carboxylic acids to alcoholic chemicals, RSC Advances, 4 (2014) 29072-29082.

[59] A. Guerrero-Ruiz, A. Sepúlveda-Escribano, I. Rodríguez-Ramos, Carbon supported bimetallic catalysts containing iron, Applied Catalysis A: General, 81 (1992) 81-100.

[60] Y.-H. Huang, S.-F. Wang, A.-P. Tsai, S. Kameoka, Reduction behaviors and catalytic properties for methanol steam reforming of Cu-based spinel compounds CuX2O4 (X=Fe, Mn, Al, La), Ceramics International, 40 (2014) 4541-4551.

[61] K. Chen, Y. Fan, Q. Yan, Metal–Support Interactions in Fe/ZrO2Catalysts for Hydrogenation of CO, Journal of Catalysis, 167 (1997) 573-575.

[62] B.S. Mitchell, The Structure of Materials, in: An Introduction to Materials Engineering and Science, John Wiley & Sons, Inc., 2004, pp. 1-135.

[63] J.-L. Cao, Y. Wang, X.-L. Yu, S.-R. Wang, S.-H. Wu, Z.-Y. Yuan, Mesoporous CuO–Fe2O3 composite catalysts for low-temperature carbon monoxide oxidation, Applied Catalysis B: Environmental, 79 (2008) 26-34.

[64] G.-S. Wu, D.-S. Mao, G.-Z. Lu, Y. Cao, K.-N. Fan, The Role of the Promoters in Cu Based Catalysts for Methanol Steam Reforming, Catalysis Letters, 130 (2009) 177-184.

[65] L. Yong-Feng, D. Xin-Fa, L. Wei-Ming, Effects of ZrO2-promoter on catalytic performance of CuZnAlO catalysts for production of hydrogen by steam reforming of methanol, International Journal of Hydrogen Energy, 29 (2004) 1617-1621.

[66] J. Ding, J. Chen, Synthesis of Cu-Zn-Zr-Al-O catalysts via a citrate complex route modified by different solvents and their dehydrogenation/hydrogenation performance, RSC Advances, 5 (2015) 82822-82833.

[67] H. Jiao, G. Jiao, J. Wang, Preparation and Magnetic Properties of CuFe2O4 Nanoparticles, Synthesis and Reactivity in Inorganic, Metal-Organic, and Nano-Metal Chemistry, 43 (2013) 131-134.

[68] R. Zhang, Y. Li, T. Zhen, Ammonia selective catalytic reduction of NO over Fe/Cu-SSZ-13, RSC Advances, 4 (2014) 52130-52139.

Chapter 5

Integration, Design and Testing of a Compact Membrane Reformer

Abstract

In this chapter, methanol steam reforming with hydrogen-selective dense Pd-Ag membranes was integrated in a single unit called a membrane reformer. It is a compact and efficient system for 'on-board' hydrogen production. The high purity hydrogen generated can be easily fed to proton exchange membrane (PEM) fuel cells for power generation in portable small scale batteries and generators. A crucial factor which may limit the performance of membrane reformers is the separation efficiency of the membrane. Hydrogen permeation through standalone dense Pd-Ag membranes is largely reported to be limited by the presence of gases such as CO, CO_2 and steam. These gas mixtures are also basic constituents of methanol reformate which contains approximately 60% hydrogen by mole. Such gas inhibition behavior is expected to significantly affect membrane reformer performance. The present work therefore compares the performance of a membrane reformer with a membrane separator under similar operating conditions using a 100μm thick self-supported dense Pd-Ag membrane. By definition, a membrane separator is principally a purifier which is used to separate hydrogen from various components such as CO_2, H_2O, CH_4 and CO. On the other hand, membrane reformer is a system which generates hydrogen from a reaction such as steam reforming and simultaneously separates it using membranes, integrated in the same physical device. Performance of the membrane reformer was optimized with respect to the effect of

steam/methanol ratio, temperature and pressure. Under optimal conditions, synthetic gas mixture of similar composition as that of the produced reformate was used to evaluate the membrane separator performance. Further, membrane reformer studies were carried out and compared between commercially available self-supported and in-house synthesized supported Pd-based membranes. Testing of membrane reformed containing multiple porous SS (PSS)-supported Pd-Ag membranes was further performed to determine the effect of multiple passes using two case studies: a) without baffle and b) with baffle. The obtained hydrogen flow rate in the membrane reformer having four Pd-Ag membranes supported on PSS was compared with the hydrogen output rate required for a 200W PEM fuel cell.

5.1 Membrane reformers: process integrated units

Integration of hydrogen generation with simultaneous separation in a single compact unit introduces the concept of membrane reformers. Integrated reaction-separation was first proposed by Professor Vladimir Gryaznov (Moscow University) in the year 1964 [1, 2]. He proposed a method to carry out simultaneous evolution and consumption of H_2 in a dense tubular palladium membrane reactor where Pd is permeable to H_2 and also serves as a catalyst for the dehydrogenation of cyclohexane to benzene [1, 2]. The potential advantage of membrane reformers is that higher conversion rates can be achieved compared to traditional reformers. According to Le Chatelier's principle, selective removal of one of the reaction products results in a shift in equilibrium towards the product side thereby increasing conversion. Hence, for the same conversion as of the traditional reactor the membrane reformers can be operated at much lower temperature. Therefore, membrane reformer overcomes thermodynamic limitations of the reversible

chemical reactions, uses less severe conditions (temperature and pressure), requires smaller volume and consumes less energy.

Using high energy density alcohols such as methanol, these membrane reformers are applied 'on-board' to produce high purity hydrogen. Increase in conversion increases the trans membrane hydrogen partial pressure difference which results in better hydrogen permeation. Further, being an integrated assembly, membrane reformer does not require a dedicated separation unit which significantly reduces the size of the system and minimizes the downstream processing cost. This makes the membrane reformer more feasible for commercial applications, particularly for 'on-board' or 'on-demand' hydrogen generation [3-5]. Hydrogen purity is determined by membrane material's selectivity to hydrogen preventing all other undesired reaction products and unreacted feed from passing through. Therefore, a successful operation in a membrane reactor requires sufficient kinetic compatibility between the rates of the reactions of interest and the rates of transport through the membranes. Thus, the most crucial aspects that affect membrane reformer performance are as follows:

a) **Property of membrane**: For membrane materials such as palladium (Pd), higher hydrogen selectivity can only be obtained if the membrane morphology is dense or non-porous. Further, hydrogen flux is a function of palladium membrane thickness. Lower the thickness, higher is the flux. The challenge in this case is fabrication a dense Pd membranes on a porous support with lower thickness.

b) **Selectivity-conversion behaviour**: Performance of membrane reactor is dominated by the hydrogen permeability of palladium membranes. Permeability further is higher, once

the partial pressure of hydrogen in feed to membrane is high thereby maintaining a high trans membrane pressure difference. As permeation of hydrogen increases reaction conversion increases. Hence, higher hydrogen recovery and high reaction conversion are two crucial parameters hat determine the membrane reactor performance.

c) **Load to surface ratio**: It is crucial that the membrane surface area available for hydrogen permeation be always higher than the load in the membrane reformer. Here, load indicates the amount of hydrogen produced by the catalyst. By doing this, compatibility between the hydrogen flux that pass the membrane and amounts consumed or produced during the chemical reaction can be maintained [6].

The system performance in case of a membrane reformer is both kinetically as well as diffusion controlled which thereby necessitates the need of an optimal temperature, pressure and flow rate that can maintain stability of the catalysts as well as the membrane. In contrast to simultaneously integrated membrane reformers, membrane separator functions sequentially as the reaction assembly is connected in series with the membrane assembly (as discussed in chapter 3). Although such segregation makes the system bulky, it allows independent control of temperature and pressure for reaction and membrane separation. Further, as the condensates can be easily removed before the reformate mixture is fed to the separator, steam inhibition and methanol inhibition (if any) effects can be eliminated and the gaseous transport through the membrane is only diffusion-limited. This may enhance the performance as well as the life of the membrane.

In the current work, optimization of membrane reformer with effect of steam to methanol (S/M) ratio, temperature (623–723K) and pressure was performed. With the optimized

conditions, membrane reformer performance was then compared with the membrane separator for the same membranes (without having steam and unreacted methanol in the feed to separator). Simulated reformate mixture gas of composition $50H_2$:$30N_2$:$18CO_2$:2CO (mol/mol) was used to determine the standalone membrane performance in the membrane separator. No sweep gas was used and permeate end was maintained at atmospheric pressure throughout to determine the standalone membrane performance at varying temperature, pressure and feed composition. High gas flow rate of 0.3 LPM was maintained for both membrane separator as well as membrane reformer which also negates concentration polarization to affect membrane performance. The objective of this comparison was to evaluate the conditions where membrane reformer performance can be made comparable with the separator. Further, under similar operating conditions, self-supported membrane was compared with supported Pd membrane integrated with the catalyst. Lastly using a set of four supported Pd-based membranes, membrane reformer integration was performed in three manners: a) integration using multiple membrane assembly (without baffle) with 6.8 cm ID reactor, b) integration using multiple membrane assembly (without baffle) with 12.5 cm ID reactor and c) integration using multiple membrane assembly (with baffle) with 12.5 cm ID reactor.

5.1.1 H_2 production by membrane reformers

A few groups who are actively working on integrated reaction-separation membrane reformers for hydrogen production includes *Tosti and Basile groups* [7-9] and *Kuipers, Dittmeyer and Elnashaie groups [10-12]*. Studies reported with these groups comprise of feasibility of packed bed MR study with commercial self-supported membranes and catalyst available. Further, Kuipers group have reported experimental as well as fluidized

bed MR studies primarily with methane as feed. In addition to this, commercialized membrane reformer designs are also available from Reb Research and Consultancy [13]. Salient features of the membrane reactors commercialized by Reb Research and Consultancy is present in Table 5.1.

Table 5.1 Commercialized membrane reformer systems

S. No.	Membrane reactor	Dimensions	Feed mixture	H_2 flow rate
1	ME-100 [REB]	The reactor was ½" **diameter** and 8" tall. Membrane 9.5" long, 0.625" x 6.5" membrane tube sealed at top.	1.09/1 molar mix of methanol/steam Catalyst (proprietary) Operation at 260^0C and 260 psig (up to 90psig) Flow rate 85ml/min.	1.5 slpm
2	ME 100-2 [REB]	16" x 17.5" x 21";	1:1 mix methanol & water, at 70psi	12.5slpm .
3	ME 150 [REB]	58" x 16"x38"	1:1 methanol water mix at 70 psi.	75 slpm

In literature, hydrogen generation and separation studies using palladium or Pd alloyed membranes are well reported [14-21]. Studies have demonstrated the optimization of methanol-based membrane reformer to achieve high hydrogen recovery and have highlighted higher methanol conversion compared to conventional reformer [7, 16-18, 20, 22, 23]. The parameters mostly reported to optimize hydrogen recovery include effect

of counter-current sweep gas, gas hourly space velocity (GHSV), steam-to-methanol (S/M) feed ratios, membrane area, temperature and pressure. Basile et al. [7, 20] reported the performance of 50 μm self-supported Pd-Ag membrane with co-current and counter-current modes of sweep gas. Integration was performed using Ru-Al_2O_3 as catalysts. Apart from H_2, CO and CO_2, CH_4 in the reformate stream was reported. Improvement in methanol conversion with membrane reformers (MR) in comparison to traditional reactors was higher at all temperatures. A maximum hydrogen recovery of 40% was reported with counter-current mode at 450°C, pressure 1.3 bar and S/M=4.5/1. Further, using $CuO/Al_2O_3/ZnO/MgO$ with sweep gas flow in counter-current mode and pressure 1.3 bar, MR performance was reported with varying S/M ratio (from 3/1 to 9/1) and temperature (250–300°C). The catalyst was prepared using co-precipitation. It was reported that with increasing temperature, effect of S/M on methanol conversion was more prominent. No CH_4 formation was reported while CO formation existed in the range 0.2 to 0.7 that is around 2000 to 7000ppm. This is to note that PEM fuel cell cannot tolerate CO beyond 10ppm and hence CO percentage in the permeate side of MR are critical. Lastly, due to low pressure difference a low hydrogen recovery of ~10% was reported. Using similar catalyst $CuO/Al_2O_3/ZnO/MgO$ and Pd-Ag self-supported membrane, at temperature 300°C and S/M=3, Iulianelli et al. [17, 22] reported effect of increasing pressure on MR performance. With varying weight hourly space velocity (WHSV) in the range of 0.36 to 1.82 h^{-1} and sweep gas flow rate of 143.1 ml/min, hydrogen yield with co-current as well as counter-current mode was reported between 60–77%. In addition, with varying sweep factor (SF) from 1.1 to 9.7, up to 90% hydrogen recovery was reported in counter-current mode at reaction pressure 3.5 bar and SF 9.7.

However, 90% hydrogen recovery was observed that WHSV 0.2 h^{-1} whereby the permeate hydrogen flow rate will be low. Hence, it is not only hydrogen recovery but also the volumetric flow rate of hydrogen produced that is essential for MR viability for commercialization. Further, at 330°C and 2.5 bar pressure for S/M molar feed ratio of 2.5:1 and GHSV 18500 h^{-1}, Liguori et al. [18] reported 85% methanol conversion using $Cu/ZnO/Al_2O_3$ and ~ 40% H_2 recovery with commercial alumina-supported 7 µm Pd membrane. The low hydrogen recovery for membrane reformer is mostly attributed to the co-adsorbed species on the membrane which reduces the hydrogen permeance through it. Further, inlet steam/methanol (S/M) composition was reported to play a crucial role in membrane reformer performance because it directly affects the percentage of H_2, CO, CO_2, steam and unreacted methanol that comes in contact with the membrane. CO was reported in the range of 0.4 to 1.21.

Ribeirinha et al. [23] reported a theoretical study where they compared hydrogen-selective membrane efficiency with CO_2-selective ionic liquids (ILs). This work presented an interesting comparison with respect to input energy cost. Nearly 90% hydrogen recovery was obtained at 473 K using vacuum on the permeate side for H_2-selective membrane (Pd-Ag) in a packed bed membrane reactor (PBMR). On the other hand, using CO_2-selective membrane in a packed bed MR (PBMR) was reported to give 95% hydrogen recovery at a sweep factor of 5 with CO_2/H_2 selectivity of the membrane was 1000. In order to meet higher hydrogen recovery, it was suggested that CO_2-selective membranes with ideal selectivity >200 can be used. Interestingly, the CO_2-PBMR were reported to be more energy efficient than H_2-PBMR for higher hydrogen recoveries.

Table 5.2 presents the key literature reported for methanol, ethanol and methane reforming, and WGS. With the detailed literature review, it becomes clear that there is enough scope for improvement in the design of membrane reformers in order to achieve better separation and higher recoveries. Higher hydrogen recovery and flux will consequently minimize the energy cost of this system.

Table 5.2 Key literature reported on membrane reformer studies

Membrane reformers with methanol steam reforming							
Author	**System Integration**	**Operating Conditions**	**Reactor**	**X* (%)**	**HRF (%)**	**H_2 flux (mol/ m^2.s)**	**Remarks**
Basile et al. 2006 [7]	Pd membrane 50 µm thick, 10mm o.d. and 150 mm length with Ru-alumina catalyst Membrane apparent Ea=33.31kJ/mol and Pe 1.66 x 10^{-5} mol/m^2s $kPa^{0.5}$	S/M 4.5/1, 350°C 1.3 bar 0.5–12 cm^3/s sweep gas Catalyst bed height 150mm length with glass sphere mm	MR 280mm length, 20mm i.d.	83	50	0.169	Hydrogen gas selectivity up to 70% was reported constant from 350– 600^{0}C with 4.5/1 water to methanol, 1.3 bar reaction pressure
Iulianelli et al. 2008 [17, 22]	Pd/Ag membrane self-supported 50µm, o.d. 10mm and 145mm length with Cu/Al/Zn/MgO	S/M 3/1(v/v) methanol molar flow rate 7.6 x 10^{-4} and 3.8 x 10^{-3} mol/min 300°C, 1-3bar, counter flow sweep gas factor 143ml/min	MR i.d. 20mm and 280mm length	80	93 at 0.36 h^{-1} WHSV and 40% at 0.182 h^{-1} WHSV	20 x 10^{-3} with pure H_2	It was reported that CO selectivity decreases by increasing the reaction pressure confirming that the membrane provides a positive contribution to decreasing CO selectivity because of the hydrogen permeation leading to higher CO consumption.
Basile et al. 2008 [20]	Dense Pd/Ag membrane $CuO/Al_2O_3/ZnO/MgO$ catalyst	S/M 3/1 to 9/1 at temperature 250–300°C; sweep gas 1.38 x 10^{-2} mol/min	FBR 6.7mm i.d. and 250mm length MR 20mm i.d. and	100 with H_2O/CH_3OH 5 mole ratio	8, remains constant through all feed composition	2 x 10^{-3} at 400°C with pure H_2	It was reported that because of low reaction pressure, hydrogen recovery with varying feed compositions remained constant. No activation was observed up to

			280mm length				300 h while CO molar ratios remained 0.2 to 0.7. At low reaction temperature 250°C , low CO was reported for all feed compositions.
Liguri et al., 2014 [18]	7 µm Pd/alumina membrane (75mm length, 13mm o.d., 9mm i.d., effective membrane area 17cm^2) with Cu 15%/ZnO 31% /Al_2O_3 18% (0.5gm) catalyst	Water/methanol 2.5/1(v/v) 280–330°C, 1.5–2.5bar; gas with methanol-water mixture 22ml/min and 29ml/min as sweep gas, GHSV 18,500h^{-1}	Reactor dimensions not provided	85	40 at 330°C and 2.5bar	0.3	H_2 recovery 60% with 80% CO and permeate purity 95% due to loss of CO(feed) through the defects in membrane resulting in 0.21–0.25% CO at 11 bar feed pressure and permeate 1 bar. It was reported that CO mole fraction was 0.62, lowest at low temperature 280°C which further decreases with increasing pressure. CO_2 mole fraction increases with reducing CO indicating the water gas shift occurrence.
Islam and Ilias, 2012 [16]	24.3µm thick Pd supported on SS NiO/ZnO/Al_2O_3 catalyst	Temperature 200 to 300°C Pressure 14.7 to 50 psi S/M 1 to 4 Sweep gas 2.2 x 10^{-3} mol/s WHSV 6 to 9 kg/mol.s	Reactor dimensions not provided	60	50	0.2 (pure H_2)	CO selectivity between 1 to 3 % was reported in the temperature range 200 to 300°C.
Ribeirinha et al., 2017	Pd-membranes for hydrogen	Catalyst 1.5g Temperature 180	Reactor 7.5mm i.d.	90	80	-NA-	Higher WHSV resulted in increasing conversion, however CO production

[23]	selectivity; ILs were used for CO_2 separation Commercial $CuO/ZnO/Al_2O_3$	to 240°C WHSV 50–500 kg/mol.s Pressure 1 to 3bar S/M 1.5 Sweep factor 2 to 20					simultaneously increases. This led to decreasing hydrogen produced. Investigations were made on the positive effect of CO_2 removal on the reformer. It was reported that selective CO_2 removal results in slight enhancement in methanol conversion than hydrogen selective membrane.
Membrane reactors with ethanol and methane reforming, and WGS							
Tosti et al. 2003 [9]	10mm diameter and 100µm thick self-supported cold rolled Pd/Ag foils	WGS $CO/H_2O/CO_2$ 0.2/0.3/0.5 325–330°C, 100kPa, 0.0003 ml/s sweep gas	Reactor dimensions not provided	96.5	28.9	-NA-	The values of permeance were higher at temperature 135–275°C while decreased to 5.8 x 10^{-5} at 276–360°C. Notably, activation energy at lower temperatures were -1866 and -521 kJ/mol at higher temperature.
Chiappetta et al., 2010 [14]	100µm thick Pd/Ag membrane with no sweep gas i.d.= 1.6mm Commercial catalyst 31% Ni, 39% NiO, 11% Al_2O_3 and 19% $SiO_{2)}$	Methane Temperature 360–560°C Feed pressure 200–600kPa Catalyst amount 0.5 to 6.1gm GHSV 1200–4200h^{-1}	Reactor i.d. 3mm	50	43	-NA-	An optimal combination of A_m/V_{cat} (area of membrane/volume of catalyst) and L_s/A_m (limiting reagent flow rate/area of membrane) was suggested to have an optimal design for improved MR performance without sweep gas.

Cornaglia et al. 2013 [15]	150 µm Self-supported Pd/Ag membrane of 10mm o.d. and 133mm length with Catalyst 0.6% $Pt/La_2O_3.SiO_2$	WGS H_2O/CO_2 673-723K, sweep gas 500 N mL/min and pressure 100–800kPa WHSV=2.8 x 10^6 h^{-1}	Reactor dimensions not provided, membrane Pe 1.38 x 10^{-8} mol/smPa$^{-0.5}$	>95	88	1.84 x 10^{-5}	It was reported that effect of pressure is more important than temperature because H_2 flux through the membrane has low activation energy (5100 J/mol)
Borgognoni et al. 2013 [24]	150 µm thick 10mm diameter 19 Pd/Ag self-supported membrane at pressures 100–500kPa	Water/ethanol/ methane (10/1/0, 11/1/0.25, 14/1/1 and 26/1/4), 350°C at membrane and 760°C at reformer, 3bar; WHSV 1200–2400 h^{-1}	Reactor dimensions not provided, catalyst amount 200gm 0.5% Pt on alumina	71 at 500kPa	88	0.38	It was reported that at pressures up to 500kPa, the hydrogen content in retentate decrease up to 12%
Lim et al., 2012 [25]	Pd-Cu and SiO_2-Al_2O_3 MR with ethanol SR Pressure 1-10atm Temperature 623K 12.5% Na-Co/ZnO catalyst	Pressure 1, 5 and 10bar	-NA-	60	-NA-	0.04	H_2/CO_2 selectivity was reported in the range of 200 to 1000 at 623K

*Here, X refers to conversion; HRF refers to hydrogen recovery factor; i.d. refers to inner diameter and FBR refers to fixed bed reactor

5.2 Experimental setup and methodology

In the first part, membrane reformer and separator performances were tested using 100µm thick, 15.2 cm^2 area self-supported dense commercial Pd-Ag membranes, as they give no additional resistance to permeation. They also avoid the formation of micro-cracks on the metallic surfaces. These membranes were supplied by REB Research & Consultancy®, USA having tube outer diameter of 1/8 inch with one end closed and the other bonded to a metal stub that could be connected with Swagelok® fittings to the reactor as shown in Fig. 5.1.

Fig. 5.1 Self-supported Pd-Ag membrane connected to the reactor

Initial membrane surface characterization studies were performed with field emission scanning electron microscopy (FESEM) to measure the thickness and observe the surface morphology. Elemental composition of the membrane film was determined by energy dispersive X-ray spectroscopy (EDX). Membrane reformer studies were conducted in a commercial unit "ME-100®" from REB Research and Consultancy, USA. "ME-100®" is a 35cm × 60cm × 40cm assembly with in-built liquid vessel, a dosing pump and reactor that is 25.5 cm tall and 1" in outer diameter (o.d.) supported by an electric furnace. Photographs and schematic describing the membrane reformer design are shown in Fig. 5.2a and Fig. 5.2b respectively. The process design of "ME-100®" presented in Fig. 5.2b allows aqueous methanol mixture to be pumped at a constant volume rate through a pump

to the boiler which vaporizes the feed. The pre-vaporized feed then enters into the reactor which has a typical shell and tube type configuration consisting of catalyst in the shell and dense self-supported tubular Pd-Ag membranes in the inner core as shown in Fig. 5.2b. The pre-vaporized feed inside the reactor comes in contact with the catalyst, which then reforms the feed mixture into hydrogen, carbon monoxide and carbon dioxide. The reformed feed along with unreacted methanol and water simultaneously comes in contact with the dense self-supported Pd-Ag membranes, which selectively permeate hydrogen through them, leaving the rest of the mixture, including the unutilized feed, to pass through the retentate. Methanol-water mixture at different mole ratios was used as the feed. By varying the feed composition, temperature and pressure, multiple sets of experiments were performed to identify the optimum conditions for maximum hydrogen recovery and permeate side hydrogen flux. Fig. 5.2c shows the schematic of a membrane separator. The 'in-house' designed membrane separator is made of SS-310 with 40 cm height and 14.5 cm diameter. The same Pd-Ag membranes, which were used for reformer studies, were used in the separator at the optimized temperature and pressure conditions. All the gases were fed through pre-calibrated flow meters to the separator where membranes were placed. A constant flow rate of inlet gases was maintained at 0.3 LPM using mass flow meter; flow rates at the retentate as well as the permeate outlet ends were measured using soap bubble flow meters. No sweep gas was used in this study. At 3 bar feed side pressure and 1 bar permeate side pressure, system performance was investigated with pure hydrogen, binary gas mixtures of $50H_2$:$50N_2$ (mol/mol) and simulated reformate composition of $50H_2$:$30N_2$:$18CO_2$:2CO (mol/mol) to find the inhibition effect of individual/mixture of gases. It is to be noted that steam and unreacted methanol are not

used in membrane separator studies as in case of sequential integration, where reaction and separation will be performed in different vessels, condensable gases from reformate will be removed before feeding them in separator unit. This is one of the major advantages of sequential integration. In all the membrane separator experiments, hydrogen percentage in the feed was kept constant at the same value as that in the reformate gases produced at same operating temperature and pressure.

In the second part, membrane reformer runs were conducted using prepared PSS supported Pd-Ag membranes. With the optimized feed composition and 0.3 LPM flow rate, effect of temperature (573 to 723 K) and pressure (0.3 to 3 bar) was determined on the permeate hydrogen flow rate. In addition, comparison of self-supported Pd-Ag MR performance was made with PSS supported Pd-Ag membrane.

Continuous inlet, retentate outlet and permeate outlet compositions were measured using gas chromatography (GC) at constant temperature with porapak Q column connected in parallel with molecular sieve. Membrane reformer reaction performance was determined using Eq. (5.1, 5.2, 5.3, 5.4) on dry reformate basis. On the other hand, Eq. (5.5 and 5.6) were used to determine membrane separator performance. Permeation of hydrogen through palladium occurs by solution-diffusion mechanism which involves several steps. The value of the exponent n in equation 5.6 varies from n = 0.5 to 1 depending on the rate limiting step. If the diffusion of atomic hydrogen through the metal bulk of the membrane is the rate determining step and hydrogen concentration in the Pd-(H/Pd) based lattice is lower than 1, Sieverts' law should be valid for which the value of the exponent n is 0.5. For the membranes used in the present study, the value of exponent 'n' is determined from hydrogen permeance experiments at different pressures.

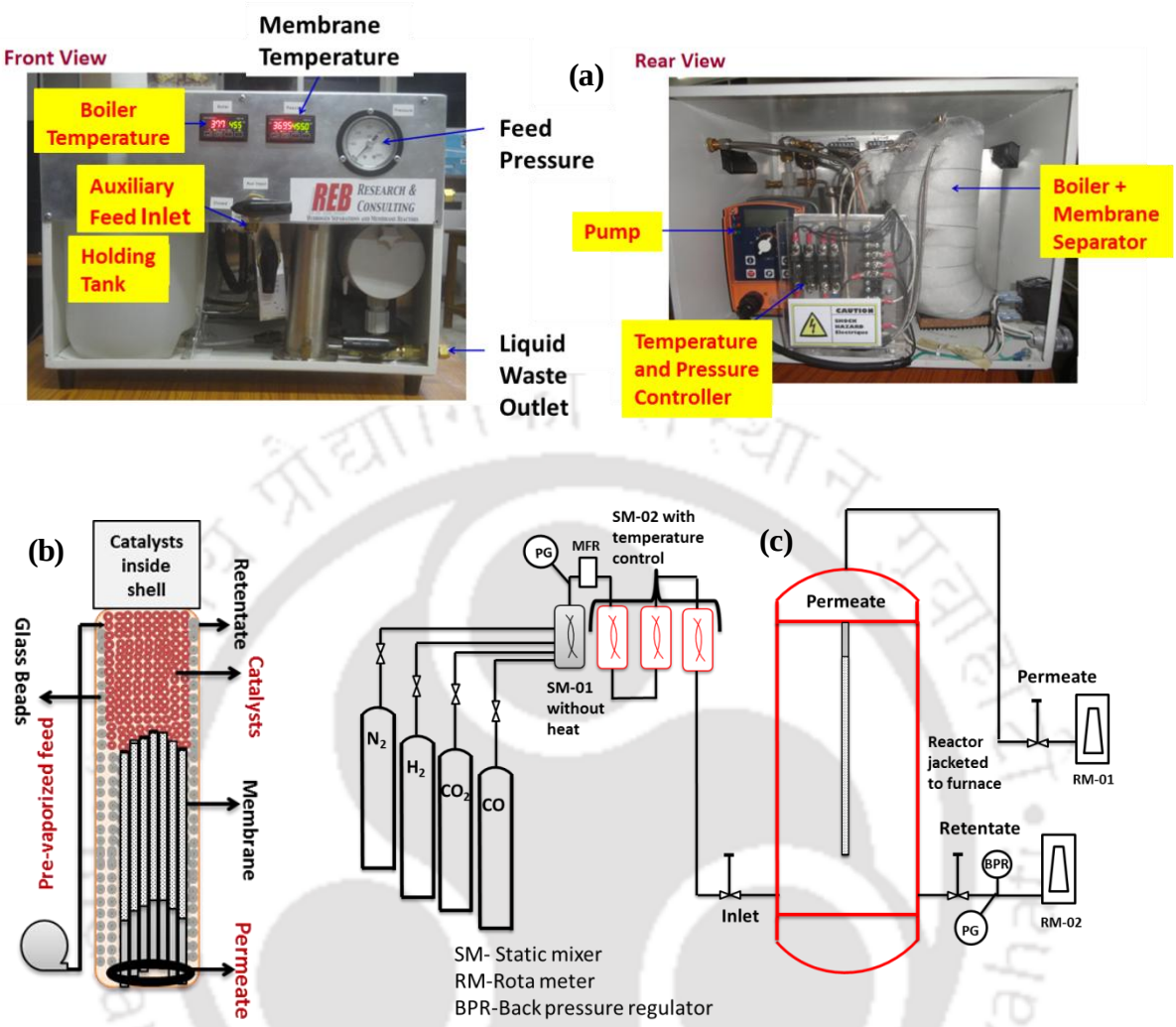

Fig. 5.2 a) Photograph of ME-100® from REB Research and Consultancy, USA and b) Schematic of ME-100® from REB Research and Consultancy and c) Schematic of Membrane Separator

$$\mathbf{H_2\ Recovery} = \frac{F_{H_{2,permeate}}}{(F_{H_{2,permeate}} + F_{H_{2,waste}})} \times 100 \qquad (5.1)$$

$$\mathbf{Total\ H_2\ Production} = \left[\left(X_{H_{2,permeate}} . F_{permeate}\right) + \left(X_{H_{2,waste}} . F_{waste}\right)\right] \qquad (5.2)$$

$$\mathbf{Methanol\ Conversion}\ (\%) = \frac{nCO_2 + nCO}{nCH_3OH} \times 100 \qquad (5.3)$$

$$\textbf{Theoretical Hydrogen} = 3 \times \mathrm{nCH_3OH} \tag{5.4}$$

$$\textbf{Permeate } \mathbf{H_2} \textbf{ Flux } (\boldsymbol{j_{H_2}}) = \frac{\mathrm{nH_{2,permeate}}}{\mathrm{A}} \tag{5.5}$$

$$\textbf{Permeability (Pe)} = \frac{\mathrm{j_{H_2} \times \delta}}{\left(\mathrm{p^{0.5}_{H_{2retentate}}} - \mathrm{p^{0.5}_{H_{2,permeate}}}\right)} \tag{5.6}$$

Lastly, three sets of runs were conducted for each set of operating variables. The resulting data showed ±5% error, after studying the responses (permeate flow rate, retentate flow rate, composition analysis) in a kinetically controlled regime. Mass balance for the inlet, permeate outlet and retentate outlet flow rates was also performed for both membrane separator and membrane reformer studies.

5.3 Membrane permeation studies with pure hydrogen

Once connected to the reactor, the membranes were heated in the presence of continuous nitrogen gas (99.999% purity) supply to bring the system at desired operating temperature and pressure. After the required temperature was reached, the membranes were kept under continuous flow of pure hydrogen for nearly 5 hours for complete reduction and removal of impurities. It is known that bulk diffusion of hydrogen through palladium is the rate limiting step when pressure exponent "n" in the flux equation (equation no 5.6) is equal to 0.5 according to Sieverts' Law. In order to determine the ideal hydrogen flux for the membranes, experiments were performed using pure H_2 as feed with increasing pressure difference. Fig. 5.3 shows that permeate hydrogen flux through membrane increases with increase in trans membrane pressure difference. The high thickness of self-supported membrane results in bulk diffusion of hydrogen through

membrane as the rate limiting step. However, the value of n is found to be 0.5 which deviates from Sievert's law exponent value. Since no pin-holes were observed on the membrane surface, this deviation mainly indicates either rate limitation by adsorption/desorption or a contribution from other transport mechanisms to hydrogen flux through the membrane. A maximum hydrogen flux of 0.16 mol/m^2.s was achieved using pure H_2 as feed with increasing pressure difference.

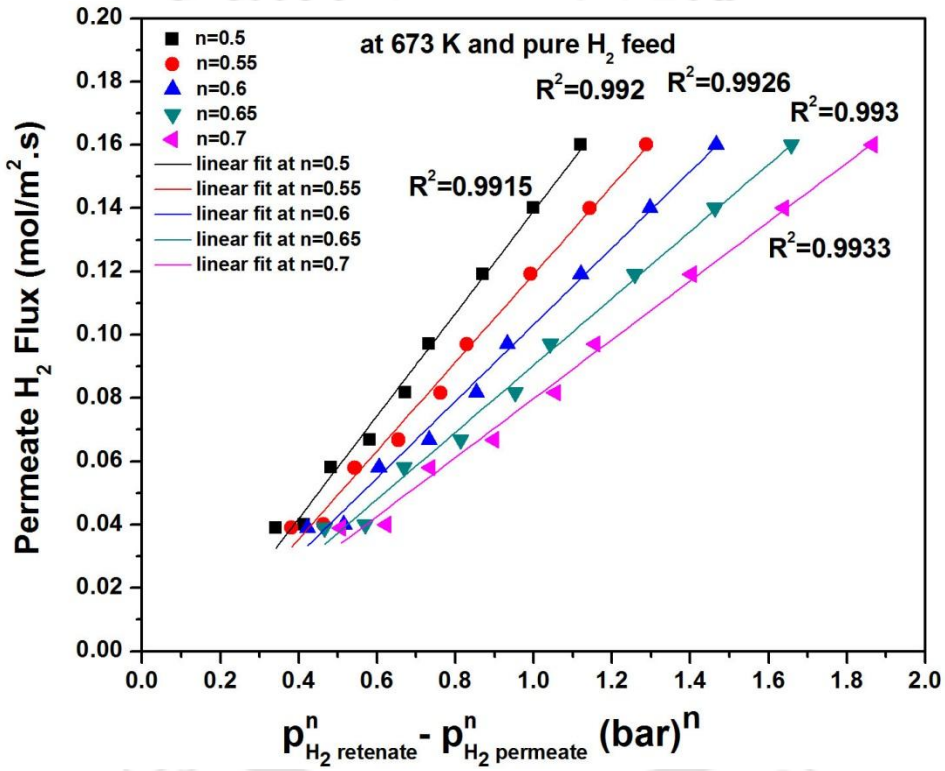

Fig. 5.3 Ideal hydrogen flux and recovery of self-supported Pd-Ag membrane with increasing trans membrane pressures at 673K using pure H_2 as feed

5.4 Self supported membrane reformer performance studies

Membranes which were reduced under high purity hydrogen for sufficiently long time (more than 5 hours) were used in membrane reformer or separator for further studies. In reformer, methanol reforming studies were carried out by using the 'proprietary' high

temperature methanol reforming catalyst, placed in the shell of the membrane reformer as shown in Fig. 5.2b. In order to determine the membrane reformer performance, the parameters as defined in Eq. 5.1 to 5.6 were evaluated. Using mass balance, amount of H_2, CO, CO_2, unreacted methanol and water in the reformate mixture at varying feed compositions, temperature and pressure was also calculated. Experiments were performed to optimize the following parameters: a) feed composition (varied in the molar ratio of 1:1 to 1:18 methanol:water) b) temperature (between 623−723K) and c) pressure (between 3 and 5 bar).

5.4.1 Effect of feed composition

To find the effect of feed composition on performance of membrane reformer, experiments are performed for different methanol/steam ratio keeping flow rate of the feed constant. It has been observed that with increase in dilution, increase in conversion only occurs up to a methanol/steam mole ratio of 1:2.2 as shown in Fig. 5.4a and thereafter the conversion remains almost constant. In methanol reforming, methanol adsorbs on the catalyst surface as methoxy species which oxidizes to formate species and subsequently decomposes into CO_2 and H_2. Initial increase in conversion with dilution of methanol was observed due to enhanced hydrogen recovery which occurs mainly because of shift in equilibrium towards water gas shift reaction thereby producing more H_2 and less CO. Further increase in dilution reduces the methanol adsorption on catalyst surface, thus giving a constant conversion. Thus, increasing water in feed showed a minimal effect on methanol conversion. Increasing water minimizes the CO content in reformate largely by reducing the possibility of reverse water gas shift reaction to occur. Thus, with

increasing feed dilution, for methanol-to-water feed ratio in the range 1:8.9 to 1:18 (mol/mol), negligible CO production was observed as shown in Fig 5.4b.

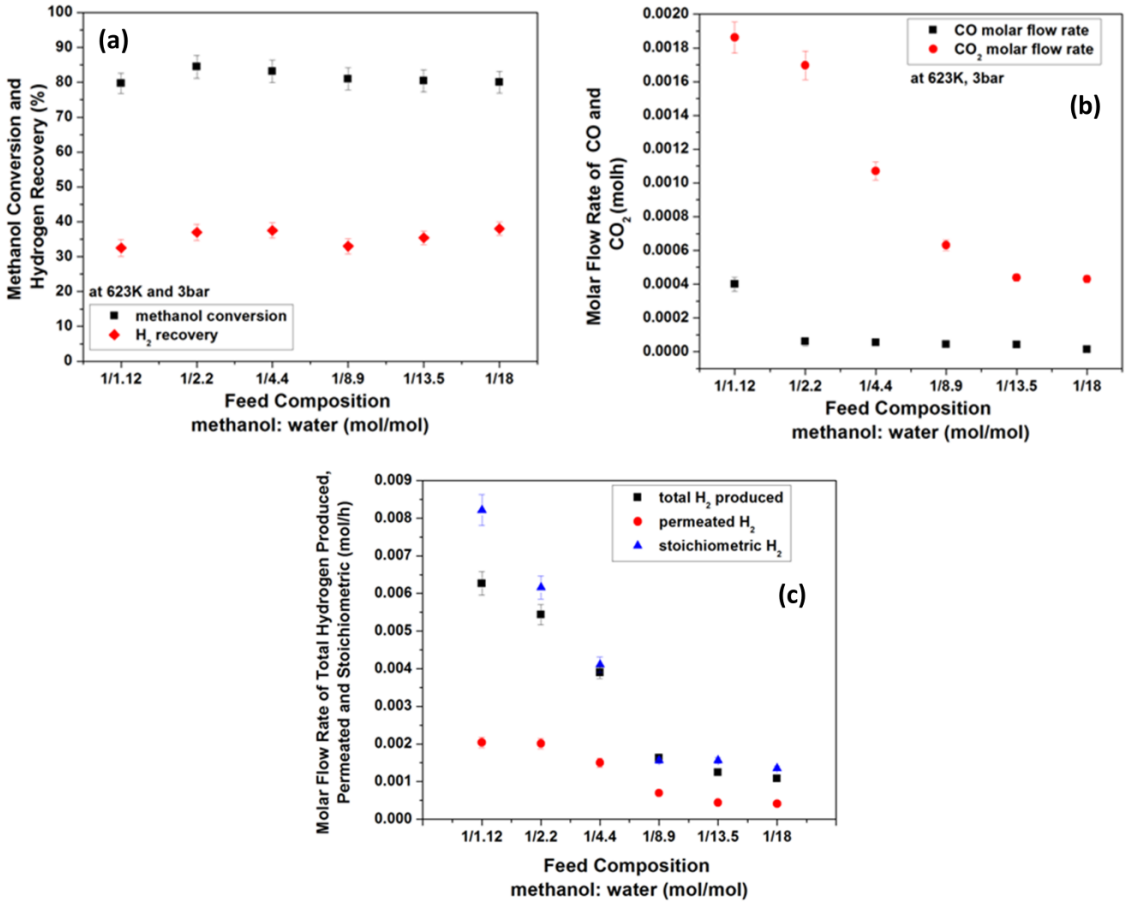

Fig. 5.4 Effect of increasing water dilution on a) permeate hydrogen recovery and methanol conversion at 623 K and 3 bar, b) molar flow rate of CO and CO_2 produced and c) theoretical hydrogen per mole methanol and permeate hydrogen molar flow rate

Further, at constant inlet feed rate, increasing methanol dilution decreases the total hydrogen produced because of decrease in absolute methanol supply. Therefore the trans membrane pressure difference decreases due to reduction in hydrogen partial pressure in the feed to membrane. Hence, hydrogen permeation rate through the membrane is also reduced as shown in Fig. 5.4c. For higher methanol/steam ratio, 1:1.12 to 1:4.4, a large

gap between permeated hydrogen and the total hydrogen produced was observed due to the higher concentration of CO and CO_2 produced. On the other hand, with higher steam concentrations in feed, decrease in total hydrogen produced results in a smaller gap between permeated hydrogen and total hydrogen produced. This clearly indicates that the performance of membrane changes drastically with the feed composition mainly because of the reformate gas composition (CO and H_2O). To find the effect of CO and CO_2 on membrane reformer performance at different operating conditions, all other studies are performed for 1:1.12 and 1:4.4 methanol-to-water (mol/mol) feed composition.

5.4.2 Effect of temperature and pressure

Steam reforming is an endothermic reaction and hence, increase in temperature enhances conversion. Fig. 5.5a and Fig. 5.5b show the effect of temperature and pressure on methanol conversion and hydrogen recovery for the self-supported dense Pd-Ag Membrane reformer. It can be observed that with increase in temperature both conversion and recovery increase for both the feed compositions.

Increase in temperature improves hydrogen flux through the membranes as diffusivity of hydrogen through membrane increases. This corresponds with a typical Arrhenius-type dependence as shown in Eq. 5.7.

$$Pe_{H_2} = Pe_{H_{2,0}} . e^{\left(\frac{-E_a}{R.T}\right)} \quad (5.7)$$

where the pre-exponential factor, $Pe_{H_{2,0}}$, represents the permeability at infinite temperature (mol m^{-1} s^{-1} $bar^{-0.5}$), E_a the activation energy (kJ/mol), R the universal gas constant (kJ/mol K) and T the temperature (K).

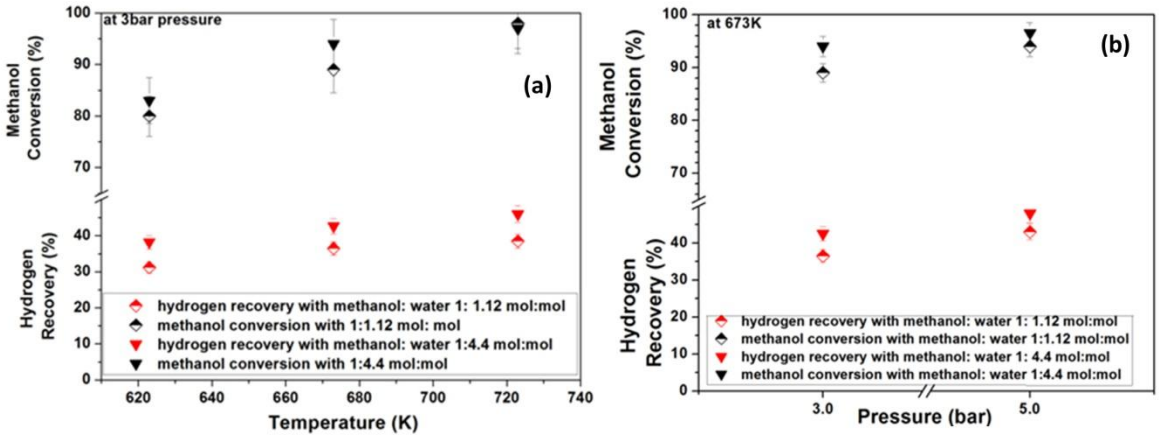

Fig. 5.5 Effect of reaction temperature and pressure on methanol conversion and hydrogen recovery using methanol: water 1/1.12, 1/4.4 mol:mol as feed: a) effect of temperature and b) effect of pressure

Therefore, increase in hydrogen removal at higher temperature shifts the reaction equilibrium towards products and hence, increases the conversion at both the feed compositions. For all the temperatures, hydrogen recovery in the case of methanol to steam ratio 1:4.4 is higher compared to 1:1.12. This is mainly because for 1:1.12 (methanol/steam) feed composition, high CO formation was observed at elevated temperatures. Further, increase in pressure enhances the trans membrane pressure difference, which increases the hydrogen permeation through the membrane. The continuous permeation of hydrogen from reformate side shifts the reaction equilibrium towards product thereby enhancing conversion as shown in Fig. 5.5b. Moreover, with increase in conversion the partial pressure of hydrogen in the feed to membrane remains high that maintains the hydrogen permeation drive and hence high hydrogen recovery as well. At 673 K and 0.003 L/min liquid flow rate, the maximum hydrogen recovery observed in this study was 48% at 5 bar using methanol: water 1:4.4 molar ratio feed. The

results from the present work are compared to those reported by other authors in literature in Table 5.3. The total CO and CO_2 produced for both 1:1.12 and 1:4.4 methanol: water (mol:mol) feed composition is presented in Fig. 5.6a and 5.6b respectively. Fig. 5.6a shows the total CO and CO_2 produced for 1:1.12 methanol: water (mol:mol) feed composition at two different temperatures (623 K, 673 K) and pressures (3bar, 5bar). Results clearly show that with increase in temperature, rate of CO formation increases for methanol to steam ratio 1:1.12. This is mainly because of methanol decomposition at elevated temperature, which is more prominent in case of higher methanol concentration. Further, reverse water gas shift reaction also increases the CO formation for 1:1.12 feed ratio, which can be observed through reduction in CO_2 formation with increase in operating temperature for both the pressures. However, for 1:4.4 methanol:water (mol:mol) feed composition, Fig. 5.6b shows prominent increase in CO_2 formation with increasing temperature. For this feed composition, formation of CO at all the operating temperatures and pressures is observed to be low compared to feed composition of 1:1.12.

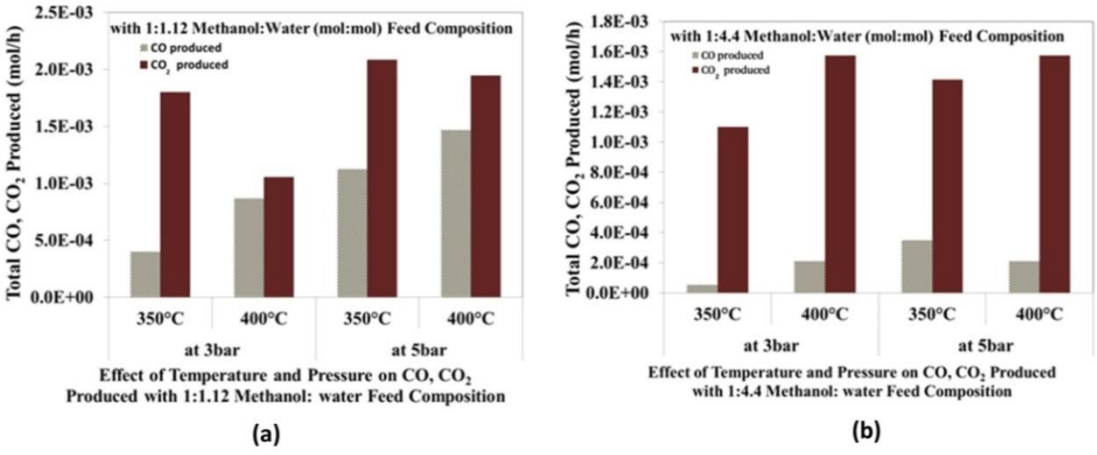

Fig. 5.6 Effect of increasing temperature and pressure on CO, CO_2 produced a) with 1:1.12 methanol:water mol:mol as feed and b) with 1:4.4 methanol:water as feed

This indicates presence of water gas shift reaction at 1:4.4 methanol:water (mol:mol) feed composition which produces H_2 and CO_2. Hence, hydrogen recovery is higher in case of diluted feed (1/4.4) compared to high methanol, concentrated feed (1/1.12) mainly because of low CO content in feed to membrane. However, it should be noted that for the self-supported Pd-Ag membranes and for both the feed compositions at all the operated temperatures and pressures, high purity hydrogen was observed on the permeate side. This shows that the membrane is stable at these operating conditions and can be used at higher temperatures to achieve almost 100% conversion, which is significantly higher compared to conventional reformer where typically 80% conversion is reported.

5.4.3 Effect of excess steam in a membrane reformer

Table 5.4 shows the reformate composition for different methanol-to-steam ratios in the feed at different temperatures. It shows that CO generation remains low for diluted feed compositions, which is also reported in literature [19-21]. Fig. 5.7 shows that at each temperature, the permeate hydrogen flux for feed having higher steam mole fraction is reduced.

For a constant feed rate, excess methanol dilution reduces the net hydrogen yield (Fig. 5.7). This reduces the trans-membrane hydrogen partial pressure and limits the hydrogen permeability through membrane. Further, H_2O also "*adsorbs*" at the Pd surface causing reduction in the active sites where hydrogen dissociation takes place. At higher temperatures, it has been reported [26] that steam reacts with carbon present on the Pd surface by the following reaction: $H_2O + C \rightarrow CO + H_2$. Since inhibition effect of CO

formed is relatively lesser than steam, steam is also reported to have a cleaning effect. Once steam is stopped H_2 flux reverses back to its original state.

Table 5.3 Comparison of methanol membrane reformer performance in the present work with studies reported in literature

Feed	Feed Ratio (mol/ mol)	T (K)	P (bar)	System Integration	Sweep Gas (cm^3/s)	X (%)	HRF (%)	H_2 Flux ($mol/m^2.s$)	Ref
Water / methanol	4.5/1	623	1.3	Pd membrane with Ru-alumina catalyst	0.5	83	50	0.05	[8]
Water / methanol	1.2/1	473	2	Pd-Ru-In self - supported membrane with Cu/Zn/Alumina	0.16	88	20	-nil-	[18]
Water / methanol	2.5/1	573	1.5–2	7µm thick Pd/alumina membrane with $Cu/ZnO/Al_2O_3$ catalyst	-nil-	85	>40	-nil-	[22]
Water / methanol	5/1	573	1.3	50µm thick Pd membrane with Cu/Zn/Mg-alumina catalyst	0.0012	100	8	0.024	[9]
Water / methanol	3/1	573	3	50µm thick Pd/Ag membrane self-supported with Cu/Al/Zn/MgO	Counter flow SF=1.1	~ 80	40	-nil-	[24]
Water/ Methanol	**4.42/1**	**673**	**3**	**100 µm thick 7 Pd-Ag self – supported membranes with proprietary catalyst (ME_100®)**	**Nil**	**>90**	**43**	**0.05**	**This work**

Thus, to avoid such differences in flux, feed with 1: 2.2 molar ratio of methanol: water may be used which shows negligible steam dilution effect on hydrogen flux with increasing temperature. This feed composition therefore can be considered as a relevant trade-off between recovery and flux for enhanced membrane reformer performance.

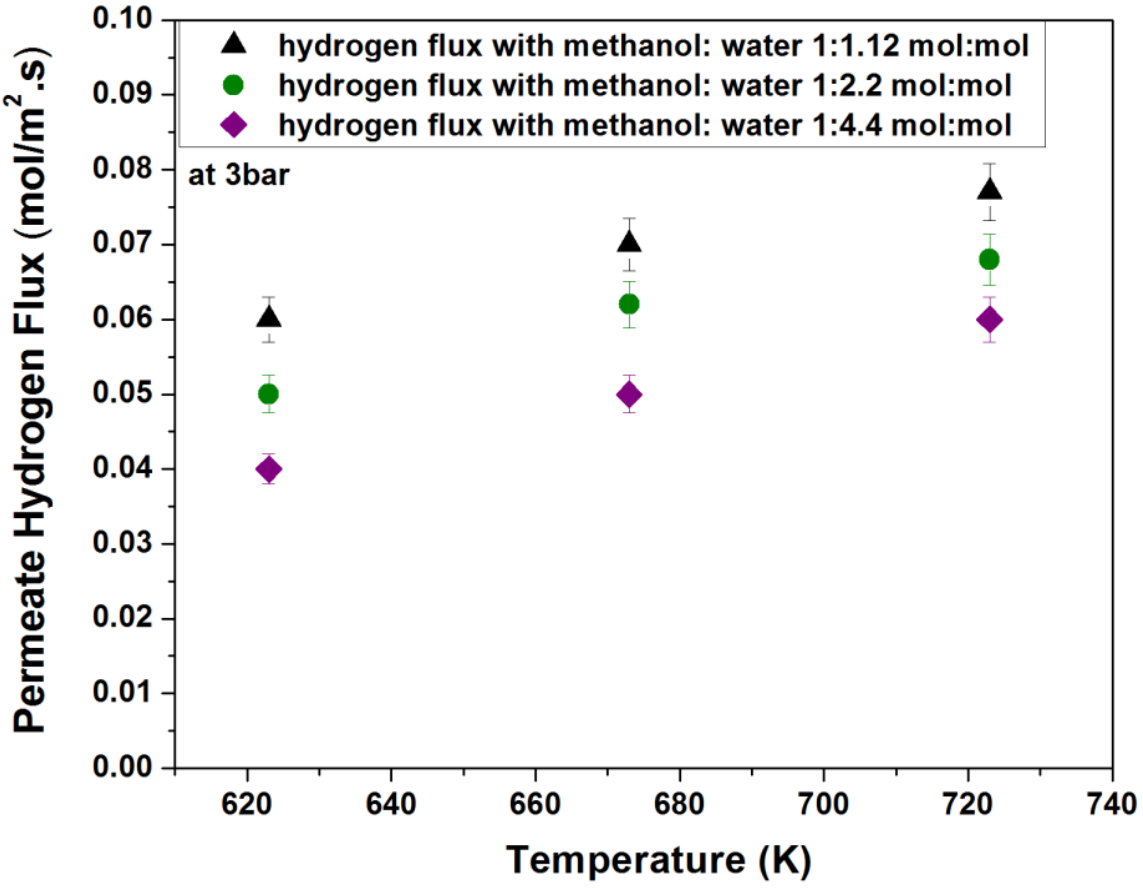

Fig. 5.7 Effect of steam on permeate hydrogen flux

Table 5.4 Composition of product reformate mixture (in mole %) produced with methanol: water ratio of 1:1.12, 1:2.2 and 1:4.4 (mol: mol) at different temperatures (calculation based on wet reformate basis)

Temperature (K)	1:1.12 Methanol:water feed composition (mol:mol)				
	H_2	**CO**	**CO_2**	**Methanol**	**Water**
623	66.7	8.9	19.8	0.2	10.2
673	65.7	8.8	16.0	3.0	6.5
723	67.4	11.3	16.8	0.5	4.0
Temperature (K)	**1:2.2 Methanol:water feed composition (mol:mol)**				
	H_2	**CO**	**CO_2**	**Methanol**	**Water**
623	54.8	4.9	17.1	0.7	22.5
673	57.0	5.8	16.0	1.9	19.3
723	61.0	6.6	17.1	0.4	14.8
Temperature (K)	**1:4.4 Methanol:water feed composition (mol:mol)**				
	H_2	**CO**	**CO_2**	**Methanol**	**Water**
623	33.9	1.9	11.2	1.33	51.6
673	45.0	2.2	13.0	0.8	39.0
723	52.0	2.4	14.8	0.4	30.0

Fig. 5.8 shows Arrhenius plot of permeate flux measured at three different feed compositions. A linear fit was made to the data in Fig. 5.8 to calculate the activation energies by applying the Arrhenius equation.

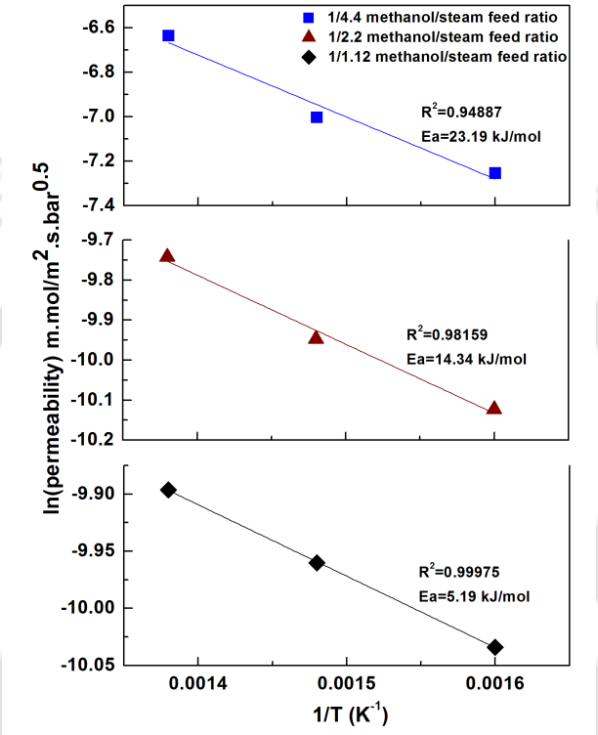

Fig. 5.8 Effect of increasing steam in the feed on activation energy of hydrogen permeation through Pd-Ag membrane

It is observed that the value of activation energy increases with increasing feed dilution. The higher value of activation energy suggests that rate controlling step shifts from bulk diffusion to surface chemisorption. Therefore, the observed decrease in permeate hydrogen flux in Fig. 5.7 may be caused primarily due to excess dilution. To verify this hypothesis, both membrane reformer and separator were compared. The separator performance was evaluated using a feed mixture having similar composition as that of the reformate gas in the membrane reformer at optimal operating temperature and pressure. It

should be noted that in the membrane separator study, steam and unreacted methanol are not considered as these condensable gases can be easily separated before the reformate mixture is fed to the standalone membrane separator.

5.4.4 Membrane reformer vs. membrane separator

In the membrane separator, effect of feed composition on performance of membrane as a standalone separator was studied. Four different feed compositions, namely a) pure H_2 b) $74H_2$:$26N_2$ (mol/mol) c) $50H_2$:$50N_2$ (mol/mol) and d) $50H_2$:$30N_2$:$18CO_2$:2CO (mol/mol), are used at a temperature of 673 K and pressure of 3 bar. In cases (a), (b) and (c), partial pressure of hydrogen is changed to evaluate the membrane performance as a separator when used at different feed compositions. It is well known that N_2 has no inhibition effect on Pd-Ag membrane. Therefore, N_2 is used as an alternate gas to prepare the mixtures of different composition. In cases (c) and (d), hydrogen mole fraction is kept constant so that partial pressure of hydrogen in the feed to membrane remains same for both the cases. This will enable us to find the effect of CO and CO_2 inhibition in case of membrane separator. The composition of gases in case (d) is maintained the same as that of the reformate gas composition when reaction is conducted at the same temperature and pressure in conventional reformer.

Fig. 5.9 shows the direct comparison of membrane separator performance with membrane reformer when both are operated at same temperature, pressure and inlet feed composition. The only difference is that in case of membrane reformer reaction and separation occur simultaneously in same vessel while in case of membrane separator these operations are performed in different vessels. In Fig. 5.9 starting from the left, it

can be observed that in the case of membrane separator, increasing the dilution of hydrogen reduces the partial pressure of hydrogen in feed to the membrane which reduces the hydrogen permeate flux. However, when CO and CO_2 are introduced in the feed keeping hydrogen fraction constant, marginal decrease in flux is observed.

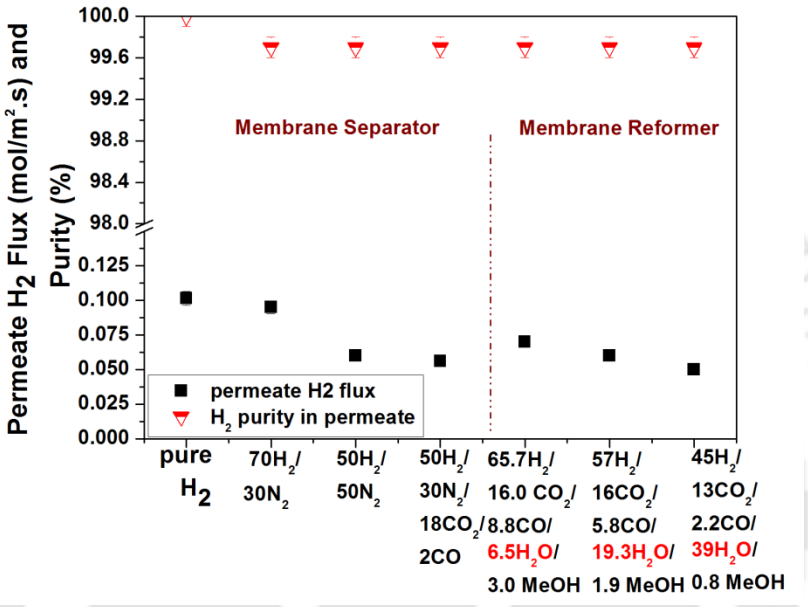

Fig. 5.9 Membrane Separator vs. Membrane Reformer: Effect of Steam, CO and CO_2

This indicates that at the operating temperature of 673 K, CO and CO_2 have minimal inhibition effect on permeate hydrogen flux in case of membrane separator. In the present study with membrane separator, negligible CO inhibition to hydrogen permeation was observed with ~8.8% CO in feed for self-supported dense Pd-Ag membrane at a temperature of 673K. This inference is in agreement with the reported literature where Peterson et al. [27] have found no CO inhibition for 200 µm thick Pd membrane at 553 K for up to 5% CO concentration in feed. Further, on comparison of membrane separator with membrane reformer for the same membranes, it was observed that the presence of

steam in reformate causes only a marginal decrease in hydrogen flux from 0.07 to 0.05 mol/m^2.s. Continuous permeation of hydrogen in a membrane reformer not only maintains the forward reaction but the diluted reformate stream also negates the occurrence of concentration polarization. Therefore, overall membrane reformer performance is either equivalent or even better than that of a membrane separator having comparable hydrogen purity. Therefore, it can be concluded that membrane reformer is indeed an advantageous system for on-board generation of ultra-pure hydrogen in a compact single assembly. Membrane reformer integration lowers the thermodynamic requirements of the reaction to attain complete conversion and therefore minimizes the energy requirements. However, the effective operation of a membrane reformer depends on finding a suitable trade-off between reaction and membrane separation, so as to operate the reformer at optimal condition. In the present study, effort has been made to find suitable operating condition for the self-supported Pd-Ag membrane reformer. On the contrary, membrane separator (sequential integration of reactor and separator) provides operational flexibility at the cost of reduced conversion. Further, the installation cost of membrane separator is relatively high due to increased assembly requirement and it makes the overall system bulky.

5.5 Design of a PSS supported membrane reformer

In-house' prepared Pd-Ag membranes supported on PSS were integrated with Cu-Fe supported on AZZ catalyst in an in-house designed packed bed membrane reformer. The reaction was carried out with S/M 3 at 573-723 K and 1.8 bar feed pressure. Further, a total 30 gm of catalyst was used and mixed with quartz twice in mass. Membrane reformer integration was performed with single membrane as well as four membrane

assembly. Further, with the four membranes assembly effect of baffle on the membrane reformer performance was also investigated.

Fig. 5.10 shows the photograph and schematic of the system used for single membrane integration study. The inner diameter of single membrane MR was 6 cm.

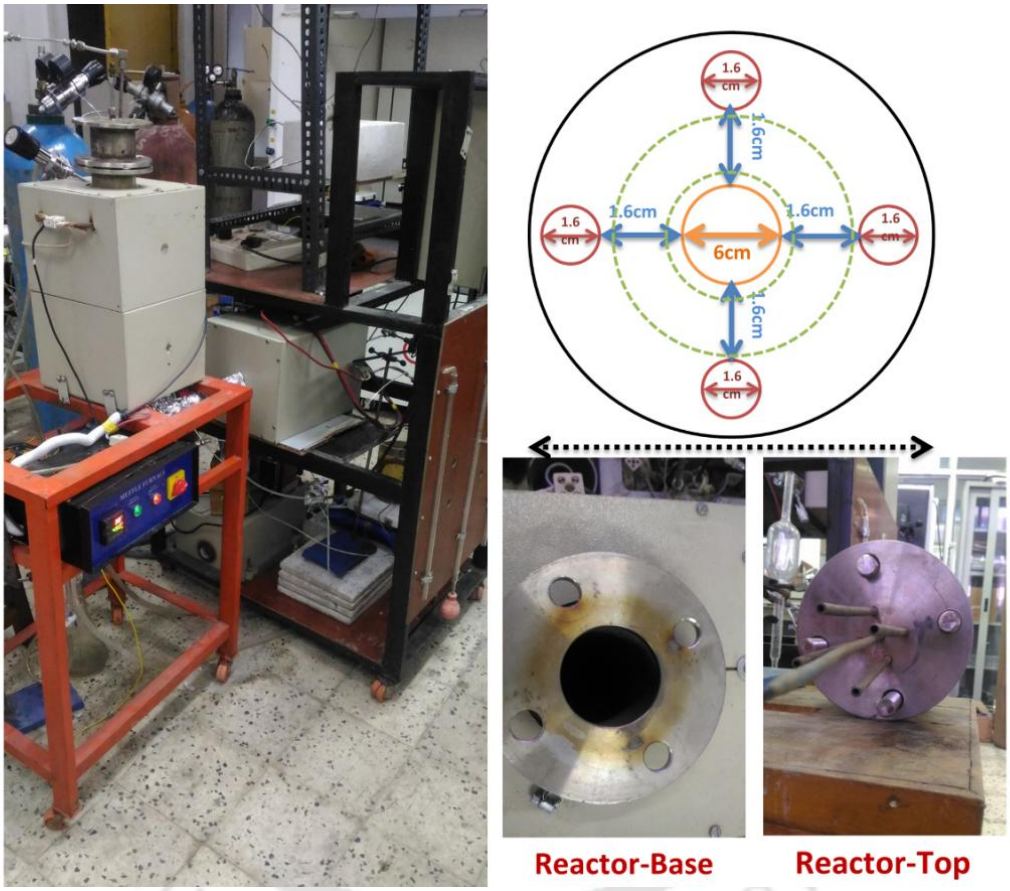

Fig. 5.10 Membrane reformer without baffle

Catalyst mixed with quartz was placed at the bottom of the reactor and membrane was placed on the top of the catalyst bed as shown in Fig. 5.10). The reactor temperature was maintained through the external furnace by using PID controller and reactor pressure was maintained through the back pressure regulator which was placed in outlet line. The feed was pre-vaporized before entering in to the membrane reformer.

Further, four membrane integration was performed with the same amount of catalyst and operating conditions in the membrane reactor 14.5 cm inner diameter. Two different integration assembly namely, single pass and multi-pass, was studied to achieve the maximum hydrogen recover and flux and to determine the effect of baffle in case of membrane reformer The arrangement used for the four membrane integration (single and multi-pass assembly) was selected based on the best membrane arrangement identified in the multi-pass separator detailed in Chapter 3. Fig. 5.11 (a-b) shows the membrane reformer used for four membrane assembly. In the four membrane assembly integration study, for both cases (single and multi-pass), catalyst was placed in the inlet zone where the inner diameter was approximately 5 cm. Further, to observe the effect of baffles on membrane reformer performance, the first case was run with four membranes placed directly on top of catalyst while in case 2 the two-two membranes were placed on each side of the baffle and catalyst was placed at inlet zone which is separated by another baffle as shown in Fig. 5.16..

Fig. 5.11a Photograph of the multi-pass membrane reformer, tube sheet and baffle arrangements

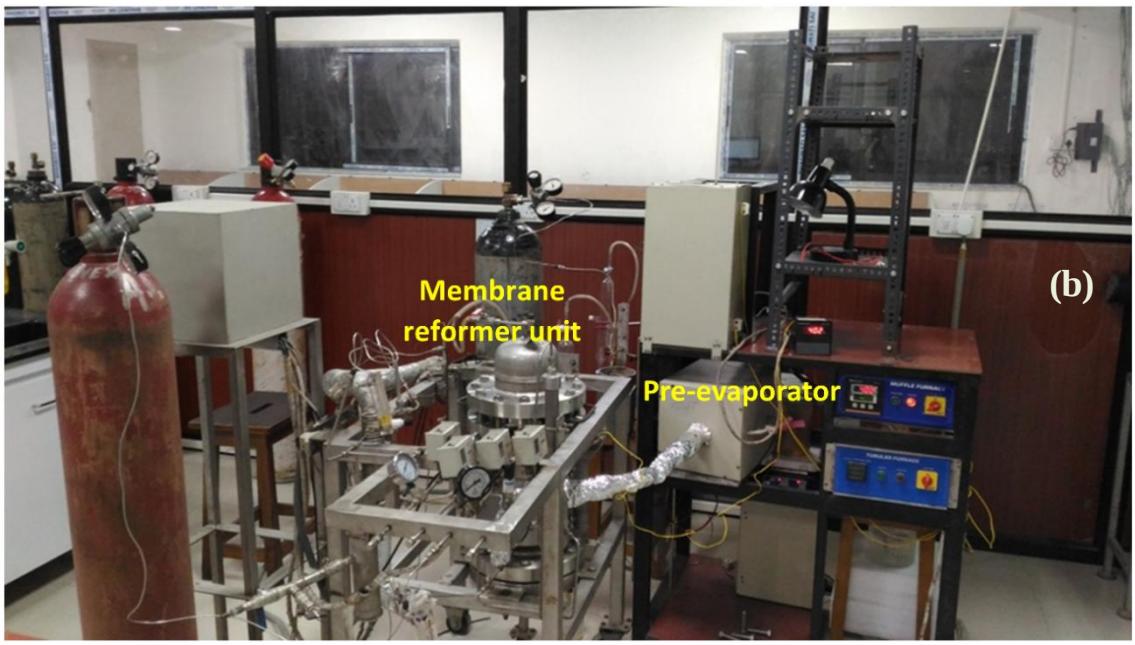

Fig. 5.11b Image of the membrane reformer set up with pre-evaporator and gas supply

5.5.1 Supported Pd-Ag single membrane single pass MR performance

In-house membrane reformer performance was determined with varying pressures and temperature. Fig. 5.12 shows hydrogen flux and recovery at constant temperature of 573 K and increasing retentate gauge pressure from 0.5 to 1.2 bar. Increased pressure difference is the driving force to enhance hydrogen permeation. Increased hydrogen permeation causes the reaction to shift forward as discussed in section 5.4.2. Further, Fig. 5.12b shows the effect of temperature on the methanol conversion and hydrogen recovery using PSS supported Pd-Ag membrane. As discussed in section 5.4.2, increase in temperature results in enhanced methanol conversion thereby resulting in higher hydrogen partial pressure on the feed side of the membrane.

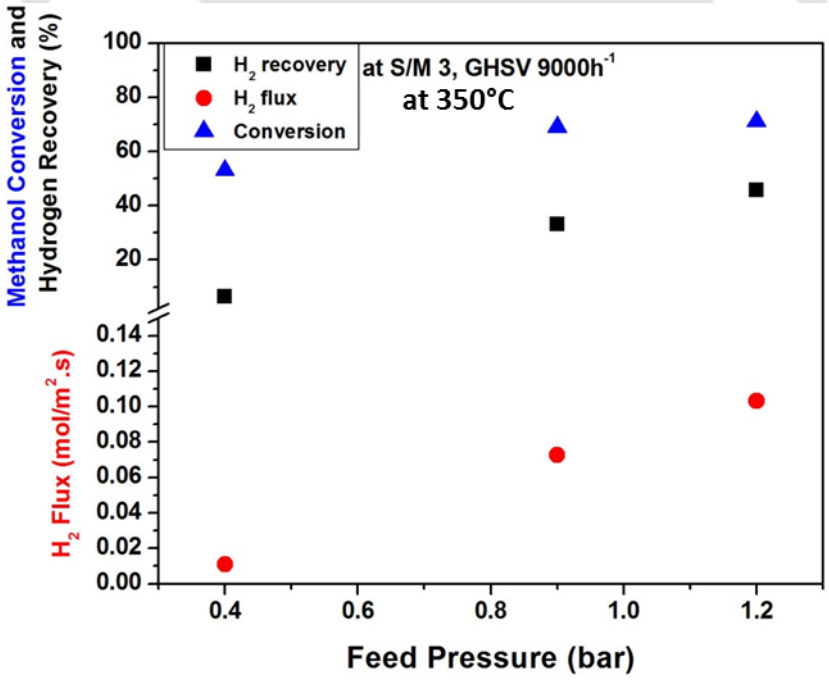

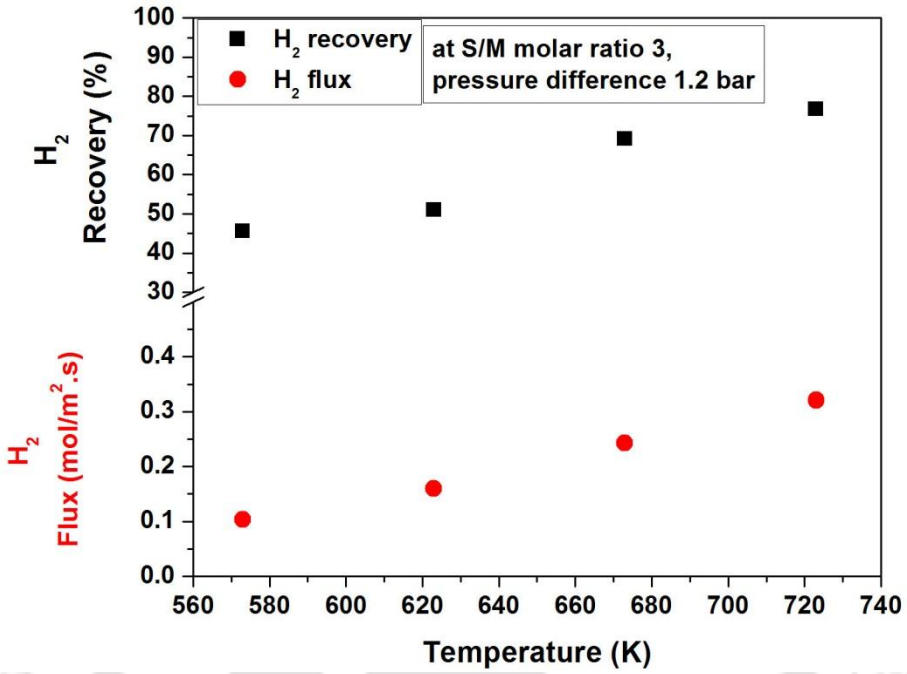

Fig. 5.12 PSS supported Pd-Ag membrane performance: a) Effect of pressure and b) Effect of temperature

The enhanced hydrogen partial pressure difference, with increase in temperature due to higher conversion, improves hydrogen recovery. Further, the obtained conversion in MR was higher for the same catalyst and sane operating condition compared to the conventional reactor shown in chapter 4. Hence, integration of hydrogen-selective separation with reformer resulted in higher methanol conversion with increasing pressures as well as temperature. This resulted in a maximum methanol conversion up to 95% and hydrogen recovery up to 75 % using a single membrane at 450°C. Comparison of methanol conversion vs. H_2 flux for MR containing PSS-supported Pd-Ag membranes is shown in Fig. 5.13. It can be observed that higher is the flux better is the conversion which forms the basis of membrane reformers. Further, methanol conversion vs. H_2/Ar selectivity was also compared between Pd-Ag membranes supported on PSS with self-

supported membrane shown in Fig. 5.14. Hydrogen selectivity for both membranes were observed similar under increasing temperatures as well as pressures.

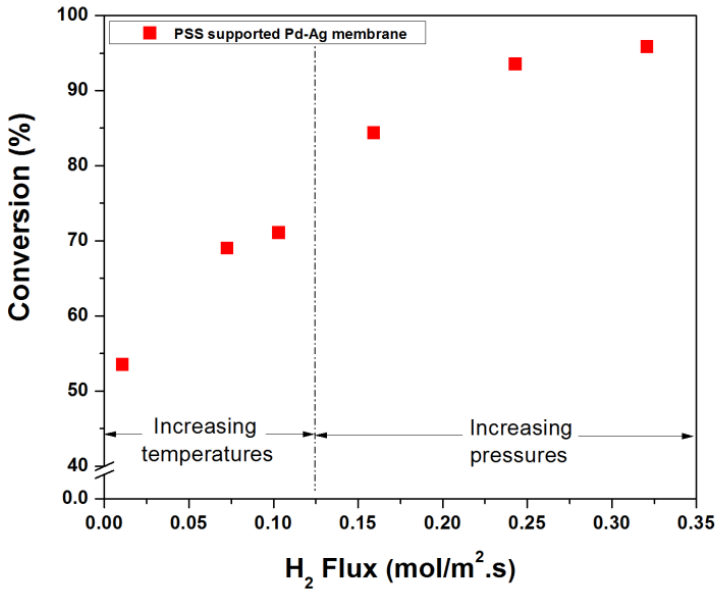

Fig. 5.13 Conversion vs. H_2 flux using self-supported and PSS supported Pd-Ag membrane

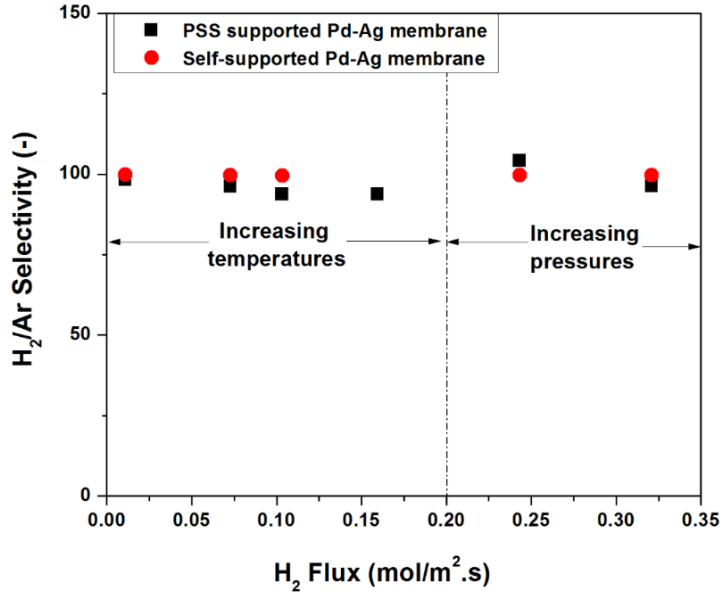

Fig. 5.14 H_2 flux vs. selectivity using self-supported and PSS supported Pd membrane

5.5.2 Supported Pd-Ag multiple membrane MR performance: with single and multi-pass

Membrane reformer run in this section was carried out for four membranes with two assemblies: a) single pass and b) multi-pass. In both the cases, catalyst mixed with quartz was placed in the inlet zone of the reactor. The pictorial representation of membrane placement for both the cases is shown in Fig. 5.15. A schematic representation of the same is presented in Fig. 5.16. Hydrogen recovery for both the designs was compared. It should be noted that catalyst lies in the inlet zone (see Chapter 3, Fig. 3.2). Hence, in single pass assembly, the first two membranes lie directly above the catalyst in the same inlet side and the other two membranes at the center. Hence, this arrangement more so depicts the case II mentioned in Chapter 3, Fig. 3.10a. Further, in multi-pass assembly, catalysts remain at the same inlet side while the membranes are connected at the center (two on both sides of the baffle).

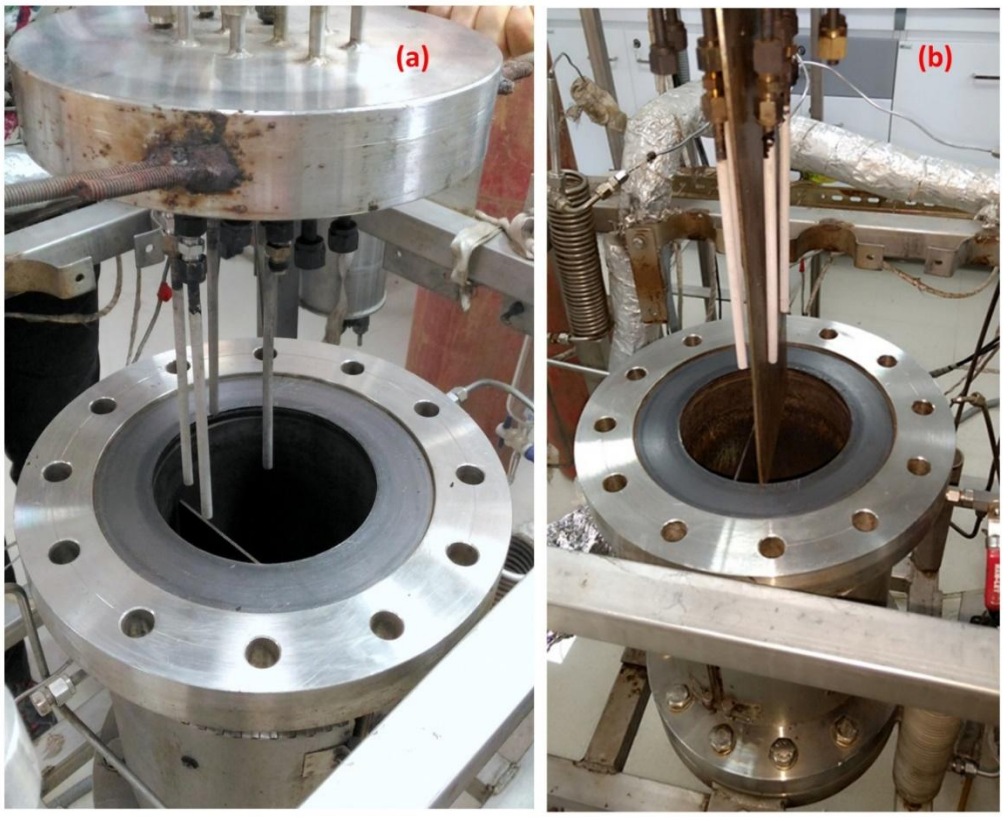

Fig. 5.15 Membrane reformer arrangement a) membrane with no baffle and b) membranes with baffle

Thus, the membrane arrangement in multi-pass assembly of Fig. 5.15 depicts the case I mentioned in Chapter 3, Fig. 3.10a. The results observed with Fig. 5.17 clearly indicate that hydrogen recovery in case of multi-pass membrane reformer is higher compared to single pass membrane reformer. This is because of the better contacting and enhanced contact time achieved in case of multi-pass membrane reformer compared to single pass membrane reformer due to presence of two extra baffles and the multi-pass membrane reformer design results in 80% hydrogen recovery. However, the recovery was slightly less compared to the case when same four membranes were used in a multi-pass membrane separator. The recovery in multi-pass membrane separator case was 61.86%.

The marginal reduction in recovery can be attributed to excess steam which dilute the reformate feed and reduces the hydrogen partial pressure. Permeate hydrogen flow rate with multi-pass membrane reformer was observed 0.92 LPM. Further, in comparison with commercial membrane reformer ME-100® (that consists of nearly 7 self-supported membranes in its assembly) the hydrogen recovery with in-house designed multi-pass MR (with 4 supported Pd-Ag membranes on PSS) was much higher. Moreover, it should be noted that even with single pass the four membrane assembly of Pd-Ag supported on PSS performs at par with the ME-100®. Therefore, in-house designed multi-pass membrane reformer with supported Pd-Ag membrane in current study performs better than commercially available membrane reformer for the same output.

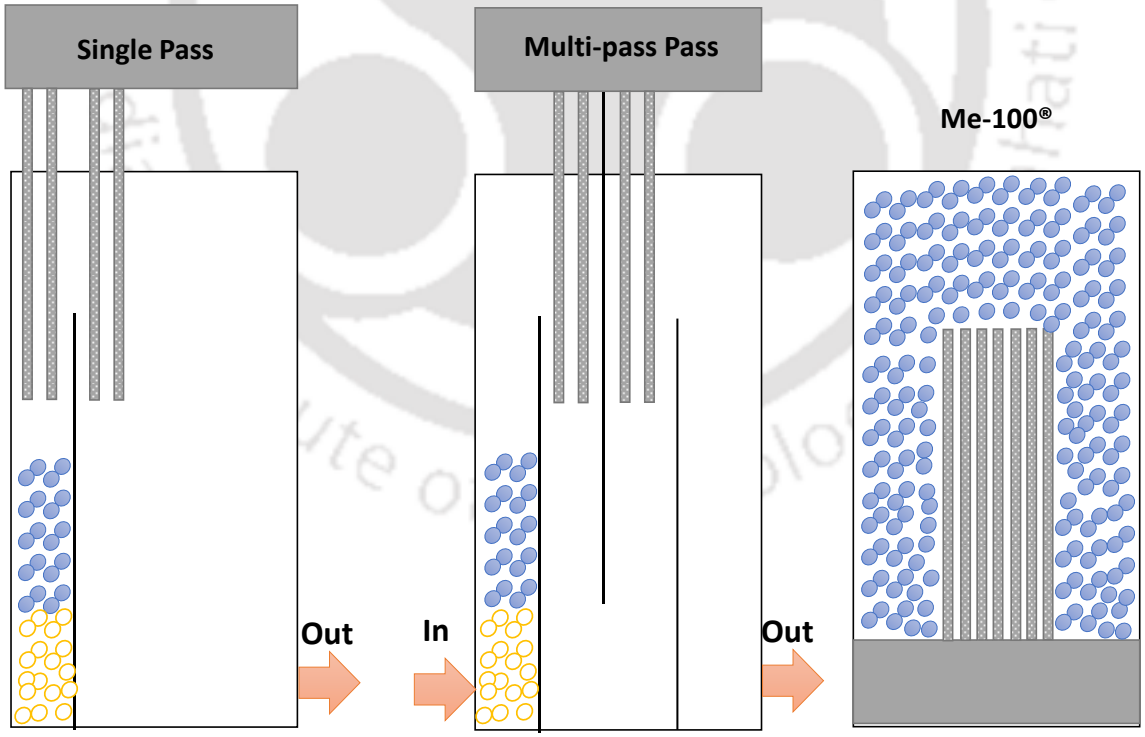

Fig. 5.16 Schematic of membrane reformers tested

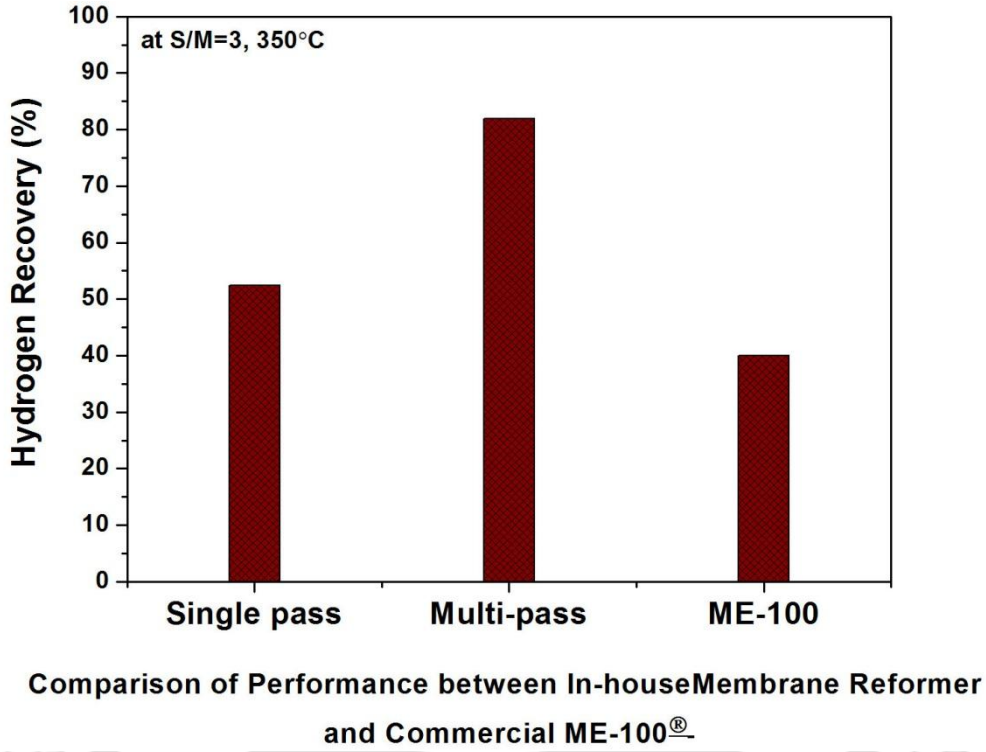

Fig. 5.17 Comparative membrane reformer performance using membrane with and without baffles

5.6 Summary

In this chapter, membrane reformer performance was analyzed using a

a) Self-supported Pd-Ag membrane

b) PSS supported Pd-Ag membrane

Further, a comparison of MR performance using both was performed using a multi-pass (baffle) membrane reformer designed in-house. Baffles allowed determining the effect of multi-pass on MR performance with respect to hydrogen recovery. It is noteworthy that high hydrogen flux and high recovery are two crucial parameters that determine the efficiency of MR. The following are the conclusions drawn from this chapter:

- Performance of membrane reformer was studied using varying feed ratios of methanol: water (1:1.12 to 1:18), temperature (623–723 K) and pressure (3, 5 bar) for 100 µm thick self-supported dense Pd-Ag membrane. The maximum hydrogen recovery with this study was observed to be ~48% with 0.05 mol/m^2.s permeate H_2 flux at 673 K temperature and 3 bar pressure for 1:4.4 methanol: steam molar ratio of feed.
- The performance of self-supported Pd-Ag membrane reformer was compared with membrane separator (sequential integration of reaction and separation unit). No significant inhibition of CO and CO_2 was observed on the performance of membrane for both membrane separator and membrane reformer. However, effect of excess steam was observed which reduces the hydrogen flux due to dilution of feed to membrane but causes no inhibition to hydrogen permeation by Pd-Ag membrane.
- On comparison of membrane reformer with membrane separator, it was observed that permeate hydrogen flux in the membrane reformer for a range of hydrogen mole percentage in the reformate mixture (65.7 to 45) remained nearly equivalent to the hydrogen flux in the separator. This confirms that membrane reformer performance is largely dominated by the membrane performance. Further, hydrogen purity also remained comparable for both the systems.
- Effect of temperature and pressure on the performance of supported Pd-Ag membrane reformer was evaluated. It was found that conversion in case of membrane reformer with single membrane was higher compared to the conventional reactor used in chapter 4.

- With single pass single membrane, MR 53% hydrogen recovery was observed which enhances significantly by increasing the number of membranes.
- The performance of supported single pass and multi-pass membrane reformer was compared. It was observed that performance of multi-pass membrane reformer was higher compared to single pass membrane reformer. Further, newly designed multi-pass membrane reformer was compared with commercially available membrane reformer (ME 100). It was observed that performance of multi-pass membrane reformer with 4 supported membrane was better compared to commercially available membrane reformer with 7 self-supported membranes.

The maximum flow rate obtained with the current work was 0.92 LPM using 4 Pd-Ag membranes supported on PSS and Cu-Fe catalyst supported on AZZ.

5.7 Notations

A	**Area of membrane, m^2**
$F_{H_2,permeate}$	**Hydrogen mass flow rate at the permeate side, kg/h**
$F_{H_2,waste}$	**Hydrogen mass flow rate at the waste/retentate side, kg/h**
j_{H_2}	**Hydrogen permeate flux, mol/m^2.h**
nCO_2	**Molar flow rate of CO_2 in reformate, mol/h**
nCO	**Molar flow rate of CO in reformate, mol/h**
nCH_3OH	**Molar flow rate of CH_3OH in reformate, mol/h**
$nH_{2,\ permeate}$	**Molar flow rate of H_2 in permeate, mol/h**
$p^{0.5}_{H_2,permeate}$	**Partial pressure of hydrogen in permeate, n=0.5**
$p^{0.5}_{H_2,retentate}$	**Partial pressure of hydrogen in retentate, n=0.5**
$X_{H_2,permeate}$	**Mass fraction of hydrogen in permeate**
$X_{H_2,waste}$	**Mass fraction of hydrogen in waste/retentate**
δ	**Membrane thickness**

References

[1] V.M. Gryaznov, V.S. Smirnov, V.M. Vdovin, M.M. Ermilova, L.D. Gogua, N.A. Pritula, I.A. Litvinov, Method of preparing a hydrogen-permeable membrane catalyst on a base of palladium or its alloys for the hydrogenation of unsaturated organic compounds, in, Google Patents, 1979.

[2] V.M. Gryaznov, V.S. Smirnov, V.M. Vdovin, M.M. Ermilova, L.D. Gogua, N.A. Pritula, G.K. Fedorova, Membrane catalyst for hydrogenation of organic compounds and method for preparing same, in, Google Patents, 1983.

[3] D. Jansen, J.W. Dijkstra, R.W. van den Brink, T.A. Peters, M. Stange, R. Bredesen, A. Goldbach, H.Y. Xu, A. Gottschalk, A. Doukelis, Hydrogen membrane reactors for CO2 capture, Energy Procedia, 1 (2009) 253-260.

[4] G. Manzolini, D. Jansen, 14 - Economic analysis of systems for electrical energy and hydrogen production: fundamentals and application to two membrane reactor processes A2 - Basile, Angelo, in: Handbook of Membrane Reactors, Woodhead Publishing, 2013, pp. 528-550.

[5] M. Bracht, P.T. Alderliesten, R. Kloster, R. Pruschek, G. Haupt, E. Xue, J.R.H. Ross, M.K. Koukou, N. Papayannakos, Water gas shift membrane reactor for CO2 control in IGCC systems: techno-economic feasibility study, Energy Conversion and Management, 38, Supplement (1997) S159-S164.

[6] S. Thomas, C. Hamel, A. Seidel-Morgenstern, Basic Problems of Chemical Reaction Engineering and Potential of Membrane Reactors, in: Membrane Reactors, Wiley-VCH Verlag GmbH & Co. KGaA, 2010, pp. 1-27.

[7] A. Basile, S. Tosti, G. Capannelli, G. Vitulli, A. Iulianelli, F. Gallucci, E. Drioli, Co-current and counter-current modes for methanol steam reforming membrane reactor: Experimental study, Catalysis Today, 118 (2006) 237-245.

[8] S. Tosti, A. Basile, L. Bettinali, F. Borgognoni, F. Gallucci, C. Rizzello, Design and process study of Pd membrane reactors, International Journal of Hydrogen Energy, 33 (2008) 5098-5105.

[9] S. Tosti, A. Basile, G. Chiappetta, C. Rizzello, V. Violante, Pd–Ag membrane reactors for water gas shift reaction, Chemical Engineering Journal, 93 (2003) 23-30.

[10] S.A.R.K. Deshmukh, S. Heinrich, L. Mörl, M. van Sint Annaland, J.A.M. Kuipers, Membrane assisted fluidized bed reactors: Potentials and hurdles, Chemical Engineering Science, 62 (2007) 416-436.

[11] R. Dittmeyer, T. Boeltken, P. Piermartini, M. Selinsek, M. Loewert, F. Dallmann, H. Kreuder, M. Cholewa, A. Wunsch, M. Belimov, S. Farsi, P. Pfeifer, Micro and micro membrane reactors for advanced applications in chemical energy conversion, Current Opinion in Chemical Engineering, 17 (2017) 108-125.

[12] M.A. Rakib, J.R. Grace, C.J. Lim, S.S.E.H. Elnashaie, Steam reforming of heptane in a fluidized bed membrane reactor, Journal of Power Sources, 195 (2010) 5749-5760.[13] R. Buxbaum, H. Lei, Power output and load following in a fuel cell fueled by membrane reactor hydrogen, Journal of Power Sources, 123 (2003) 43-47.

[14] G. Chiappetta, G. Barbieri, E. Drioli, Pd/Ag-based membrane reactors on small scale: Assessment of the feed pressure and design parameters effect on the performance, Chemical Engineering and Processing: Process Intensification, 49 (2010) 722-731.

[15] C.A. Cornaglia, S. Tosti, M. Sansovini, J. Múnera, E.A. Lombardo, Novel catalyst for the WGS reaction in a Pd-membrane reactor, Applied Catalysis A: General, 462–463 (2013) 278-286.

[16] M.A. Islam, S. Ilias, Steam Reforming of Methanol in a Pd-Composite Membrane Reactor, Separation Science and Technology, 47 (2012) 2177-2185.

[17] A. Iulianelli, T. Longo, A. Basile, Methanol steam reforming reaction in a Pd–Ag membrane reactor for CO-free hydrogen production, International Journal of Hydrogen Energy, 33 (2008) 5583-5588.

[18] S. Liguori, A. Iulianelli, F. Dalena, V. Piemonte, Y. Huang, A. Basile, Methanol steam reforming in an Al2O3 supported thin Pd-layer membrane reactor over Cu/ZnO/Al2O3 catalyst, International Journal of Hydrogen Energy, 39 (2014) 18702-18710.

[19] M.M. Barreiro, M. Maroño, J.M. Sánchez, Hydrogen permeation through a Pd-based membrane and RWGS conversion in H2/CO2, H2/N2/CO2 and H2/H2O/CO2 mixtures, International Journal of Hydrogen Energy, 39 (2014) 4710-4716.

[20] A. Basile, A. Parmaliana, S. Tosti, A. Iulianelli, F. Gallucci, C. Espro, J. Spooren, Hydrogen production by methanol steam reforming carried out in membrane reactor on Cu/Zn/Mg-based catalyst, Catalysis Today, 137 (2008) 17-22.

[21] S.H. Israni, M.P. Harold, Methanol Steam Reforming in Pd−Ag Membrane Reactors: Effects of Reaction System Species on Transmembrane Hydrogen Flux, Industrial & Engineering Chemistry Research, 49 (2010) 10242-10250.

[22] A. Iulianelli, T. Longo, A. Basile, Methanol steam reforming in a dense Pd–Ag membrane reactor: The pressure and WHSV effects on CO-free H2 production, Journal of Membrane Science, 323 (2008) 235-240.

[23] P. Ribeirinha, M. Abdollahzadeh, M. Boaventura, A. Mendes, H2 production with low carbon content via MSR in packed bed membrane reactors for high-temperature polymeric electrolyte membrane fuel cell, Applied Energy, 188 (2017) 409-419.

[24] F. Borgognoni, S. Tosti, M. Vadrucci, A. Santucci, Combined methane and ethanol reforming for pure hydrogen production through Pd-based membranes, International Journal of Hydrogen Energy, 38 (2013) 1430-1438.

[25] H. Lim, Y. Gu, S.T. Oyama, Studies of the effect of pressure and hydrogen permeance on the ethanol steam reforming reaction with palladium- and silica-based membranes, Journal of Membrane Science, 396 (2012) 119-127.

[26] D.R. Alfonso, Comparative studies of CO and H2O interactions with Pd(111) surface: A theoretical study of poisoning, Applied Physics Letters, 88 (2006) 051908.

[27] K. Aasberg-Petersen, C.S. Nielsen, S.L. Jørgensen, Membrane reforming for hydrogen, Catalysis Today, 46 (1998) 193-201.

Chapter 6

Conclusions and Recommendations

6.1 Conclusions

The objectives of the current thesis was to integrate methanol steam reforming with palladium based alloy membranes into a single unit called as membrane reformer for the power generation once combined with PEM fuel cell. The key parameter was to synthesize and optimize the catalyst performance in order to achieve minimal CO selectivity. In order to achieve the same, various mono-metallic and bi-metallic catalysts were synthesized, characterized and tested. The performance of the catalysts was optimized at variable conditions to achieve maximum hydrogen yield and minimum CO selectivity. To separate the ultra-pure hydrogen, as per the requirement of PEM fuel cell, from the produced reformate mixture palladium based membranes were used. Supported Pd-Ag membranes were prepared on porous SS and porous ceramic supports. The performances of both the membranes were optimized to achieve high purity, maximum recovery and high flux. Further, the performance of supported membranes was compared with the performance of commercially available self-supported Pd-Ag membranes. An 'in-house' membrane separator unit was designed by introducing baffles to enhance the recovery and flux of hydrogen through permeates line. Finally, both reaction (catalyst) and separation (membranes) were integrated to design a 'single pass' and 'multi-pass' membrane reformer for enhanced conversion, recovery and flux. The performance 'in-house' designed single pass and multi-pass membrane reformer was compared with commercially available self-supported membrane reformer. It was found that 'in-house' designed four membrane based multi-pass membrane reformer provides better recovery

and flux compared to commercially available seven membrane based membrane reformer. The individual summary of each chapter is presented at the end of the chapter to elaborate detailed finding. The broad conclusions of the thesis are as follows:

- ✓ Membrane composition was optimized by systematic synthesis, characterization and testing of palladium based membranes such as a) pure Pd, b) 90%Pd-10%Ag and c) 90%Pd-8%Ag-2%Au on porous alumina using electroless deposition. For the addition of silver and gold, sequential electroless deposition and galvanic displacement respectively was performed. All membranes developed were tested up to 2 bar using bubble point method for the extent of densification. Optimal hydrogen permeability using Pd-Ag membranes was observed. The same composition was then deposited on to porous SS support and tested. Maximum hydrogen permeation using Pd-Ag membrane on PSS was established. Higher membrane surface area on PSS and larger pore size of PSS in comparison with porous alumina resulted in an improved hydrogen permeation. Further, the brittle nature of porous alumina also hindered its connections with SS fittings and therefore was only used for preliminary optimization of membrane composition.
- ✓ Enhancement in hydrogen recovery using the developed Pd-Ag membrane on PSS was then established using an 'in-house' designed multi-pass membrane separator. Gas permeation testing was performed with $50H_2$: $50N_2$ (v/v) and $50H_2$:$30N_2$:$18CO_2$:2CO (v/v) as feed at optimized temperature, pressure and GHSV. Modular assembly of longitudinal baffles in the multi-pass membrane separator allowed determining single membrane performance change by changing its location inside reactor shell (inlet, center and outlet). Using self-supported commercial Pd-Ag

membranes, hydrogen recovery was identified higher at center than the inlet and outlet zone. Further, using six different arrangements of four membranes set, the best design for a high throughput membrane separator was established. Using the multi-pass membrane separator, nearly 2-3% improvement in hydrogen recovery was determined using single membrane whereas up to 33% improvement was observed with the multiple membranes.

- ✓ Finally, the performance of prepared supported Pd-Ag membranes (both on porous SS and porous alumina) were compared with commercially available self-supported membranes in a single pass and multi-pass membrane separator. Both porous SS and porous alumina supported membranes give higher flux compared to self-supported membranes in both single pass and multi-pass membrane separator. Among the porous SS and porous alumina supported membranes, porous SS supported membranes provide maximum flux due to enhanced surface area.
- ✓ Methanol steam reforming activity for different mono-metallic as well as bi-metallic catalysts was determined with effect of temperature, S/M ratio and W/F. Minimal CO selectivity at high temperatures (up to 400°C) was obtained using Cu-Fe supported on Al_2O_3-ZnO-ZrO_2. Characterization of this catalyst using TPR and XRD exhibited a shift which indicated alloy formation. This was also confirmed using TEM that showed a much reduced metal particle size in comparison to mono-metallic Cu and Fe catalysts. Using DRIFT study no adsorbed CO was observed. Stability in methanol conversion was also established up to a period of 100 hrs.
- ✓ The best performing Cu-Fe supported on AZZ catalyst was integrated with Pd-Ag on PSS membrane in and in-house designed membrane reformer unit to conduct the

membrane reformer study. Membrane reformer performance was tested for single and multi-pass assembly by using synthesized catalyst and prepared supported membrane. Further, 'in-house' designed membrane reformer performance was compared with commercially available self-supported Pd-Ag membrane reformer ME-100®.

- ✓ Hydrogen selectivity of prepared PSS supported membrane was at par with commercially available self-supported membrane for both increasing temperature and pressure and almost remains same for all the conditions.
- ✓ It was observed that hydrogen recovery increases with increase in number of membrane for same conditions. Further, multi-pass membrane reformer performance was significantly higher compared to single pass membrane reformer. Hence, multi-pass membrane reformer can be opted for possible integration and scale-up studies.

6.2 Recommendations and future directions

- ✓ In order to enhance the hydrogen separation efficiency, it is vital to fabricate thinner membranes. However, with electroless deposition methodology, it is extremely challenging to produce a thinner and dense Pd-alloy membrane unless the support characteristics and its pore network are controlled. Use of deposition tools such as physical vapor deposition (PVD) and chemical vapor deposition (CVD) may be investigated for the fabrication of thinner and dense Pd films. Further, a hybrid deposition methods based on combination of two or three techniques, like CVD followed by electroless deposition or PVD followed by electroless deposition, can be used for effective densification.

- ✓ The surface morphologies of the porous SS support (PSS) used in the current study showed very large pore size distribution. Despite controlling the pore structure with 'in-house' prepared pre-defined particle size yttria stabilized zirconia (YSZ), a significant benefit to achieve thinner Pd-alloy membrane was not observed. Further, in case of alumina the challenge was to connect the ceramic with SS fittings and make it leak proof. Despite using graphite ferrules, obtaining an absolute leak proof connection was observed to be a trial and error based success along with huge losses. Hence, it is highly recommended to look for optimization of support structure which is the core of these deposition methodologies. It is advisable to develop porous structure in-house with a controlled pore size and network. Further, materials such as zirconia-alumina alloy composites may also be investigated in the development of same.
- ✓ For future directions, catalysts with higher reactivity at low temperatures may be investigated. Further, Fe as promoter can also be further investigated to demonstrate differences in activity with varying catalysts formations such as hetero-atom, alloy, inter-metallic and core shell. Moreover, catalysts performance with increasing pressures needs to be investigated as the product selectivity may change with pressure that affects the membrane reformer integration.
- ✓ Finally, 'multi-pass membrane reformer' arrangement is recommended for the future integration and scale-up studies.

Appendix A

Atomic Absorbance Spectroscopy (AAS) for Standard Solutions

The calculation for the amount of metal deposited was performed after the calibration graph for pure metal with known concentration was generated as shown in Fig. A1. The sensitivity of the AAS instrument is high if the metal concentration is below 100 ppm. Hence, during deposition, 0.1 mL sample was collected for multiple cycles and were analyzed with AAS using dilution factor of 100. An example of the calculation done is shown in Table A1 below

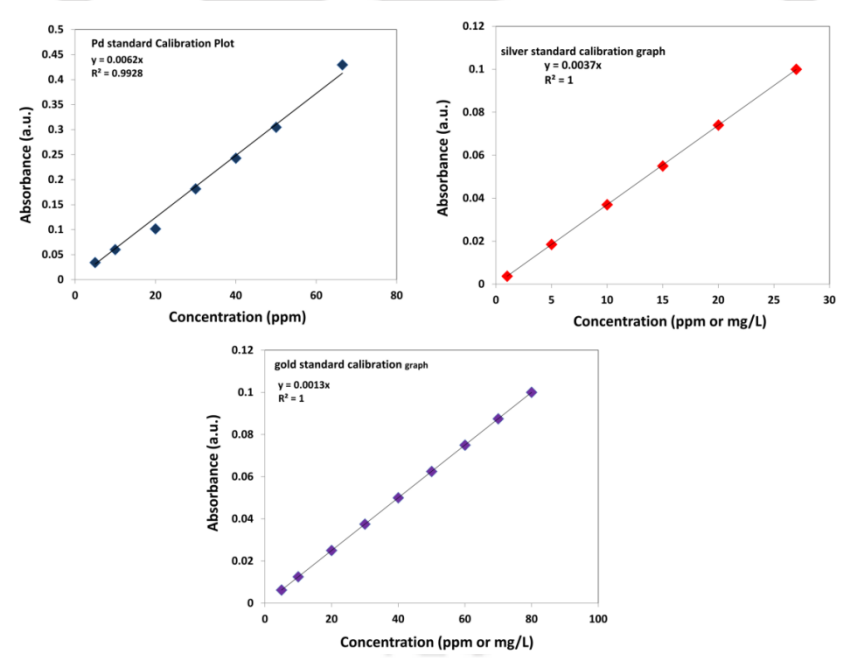

Fig. A1 Standard Pd, Ag and Au solution calibration graph

Table A1 Example for Calculation for AAS

Time (mins)	Sample	Absorbance	df*	Concentration mg/L	amount of Pd mg/50mL	Conversion (%)	Cumulative Pd Deposited in mg	area of tube (cm^2)	Thickness (µm)
	INITIAL	0.7677	100	6141.6	307.08			28.3	0
30	T1	0.5057	100	4045.6	202.28	34.13	104.8	28.3	3.114
60	T2	0.3979	100	3183.2	159.16	48.17	147.9	28.3	4.396
90	T3	0.2186	100	1748.8	87.44	71.53	219.6	28.3	6.527
120	T4	0.1885	100	1508	75.40	75.45	231.7	28.3	6.885
150	T5	0.1653	100	1322.4	66.12	78.47	241.0	28.3	7.161
Cumulative Thickness									28

***Here df stands for dilution factor**

BIO-DATA

Name: Richa Sharma

Date of Birth: 06/11/1984

Place of Birth: Delhi, India

Email: richa.s.84@gmail.com / richa.sharma@iitg.ernet.in

Educational Qualifications:

	Educational Qualification
2012 - present	Ph. D., Chemical Engineering Indian Institute of Technology Guwahati
2010-2012	M. Tech., Chemical Technology (Bio-chemical Engineering) HBTI, Kanpur
2003-2007	B. Tech., Biotechnology Rai Foundation Colleges, Maharashtra

Awards and Achievements

- Best paper presentation on "Performance of Palladium Membrane based Hydrogen Generator cum Separator" at CHEMCON "13", ICT-Mumbai.
- Second Prize in Poster on "On-board hydrogen generator-design, material synthesis and Integration" at 3rd INDO-GERMAN Workshop 2016, jointly organized by IITGuwahati, India and Max Planck Institute, Magdeburg, Germany
- Asset best paper presentation award on Dense supported palladium membrane performance in a multi-tubular reactor at Seventh DAE-BRNS symposium "SESTEC-2016"

Publications

- Richa Sharma, Amit Kumar, Rajesh K. Upadhyay, Catalytic Sol Assisted Dense Pd/γ-Al_2O_3 Membrane using Modified Electroless Plating: Effect of Process on Surface Morphology, *Chemical Product and Process Modeling, 12 (2016) 10-28*

- Richa Sharma, Amit Kumar, Rajesh K. Upadhyay, Performance Comparison of Methanol Steam Reforming Integrated to Pd-Ag Membrane: Membrane Reformer vs. Membrane Separator, *Separation and Purification Technology, 183 (2017) 194-203*

- Richa Sharma, Amit Kumar, Rajesh K. Upadhyay, "Design of a Multi-pass Membrane Separator for Hydrogen Separation through Self-supported Pd-Ag Membranes " *International Journey of Hydrogen Energy 43 (2018) 5019-5032*

- Richa Sharma, Amit Kumar, Rajesh K. Upadhyay, "Methanol Steam Reforming with Fe-based Catalyst: Targeting Zero CO Selectivity" (Manuscript to be communicated)

- Richa Sharma, Amit Kumar, Rajesh K. Upadhyay, "Multi-pass Membrane Reformer Performance in Packed and Fluidized Bed" (Manuscript to be communicated)

- Richa Sharma, Amit Kumar, Rajesh K. Upadhyay, "Kinetic modeling of high temperature CO free methanol steam reforming activity using Cu-Fe bi-metallic alloy" (under processing)

Conferences Presented

- "Performance of Palladium Membrane Based Hydrogen Generator cum Separator", Richa Sharma, Amit Kumar and Rajesh K. Upadhyay, CHEMCON 2013, Mumbai, India, 27-30 December, 2013. (Best Paper Award)

- "Comparative Study on Pd Based Membrane Separator and Reformer: Effect of Membrane Stacking", Richa Sharma, Amit Kumar, Rajesh K. Upadhyay, ISCRE 23 & APCRE 7, Bangkok, Thailand, 7-10 September 2014.

- "Hydrogen Recovery from a Palladium Membrane Reformer: Optimizing Reaction and Separation Effect", Richa Sharma, Amit Kumar, Rajesh K. Upadhyay, CAMURE-9 & ISMR-8, Lyon, France, 7-10 December 2014.

- "Process Optimization of Palladium Membrane Performance for Hydrogen Separation", Richa Sharma, Amit Kumar, Rajesh K. Upadhyay, CHEMCON 2014, Chandigarh, India, 27-30 December, 2014.

- "A Comparative Study of Integration Approaches in a Palladium Membrane Reformer for Ultra-Pure H_2 Production" Richa Sharma, Amit Kumar, Rajesh K. Upadhyay, 4^{th} International Hydrogen & Fuel Cell Conference, AGRA 6-8 December 2015.

- "Integration Approaches in a Palladium Membrane Reactor for Ultra-Pure H_2 Production" Richa Sharma, Amit Kumar, Rajesh K. Upadhyay, CHEMCON 2015, Guwahati, India, 27-30 December, 2015.

- "Methanol fed On-board Hydrogen Generator: Design, Material Synthesis and Integration", Richa Sharma, Amit Kumar, Rajesh K. Upadhyay, 3rd INDO GERMAN WORKSHOP, Guwahati, 23-26 February 2016. (Awarded 2^{nd} Prize)

- "Hydrogen separation using dense supported palladium membranes in a multi-tubular in-house membrane reactor", Richa Sharma, Amit Kumar, Rajesh K. Upadhyay, SESTEC 7, Guwahati, 17-20 May 2016. (Best Paper Award)

- "Palladium Based Membrane Separator for Generation of Ultra-Pure Hydrogen: Design, Preparation and Testing", Richa Sharma, Amit Kumar, Rajesh K. Upadhyay, SESTEC 7, Guwahati, 17-20 May 2016. (**Invited talk**)

- "Generation of H_2 for 200W PEM Fuel Cells from supported Cu-Fe based Catalysts using Membrane based Methanol Steam Reforming" Richa Sharma, Amit Kumar, Rajesh K. Upadhyay, ACS-On Campus, Guwahati, January 2017

- "Low Temperature Methanol Steam Reforming using Cu-Fe Bi-metallic Catalysts" Abstract Accepted-Oral Presentation" Richa Sharma, Amit Kumar, Rajesh K. Upadhyay, Camure-10 and ISMR-9, Qingdao, China, July 7th-10th 2017. (oral Presentation)

- "Production of High Purity Hydrogen through Methanol Based Membrane Reformer" Richa Sharma, IIChE Lecture at Assam Engineering College (AEC) August 2017, Guwahati (**Invited Talk**)

Conferences Accepted

- "Integration of Synthesized Catalysts and Membrane in Packed and Fluidized Bed Membrane Reformer for Production of Hydrogen through Steam Reforming" Richa Sharma, Amit Kumar, Rajesh K. Upadhyay, **17 AIChE Annual Meeting**, Minneapolis, USA, 29th Oct-3rd Nov, 2017.
- "Membrane Reformers: Optimization of Catalysts and Membranes for Production of Ultra-Pure Hydrogen through Steam Reforming of Methanol" Richa Sharma, Amit Kumar, Rajesh K. Upadhyay, **17 AIChE Annual Meeting**, Minneapolis, USA, 29th Oct-3rd Nov, 2017.

Date: 14-05-2018

Place: IIT-Guwahati **Signature**